TOOL WEAR PREDICTION IN MACHINING
A HYBRID FINITE ELEMENT AND EMPIRICAL METHODOLOGY

TOOL WEAR PREDICTION IN MACHINING
A HYBRID NUMERICAL AND EMPRICAL METHODOLOGY

By

KEYVAN HOSSEINKHANI KARGAR, B.Sc., M.Eng.

A Thesis
Submitted to the School of Graduate Studies
in Partial Fulfillment of the Requirements
for the Degree
Doctor of Philosophy

PREFACE

This Ph.D. thesis presents the development of a unique tool wear prediction methodology by combining the advantages of the finite element simulation and the available empirical wear rate characteristic models. The contents of this thesis are presented as an integrated article thesis which is also known as sandwich thesis, and it includes nine chapters.

Chapter one presents a very brief introduction to the objectives and contents of each chapter.

Chapters two provides a literature review on the mechanics of cutting process, tool wear type, mechanisms as well as tool wear predictions methodologies. This chapter also reviews empirical tool wear models and the previous researches on finite element-based tool wear prediction methodologies.

Chapter three reviews the different techniques used in finite element simulating the cutting process and the fundamentals of assembling an ALE cutting model which has been used throughout this thesis.

Chapter four explores the viability of the most widely used frictional models for simulating the contact condition at the tool-chip interface. This chapter is the copy of the collaborative paper that has been published in the Journal of Advanced Manufacturing Technology in 2017 by Amir Malakizadi, Keyvan Hosseinkhani, Emilia Mariano, E. Ng, Antonio Del Prete, Lars Nyborg.

Chapter five discusses the accuracy of finite element simulation of cutting process under the worn tool geometry. This chapter is a copy of the paper published in the Journal of Advanced Manufacturing Technology in 2021 Keyvan Hosseinkhani and Eugene Ng.

Chapter six evaluates the calibration of the empirical tool wear rate models. This chapter is the copy of the paper published in the International Journal of Advanced Manufacturing Technology in 2018 by Keyvan Hosseinkhani and Eugene Ng.

Chapter seven presents a unique approach for estimating tool life. This chapter is the copy of the paper published in the Journal of Manufacturing and Materials Processing in 2020 by Keyvan Hosseinkhani and Eugene Ng.

Chapter eight summarizes the key discovery in this research. Following that the ideas that can potentially improve the current achievements and enhance their applications are presented in the future work section.

I declare that this Ph.D. thesis is an original research and has been written by me and has not been submitted for any previous degree.

Keyvan Hosseinkhani
December 2022.

ABSTRACT

Tool wear rate prediction using either empirical or finite element (FE) method has its respective advantages and drawbacks. Major drawbacks with empirical approaches are extensive experimental data are required to calibrate the empirical model constants and are bounded by the unique combination of the tool/workpiece material. Whereas with FE approach, long computational time are required even with current central processing unit speeds and peripheral component interconnection frequencies. The ratio between computation time and real cutting time is about 9600.

The objective of this research is to develop and validate a unique hybrid empirical and finite element approach to predict tool wear rate that is computationally efficient and limited number of tests required to calibrate the empirical model. Four different empirical wear rate models were evaluated based on least number of quantitative assumptions involved and independency from the proportion of dominant wear mechanisms. The empirical wear rate models selected for evaluation are dependent on stresses and temperatures rather than process parameters. The stresses and temperature predicted by the FE model served as input for the empirical wear rate models. FE computational time was substantially reduced as this approach only needs to simulate the cutting process up to steady state with different flank wear length. Each unique flank wear length simulations are not dependent on the other. Therefore, the simulation can be performed in parallel, which increased computation efficiency in an exponential rate. An initial wear rate model was also developed, which is dependent on average stresses acting on the cutting edge.

Experimental orthogonal cutting tests of AISI 1045 (165-190 BHN) with uncoated tungsten carbide were carried out to calibrate and validate the wear rate models. Usui wear rate model was the most robust when compared to the other models investigated. This was because there is unbounded restriction in selecting process parameters during model calibration. Good agreement between predicted and experimental tool wear rate with only two tests required to calibrate the empirical model. The computation time with such an approach is independent on tool wear rate. The initial wear rate model substantially improved the accuracy of the prediction only at the more aggressive cutting conditions as the wear mechanism were based on mechanical effect rather than thermal.

ACKNOWLEDGEMENT

First, I would like to give special thanks to my supervisor, Dr. Eu-Gene Ng, for his continuing support, motivations and guidance throughout the course of this research. His guidance and support have been invaluable in shaping the direction of my research. The opportunities provided by Dr. Eu-Gene Ng in allowing me to be involved in industrial projects and participating in multiple domestic and international conferences are highly appreciated.

I would also like to thank Dr. Philip Koshy and Dr. Joseph McDermid for honoring me by being a part of my PhD supervisory committee. Their support and advice are deeply appreciated.

I also owe a special thank to Nima Zarif Yussefian for assisting me in gaining more insights into the mechanics of metal cutting and tool wear. Another special thank goes to Youssef Ziada for assisting me in finite element simulation of cutting process.

I am extremely grateful to my lovely mother for her limitless support and continuous encouragement during all these years. I give a special thank to my beautiful wife, Somayeh, for her understanding and support through these years.

I would also like to thank the former leadership team at Burloak Technologies Inc. and Additive Metal Manufacturing Inc.; Mr. Peter Adams, the former president and founder of Burloak Technologies, Mr. Stew Deadman, the former vice president of technology at Burloak, as well as Mr. Nigel Southway, the former vice president of engineering at Additive Metal Manufacturing for giving me the opportunity while I was completing my PhD.

At the end, none of this work would have been possible without the financial assistance of the NSERC Canadian Network for Research and Innovation in Machining Technology (CANRIMT).

TABLE OF CONTENT

LIST OF FIGURES

LIST OF TABLES

1 INTRODUCTION

In machining workpiece material undergoes large plastic deformation which is coupled with high strain rate and temperature. This complex nature of deformation makes the development of predictive, rather than descriptive, analytical models very challenging. At the same time, experimentally developed empirical models are highly limited to specific boundary conditions and time consuming and expensive to calibrate.

With the improvements in computational capabilities, the finite element method has been used as a powerful tool for simulating the machining process [Ceretti, 1999, Klocke, 2002, Ng, 2002a]. Finite element (FE) models are physics-based models which incorporate the constitutive material model as well as the friction model to simulate the complex workpiece deformation and tool-workpiece contact. Once a finite element cutting model is validated, it can provide a unique insight into the process mechanics and consequently reduce the number of design iterations required for the process optimization and tool design. Also, in contrast to analytical models, FE models keep the history of the cutting process required for the analysis of sequential cuts.

Contact and friction in machining affect the cutting power, surface integrity of interacting tool and workpiece as well as tool wear and tool life. Wear on the cutting tool changes the optimum geometry of its cutting edge and increases the forces, temperature, and vibration. When wear on the tool reaches to a critical size, it must be replaced otherwise it affects the integrity of the machined component as well as the components of machine tool. Therefore, tool wear in machining directly relate to the economics of the process and modeling and prediction of them is of significant value for process optimization.

In this context, this PhD thesis presents the proof-of-concept of a tool wear and tool life prediction methodology based on a hybrid empirical / finite element approach.

Chapter two introduces the mechanics of metal cutting with the focus on the principle of chip formation process, the tool wear types and mechanisms, tool wear prediction approaches and well-known empirical models. Following the initial introduction, chapter two reviews the latest advancements in finite element-based tool wear prediction approaches and discusses the limitation and required improvements. The last section of chapter two presents the objectives and outline of the thesis.

Chapter three introduces the various techniques which have been used in finite element simulation of the cutting process. In this chapter the fundamentals of building a finite element cutting model are explained and the basics of the material constitutive model and contact and friction models are explained.

Chapter four to seven are the re-production of the research works associated with the current thesis that have been published in peer reviewed academic journals.

At the end chapter eight states the conclusions and covers the proposed future works.

2 LITERATURE SURVEY

2.1 Mechanics of Metal Cutting

The machining process considered in the present thesis is a conventional type in which a wedge-shaped tool with specific cutting edge geometry cuts through the workpiece material and removes a thin layer. The removed layer is known as the chip and the removal process is known as the chip formation process [Shaw, 2005]. In terms of analyzing the chip formation, the most common types of conventional machining processes such as shaping, broaching, turning, milling, and drilling, as shown in Figure 2-1, can be studied with similar approach.

For simplification purposes, the experimental and numerical works in the context of present research are based on the orthogonal chip formation process. The general configuration of an orthogonal chip formation process has been illustrated in Figure 2-2 (a) and (b). In an orthogonal process tool cutting edge is perpendicular to the cutting direction or velocity, width

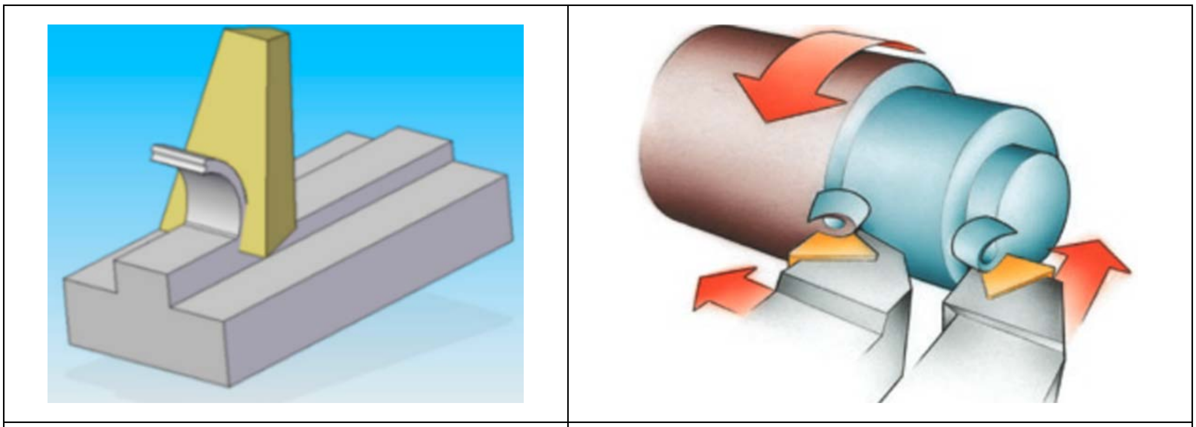

(a) Shaping (b) Turning

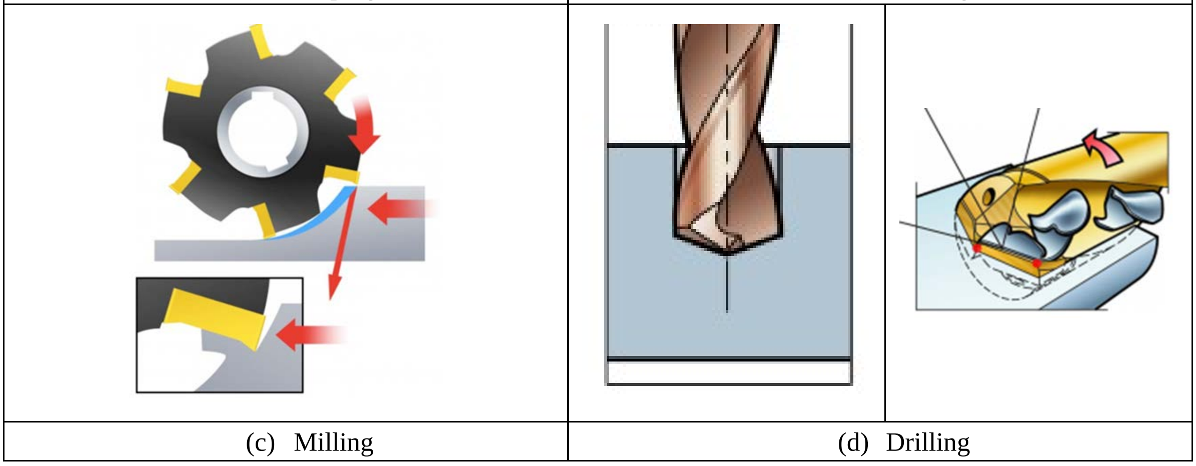

(c) Milling (d) Drilling

Figure 2-1. Chip formation in turning, milling, and drilling processes [Coromant, 1994].

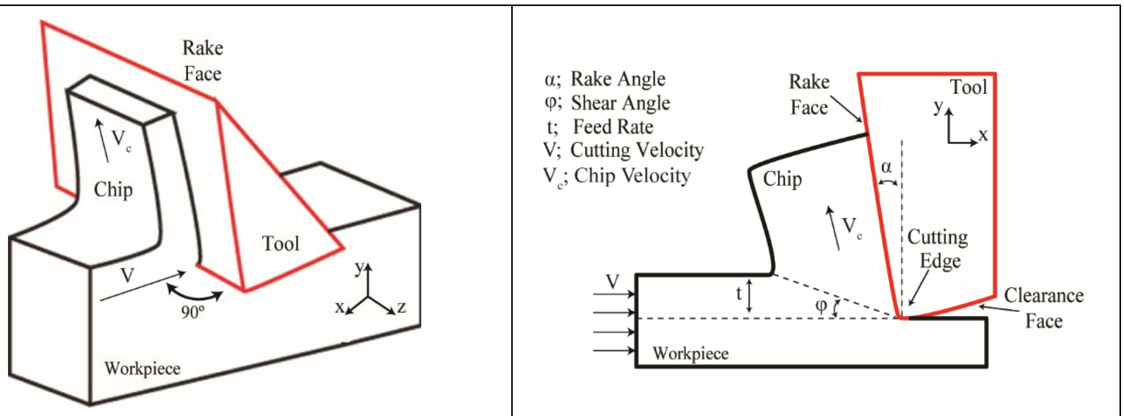

(a) (b)

Figure 2-2. Orthogonal chip formation (a) 3D and (b) 2D.

of cutting edge is larger than the width of workpiece material, width of the workpiece material is larger than the uncut chip thickness/feed rate by at least ten times. With reference to Figure 2-2 (a), the chip only flows in the x-y plane and does not flow in the z direction [Merchant, 1945, Oxley, 1989, Shaw, 2005]. As the result, forces are only acting on one plane and chip formation would be simplified to a two-dimensional plane strain process. Figure 2-2 (b) also illustrates the parameters involved in the chip formation process such as tool rake angle, tool cutting edge and the shear angle of the workpiece material. The angle between tool rake face and normal to the cutting direction is known as the rake angle and depending on the applications can be either positive or negative. Lower machining forces and smaller shear plane length are usually achieved whit positive rake angle tools. However, a tool with negative rake angle is able to withstand higher stresses and to go thorough heavier cuts. The geometry that connects tool rake and clearance faces is known as the cutting edge geometry. The cutting edge geometry has large influence on the machining forces, stress, strain as well as the temperature distribution in the cutting zone [Yen, 2004a, Yussefian, 2010]. The round and chamfered cutting geometries are shown in Figure 2-3.

In the cutting zone, there are three regions of interest, as shown in Figure 2-4. The first region is the boundary between the undeformed (workpiece) and deformed (chip) material. The second region is contacting interface between the tool rake face and moving chip and the third region is the contacting interface between the cutting edge of the tool and machined surface [Trent, 2000, Toenshoff, 2013]. As the cutting tool advances into the workpiece, a thin layer of the workpiece undergoes severe plastic deformation due to shearing by passing thorough the shear zone which is known as the primary shear deformation zone (PSDZ). The shear angle, φ, dictates the orientation of PSDZ as shown in Figure 2-2. In machining even with a very sharp cutting edge, a finite edge geometry or radius exists at the intersection of clearance and rake faces [Albrecht, 1960]. Therefore, the primary shear deformation zone is not just a single plane but a region, as shown in Figure 2-4. The interface contact between the underside of the chip and rake face is known as the secondary deformation zone (SDZ). The interface contact between the tool cutting edge and newly generated surface forms the tertiary deformation zone (TDZ).

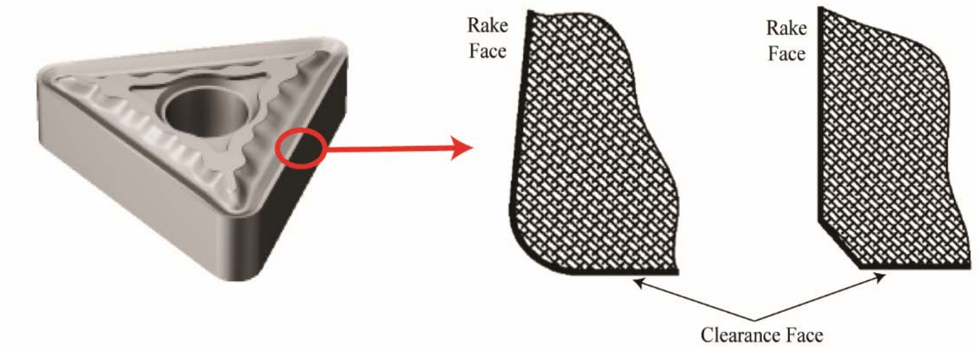

Figure 2-3. Different cutting edge geometries [Yen, 2004].

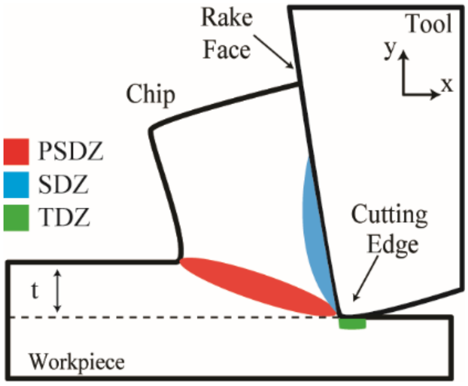

Figure 2-4. Three deformation zones in orthogonal cutting process.

2.2 Mechanics of Tool Wear in the Cutting Process

Tool wear is defined as the gradual loss of tool material in the cutting zone. Due to the extreme thermal and mechanical loadings generated in the cutting zone, tool wear is an inevitable phenomenon which gradually changes the initial cutting edge geometry. The worn cutting edge affects the mechanics of cutting by increasing the machining forces, temperature, and tensile residual stresses in the machined component component [Yen, 2004a, Chen, 2004, Denkena, 2011, Saini, 2012]. Flank and crater wear are considered as the most common measured form of tool wear in conventional machining processes [Astakhov, 2008, Li, 2012].

Crater wear is usually formed on the rake face of the tool where the tool is under high temperature and pressure induced by chip formation and sliding, as shown in Figure 2-5. Crater wear is represented by its depth, K_T, and the maximum depth of crater pattern is usually located at the midpoint of tool-chip contact length where the maximum temperature has been reported to exist, [Astakhov, 2004, 2006]. Progression of crater wear is not desirable as it weakens the cutting edge and results in edge chipping or edge catastrophic failure.

Flank wear is usually formed on the clearance face of the tool and mainly due to the high sliding velocity of hard inclusions of workpiece material passing over the tool clearance face, The length of the flank wear is represented by the length V_B, as detail in Figure 2-5. Progression of flank wear increases the contact area between the tool and machined surface which increases plastic deformation and heat generation rate. As the result, increase in the flank wear length is

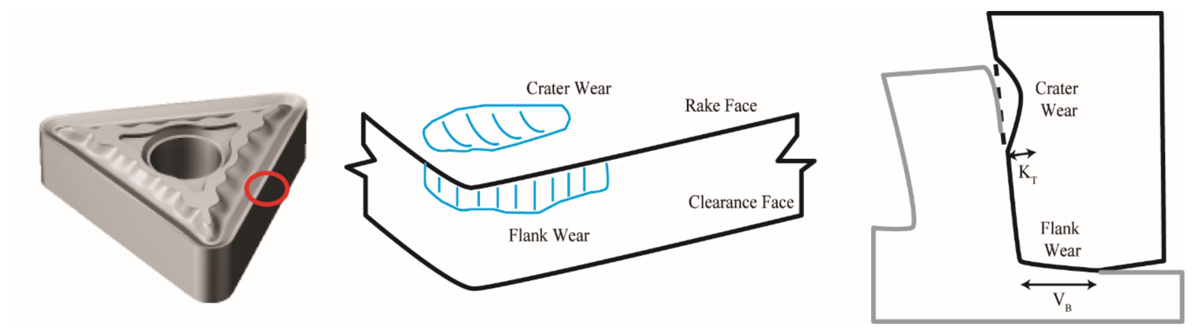

Figure 2-5. Schematic of (a) crater wear and (b) flank wear.

directly related to the increase in the cutting power and the “unwanted” tensile residual stresses in the machined component.

Tool life is defined as the productive cutting time during which tool cutting edge can generate a surface within acceptable integrity and requirements. In case of crater wear tool life is defined with respect to the size of crater depth, and for flank wear tool life is defined with respect to the size of wear length.

Figure 2-6 shows the tool life diagram in terms of flank wear length with cutting time. A general tool life trend consists of three periods which are: a) the initial or running-in period, b) the secondary or steady-state period and c) the tertiary period [Shaw, 2005, Boothroyd, 1985]. The initial period is basically categorized as the time period in which the cutting tool engages into a cut and is generally accompanied by high wear rates induced from high stresses acting on a smaller initial cutting edge radius resulting in micro chipping or fracture. After the initial fracture, cutting tool is completely engaged into the cut and the gradual formation of wear is experienced in a long steady-state period. The tertiary period is emerged following the steady-state period when tool wear has reached to a critical size and extensive thermal and mechanical loads are generated in the cutting zone which extremely increase the wear rate.

Mechanisms responsible for tool wear formation have been mainly categorized as abrasion, adhesion, diffusion, oxidation, fatigue, and delamination. While all these

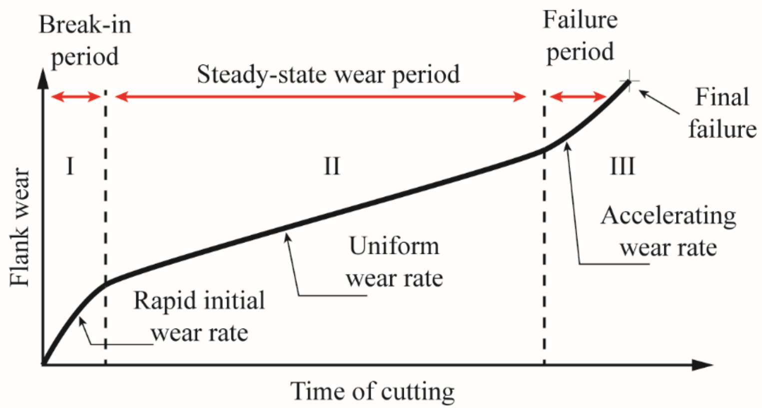

Figure 2-6. Tool life diagram – relationship between flank wear length and cutting time [Boothroyd, 1985].

mechanisms are usually existing in a practical cutting process, the dominant mechanism depends on the tool-work material combination as well as the overall cutting conditions. In terms of analyzing crater and flank wear, which were mentioned as the two most common forms of tool wear, the main mechanisms are abrasion, adhesion, and diffusion [Altintas, 2000].

2.2.1 Abrasion

Abrasion is generally defined as the process of shearing away the small particles from a soft body when it comes into the contact with a harder body [Rabinowicz 1966, Glaeser, 1971, Hoier, 2019]. In the cutting process, abrasive wear is referred to the situations where particles of the tool are sheared off by the mechanical action of hard inclusions in the workpiece material as they slide over the tool face, as shown in Figure 2-7. Signs of grooving are usually observed on the abraded surfaces. Sand particles in castings, carbide inclusions in steel and silicon particles in Al-Si alloys are the examples of hard inclusions [Koshy, 2011]. This mechanism is similar to the grinding process and the typical wear type due to abrasion is the flank wear on the tool clearance face [Sadik, 2014]. Sliding velocity of the workpiece material over the tool clearance face is higher compared to sliding velocity of the chip over the tool rake face. Also the workpiece temperature in the clearance face region is lower than the temperature on the rake face. Combination of higher sliding velocity and lower temperature results in higher rate of abrasion on the clearance face of the tool.

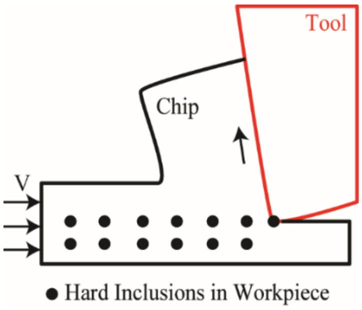

Figure 2-7. Schematic of abrasion in the abrasive wear in the cutting zone.

2.2.2 Adhesion

Adhesion occurs during the relative movement between two bodies under normal load when fragments of the softer body adhere to the fragments of the harder body [Rabinowicz, 1980]. In the cutting process, adhesive wear is referred to the situations where the fragments of the work material are welded to the tool material and form junctions due to friction mechanism. The adhered junctions are unstable and fracture due to the relative movement between tool and work, as detailed in Figure 2-8. The fractured junctions carry small fragments from the tool body, which is referred to as adhesive wear [Altintas, 2000].

An example of adhesive wear is the built-up edge (BUE). At low cutting speed, which result in low cutting temperatures, and together with good affinity between tool and workpiece material, part of the chip an get welded and hardened on the tool rake face. This is referred to as built-up edge. Built-up edge is periodical an unstable and every time it is fractures, it removes a piece of cutting tool material or its coating. Notch wear on the cutting tool is also considered to be the result of adhesive wear.

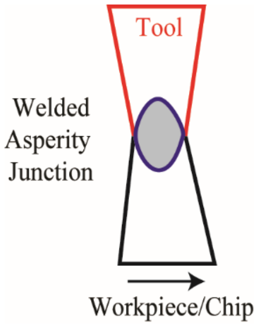

Figure 2-8. Schematic of adhesion – model of a junction about to be broken.

2.2.3 Diffusion

Diffusion is referred to the movement of the atoms in a metallic crystal lattice from one region of high concentration to a region of low concentration. Diffusion is a thermo-mechanical process and rate of diffusion is exponentially dependent on temperature [Boothroyd, 1985]. In the cutting process, diffusion depend on the chemical stability of the tool material and occurs when the atoms of the tool move to the work material as the result of high contact normal load and high temperature. This process occurs in a small reaction zone at the interfaces of contact and gradually creates an indentation in the tool surface which is referred to as diffusive wear. For example, when cutting steel (iron F_e) with tungsten carbide tool (WC) the cobalt particles in the tungsten carbide diffuse into the moving steel chip and ferrite atoms move into the tool, as illustrated in Figure 2-9. The moving ferrite particles together with tungsten carbide from a very brittle and low wear resistance carbide. The typical wear type due to diffusion in cutting is the crater wear on the tool rake face [Sadik, 2014]. The metal-on-metal contact under high temperature and low sliding speed on the tool rake face result in the occurrence of diffusion. Choosing a tool material with high thermal conductivity and low solubility in the workpiece material as well as coating on the tool face will reduce the rate of diffusion.

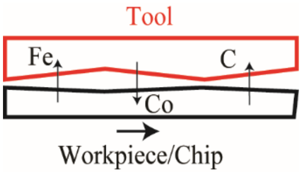

Figure 2-9. Schematic of diffusion when cutting steel with uncoated tungsten carbide.

2.3 Tool Wear Prediction

Traditionally, there have been two main approaches toward tool wear and tool life prediction [Palmai, 2013]. In the first approach, empirical equations were developed by relating tool life to the process parameters such as cutting speed, feed rate and depth of cut. These models are generally being referred to as the tool life models. In the second approach, empirical equations were developed by relating the rate of tool wear to the wear mechanisms such as abrasion, adhesion, and diffusion in the cutting zone. These models are generally being referred to as the tool wear models.

2.3.1 Empirical tool life models

One of the most famous tool life models is the equation developed by Taylor [1907]. Table 2-1 lists the Taylor's basic tool life equation and its extensions. In the equations listed in Table 2-1, L is the tool life, V is the cutting speed, f is the feed rate, d is the depth of cut, T is the temperature and n, m, p, q, r, C_1, C_2, C_3 *and* C_4 are the constants to be determined experimentally. In Eq. 2-1, which is the most widely used equation among the four equations listed, constants C_1 and n are determined experimentally for every combination of tool and workpiece materials and currently available in many available references [Mills, 1983, Schey, 1987]. In Eq. 2-2, it has been observed experimentally that $r < q < p$. This indicates that the tool life is most sensitive to cutting speed and followed by feed rate and lastly to depth of cut. Eq. 2-2 results in more accurate prediction of tool life compared to the basic Taylor's tool life equation, Eq. 2-1. However, more experiments are required for its calibration [Niebel, 1989, Hoffman, 1984]. Eq. 2-3 includes the hardness of workpiece materials in addition to the parameters included in Eq. 2-2. But studies have concluded that its accurate estimation is limited for tool life between 10 to 60 minutes [Wang, 1986, Hoffman, 1984]. Eq. 2-4 includes the effect of cutting temperature on the tool life and n has been found to be between 0.01 and 0.1. Eq. 2-4 requires temperature measurement for its calibration and implementation. Therefore, it has been considered as an inconvenient tool life equation in the machine shop environment [Quinto, 1988, Oxley, 1989].

It has been concluded that Taylor's basic and extended equations need to be calibrated experimentally for every combination of tool and workpiece materials as well as cutting operating conditions. Thus, these equations are convenient to be used in limited range of cutting conditions. Furthermore, except the tool life, these models do not provide any information regarding the wear rate and worn profiles which are important data when it comes to process optimization and tool design [Marksberry, 2008, Poulachon, 2001, Choudhury, 2000].

$VL^n = C_1$	Taylor's basic equation.	Eq. 2-1
$L = C_2 / V^p f^q d^r$	Taylor's extended equation including the cutting parameters	Eq. 2-2
$V = C_3 / \left(L^m f^p d^q (BHN/200^n) \right)$	Taylor's extended equation including the cutting parameters and workpiece material's hardness	Eq. 2-3
$TL^n = C_4$	Taylor's extended equation including the cutting temperature	Eq. 2-4

Table 2-1. Taylor tool life model and its extensions [Marksbrry, 2008].

2.3.2 Empirical tool wear models

Table 2-2 below lists the most famous models developed based on the second approach The first relations developed by this approach were probably those resulted from works done

Wear Rate Models	**Reference**
$dW/dL = A_r (c/b) Z$	[Archard, 1953]
$dW/dL = Z\ (P/H)$	[Shaw, 1956]
$dW/dt = F(V, f).C + D \exp(-E/RT)$	[Takeyama, 1963]
$dW/dt = A\sigma_n v_s \exp(-B/T)$	[Usui, 1984]
$VB = K\left(2\ V / \tan\theta\, b^2\right)^{1/3} (F_t t / H_t)^{1/3}$	[Zhao, 2002]
$dW/dt = \left\{ (A/H) \left(F_f / Vf \right) v_s \right\} + B \exp(-E/RT)$	[Luo, 2005]
$dW/dt = Av_s (H_w/H_t) + Bv_s \exp(-C/T)$	[Akawawa, 2009]
$dW/dt = A\sigma_n v_s \exp(-B/T) + D \exp(+E/RT)$	[Attanasio, 2010]

Table 2-2. List of selected tool wear rate models

by Shaw and Dirke [1956] and Trigger and Chao [1956]. Half a century later Zhao et al. [2002], and Akazawa et al. [2009] enhanced this approach by including the effect of temperature on the thermal softening of cutting tool. Among the tool wear rate models listed in Table 2-2, those proposed by Takeyama and Murata [1963] and Usui et al. [1984] are the most famous and have been used widely in numerical studies of tool wear.

2.3.3 Takeyama and Murata wear rate model

Takeyama and Murata [Takeyama, 1963] developed their tool wear model based on turning cast iron and heat resistant alloy with carbide tools, P10 and K20. From their observation during turning, the total amount of tool wear was due to the combination of mechanical abrasion and diffusion as shown in Eq. 2-5:

$W = W_a + W_d$…………………………………………………………………	Eq. 2-5

Based on Takeyama and Murata, wear due to mechanical abrasion, W_a, was directly related to the length of cut and independent from temperature. On the other hand, wear due to diffusion was a rate process and according to the Arrhenius law depends on temperature. Referring to Eq. 2-5 the total wear rate has been then presented in Eq. 2-6:

$dW/dt = F(V, f).C + D \exp(-E/RT)$……………………………………………	Eq. 2-6

where V is the cutting speed, C and D are the constants associated with the tool and work material, f is the feed rate, E is the activation energy of the diffusion process containing both entropy and enthalpy terms, R is the universal gas constant, and T is the temperature.

Based on the experimental tool wear tests, Takeyama and Murata concluded that under the mild cutting conditions or when the temperature is lower than the activation temperature of diffusion, T_{act}, wear due to the mechanical abrasion is predominant and the second term in Eq. 2-5 and Eq. 2-6 approaches zero. On the other hand, when the temperature is higher than T_{act}, the tool wear rate is mainly due to temperature the first term of Eq. 2-5 and Eq. 2-6 was considered as zero. In the original work done by Takeyama and Murata, temperature was the only process variable required to be measured from the cutting process and it was obtained experimentally.

Mathew [1989] investigated the tool wear rate of carbide tools when machining mild steel and observed the effectiveness of the Takeyama's proposed diffusion equation in relating the tool wear to temperature.

Arsecularatne et al., [1996] investigated the effect of temperature on the tool life in oblique machining (turning) of mild steel using brazed-on tungsten carbide cutting tool. The investigation showed similar effect of temperature on tool life as was described in Takeyama's wear rate model. One decade later, Arsecularatne et al., [2006] extended his investigation and studies the influence of temperature on the wear rate of the cutting tools when machining mild steel with tungsten carbide The investigation showed that at low temperature abrasion was the dominant wear mechanism while at diffusion was the dominant wear mechanism at higher temperature. This agreed with observation of Takeyama and Murata's model.

Akazawa et al., [2009] proposed a combined abrasive and diffusive wear rate equation when machining medium carbon steel with P10 tool, as shown in Eq. 2-7:

$$dW/dt = Av_s\,(H_w/H_t) + Bv_s\,\exp(-C/T) \quad \text{Eq. 2-7}$$

The first part of the equation indicates wear rate due to abrasion, and the second part the wear rate due to diffusion. In Eq. 2-7, dW/dt is the rate of volume loss per unit contact area per unit time, v_s is the sliding velocity of the work material and T is the tool face temperature. A and B are the constants which depend on the cutting conditions and combination of work and tool materials. H_t, and workpiece, H_w are the hardness of tool and workpiece material respectively.

In Akazawa's equation the wear rate due to abrasion is similar to the abrasive wear rate proposed by Takeyama & Murata [Takeyama, 1963] except that the effect of relative hardness of the tool, H_t, and workpiece, H_w, has been included. Based on the experiments in Akazawa's study, the hardness of workpiece material, H_w, was observed to be decreased exponentially by the temperature increase. This relationship has been shown in Eq. 2-8 in which C_1 and C_2 are the material constants and T is the temperature.

$H_w = C_1 exp(-C_2 T)$	Eq. 2-8

In Akazawa's study, the hardness of tool material was observed to be decreased linearly by the temperature increase. This relationship has been shown in Eq. 2-9 in which C_3 and C_4 are the material constants and T is the temperature.

$H_t = -C_3 T + C_4$	Eq. 2-9

It should be noted that, while not included in the original model, Takeyama & Murata [Takeyama, 1963] discussed the importance of including the effect of temperature on the hardness of both tool and work when estimating the abrasive wear. Takeyama & Murata believed that the higher temperature will soften the tool and also reduces the abrasiveness of hard inclusions in the work material. The amount of abrasive wear is dependent on the relative hardness between the tool and work materials. In Eq. 2-7, the constant A is the coefficient of abrasive wear and dependent on the rate of hard inclusions in work material. Similar to the Takeyama & Morata model, Akazawa considered the diffusive wear as a rate process and according to the Arrhenius law dependent on temperature.

2.3.4 Usui wear rate model

Usui et al. [Usui, 1984], developed an empirical equation for estimating the crater and flank wear rate when turning mild carbon steel with uncoated carbide, P20. Eq. 2-10 details the Usui's wear rate relations.

$dW/dt = A\sigma_n v_s \exp(-B/T)$ ………………………………………………………	Eq. 2-10

In Eq. 2-10, dW/dt is the rate of volume loss per unit contact area per unit time, σ_n and T are the normal stress and temperature on the tool face respectively while v_s is the sliding velocity of the work material. *A* and *B* are the constants which depend on the cutting conditions and combination of work and tool materials.

Usui's equation was developed by modifying the terms in Shaw and Dirke's model [Shaw, 1956, Usui, 1978a, 1978b], which was proposed based on the Archard [Archard, 1953] type model for adhesive wear, as shown in Eq. 2-11:

$dW = A_r\,(c/b)\,Z\,dL$……………………………………………………….	Eq. 2-11

In Eq. 2-11, dW is the rate of volume loss in the sliding distance dL, A_r is the real area of contact between the bodies, c is the height of the postulated plate like wear particle, b is the mean spacing of the asperities, and Z is the probability of producing a wear particle per asperity encounter. In Eq. 2-11 Usui replaced the real area of contact, A_r, with the ratio of the normal stress and the hardness of asperity junctions, σ_n/H. The hardness was related to the temperature as detailed in Eq. 2-12:

$H=A_1 exp(A_2/T)$……………………………………………………….	Eq. 2-12

where A_1 and A_2 were constants and depending on the material combinations. The probability parameter was also expressed based on Arrhenius law, as shown in Eq. 2-13:

$Z=B_1 exp(-\Delta E/\lambda T)$……………………………………………………….	Eq. 2-13

where B_1 was a constant depending on material type, λ was the Boltzmann's constant, and ΔE was the activation energy of thermally activate rate process.

Tool wear investigations by Kitagawa [1988, 1989] showed that both flank and crater wear can be predicted by Usui's equation when turning carbon steels (0.15-0.46% C) with uncoated carbide tools.

Zhao et al., [2002] extended Usui's model by including the effect of tool thermal softening on the wear rate and proposed an equation for relationship between tool hardness and cutting temperature. Results showed well agreement between the predicted wear and experimental data of turning annealed AISI4142 steel using steel grade carbide tool.

Wanigarathne et al. [2005] investigated the effect of temperature on the tool wear progression when machining mild steel with coated tungsten carbide (TiN/TiCN/TiC) grooved tools. The results showed the similar relationship between temperature and wear rate as it was proposed by Usui.

Combining the Takeyama and Usui equations, Attanasio proposed a coupled abrasive-diffusive model for estimating the crater and flank wear rates of P40 uncoated carbides in turning AISI 1045, [Attanasio, 2010, 2011]. Based on their approach, in the regions where temperature is lower than the activation temperature of the diffusion, T_{act} the dominant wear mechanism is abrasion and wear rate would be calculated only based on Usui's equation, as shown in Eq. 2-14 which is the same as Eq. 2-10. On the other hand, in the regions where temperature is higher than the activation temperature, the combination of Usui and Takeyama& Murata's equations would be used for wear rate estimation, as shown in Eq. 2-15.

$$dW/dt = dW_a/dt = A \sigma_n v_s \exp(-B/T) \ldots\ldots\ldots\ldots\ldots\ldots\ldots\ldots T \le T_{act} \qquad \text{Eq. 2-14}$$

$$dW/dt = dW_a/dt + dW_d/dt = A \sigma_n v_s \exp(-B/T) + D \exp(+E/RT) \ldots\ldots\ldots T > T_{act} \qquad \text{Eq. 2-15}$$

2.4 Tool Wear Predictions using Finite Element Methods and Empirical Models

In recent years with the improvements in computational capabilities, employing the finite element (FE) method to simulate the tool wear has been increased. By employing FE as a solid mechanics technique to simulate the mechanical and thermal fields or distributions required by empirical wear rate models, researchers have attempted to develop physics-based methodologies for two dimensional and three-dimensional tool wear predictions. Table 2-3 lists the selected publications on this topic and indicates the machining process, tool and workpiece material combination, and the type of tool wear that was predicted. With reference to

Reference	Machining Process	Workpiece/Tool Material	Tool Wear Type
[Malakizadi, 2020]	Turning	(C50 steel/uncoated cemented carbide; WC-10% Co)	Flank wear
[Wang, 2019]	Turning	(Ti6Al4V/uncoated cemented carbide)	Crater wear
[Xiang, 2018]	Drilling	(SiCp/Al Composites/ diamond)	Flank wear
[Binder, 2017]	Turning	AISI 1045/uncoated and coated cemented carbide	Flank and crater wear
[Malakizadi, 2016]	Turning	(Case hardened steel/cemented carbide)	Flank wear
[Lotfi, 2016]	Turning	IN625/ceramic and coated tungsten carbide	Flank and crater wear
[Thepsonthi, 2015]	Milling	(Ti6Al4V/uncoated cemented carbide)	Flank wear
[Binder, 2015]	Turning	AISI 1045/uncoated and coated cemented carbide	Flank and crater wear
[Schulze, 2011, Zanger, 2013]	Turning	(Ti6Al4V/uncoated cemented carbide)	Flank wear
[Thepsonthi, 2013]	Milling	(Ti6Al4V/coated CBN)	Flank wear
[Yang, 2013]	Turning	(Ti6Al4V/uncoated cemented carbide)	Flank and crater wear
[Salvatore, 2013]	Turning	42CD4 steel/uncoated tungsten carbide	Flank and crater wear
[Malakizadi, 2013]	Turning	Aged IN718/ uncoated cemented carbide	Flank wear
Haddag, 2013	Turning	AISI 1045/uncoated cemented carbide	Flank and crater wear
[Attanasio, 2009, 2010, 2011]	Turning	AISI 1045/uncoated cemented carbide	Flank and crater wear
[Özel, 2010]	Turning	(Ti6Al4V/multi-layer coated cemented carbide)	Flank and crater wear
[Lorentzon, 2008]	Turning	Forged IN718/ uncoated cemented carbide	Flank and crater wear
[Attanasio, 2008a, 2008b]	Turning	AISI 1045/uncoated cemented carbide	Crater wear
[Filice, 2007a]	Turning	AISI 1020/uncoated cemented carbide	Flank and crater wear
[Xie, 2004, 2005]	Turning	AISI 1045/uncoated tungsten carbide	Flank and crater wear
[Yen, 2004c]	Turning	AISI 1045/uncoated tungsten carbide	Flank and crater wear

Table 2-3. Selected publications on employing FE to simulate tool wear in machining.

Table 2-3, most of the published work focused on orthogonal turning operating with AISI 1045 steel or Ti6Al4V. Majority of the research could predict flank wear. In majority of wear prediction attempts, the cutting process with defined tool edge geometry was simulated with FE until the mechanical and thermal loadings on the cutting tool reached steady state. Depending on the wear rate equation the required variables on interfacial nodes such as temperature, contact pressure, and sliding velocity were determined from the simulation. Following on from here, the wear rate at each node and the interfacial nodal displacements were calculated at a specified time increment. Finally, the tool geometry was updated, and the length of flank wear, *VB*, or depth of crater, *KT*, was determined. If the tool wear criterion has not been reached, the updated tool geometry was inserted back in the cutting simulation and same cycle was continued until the wear criterion was achieved. The flow chart of this methodology is shown in Figure 2-10.

Based on this approach, Binder, et al. [2017] predicted flank and crater wear of carbide tool in machining AISI 1045 with uncoated and coated carbides. Lotfi, et al. [2016] estimated the wear formation on the cutting edge of ceramic and coated carbide tools when turning Inconel 625 in 3 dimensional configurations. Malakizadi, et al. [2016] predicted flank wear of the uncoated cemented carbide tools in turning 20MnCrS5 case hardened steel in 3 dimensional configurations Zanger and Schulze [Zanger, 2013, Schulze, 2011] predicted flank wear when machining titanium alloy Ti-6Al-4V with uncoated tungsten carbides. Malakizadi et al. [2013] developed a 3D FE based methodology for prediction of flank wear when turning alloy 718 with uncoated tungsten carbide. Haddag and Nouari [2013] predicted flank and crater wear in dry cutting of AISI 1045 with uncoated carbides. In this study the influential parameters on tool wear were extracted from stabilized 3D finite element models. Attanasio, et al. [2010, 2011] predicted three-dimensional crater and flank wear when turning AISI 1045 with uncoated carbide. Filice, et al. [2007b] predicted the two-dimensional evolution of flank and

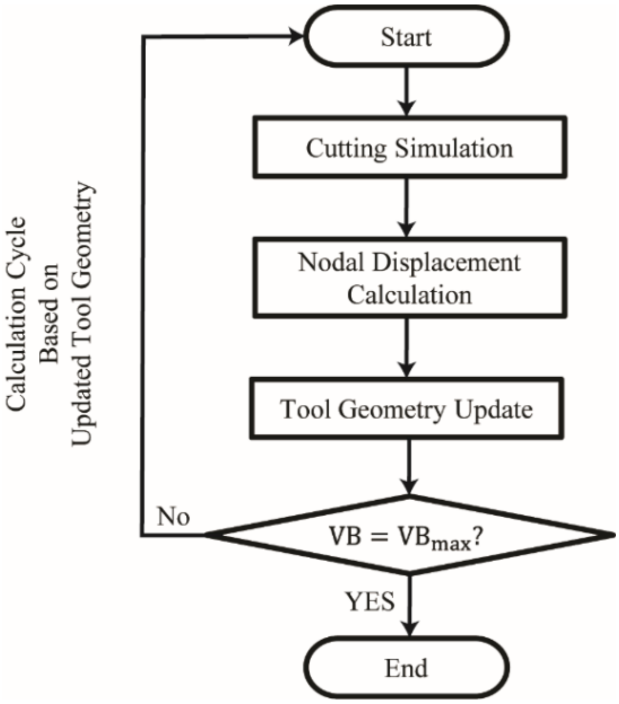

Figure 2-10. Regular approach in finite element based prediction of tool wear.

crater wear in orthogonal cutting of AISI 1020 with uncoated carbide. Yen, et al. [2004c] and Xie, et al. [2005] modeled the two-dimensional progression of both flank and crater wear in orthogonal turning of AISI 1045 with uncoated tungsten carbide. In this approach, the efficiency of the FE in simulating the process variables and the selection and calibration of wear rate models are the key factors for achieving an accurate prediction.

2.4.1 Finite element simulation of cutting process

Majority of the published FE based tool wear prediction provided limited information regarding the accuracy of finite element techniques in simulating the mechanical and thermal process variables under the worn cutting edge geometries. Yen, et al. [2004c], Xie, et al. [2004] and Zanger and Schulze [2013] considered the accuracy of the simulated process variables only under the sharp cutting edge. Binder et al. [2017] and Attanasio et al. [2010, 2011] and Filice, et al. [2007b] did not discuss the accuracy of the simulated mechanical and thermal loadings in cutting with sharp and worn cutting edge geometries.

2.4.2 Calibration of empirical wear rate models

In general, the wear rate models should be calibrated based on the unique combination of tool and workpiece materials and for specific cutting conditions. Calibration refers to the process of determining the model's constants which would result in the minimum difference between the model output and the those acquired experimentally. It has been realized that in previous wear estimation attempts, the calibration frameworks have not been clearly set in terms of the procedure for data collection and the optimum number of the experiments/simulations performed for data collection.

Lotfi et al. [2016] and Filice et al. [2007b] used eleven and nine cutting conditions to calibrate the models respectively. While the predicted tool wear was in good agreement with experiment, the large number of cutting experiments seemed to be excessive and time intensive. On the other hand, Malakizadi et al. [2013] and Attanasio et al. [2010] employed one cutting condition to calibrate the wear rate model. Unfortunately, the wear rate predictions were different from experiment especially when there was a large difference between the cutting parameters and those used during calibration. Other published research did not elaborate on the cutting conditions and number of experiments performed during calibration, [Binder, 2017, Haddag, 2013, Xie, 2005, Yen 2004c, Zanger, 2013] did not calibrate the wear rate models for specific cutting conditions and tool/workpiece material combinations but rather used the calibration constants from literature [Kitagawa, 1988, 1989]. Table 2-4 lists these calibration details.

2.4.3 Tool life prediction

Regardless of the wear prediction accuracy in the previous attempts, two key factors have been identified. The first factor is the nodal wear rate and displacement calculation. Calculating the

Reference	Was the calibration procedure explained?	Was calibration performed?	Number of cutting conditions used for calibration
[Malakizadi, 2020]	No	Yes	1
[Binder, 2017]	Yes	Yes	Not Specified
[Lotfi, 2016]	Yes	Yes	15
[Malakizadi, 2016]	Yes	Yes	4
[Thepsonthi, 2015]	No	No	Not Specified
[Zanger, 2013]	Yes	Yes	Not Specified
[Haddag, 2013]	No	No	Not specified
[Malakizadi, 2013]	Yes	Yes	1
[Özel, 2010]	No	No	Not specified
[Attanasio, 2010]	No	Yes	1
[Filice, 2007b]	Yes	Yes	9
[Xie, 2005]	No	No	Not specified
[Yen, 2004c]	No	No	Not specified

Table 2-4. Summary of calibration details.

displacement rate of each node along the tool-workpiece interface highly relies on the state of contact simulation, which is very complex in metal cutting. The complexity generally results in uncertainties in the simulated process variables such as sliding velocity which could lead to errors in nodal displacement calculation and consequently irregularity on updated worn geometry. Xie, et al. [2005] reported the poor mesh control at the interfaces of contact which resulted in contact noise and inaccurate prediction of process variables such as heat flux, temperature, and contact pressure. To overcome this issue, Hosseinkhani and Ng [2015] and Malakizadi et al. [2016] developed methodologies to determine the rate of tool material loss on the flank face from average values of interface temperature and contact pressure instead of calculating the individual nodal displacement rates.

The other factor is the iterative nature of tool wear prediction procedure which makes the overall computational time long and expensive. When using the approach detailed in Figure 2-10, a simulated cutting time increment should be defined based on which nodal displacements are calculated and cutting edge geometry is updated. Generally, the magnitude of simulated cutting time increment with respect to the total cutting time specifies the number of iterations required until the wear criterion is reached. Based on the selected time increment, Filice et al. [2007b], Attanasio et al. [2010], and Malakizadi et al. [2013] went through 10, 16, and 8 iterations, respectively. The iterative approach of Figure 2-10 is referred to as the series since the start of each iteration depends on the completeness of the previous iteration.

2.4.4 Tool wear estimation in the initial break-in cutting period

The Takeyama & Murata and Usui as well as Akazawa and Attanasio equations have been mainly developed based on the wear mechanisms in the steady-state wear period. However, the condition in the initial break-in cutting period is different. According to Shaw [Shaw, 2005], the trend observed in tool wear progression during machining is very similar to the wear rate of a loaded conical slider on a hard disk, as shown in Table 2-5 and Figure 2-11. Based on Shaw’s observations the wear rate of the loaded slider was high at the beginning of the test as $P/A > H/3$ because A was approximately zero. This is similar to the initial break-in period in cutting. P, A, and H were the normal load, apparent area of contact, and the hardness of the slider pin respectively. $H/3$ was the uniaxial flow stress of the pin. As the tip of the pin was worn due to the initial high pressure and apparent contact area increased and reached to the first critical value A_1, the wear rate dropped because $P/A < H/3$. This is similar to the steady state wear period in cutting. As the apparent area of contact reached the second critical value

Region I	$P/A > H/3$	Initial break-in period	Initial rapid wear rate
Region II	$P/A < H/3$	Steady-state wear period	Uniform wear rate
Region III	$P/A > H/3$	Failure period	Accelerated wear rate

Table 2-5. Three regions due to variation of wear volume with respect to time in a loaded conical slider.

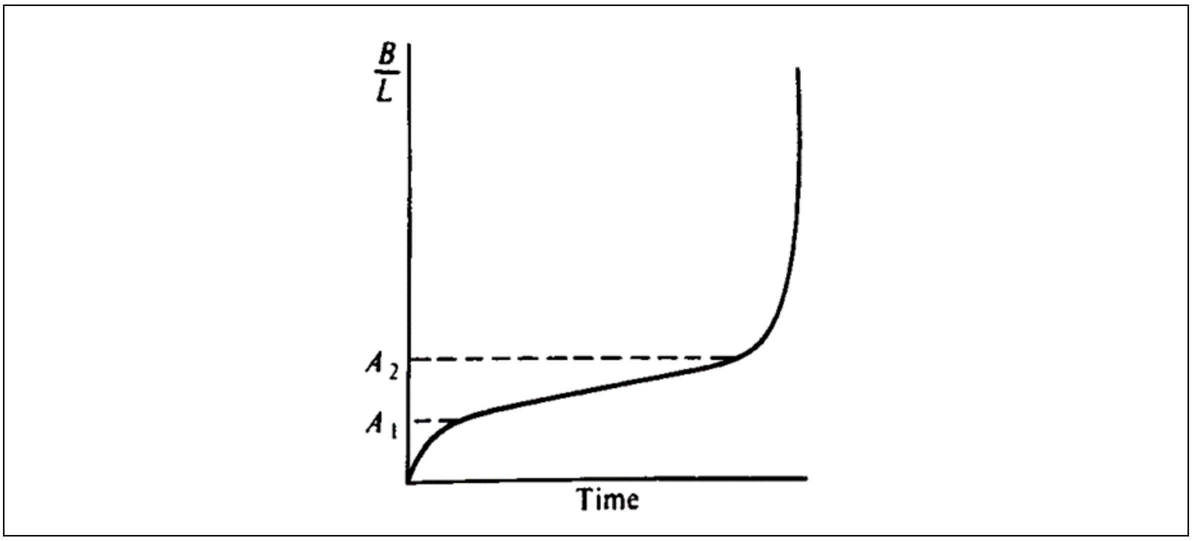

Figure 2-11. Variation of wear volume with respect to time in a loaded conical slider.

A_2, the temperature increased to the point of thermal softening, consequently decreased the H, and $P/A > H/3$ occurred again. This is similar to the failure period in cutting. The tool wear graph in Figure 2-6 can be also represented by Table 2-5.

Due to these differences in wear rate mechanisms as the contact area and temperature increased, it is not obvious that the wear mechanisms based on which the Takeyama and Murata, Usui and other described equations have been developed are representing the wear situations in the initial break-in cutting period.

Regardless of the accuracy of the reviewed tool wear prediction studies in section 1.4, different views existed toward the capability of the empirical equations in estimating wear rate in the initial break-in cutting period. By referring to the Usui’s equation as an expression developed based on the principles of adhesive wear, which may be better describing the flank wear at higher temperature during the cut, Yen et al. [2004c] started his prediction procedure on a tool with a pre-defined 60 µm flank wear. Filice et al., [2007b], also started the prediction on a tool with an initial flank wear of 50 µm by referring to Takeyama & Murata's equation as an expression which is unable to capture the effect of initial sudden wear. On the other hand, [Attanasio, 2010, Haddag, 2013, Malakizadi, 2013, Xie, 2005, Zanger, 2013] used the empirical equation from the beginning of the process by assuming that they are able to capture the wear rate throughout the whole process.

It should be noted that the importance of the successful estimation of wear rate in the initial period has its direct influence on the tool cutting edge design as well as substantial influence on the overall prediction accuracy of the model.

2.5 Thesis Objectives and Outline

2.5.1 Thesis objectives

1. The first objective is to evaluate the results of mechanical and thermal process variables from FE simulation of the cutting process based on sharp (new) and worn tool edge geometries. This objective refers to the fact that an important part of the finite element (FE) based tool wear prediction process refers to the ability of the FE models to simulate the mechanical and thermal process variables in the cutting zone effectively.
2. The second objective is to define the calibration framework for the empirical wear rate models which have been widely used in the tool wear prediction studies. This objective refers to the fact that the other important part of the finite element (FE) based tool wear prediction process refers to the selection and calibration of the empirical wear rate models which relate the tool wear rate to the wear mechanisms in the cutting zone.

3. The third objective is to develop a methodology for tool life prediction using a hybrid finite element simulation coupled with calibrated empirical wear rate models. This methodology should minimize the challenges involved in the nodal displacement calculations and should reduce the computational time when compared to nodal movement technique.

2.5.2 Thesis outline

Chapter three reviews the principles of finite element simulation of the cutting process. In this chapter, different techniques for simulating the cutting process are introduced and the most efficient technique for the purpose of current research is selected. The material model, the contact algorithm and the boundary conditions are also reviewed.

In Chapter four, the viability of the most widely used frictional models for simulating the contact condition at the tool-chip interface has been evaluated. In addition, the performance of three different FE commercial software, Deform 2D, Abaqus/Explicit and AdvantEdge, under nearly similar thermal and frictional boundary conditions has been investigated. In order to develop a systematic approach to evaluate the performance of friction models, the optimum sets of friction coefficients were initially determined, where the criterion was set as the minimum average prediction error of all the simulated responses including the cutting force, feed force, chip thickness and the contact length. The results indicated nearly a similar range of minimum average error for all the adopted friction models, independent of FE commercial code used for simulation of cutting process. The reasons for such behaviour were discussed critically, and the most viable models to represent the contact condition at the tool-chip interface were identified. This part of the thesis has been published in Journal of Advanced Manufacturing Technology in 2016.

Chapter five investigates the mechanical and thermal process variables when simulating the cutting process with sharp (new) and worn edge geometries. Cutting experiments are performed in specific ranges of cutting speed and feed rate. Tool cutting edge is analyzed in different steps of the process and worn edge geometries are obtained. The worn edge geometries are then used to build the Arbitrary Lagrangian - Eulerian FE cutting models in ABAQUS/Explicit. To validate the models, the simulated results of the machining forces and temperature were compared to the experiment. To further validate the models, the obtained temperature, contact pressure and sliding velocity were used as input in the Usui’s wear rate model to estimate the rate of flank wear. This chapter is the reproduction of the content that has been submitted for publication to the International Journal of Advanced Manufacturing Technology.

Chapter six focuses on the calibration of the empirical models which relate the tool wear rate to the wear mechanisms in the cutting zone. This chapter defines the calibration framework for the Takeyama & Murata, Usui, Attanasio, and Akazawa models based on a hybrid simulation/experimental approach with emphasis on the flank wear. The framework specifies the required data to be collected for efficient calibration of wear rate models. This ultimately will assist in the selection of appropriate wear rate model. The framework also suggests the optimum number of experiments and simulations to be performed for data collection which will prevent the excessive and redundant experiments and simulations. This chapter is the reproduction of the paper that has been published in International Journal of Advanced Manufacturing Technologies in 2018.

Chapter seven proposes a unique hybrid experimental / numerical methodology for tool life and investigates its feasibility. The research outcomes from chapter 3 and 4 have been used as the inputs in the proposed methodology. This methodology also minimizes the challenges involved in the nodal displacement calculations and reduces the computational time when compared to nodal movement technique. Chapter seven also investigates the capability of the existing empirical wear rate models in predicting the wear rate in the initial cutting period. Alternatively, based on the experimentally obtained wear rates and simulated stresses, a new equation is proposed for wear rate prediction in the initial cutting period and its feasibility is investigated. This chapter is the reproduction of the paper that has been published in the Journal of Manufacturing and Materials Processing in 2020.

Chapter eight concludes the outcomes of this thesis and explains the limitations of the proposed tool wear/life prediction methodology. Chapter eight also provides insight for the future work for improving and advancing this methodology.

2.5.3 Contributions to articles

Chapter four to seven of this thesis are reproductions of published articles in the top journals in the fields of advanced manufacturing.

Chapter four represent the research works that were performed in collaboration with other researchers during the initial stage of the current thesis. In these chapters, the author of the current thesis collaborated mainly on assembling the finite element models, running the simulations in ABAQUS/CAE and data analysis.

With respect to chapters five to seven, which are the core of the current thesis, all the tests measurements and computations are original research results and performed at McMaster University. The original idea of employing finite element simulation for tool wear prediction came from Dr. Ng. The methodology of how to combine the advantages of finite element simulation and empirical tool wear rate models was developed over numerous in-person meetings and discussion between myself and Dr. Ng. I wrote the first draft of the papers in chapter five, six and seven and prepared all the figures and graphs. They were then modified in accordance with Dr. Ng’s instruction.

3 FINITE ELEMENT SIMULATION OF CUTTING PROCESS

In this chapter, the different techniques used in simulating the cutting process are reviewed and the fundamentals of assembling an ALE cutting model which has been used throughout this thesis are explained.

3.1 Introduction

In recent years with the rapid advancement in computational capabilities, employing the finite element (FE) models for simulating the cutting process has been increased [Denkena, 2012, Kalhori, 2001, Li, 2002, Movahhedy, 2000, Ng, 2002b, Sanchez, 2011, Simoneau, 2006, 2007] (Ng, et al., 2002). Finite element models are physics-based models in contrast to experimentally oriented empirical models. Also, in contrast to analytical models, they keep the history of the cutting process required for the analysis of sequential cuts. Furthermore, once a finite element cutting model is validated, it could be used for analysis of the stresses, plastic strain, sliding velocity, and temperature which are difficult or impossible to analyze using experimental and even analytical approaches.

3.2 Finite Element Techniques

Three type of finite element techniques are commonly used in the simulation of cutting process. These are known as Lagrangian, Eulerian and Arbitrary Lagrangian-Eulerian techniques [Halim 2008]. Each one of these techniques has its advantages and disadvantages which are being reviewed in the following sections.

3.2.1 Lagrangian technique

In Lagrangian technique the FE mesh grids are attached to the material and are displaced due to deformation of material. This has been illustrated in Figure 3-1. In Figure 3-1 (a) both material and mesh grids are in the initial state. In Figure 3-1 (b) material and mesh grids are in the deformed and displaced state where the mesh grids were displaced by the deformation of material.

When cutting process is simulation based on the Lagrangian technique, the chip and its contact length on the tool is formed based on the natural deformation of material being cut. Based on this advantage the Lagrangian technique has been successfully used for simulating the 2-dimaneional continuous and segmental chip formations [Ng, 2002a], 3-dimensional continuous chip formation [Ng, 2002b] as well as the chip formation that includes the microstructure of workpiece material [Simoneau, 2006]. However, there are two main

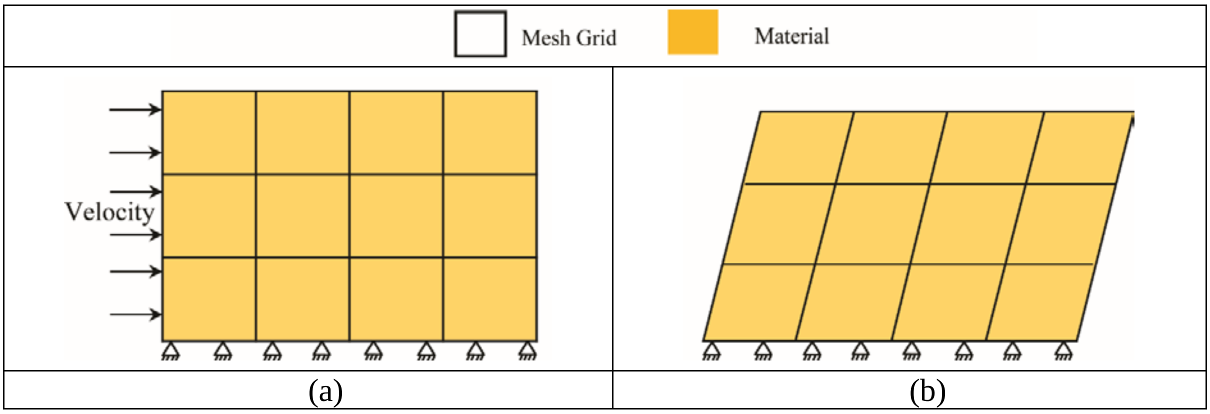

Figure 3-1. Schematic of mesh grids and material in un-deformed and deformed state in Lagrangian simulation.

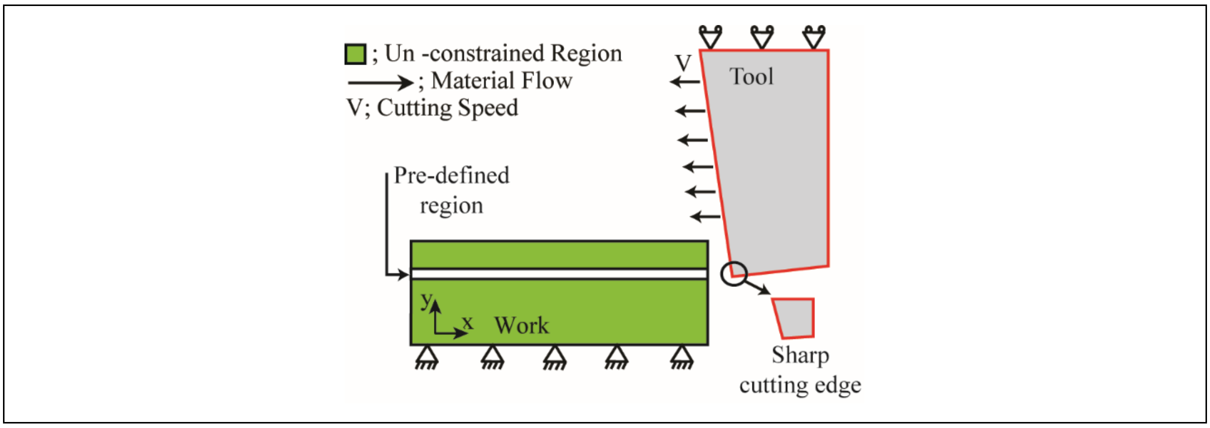

Figure 3-2. Schematic of separation zone in Lagrangian simulation.

disadvantages associated with the Lagrangian technique. When simulating the cutting process based on this technique, a damage criterion needs to be used to define the separation of chip from workpiece material as tool cuts thorough the workpiece, as shown in Figure 3-2. A detailed study by Huang and Black [1996] on different types of damage or separation criteria has shown that neither geometrical nor physical criterion can simulate the separation correctly. Also, because of the need to define a damage criterion, the cutting tool should be considered as perfectly sharp in the simulation, which is considered as another disadvantage. Assuming a sharp cutting tool and neglecting the cutting edge geometry affects the simulation of process variables such as the stagnation zone and plowing as well as the feed force [Fang, 2007, Halim, 2008, Joyot, 1998, Komvopoulos, 1991].

3.2.2 Eulerian formulation

In Eulerian technique the FE mesh grids are fixed spatially, and material flows through them and they are not displaced by the deformation of material. This has been illustrated in Figure 3-3. In Figure 3-3 (a) both material and mesh grids are in the initial state. In Figure 3-3 (b) material and mesh grids are in the deformed state where the mesh grids were fixed and have not been displaced by the deformation of material.

Figure 3-4 shows the schematics of chip formation in Eulerian simulation. When cutting process is simulation based on the Eulerian technique, because the mesh grids are not attached to the material, chip does not form based on the natural deformation of the material. Therefore, there is no need for a damage or separation criterion to be defined. Since there is not separation line, the cutting edge geometry can be included in the simulation [Rczy, 2004]. However, the prior knowledge of chip geometry and tool-chip contact length is required to initiate the simulation. Also in the Eulerian technique the elastic properties of the workpiece material is ignored and its being considered as viscoplastic. This limits the capability of this technique in

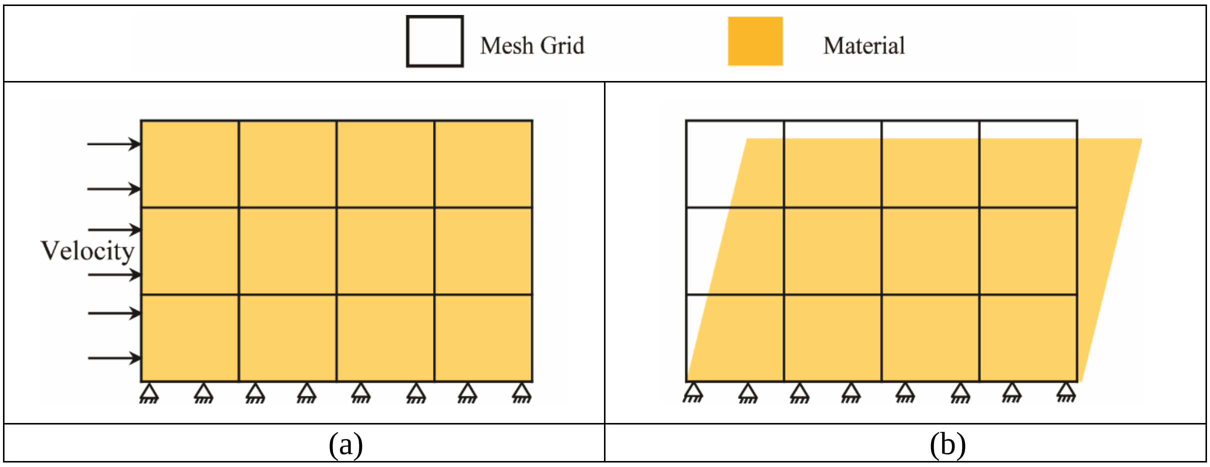

(a) (b)

Figure 3-3. Schematic of mesh grids and material in un-deformed and deformed state in Eulerian simulation.

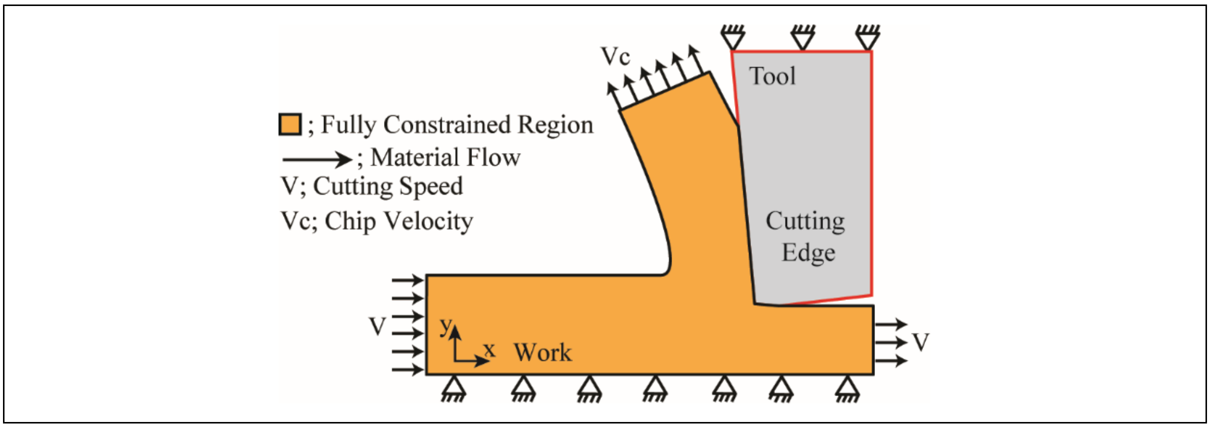

Figure 3-4. Schematic of chip formation in Eulerian simulation.

prediction of residual stresses in the machined surface [Halim, 2008]. Furthermore, the workpiece material should be considered as homogenous, and the effect of its microstructure cannot be included.

3.2.3 Arbitrary Lagrangian-Eulerian (ALE) formulation

In ALE technique the advantages of both Lagrangian and Eulerian techniques are combined. Figure 3-5 shows the schematics of an ALE cutting model. In a model built based on the ALE technique, the workpiece mesh elements in the region in front of the tool cutting edge are fixed spatially, as in the Eulerian technique. As the result, no damage criterion for the chip separation is required and cutting edge geometry can be included in the simulation. Also, since the material flows through these mesh elements, the severe deformation of material in

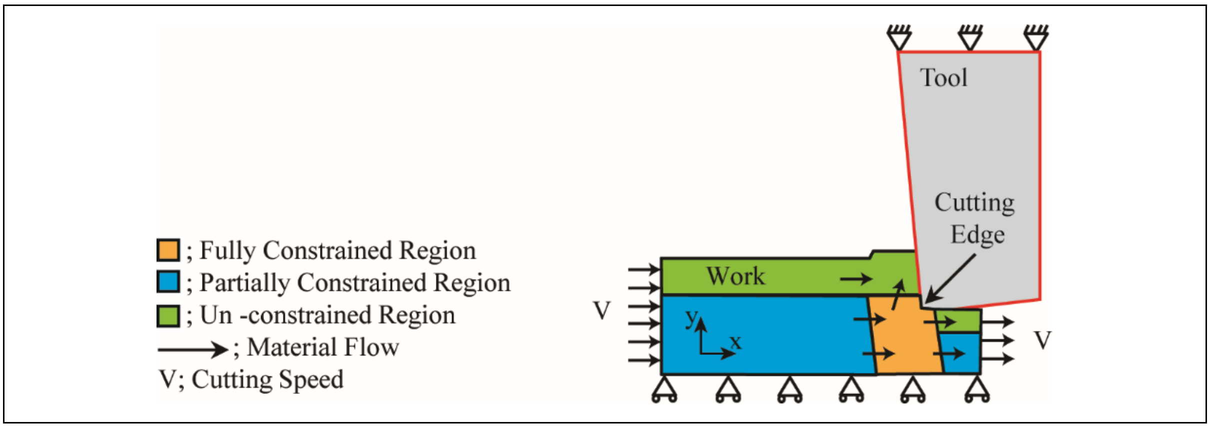

Figure 3-5. Schematic of mesh grids and material in un-deformed and deformed state in the ALE simulation.

front of the tool tip is minimized and does not lead to the severe mesh element distortion. In the ALE technique, the workpiece mesh elements in the region which forms the chip and those hich form the machined surface were not fixed and were attached to the workpiece material, as in the Lagrangian technique. Therefore, the final chip geometry and the tool-chip contact length would be formed based on the natural deformation of the material [Nasr, 2007].

ALE cutting models have been used for prediction of residual stresses in the machined surface [Ziada, 2013], simulation of process variables based on different cutting edge geometries [Nasr, 2007] and modelling of temperature [Coelho, 2007]. Also with the advantages of the ALE technique, in terms of including the tool cutting edge geometry in the simulations, the feed forces can be predicted more efficiently when compared to the Lagrangian technique. However, the predicted feed forces have been reported to still be 30-70% lower than the feed forces obtained experimentally [Arrazola, 2008]. It should be mentioned that so far the ALE technique has been used successfully in the orthogonal cutting models with continuous chip formation where the workpiece material was considered homogenous.

Choosing one of the mentioned techniques for simulating a machining process really depends on the available input data and the required output information.

All the FE models in the current research are based on the ALE technique. The ALE technique was chosen over Lagrangian because including the new and worn tool cutting edge geometries are required to be employed in the simulations. The lack of data on the chip separation criteria and the large mesh distortion around the tool cutting edge were other factors for preferring the ALE technique over Lagrangian. The lack of information for the assumption of initial chip geometry was the main reason for preferring the ALE technique over Eulerian.

3.3 Material Model

One of the main challenges in finite element simulating of the metal cutting process is associated with employing the constitutive model that effectively simulates the material behaviour in this complex process. In metal cutting, workpiece material experiences large deformation at very high speed in a small localized region [Jaspers, 2002]. Therefore, strain rates as high as 10^5 1/s could result in high temperature change rate. Table 3-1 shows the strain and strain rate in metal cutting compared to some other manufacturing processes [Ziada, 2013].

Three material models that have been used in the simulation of metal cutting are the Johnson-Cook [Johnson, 1983], Oxley [1997] and Zerilli and Armstrong [Zerilli, 1987] models. The Johnson-Cook model has been widely used in the finite element simulation of metal cutting. In the present study, the Johnson-Cook model has been used to simulate the plastic response of the workpiece material.

The Johnson-Cook constitutive model [Johnson, 1983] is a type of Mises plasticity model and is suitable for applications where large nonlinearities are involved and large plastic deformation of a material is a function of strain-rate and temperature. The Johnson-Cook constitutive model relates three uncoupled terms of strain hardening, strain-rate sensitivity, and thermal softening due to temperature to the plastic deformation of the workpiece material, as shown in Eq. 3-1:

$$\sigma=\left(A+B\varepsilon_{pl}^{n}\right)\left[1+C\ln\left(\dot{\varepsilon}_{pl}/\dot{\varepsilon}_{0}\right)\right]\left\{1-\left[\left(T-T_{ref}\right)/\left(T_{melt}-T_{ref}\right)\right]^{m}\right\} \tag*{Eq. 3-1}$$

Process	Typical Strain	Typical Strain Rate (s^{-1})
Sheet Metal Forming	2-5	1 - 10^2
Rolling/Forging	0.1 – 0.5	1 - 10^3
Extrusion	0.1 – 0.5	10^{-1} – 10^2
Metal Cutting	1 - 10	10^3 - 10^6

Table 3-1. Comparing the strain and strain rate in different manufacturing processes [Ziada, 2013]

The first term in the Johnson-Cook model corresponds to the strain hardening effect. In this term “ε_{pl}” is the equivalent plastic strain and “A”, “B” and “n” are the material constants and represent the initial yield strength, strain hardening coefficient and strain hardening exponent. The second term corresponds to the strain rate sensitivity. In this term “$\dot{\varepsilon}_{pl}$” and “$\dot{\varepsilon}_0$” are the equivalent plastic strain rate and the initial or reference plastic strain rate. “C” is the strain rate coefficient. The third term corresponds to the thermal softening effect. In this term T is the current temperature of workpiece, T_{melt} is its melting temperature and “m” is the thermal softening coefficient. T_{ref} is the reference temperature that all the material constants used in the model are determined at this temperature.

3.4 Friction Model

In a simple description, friction is the resisting force one surface experiences when it slides over another surface [Shaw, 2005]. Coulomb friction law is the most well-known theory for describing the friction. Based on this theory, the friction force between the two contacting interfaces, in relative motion, is described in Eq. 3-2:

$$F=\mu N \qquad \text{Eq. 3-2}$$

where F is the friction force, N is the normal force at the interface and μ is the coefficient of friction. It should be mentioned that the Coulomb friction law was obtained under the light normal loading condition where the real area of contact, A_r, is much smaller than the apparent area of contact, A, as shown in Figure 3-6. In this situation the coefficient of friction is constant for a pair of material and is independent from the normal load, contact area and sliding velocity.

According to Shaw [2005], friction between solid bodies can be divided into three regimes as the normal stress, σ_n, increases and the real area of contact becomes closer to the apparent area of contact, as shown in Figure 3-7. Regime I referred to the conditions where normal stress is low and Coulomb friction law holds, $\mu=\tau/\sigma_n$ is constant. Regime III is referred to the conditions where normal stress is very high and apparent and real area of contacts are equal. In these situations, plastic shear deformation happens within the solid body of the softer material and the shear stress is independent from the normal stress. Regime II is considered as the transition between Regime I and III where $\mu=\tau/\sigma_n$ is not constant but decreases with the increase in normal load.

In metal cutting the contacting interfaces of tool and workpiece material undergo extreme condition. High sliding velocity, high normal load as well as high temperature are the three factors associated with extreme contact condition in the cutting zone. According to Shaw [2005], all the three mentioned regimes in Figure 3-7 exist at the different regions along the interfaces of contact in the cutting zone.

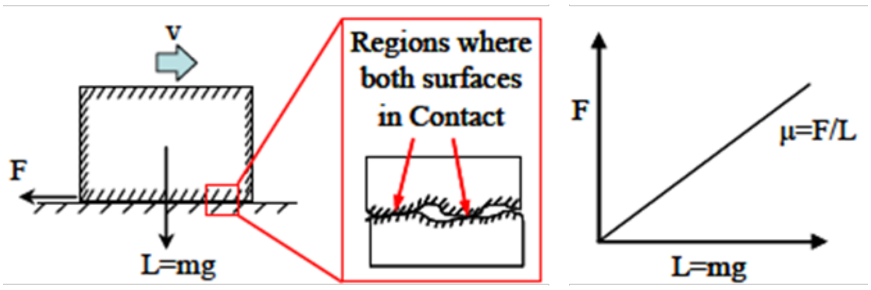

Figure 3-6. Contact condition for the original Coulomb friction law [Halim, 2008].

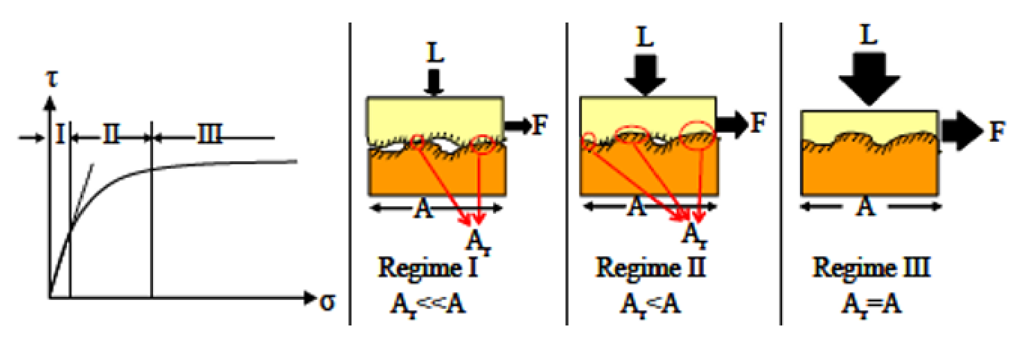

Figure 3-7. Shaw's description of three regimes of solid friction [Halim, 2008].

Experimental studies have indicated there are two distinct regions at the interface of tool and chip which are known as sticking and sliding regions [Malakizadi, 2015]. Based on these observations on the region close to the tool cutting edge where the normal stress is extremely high, workpiece or chip material may stick to the tool. As the normal stress decreases on the tool rake face, the chip material starts sliding until it leaves the tool surface. The most commonly accepted theory of contact and frictional behaviour along the tool-chip interface, in an orthogonal cutting process, has been proposed by Zorev [1963], as shown in Figure 3-8. Based on Zorev's theory, the normal stress is at its maximum at the cutting edge and decreases exponentially along the contact length, l_c, and becomes zero as the chip leaves the interface. In terms of shear or frictional stress, the interface is divided into the sticking and sliding zones. Along the sticking zone, l_p, the frictional stress is at its maximum and is constant. Along the sliding region, the frictional stress is proportional to normal stress and gradually decreases and becomes zero as the chip leaves the interface.

One challenges in finite element simulation of the metal cutting is associated with employing the friction model that efficiently simulates the contact at the tool-chip and tool-workpiece interfaces in the cutting zone. In the following sections, some of the friction models

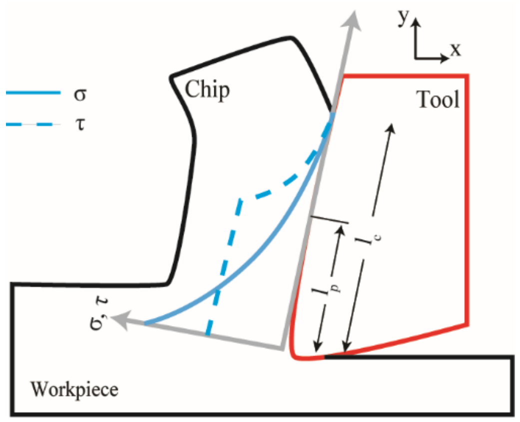

Figure 3-8. Distribution of normal and shear stresses along the tool-chip interface based on Zorev's theory [Zorev, 1963].

that have been commonly used in the finite element simulation of cutting process to model the frictional behaviour at the tool-chip interface are introduced.

3.4.1 Coulomb friction model.

In the Coulomb friction model the frictional stress on the contacting interfaces, τ, is proportional to the normal stress, σ, and coefficient of friction μ, as shown in Eq. 3-3:

$$\tau = \mu\sigma_n \qquad \text{Eq. 3-3}$$

3.4.2 Constant shear friction model

When reviewing the constant shear friction model, the shear friction on the tool-chip interface is proportional to the constant shear friction factor, m, and the shear flow stress of the workpiece material, k, as detailed in Eq. 3-4:

$$\tau = mk \qquad \text{Eq. 3-4}$$

3.4.3 Combined constant shear and coulomb friction model

The constant shear friction model is valid in the sticking region and the Coulomb friction model is valid in the sliding region, as shown in Eq. 3-5 (a) and 3-5 (b) respectively:

$\tau = mk$ *at sticking region*	Eq. 3-5 (a)
$\tau = \mu\sigma_n$ *at sliding region*	Eq. 3-5 (b)

3.4.4 Zorev's sticking – sliding model

With Zorev's model, the frictional stress is maximum and constant along the sticking region as shown in Eq. 3.6 (a). This frictional stress is equal to the shear flow stress of the workpiece material *k*, and is independent from the applied normal stress. Along the sliding region, the frictional stress is proportional to normal stress and the coefficient of friction:

$\tau = k$ *at sticking region*	Eq. 3-6 (a)
$\tau = \mu\sigma_n$ *at sliding region*	Eq. 3-6 (b)

Table 3-2 lists some of the finite element simulation studies of the cutting process based on different types of friction models used. Majority of the published work used Coulomb friction model. In addition to the models introduced above, there are other frictional model proposed such as the variable shear friction at the tool-chip interface by Usui and Shirikashi [1982] and the variable coefficient of friction along the tool-chip interface by Ozel et al., [2006], Arrozola et al. [2008], and Haglund et al. [2008].

A thorough study by Halim (Halim, 2008) on using different friction models in the simulation of metal cutting showed that regardless of using different models, the simulated results of the feed force are still under-estimating the experiment. In the context of present research, the interaction between the contacting surfaces has been modeled based on the

References	Friction Model
[Arrazola, 2008, Bil, 2004, Filice, 2007a, Haglund, 2008, Iqbal, 2007, Klock, 2001, Komvopoulos, 1991, Mamalis, 2001, Marusich, 2001, Sartkulvanich, 2005]	Coulomb Friction Model.
[Berhrens, 1999, Filice, 2007a, Iqbal, 2007, Özel, 2006, Sartkulvanich, 2006, Yen, 2004b]	Constant Shear Friction Model
[Filice, 2007a, Iqbal, 2007, Özel, 2006]	Combined Constant Shear and Coulomb Friction Model
[Filice, 2007a, Haglund, 2002, Özel, 2000, Shet, 2000, Shi, 2002, Shi 2004, Yang, 2002]	Zorev's Sticking – Sliding Model

Table 3-2. Finite element simulation studies of the cutting process based on different types of friction models.

Coulomb friction law in which the sticking and sliding conditions are the functions of normal and shear stresses. Figure 3-9 shows the principle of contact algorithm in the simulating software, ABAQUS, when the Coulomb friction model is used. Based on Figure 3-9, when the frictional stress is lower than the multiplication of normal stress and coefficient of friction, sticking occurs which has been indicated by the shaded region. When the frictional stress is larger than the multiplication of normal stress and coefficient of friction, sliding occurs which

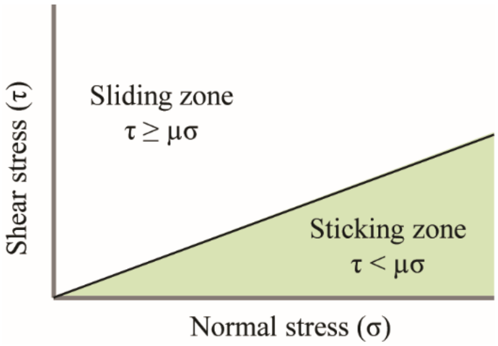

Figure 3-9. Illustration of sticking and sliding regions for Coulomb friction model in the simulation software, ABAQUS.

has been indicated by the un-shaded region.

Tribometers with pin on-rotating disk or ring systems has been one of the widely used approaches to determine the coefficient of friction to be used in the friction models. Based on this approach, the normal and tangential forces at the contact between pin and disk are recorded and based on the relation between the normal and tangential forces the coefficient of friction is determined. Various researchers have employed the pin-on-disk or ring systems with different setups with the objective to create a contact condition close to the extreme conditions in the cutting zone. In most cases the attempts have not been successful. The setup by Olsson et al. [1989] failed to establish the contract pressure that were observed in metal cutting. Grzesik et al. [2002] could not replicate the contact condition in terms of having the fresh workpiece surface at the interface of contact. Zemzemi et al. [2008] could not replicate the contact condition in terms of the chemical purity of the contact surface.

The COF used in the context of this thesis was based on the experimental study by Puls et al., [2012]. Puls et al. [2012], proposed a reverse orthogonal cutting configuration for determining the COF as a function of sliding velocity, as shown in Figure 3-10. In this configuration the workpiece was rotated in the opposite direction of the actual cutting process and clearance angle of the tool acted as a highly negative rake angle which caused severe plastic deformation of the workpiece material passing underneath. Therefore, the COF was determined as the ratio of tangential and normal forces measured on the inclined deformation plane. The calculated COFs were reported as a function of sliding velocity in Figure 3-11. The results showed that COF decreased by the increase in cutting speed and the average values ranged from 0.61 at 20 m/min to 0.23 at 200 m/min. Due to the direct relation between cutting speed and temperature, it has been also concluded that the effect of temperature on friction has been already included in the frictional data presented by Puls et al., [2012]. In the present research,

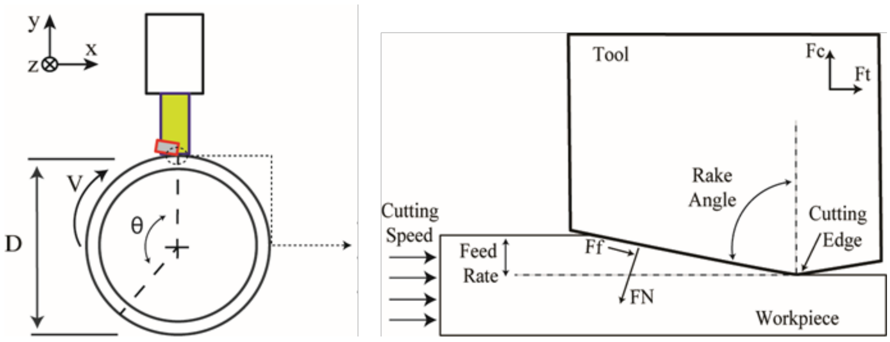

Figure 3-10. Configuration of reverse cutting experiment [Puls, 2012].

Sliding Velocity (m/min)	20	50	100	150	200
COF	0.61	0.59	0.31	0.25	0.23

Figure 3-11. Experimentally obtained COF as the function of velocity [Puls, 2012].

constant COF was used in simulation. For each simulation, the COF was chosen from the data in Figure 3-11 referring to its cutting speed.

3.5 Heat Generation

Plastic deformation of workpiece and the sliding friction at the contacting interfaces are the main heat sources during metal cutting [Filice, 2006, Huang, 2003, Rech, 2013, Trigger, 1963]. The heat generated per unit volume due to plastic deformation of workpiece material is shown in Eq. 3-7:

$$Q_{Pl}=\eta_m\sigma\dot{\varepsilon}$$

Eq. 3-7

In Eq. 3-7, η_m is the inelastic heat fraction, σ is the plastic flow stress, and $\dot{\varepsilon}$ is the strain rate [Ng, 2003]. Based on the Ng, et al. [2002b] the fraction of mechanical dissipation due to the plastic deformation of the work material which is converted into the heat is defined through the inelastic heat fraction and has been considered to be 0.9. This means that 90% of the mechanical energy due to plastic deformation has been converted into the heat.

The generated heat flux density due to the friction at interfaces is shown in Eq. 3-8:

$q_f=\eta_f\tau_f(\Delta S/\Delta t)$	Eq. 3-8

In Eq. 3-8, τ_f is the frictional stress, ΔS is the incremental slip and Δt is the time increment [Ng, 2003]. The parameter η_f defines as the fraction of dissipated energy converted into heat which has been considered as 1.0 in the present study. The percentage of heat due to the friction which is channelled into the chip or work, β_H , was related to the thermal diffusivity of the work and tool materials, as shown in Eq. 3-9 and Eq. 3-10 respectively. The In. Eq. 3-10, k is the thermal conductivity, ρ is the density, and c_p is the specific heat capacity. The subscripts w and t refer to the work and tool. It should be noted that variation in cutting speed affects the temperature which affects both thermal conductivity and specific heat capacity. However, in the ABAQUS this value must be inserted as a constant value, and its relation to cutting speed and consequently to the temperature could not be included. Also, the information about cutting speed and temperature were not known prior to the simulation.

$\beta_H= E_w/(E_w+ E_t)$	Eq. 3-9
$E_{w,t}= (k_{w,t}*\rho_{w,t}*c_{p_{w,t}})^{\frac{1}{2}}$	Eq. 3-10

The heat losses through convection or radiation were neglected [Usui, 1982] and the gap conductance between the interacting surfaces has been considered as 1E+8 W/m^2°C. An extreme value of gap conductance has been widely used in finite element simulation of cutting process [Bordin, 2015, Thepsonthi, 2015]. Such an extreme value decreased the required simulation time for reaching to a steady state condition [Malakizadi, 2016]. It should be noted that in the context of present research, thermal contact conductance has been referred to as the gap conductance. This was related to naming convention in ABAQUS software.

4 PAPER 1: INFLUENCE OF FRICTION MODELS ON FE SIMULATION RESULTS OF ORTHOGONAL CUTTING PROCESS

This chapter is a copy of the collaborative paper that has been published in the Journal of Advanced Manufacturing Technology in 2017. This paper evaluates the viability of the most widely used frictional models for simulating the contact condition at the tool-chip interface. In addition, the performance of three different FE commercial software, Deform 2D, Abaqus/Explicit and AdvantEdge, under nearly similar thermal and frictional boundary conditions has been investigated. To develop a systematic approach to evaluate the performance of friction models, the optimum sets of friction coefficients were initially determined, where the criterion was set as the minimum average prediction error of all the simulated responses including the cutting force, feed force, chip thickness and the contact length. The results indicated nearly a similar range of minimum average error for all the adopted friction models, independent of FE commercial code used for simulation of cutting process. The reasons for such behaviour were discussed critically, and the most viable models to represent the contact condition at the tool-chip interface were identified. The main goal of this collaborative research, in terms of applying to the present thesis, was to evaluate the accuracy of the finite element simulation which was part of the first phase of tool life prediction methodology. All the simulated results using ABAQUS in this publication were performed by Keyvan Hosseinkhani, McMaster University.

Authors: Amir Malakizadi, Keyvan Hosseinkhani, Emilia Mariano, E. Ng, Antonio Del Prete, Lars Nyborg

The International Journal of Advanced Manufacturing Technology volume 88, pages 3217–3232 (2017)

Abstract.

It is well-known that the reliability of Finite Element (FE) simulation results of cutting processes depends mainly on two factors; implementation of a well-defined constitutive model which can properly represent the severe deformation in chip formation process as well as the viability of the relation adopted to simulate the frictional condition at the tool-chip interface. In the current study, a systematic approach is presented to evaluate the performance of various friction models in three different FE commercial codes; Deform 2D, Abaqus/Explicit and AdvantEdge. The frictional condition was analysed for two uncoated cemented carbide- plain carbon steel combinations; K10/AISI 1045 and H13A/AISI 1080. The results indicated that approximately similar ranges of minimum average error in simulation responses can be achieved; independently of the FE code used for simulation of the chip formation process and for both tool-work material combinations. The reasons for this observation were critically discussed.

Keywords: Cutting process, friction model, Finite Element Method, Artificial Neural Network, Johnson-Cook

4.1 Introduction

Metal cutting process often plays a central role in manufacturing industrial components, where they are closely dimensioned, new features such as holes and fillets are made and the specific demands on the properties of machined surfaces are secured. In cutting operations, the work material in the vicinity of the tool edge experiences a severe plastic deformation at very high strain rates, normally in order of 10^3-10^6 s^{-1}, and a substantial amount of heat is therefore generated at the tool-chip interface [1]. As a result, the tool edge is often subjected to high contact pressures and temperatures, the amounts of which can exceed 5 GPa and 1200 °C, respectively [1, 2]. Under such extreme conditions, the cutting edge can wear down after only a short machining time. The worn tools may in turn deteriorate the surface finish properties and the dimensional accuracy of the machined parts.

For many years, costly experimental procedures have been regarded as the only reliable method to estimate the tool life and to optimise the machining operations to achieve higher efficiency in terms of time and cost. In recent years, however, the significant advances in the computing power of computers have facilitated the application of advanced numerical techniques such as Finite Element Method (FEM) in metal cutting research and development. This has provided the opportunity to simulate the responses such as tool surface temperature and stress distribution around the cutting edge under various cutting conditions and for different tool geometries, which in turn has allowed the development of cost effective and robust approaches for tool wear estimations under operational conditions [3-5]. Yet, the reliability of the FE simulation results has shown to depend largely upon the reliability of the flow stress data to describe the severe plastic deformation in shear zone and viability of the frictional and thermal boundary conditions adopted at the tool-chip interface [6-8]. A vast number of studies have been therefore dedicated to development of the experimental approaches such as Split Hopkinson Pressure Bar (SHPB) high strain rate test [9, 10] and inverse modelling of orthogonal cutting process [11-15] to determine the flow stress properties of the work material within the common range of strain, strain rate and temperature encountered during the chip formation process. In parallel, more advanced constitutive models have been proposed based on the experimental observations in order to represent the material behaviour under such extreme conditions [12, 16, 17].

The tribological conditions at the tool-chip interface have been studied using various experimental methods [18-22]. These studies have been generally aimed at understanding the tribological condition at contact regions and also development of an appropriate model that can represent the complex material deformation at the so-called secondary shear zone at the tool-chip interface. These methods involved the analysis of the frictional behaviour either directly by metal cutting tests or by tribometer instruments that can reproduce similar tribological conditions as the cutting process. A basic force analysis proposed by Merchant [23] was among the early attempts to assess the mean (apparent) friction coefficient based on the results of orthogonal cutting tests. This approach was extended by Usui et al. [24] using a more advanced slip-line field in the vicinity of the cutting edge to derive a universal expression for the mean Coulomb friction coefficient including the influence of rake angle and restricted contact length. In a more recent study, Atkins [25] presented a method to estimate the local frictional behaviour at the tool-chip interface based on the analysis of the cutting forces and the distribution of the normal stress along the contact length proposed by Zorev [26]. Tailored cutting experiments using the split and photoelastic tools have also been suggested by several authors [18, 19] to measure the local frictional condition on the rake face of the tools during chip formation process. Several attempts have also been made to develop tribometer instruments that can reproduce the tribological conditions at the tool-chip interface. For instance, Zemzemi et al. [20] and Rech et al. [21] re-designed the tribometer instrument proposed by Hedenqvist and Olsson [27] to achieve contact pressures as high as 3 GPa which can be considered within the common range of normal pressure on the rake face of the tools during chip formation process. Even though their approach ensured a reasonable range of contact pressure and interface temperature, the friction coefficient was measured on the non-fresh surfaces of the work material. To overcome this limitation, Smolenicki et al. [22] designed an in-process tribometer instrument that allowed to measure the friction coefficient on the newly generated non-oxidised pin-on-ring contact regions by pre-cutting the surfaces using a cutting tool placed at a small distance from the pin. Puls et al. [28] developed an experimental concept similar to the broaching equipment, where the clearance side of the tools was forced on thin sheets to induce local deformation in a range common in metal cutting. Under such conditions, the chip formation is supressed as a result of a very negative rake angle and a uniform distribution of contact pressure is generated across the contact region. Accordingly, based on the observations of these experimental set-ups, several friction models have been proposed to describe the frictional condition in metal cutting process. The Coulomb (sliding) friction model [6, 9, 29-32], constant or variable shear friction relations [6, 11, 31, 33, 34], temperature or strain rate modified models [19, 28, 35] and finally the velocity dependent Coulomb friction model [8, 20, 22] are the main relations presented in literature. The viability of these models has been investigated using FE commercial codes in a number of studies. Özel [6] compared the performance of a number of friction models adopted in Deform 2D FE commercial code. He showed that the variable friction models led the least deviations from the experimental measurements. Arrazola and Özel [36] used Abaqus/Explicit with Arbitrary Lagrangian Eulerian (ALE) formulation to evaluate the performance of Coulomb friction model and sticking-sliding friction relation including various limiting shear stress values in simulation of orthogonal cutting process. It was shown that sticking-sliding shear friction model Abaqus/Explicit should be used with caution, as the acceptable values for limiting shear stress differs at various cutting conditions and they should therefore be adjusted carefully. Improper adjustments led to large simulation errors in terms of cutting forces and chip thickness. Bil et al. [31] compared the performance of three different FE commercial codes: MSC Marc, Deform 2D and AdvantEdge with respect to the influence of friction coefficients, different remeshing criteria, and threshold tool penetration values on the simulation results. The shear and sliding friction models with constant values were evaluated in their investigations. They showed that the FE simulation results depend significantly upon the friction coefficients. The lowest deviations in cutting force predictions were observed for smaller friction coefficients, whereas more accurate results were obtained for thrust force and shear angles using larger friction coefficients.

A part from the study conducted by Bil et al. [31], the majority of investigations on viability of friction models have been limited to only one specific FE commercial code. Moreover, in best of our knowledge, a systematic approach for evaluation of friction models has not been presented in previous studies. In the current study, the viability of the most widely used models for simulation of the frictional condition at the tool-chip interface has been evaluated. In addition, the performance of three different FE commercial codes: Deform 2D, Abaqus/Explicit and AdvantEdge, under nearly similar thermal and frictional boundary conditions has been investigated. In order to develop a systematic approach to evaluate the performance of friction models, the optimum sets of friction coefficients were initially determined, where the criterion was set as the minimum average prediction error of all the simulated responses including the cutting force (FC), feed force (Ff), chip thickness (CT) and the contact length (CL). The results indicated nearly a similar range of minimum average error for all the adopted friction models, independence of FE commercial code used for simulation of cutting process. The reasons for such behaviour were discussed critically and the most viable models to represent the tribological condition at the tool-chip interface were identified.

4.2 Implemented Friction Models

The experimental stress measurements using split and photoelastic tools indicated two distinct contact zones on the rake face of the tools, widely referred to as sticking and sliding frictional zones. This has also been shown using other analysis techniques [37, 38]. In the sticking region, the friction stress is generally independent of the normal stress and is limited by the shear flow stress (k) of the work material. However, as the normal stress reduces on the rake face along the tool-chip contact length, the friction stress becomes proportional to the normal pressure (σ_n). This region on the rake face is referred to as the sliding zone. Shaw and his co-workers [39] characterised the sticking and sliding zones along the tool-chip interface based on the relation between the contact pressure and the real area of the contact (A_r), i.e. the total area of the asperities formed on the contact pair. According to this model, the frictional force between two contact surfaces is produced by the shearing action of the welded asperities, the amount of which supposedly varies with contact pressure as:

$A_r = A_n\left[1 - \exp\left(-\alpha\sigma_n\right)\right]$	Eq. 4-1

where A_n represents the apparent area of contact between the two surfaces and α is a constant. As evident from Eq. 4-1, the real contact area increases with an increase in the contact pressure, and it ultimately approaches the apparent area of contact at very high contact pressures. This state represents the sticking condition near the cutting edge, where the relative motion between the tool and chip material produces gross sub-surface shear plastic deformation within the adhered material on the tool surface. However, as the contact pressure reduces along the tool-chip contact length, the real area of contact reduces. Under the condition where $A_r \ll A_n$, the shear friction stress becomes linearly proportional to the contact pressure, representing the sliding contact condition far from the cutting edge. The complex frictional condition at the tool chip-interface can therefore be formulated using a single mathematical relation with reference to Eq. 4-1, as also suggested by Childs [19] and Shirakashi and Usui [40]. The experimental data presented in literature [41] indicate that the shear friction stress in the sticking region may vary between 0.5k and k for different tool-work material combinations. The frictional behaviour is also shown to be highly nonlinear with respect to the variation of the contact pressure [41]. Hence, an additional parameter would be required to describe the shear friction stress within the entire range of contact pressure at the tool-chip interface:

$\tau = \left[1 - \exp\left(-\alpha_1\sigma_n^{\alpha_2}\right)\right]k$	Eq. 4-2

Figure 4-1a shows the variation of the friction coefficient with respect to the contact pressure for different combination of friction parameters. The local frictional behaviour at tool-chip interface may also be described using the following relation:

$$\tau = \begin{cases} \mu\sigma_n & \mu\sigma_n < mk \qquad (L_{st} \le x \le L_{sl}) \\ mk & \mu\sigma_n \ge mk \qquad (0 \le x \le L_{st}) \end{cases} \tag{Eq. 4-3}$$

where L_{st} and L_{sl} represent the sticking and sliding contact lengths, respectively. μ and m are the sliding and sticking friction coefficients. Based on this model, the friction stress under sticking condition is proportional to the shear flow stress of the work material at tool-chip interface and it is proportional to the normal stress within the sliding zone. The experimental measurements presented by Childs et al. [41] showed that the shear friction coefficient, m, may take a value between 0.5 and 1 while μ can take values as high as 1.5 when cutting steels using uncoated carbide tools. Both μ and m are also shown to vary significantly with temperature and contact pressure.

The Coulomb friction law has also been implemented to describe the shear stress at the tool-chip interface, assuming the friction coefficient as a function of either sliding velocity or interface temperature [8, 20]. Puls et al. [42] developed an experimental concept to provide the apparent Coulomb friction coefficient (μ_{app}) at various sliding velocities by measuring the axial and tangential forces acting on the clearance side of the tool while being forced in transverse direction toward the disc rotating in the opposite direction compared to the conventional case of a turning operation. In this way, it was possible to supress the chip formation process as a result of a very negative rake angle (-80°) and therefore a uniform frictional condition could be reproduced across the contact region. The friction coefficient was then calculated based on the basic force analysis proposed by Merchant [23]:

$$\mu_{app} = \frac{F_t + \tan(\gamma)F_C}{F_C - \tan(\gamma)F_t} \tag{Eq. 4-4}$$

where γ is the rake angle and F_t and F_C are the tangential and normal force across the contact region. In the current study, based on the results of this experimental setup, a mathematical relation was derived for the velocity dependent Coulomb friction coefficient:

$$\mu = (0.6 - \mu_0)\exp\left(-\left((\alpha_1 V_S)^{\alpha_2}\right)\right) + \mu_0 \qquad \text{Eq. 4-5}$$

where α_1, α_2 and μ_0 are the model parameters. Here, μ_0 was assumed at 0.2, while the upper limit for friction coefficient was set at 0.6 based on the experimental measurements presented for H13A/AISI 1045 tool-work material combination [42]. Figure 4-1b shows the variation of the friction coefficient with sliding velocity for different combinations of parameters along with the experimental measurements.

Table 4-1 summarises the friction models adopted in the current study. In addition to the Eq. 4-2, Eq. 4-3, and Eq. 4-5, the Coulomb (sliding) and shear friction models with constant parameters were also adopted for simulation of the chip formation process. These models are often regarded as the standard relations for simulation of the tribological condition at tool-chip interface in metal cutting based on their availability in various FE commercial codes, as will be discussed in section 3.2.

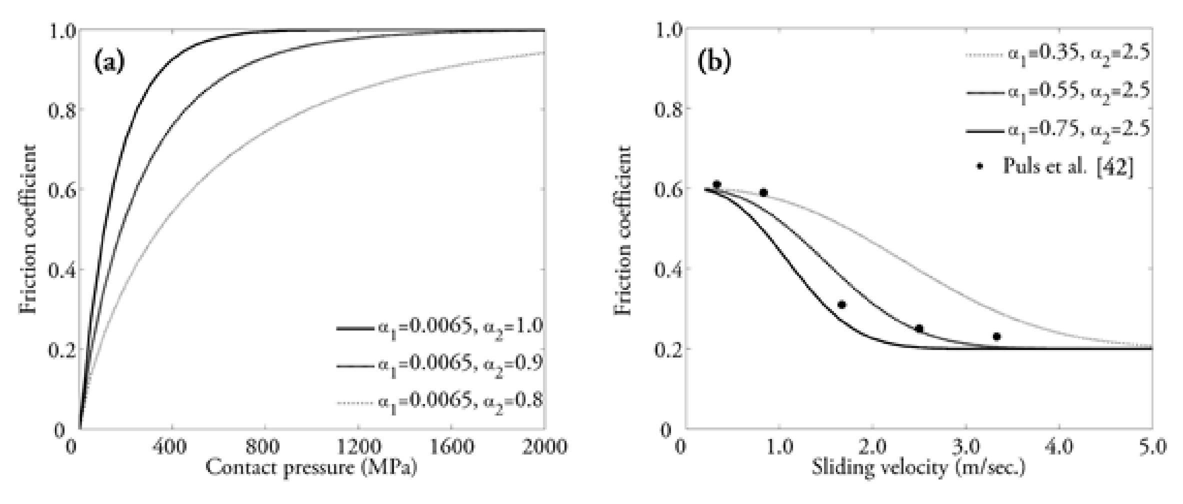

Figure 4-1. variation of pressure and velocity dependent friction coefficients with contact pressure and sliding velocity based on Equation 2 and Equation 5, respectively. Experimental data for the velocity dependent model were taken from Puls et al. [42].

Friction model	**Mathematical formulation**
Sliding friction model (SL) [7, 9, 29-32]	$\tau = \mu\sigma_n \ , \ \mu = const.$
Velocity dependent friction model (VD)	$\tau = \mu\sigma_n \ , \ \mu = (0.6 - \mu_0)\exp\left(-\left((\alpha_1 V_S)^{\alpha_2}\right)\right) + \mu_0$
Shear friction model (SH) [6, 31, 33]	$\tau = mk \ , \ m = const.$
Pressure dependent shear friction model (PD)	$\tau = mk \ , \ m = \left[1 - \exp\left(-\alpha_1 \sigma_n^{\alpha_2}\right)\right]$
Sticking-Sliding friction model (SS) [6, 36, 43]	$\tau = \begin{cases} \mu\sigma_n & \mu\sigma_n < mk \quad (L_{st} \le x \le L_{sl}) \\ mk & \mu\sigma_n \ge mk \quad (0 \le x \le L_{st}) \end{cases}$

Table 4-1. The friction models investigated in current study.

4.3 Evaluation Methodology

In order to evaluate the viability of the presented friction models to describe the frictional condition at the tool-chip interface, initially the optimum combination of friction parameters was determined for each model according to the steps shown in Figure 4-2. The aim was to ensure that the friction models were evaluated based on their optimum combinations at which the least deviations from the experimental measurements, including the chip thickness, contact length and the cutting/feed forces were achieved. This allowed for a more systematic evaluation of the performance of a certain friction model by calculation of the percentage of the average simulation errors.

As evident from Figure 4-2, initially a different combination of friction parameters were generated for each of the models presented in Table 4-1. In the case of the models with two parameters (i.e. VD, PD and SS models), the Central Composite Design (CCD) was adopted to generate nine different combinations of friction parameters in three levels. The friction coefficient for the models with only one parameter was also varied in three levels, however, the step sizes were set similar as the ones adopted in the sticking-sliding model. The chip formation process was then simulated in different FE commercial codes incorporating various combinations of friction parameters generated for each model. Two different cutting

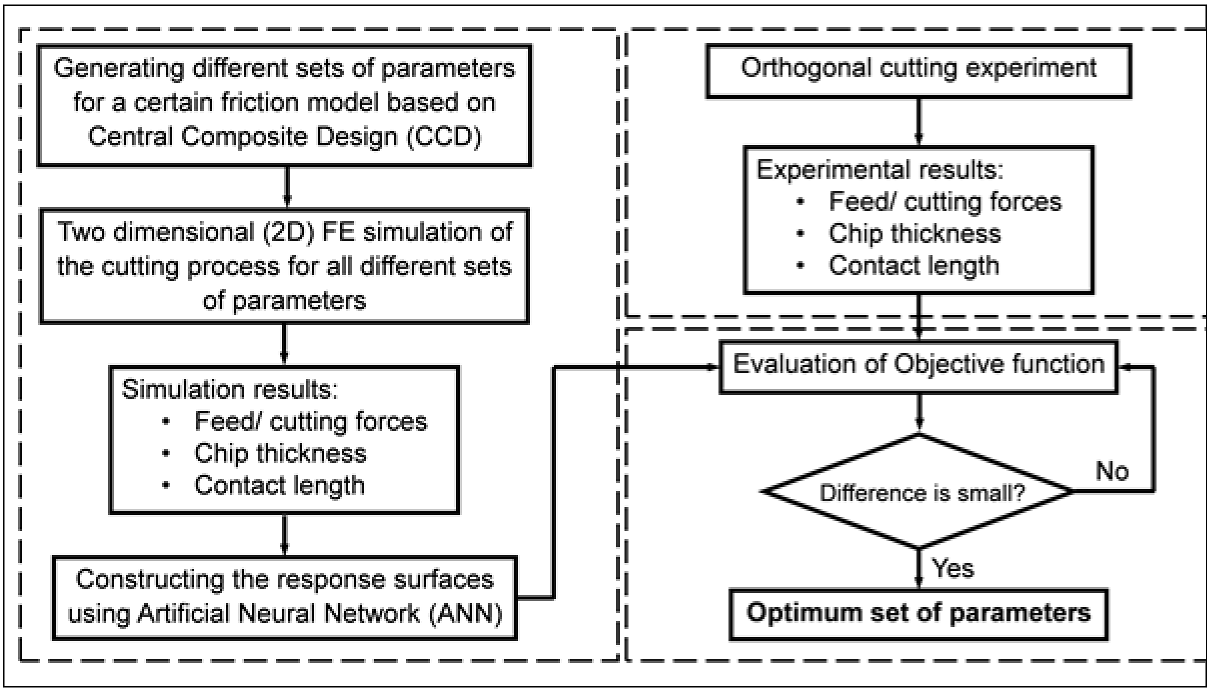

Figure 4-2. The flowchart indicating the steps of the evaluation methodology adopted in this study.

conditions; A and C were simulated in this step for both tool/material combinations (see Table 4-3). The response surfaces were then established for models with two parameters using Artificial Neural Network (ANN) platform available in MATLAB software [44] to describe the relation between friction parameters and the simulated outputs. In the case of the models with only one parameter (e.g. SL and SH models), the mathematical relations between the friction coefficient and the simulation outputs were simply expressed as third order polynomials. The optimum sets of friction coefficients were then identified by formulating an optimisation problem as:

$$\text{Min } f(x) \text{ such that } X_{lb} < X < X_{ub} \qquad \text{Eq. 4-6}$$

where X_{lb} and X_{ub} represent the vectors including the lower and upper bounds of the friction parameters for a certain model. Table 4-2 shows the upper and lower bounds set for each of the friction model as well as the total number of variations adopted for each model to determine the response surfaces (or the third order polynomials). Note that the upper and lower values of the Coulomb friction model (SL) were set based on the experimental data presented by Puls et

Friction model	Lower bound	Upper bound	Number of combinations
Sliding friction model (SL)	μ=0.2	μ=0.6	3
Velocity dependent friction model (VD)	α_1=0.35, α_2=0.5	α_1=0.75, α_2=2.5	9
Shear friction model (SH)	m=0.5	m=1.0	3
Pressure dependent shear friction model (PD)	α_1=0.0025, α_2=0.8	α_1=0.0065, α_2=1.0	9
Sticking-Sliding friction model (SS)	μ=0.2, m=0.5	μ=0.6, m=1.0	9

Table 4-2. The lower and upper bounds of the friction parameters adopted in the current study.

al. [42] for H13A- AISI 1045 tool-workpiece material combinations. $f_{(X)}$ in Eq. 4-6 represents the objective function expressed as:

$$f(\mathbf{X}) = \sum_{m=1}^{4}\left\{ w_m \left[\sum_{n=1}^{N} \left(\frac{Y_{mn,ANN} - Y_{mn,EXP}}{Y_{mn,EXP}} \right)^2 \right] \right\} \qquad \text{Eq. 4-7}$$

where X is a vector including the friction parameters. N is the number of cutting conditions used for identification of optimum friction coefficients. $Y_{mn,ANN}$ *and* $Y_{mn,EXP}$, respectively, represent the calculated responses by integration of FEM and ANN and the corresponding experimental measurements at similar cutting conditions. w_m is the weight factor for each term in Eq. 4-7, and they were assumed unitary in the current study to ensure an identical impact for each term in the objective function in the optimisation process. The interior point optimisation algorithm with multiple starting points in MATLAB was adopted to find the global optimum solution.

4.3.1 Material and experimental details

The orthogonal machining tests for AISI 1080 eutectoid steel were performed under dry condition using Sandvik N151.2-650-50-3B-H13A standard uncoated cemented carbide [11]. Prior to machining tests, a cylindrical bar with 60 mm diameter and 55 mm length was heat treated to achieve a pearlitic structure with fine lamellar spacing. The procedure involved initial austenitisation at 865 ˚C for 1 hour followed by 10 minutes cooling within a salt bath with 590

˚C and air cooling to room temperature. The heat treatment procedure resulted in a fully pearlitic structure with 0.274 µm mean true lamellar spacing. All machining tests were performed on an EMCO 365 CNC lathe equipped with a Kistler 9275A three component dynamometer to measure the cutting forces. Orthogonal cutting condition was met through transverse machining of flanges with 2 mm thickness, generated on the cylinder prior to machining tests. Each cutting test was repeated three times with fresh inserts to ensure reproducibility of the experimental results.

A Leitz DMRX light optical microscope equipped with AxioVision digital image processing software was used to measure the thickness of randomly selected chips produced under various cutting condition. The chip-tool contact lengths were also measured by means of EDS (Energy Dispersive Spectroscopy) analysis on the rake face of the inserts after machining using Iron elemental mapping.

The experimental data for AISI 1045 alloy were taken from [45]. The author used K10 uncoated carbide with 6˚ rake angle and no chip breaker for orthogonal cutting tests. The orthogonal cutting tests were performed on tubes with cutting width at least ten times larger than the feed rates. Table 4-3 shows the cutting conditions used in the current study for evaluation of the friction models. Table 4-4 shows the experimental measurements.

Work Material	Condition	Tool material	Cutting speed (m/min)	Rake angle (°)	Feed rate (mm/rev)	Depth of cut (mm)
AISI 1080	A	H13A	90	0	0.1	2
	B		120			
	C		180			
AISI 1045	A	K10	120	6	0.1	NA*
	B		120		0.2	
	C		240		0.1	
	D		240		0.2	

Table 4-3. The cutting data used in the current study.

Work Material	Condition	CT (mm)	CL (mm)	F_C (N/mm)	F_f (N/mm)
AISI 1080	A	0.279	0.524	278	226
	B	0.244	0.425	263	197
	C	0.219	0.423	267	180
AISI 1045	A	0.320	1.000	287	259
	B	0.500	1.325	459	302
	C	0.290	0.725	234	179
	D	0.450	1.089	413	224

Table 4-4. The experimental measurements during orthogonal machining AISI 1080 and AISI 1045 steels.

4.3.2 Finite element modelling of cutting process

The chip formation process in Deform 2D and AdvantEdge was simulated using Lagrangian formulation, while the FE models in Abaqus/Explicit were constructed using Arbitrary Lagrangian-Eulerian (ALE) formulation. Figure 4-3 shows the adopted structural boundary conditions for the FE models based on ALE and Lagrangian formulations. In ALE approach, the mesh around the cutting edge, where the work material undergoes severe plastic deformation is fixed in space and it follows the Eulerian formulation. However, the mesh at the machined surface and also within the part of the work material which forms the final geometry of the chip is left unconstrained and follows Lagrangian formulation. Hence, the elements on the chip tail are steadily expanded and the final chip is produced during FE analysis. The chip separation in Deform 2D and AdvantEdge is undertaken by continuous remeshing to eliminate the distorted elements during the analysis [31, 46]. Once the new mesh is generated, the calculated outputs from the step prior to the remeshing stage are interpolated on the new mesh. The details of ALE and Lagrangian formulations adopted for FE modelling of the cutting process can be found in [33, 47].

The tool in Deform 2D was assumed to be rigid due to its relatively high elastic modulus, while the elastic properties of the tool were directly included in the FE model built in

Abaqus/Explicit and AdvantEdge. Johnson-Cook constitutive model was incorporated in all FE codes to simulate the visco-plastic behaviour of the work material within the range of strain, strain rate and temperature encountered during the chip formation process:

$$\sigma = \left(A + B\varepsilon^{n}\right)\left[1 + C\ln\left(\frac{\dot{\varepsilon}}{\dot{\varepsilon}_0}\right)\right]\left[1 - \left(\frac{T - T_r}{T_m - T_r}\right)^{m}\right]$$

Eq. 4-8

In this model, σ is the flow stress of the work material, ε is the strain, T is the temperature and $\dot{\varepsilon}$ is the strain rate. A, B, C, n and m represent the material parameters. $\dot{\varepsilon}_0$ is the reference strain rate and T_m and T_r represent the melting and room temperatures, respectively. The constitutive data for AISI 1045 were taken from [45], where the author used SHPB high strain rate test for calibration of the Johnson-Cook material model. In the case of AISI 1080, the material parameters were obtained using inverse modelling of orthogonal cutting process [11]. In this approach, the author combined Response Surface Methodology (RSM) and Oxley's machining theory to determine the mathematical relation between the material parameters and the outputs of interests including the feed force, cutting force, chip thickness and contact length for a certain cutting data. The optimum set of material parameters were then identified by minimising the difference between the estimation of the outputs based on the established mathematical relations and the corresponding experimental measurements at similar cutting conditions. Table 4-5 shows the material parameters of the Johnson-Cook model incorporated in this study for AISI 1045 and AISI 1080. The thermal properties of the tool and workpiece material are also shown in Table 4-6. The temperature dependent data for AISI 1045 were taken from [48], while JMatPro^{TM} commercial software [49] was used to obtain the thermal properties for AISI 1080.

Material	A	B	C	n	m	$\dot{\varepsilon_0}$	T_m (K)
AISI 1045	553.1	600.8	0.0134	0.234	1	1	1773
AISI 1080	534.6	410	0.0062	0.137	1.01	1	1738

Table 4-5. The Johnson-Cook material parameters for AISI 1045 [45] and AISI 1080 [11].

Material	$\lambda (W/m.K)$	$\rho \times C_p$ $(J/cm^3.K)$
AISI 1045 [48]	25˚C <T<600 ˚C: $3.91\times10^{-8}T^3-4.74\times10^{-5}T^2-0.0121T+46.1$	25˚C <T<600 ˚C: $4.685\times10^{-6}T^2+1.527\times10^{-3}T+3.664$
	T>600 ˚C: 26	T>600 ˚C: 6.28
AISI 1080 [11]	25˚C <T<900 ˚C: $4\times10^{-8}T^3-4\times10^{-5}T^2-0.0195T+50.32$	25˚C <T<900 ˚C: $9\times10^{-7}T^2+0.0022T+3.735$
H13A [11]	25˚C <T<1000 ˚C: $6\times10^{-8}T^3-9\times10^{-5}T^2-0.0083T+94.834$	25˚C <T<1000 ˚C: $3\times10^{-9}T^3-5\times10^{-6}T^2+0.0041T+2.886$
K10 [50]	80	5.7

Table 4-6. The thermal properties of the tool and work materials.

As mentioned before, AdvantEdge FE commercial code only supports the Coulomb friction model (SL) with constant values. In addition to the standard Coulomb friction model, it is also possible to provide the velocity dependent Coulomb friction coefficients in Abaqus/Explicit using tabulated data. Hence, both the constant and velocity dependent friction models were implemented for FE modelling of the cutting process using Abaqus/Explicit. A wider range of friction models including the Coulomb, shear and sliding-sticking friction models are available in Deform 2D, where the friction coefficients can be defined either as a constant or as a function of temperature and/or pressure using tabulated data. In addition, Deform 2D provides a platform to adopt a user-defined friction coefficient as a function of temperature, shear flow stress, contact pressure and sliding velocity for each of the aforementioned friction models by developing FORTRAN sub-routines. In this study, the velocity and pressure dependent friction models presented in Table 4-1 were implemented using this platform. Table 4-7 shows the summary of the friction models implemented in different FE codes in the current study.

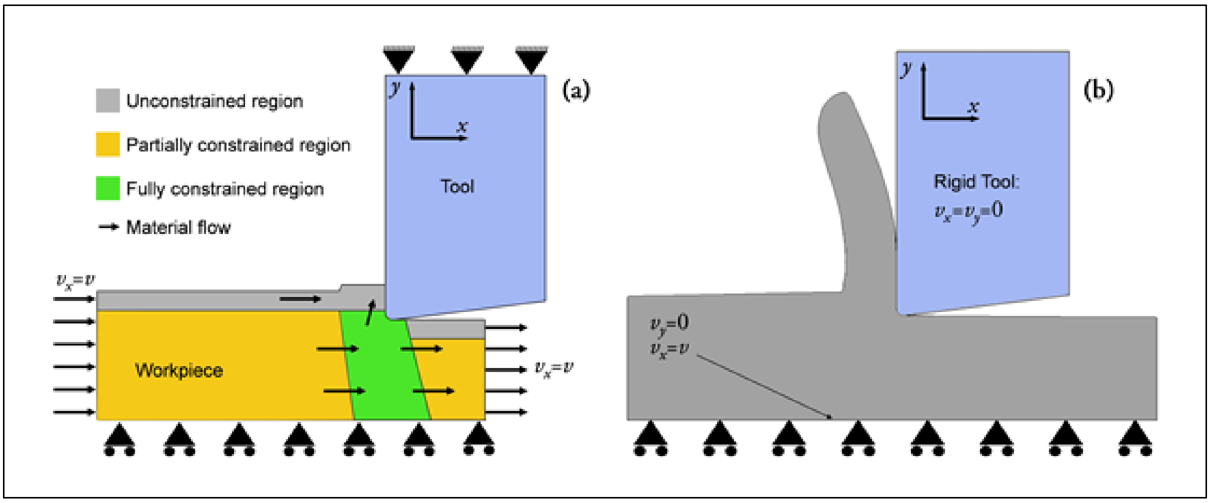

Figure 4-3. The boundary conditions adopted for ALE (a) and Lagrangian (b) FE models.

FE code	VD	PD	SL	SH	SS
Deform 2D	✓	✓	✓	✓	✓
AdvantEdge	—	—	✓	—	—
Abaqus/Explicit	✓	—	✓	—	—

Table 4-7. The friction models adopted in different FE codes in the current study.

Perfect thermal condition was assumed at tool-chip interface in Deform 2D and Abaqus/Explicit. This was achieved by adjusting a very heat transfer coefficient and high gap conductance at the tool-chip contact surfaces in the FE models. The ideal thermal condition at the tool-chip interface has been widely accepted for the simulation of cutting process [32, 43, 51], which has been experimentally verified for a number of tool-work material combinations through temperature measurements [52, 53]. The AdvantEdge FE commercial code, however, does not take into account the heat conduction between the tool and work material, and therefore it is not possible to adjust interface properties as such in the FE models. Furthermore, a different partitioning assumption has been made in Deform 2D, Abaqus/Explicit and AdvantEdge FE codes to apportion the heat due to frictional work between the tool and chip material. Deform 2D and AdvantEdge commercial codes adopt predefined values to divide the generated heat between the tool and chip, whereas it is possible to adjust the heat partitioning coefficient in Abaqus/Explicit for the frictional contacts. AdvantEdge adopts the approach proposed by Sekhon and Chenot [54] to compute the ratio of heat supply to the tool and chip [46]. A similar approach was also followed to calculate the heat partitioning coefficient for FE models in Abaqus/Explicit [30]. The generated heat through friction is, however, evenly distributed between the tool and chip in Deform 2D. These differences in FE formulations and thermal boundary conditions should be taken into account while comparing the FE simulation results.

4.4 Evaluation of simulation results

Figure 4-4 and Figure 4-5 show the FE simulation results of the chip formation process, indicating the temperature distribution in the vicinity of the cutting edge for AISI 1080 and AISI 1045 carbon steels at cutting conditions B and D, respectively, using Deform 2D, AdvantEdge and Abaqus/Explicit FE commercial codes. In all cases, the Coulomb friction model with a constant friction coefficient of 0.40 was adopted for FE modelling of the cutting process. Figure 4-6 summarises the other simulated responses at the corresponding cutting conditions for each material. As evident from these figures, a similar frictional condition led to different simulation results in various FE codes.

Figure 4-7 shows the established response surfaces by ANN based on the FE simulation results of the cutting process, incorporating the pressure dependent shear friction model (PD),

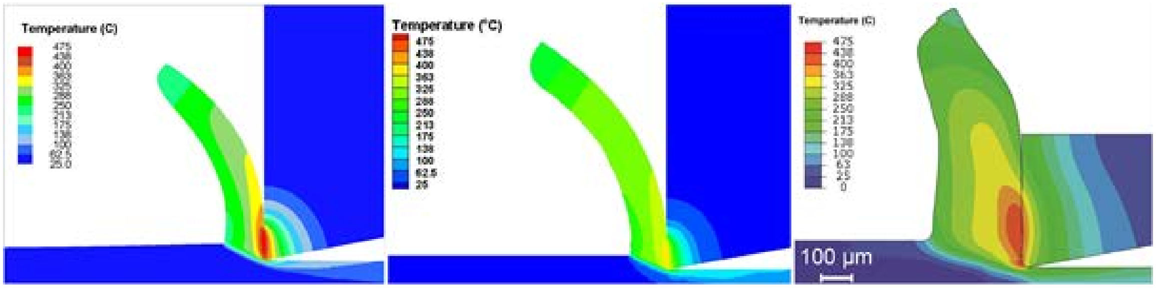

Figure 4-4. Calculated temperature distribution in the vicinity of tool edge at cutting condition B using Deform 2D (a), AdvantEdge (b) and Abaqus/Explicit (c). Work material: AISI 1080, Coulomb friction model, COF: 0.4.

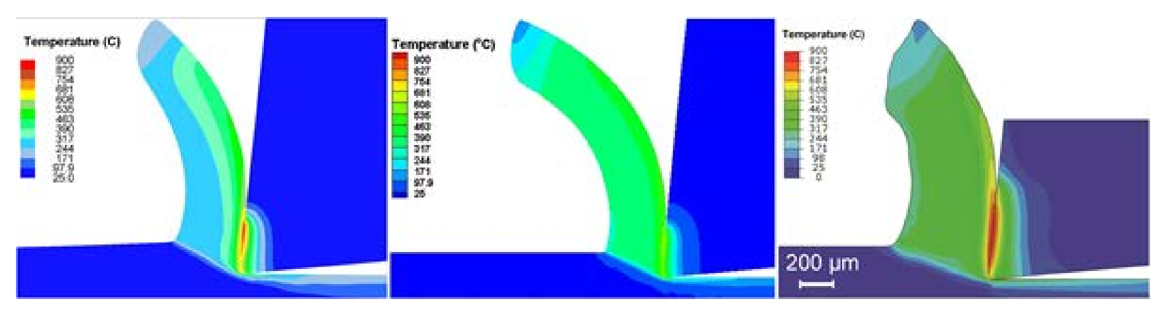

Figure 4-5. Calculated temperature distribution in the vicinity of tool edge for cutting condition D using Deform (a), AdvantEdge (b) and Abaqus/Explicit (c), Work material: AISI 1045, Coulomb friction model, COF: 0.4.

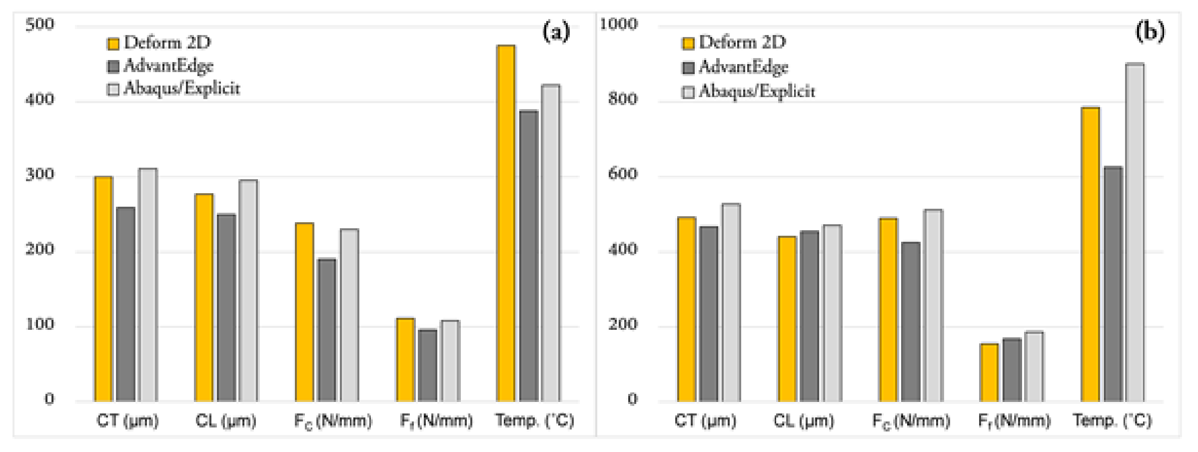

Figure 4-6. Summary of the FE simulation results of the chip formation process using different FE codes for AISI 1080 at cutting condition B (a) and AISI 1045 at cutting condition D (b) Coulomb friction model, COF: 0.4.

for AISI 1080 carbon steel at cutting condition A. As evident, different combinations of the friction parameters give rise to the varying simulation results; however the degree of variation differs for each response. Figure 4-8 also shows the simulated cutting and feed forces for AISI 1045 plain carbon steel at cutting condition A, using the adopted velocity dependent friction model in Deform 2D and Abaqus/Explicit. Evidently, the FE simulation results substantially varied between different FE codes. In addition, the maximum response was achieved at different combinations of friction parameters. For instance, the maximum cutting and feed forces were observed at (α1, α2) =(0.35, 2.5) and (α1, α2)=(0.35, 0.5) when modelling the cutting process in Deform 2D and Abaqus/Explicit, respectively. It should be noted, however, that the variations in the FE simulation results were relatively small in Abaqus/Explicit between different combinations of friction parameters, as can be seen in Figure 4-8b and Figure 4-8d.

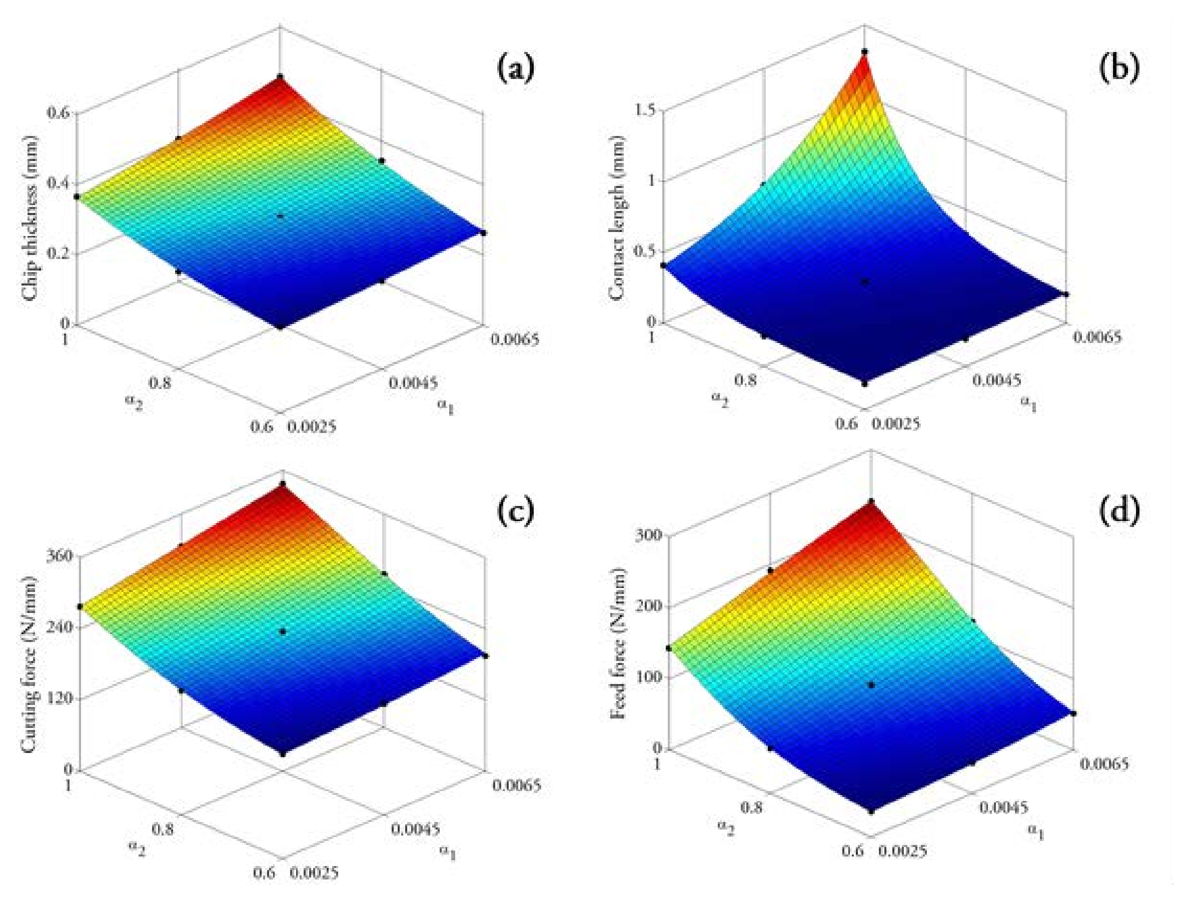

Figure 4-7. The influence of the pressure dependent (PD) friction model parameters on chip thickness (a), contact length (b), cutting force (c) and feed force (d): AISI 1080 at cutting condition A.

The optimum sets of friction coefficients were obtained by implementation of the methodology shown in Figure 4-2. The results are summarised in Table 4-8 and Table 4-9 for the investigated tool/work material combinations. The error in the simulated responses after implementation of the optimum sets of friction parameters in FE models is also shown in Figure 4-9 to Figure 4-12 for AISI 1045 at cutting conditions A and B and AISI 1080 at cutting conditions B and C.

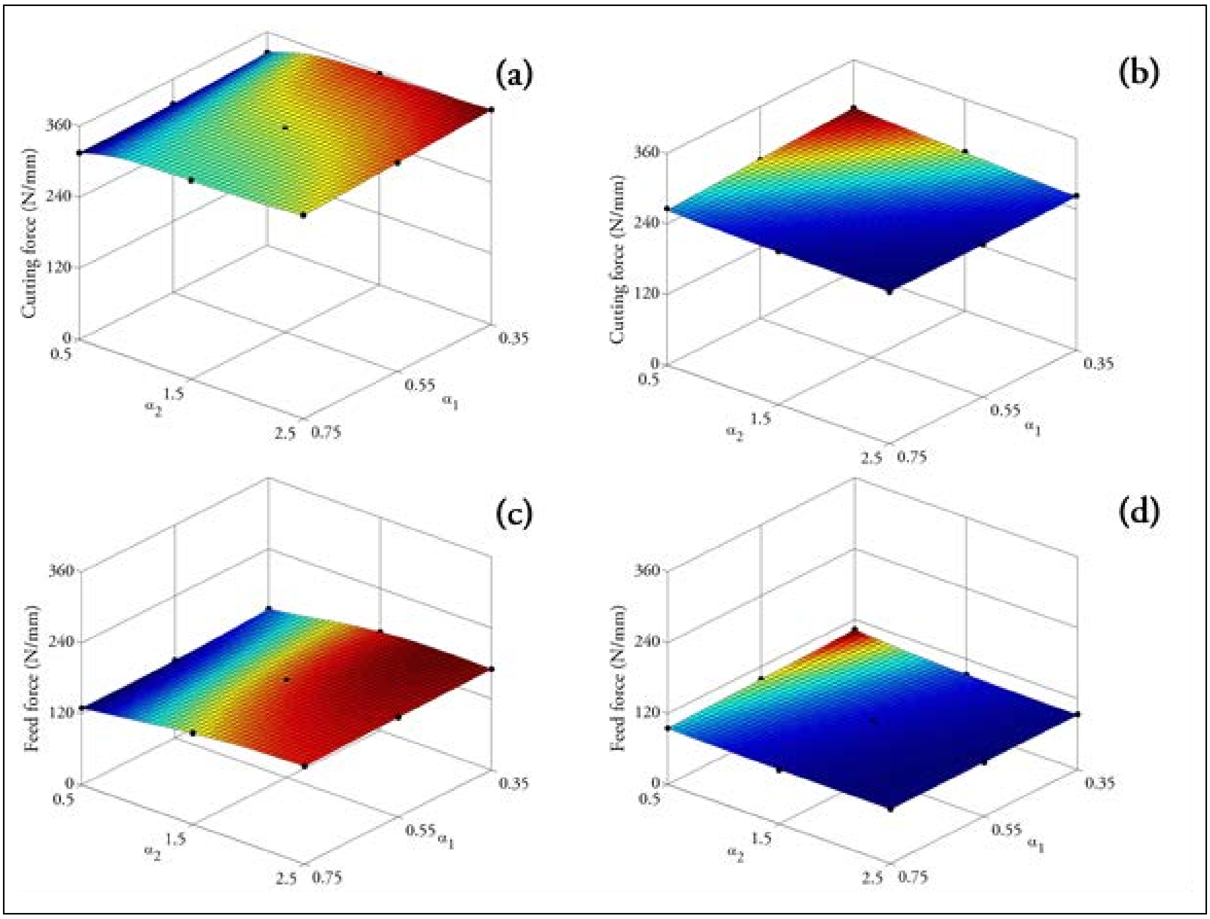

Figure 4-8. The influence of the parameters of the velocity dependent (VD) friction model implemented in Deform 2D (a and c) and Abaqus/Explicit (b and d) FE commercial codes on cutting and feed forces for AISI 1045 at cutting condition A.

Friction model	Deform 2D	Abaqus/Explicit	AdvantEdge
Sliding friction model (SL)	μ=0.6	μ=0.6	μ=0.6
Velocity dependent friction model (VD)	α_1=0.44, α_2=2.26	α_1=0.35, α_2=0.5	—
Shear friction model (SH)	m=0.83	—	—
Pressure dependent shear friction model (PD)	α_1=0.0065, α_2=0.92	—	—
Sticking-Sliding friction model (SS)	μ=0.6, m=1.0	—	—

Table 4-8. The optimum sets of friction parameters obtained for K10/AISI 1045 tool-work material combinations within the range of DOE given in Table 4-2.

Friction model	Deform 2D	Abaqus/Explicit	AdvantEdge
Sliding friction model (SL)	μ=0.6	μ=0.4*	μ=0.6
Velocity dependent friction model (VD)	α_1=0.75, α_2=2.5	α_1=0.35, α_2=0.73	—
Shear friction model (SH)	m=0.79	—	—
Pressure dependent shear friction model (PD)	α_1=0.0065, α_2=0.88	—	—
Sticking-Sliding friction model (SS)	μ=0.6, m=1.0	—	—

*FE simulations did not reach the thermal steady state condition for the larger friction coefficients after 5 mm of cut.

Table 4-9. The optimum sets of friction parameters obtained for H13A/AISI 1080 tool-work material combinations within the range of DOE given in Table 4-2.

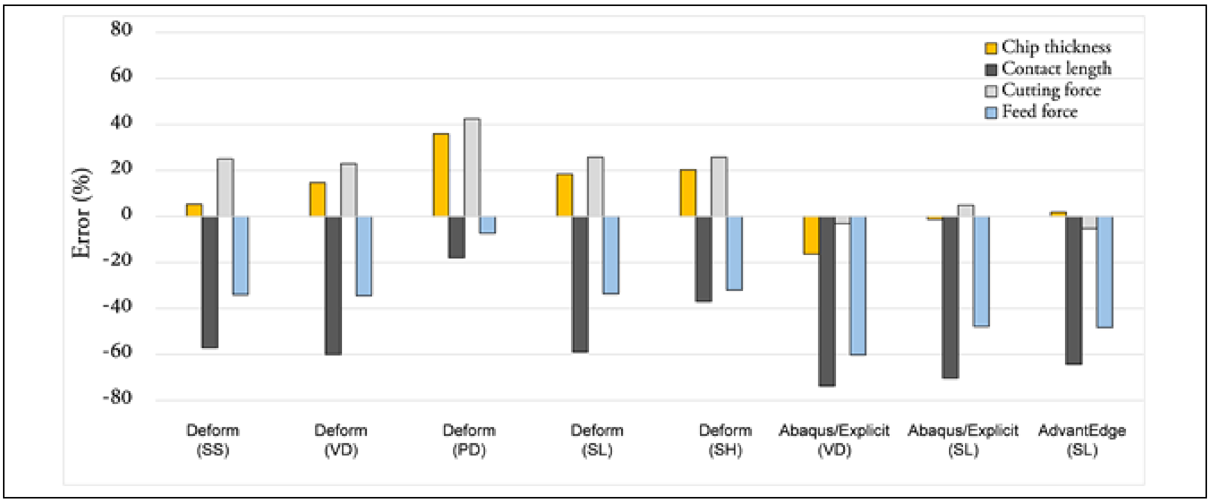

Figure 4-9. The error percentage in simulated responses using different FE codes and friction models: AISI 1045, cutting condition A. The experimental results given in Table 4 was considered as the reference.

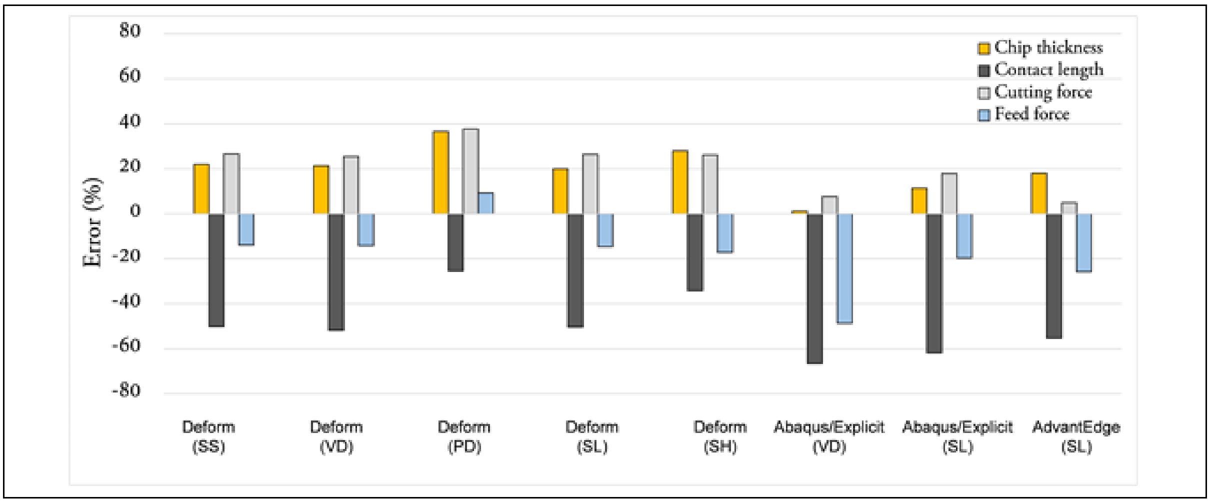

Figure 4-10. The error percentage in simulated responses using different FE codes and friction models: AISI 1045, cutting condition B. The experimental results given in Table 4 was considered as the reference

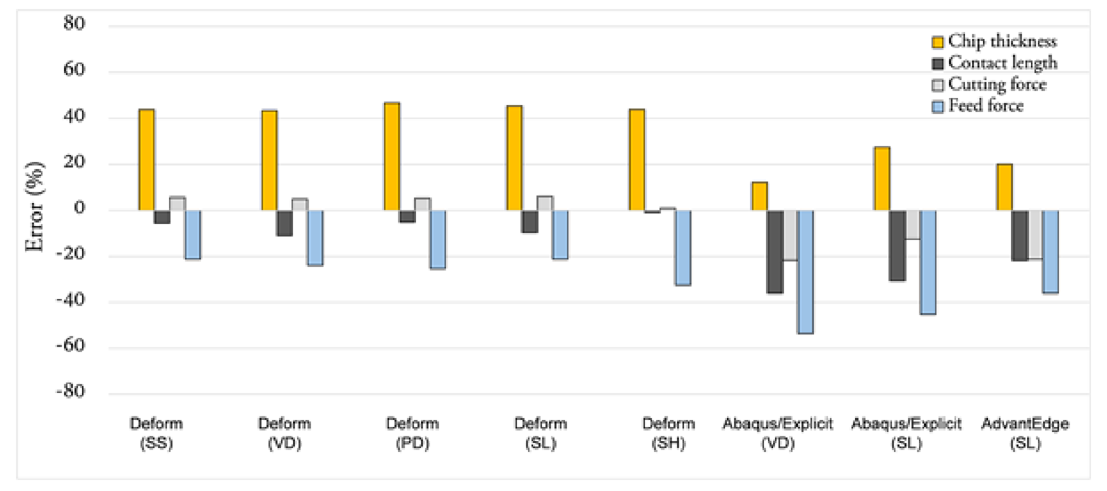

Figure 4-11. The error percentage in simulated responses using different FE codes and friction models: AISI 1080, cutting condition B. The experimental results given in Table 4 was considered as the reference.

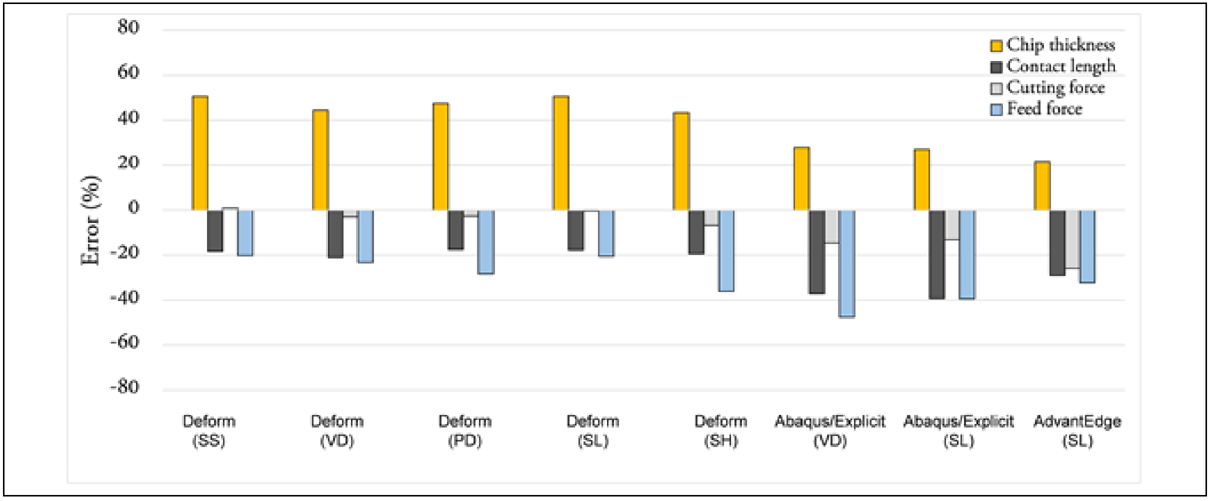

Figure 4-12. The error percentage in simulated responses using different FE codes and friction models: AISI 1080, cutting condition C. The experimental results given in Table 4 was considered as the reference.

4.5 Discussion

The methodology presented in the current study provided a more systematic evaluation of the friction models compared to the previous attempts, where often the error in feed force predictions was considered as the main factor for the assessment of the viability of the adopted friction models [6, 8]. In the current approach, on the contrary, the optimum friction parameters were initially determined for each model by adjusting an identical impact for all the responses under investigation during the optimisation process. Evaluation of the FE simulation results utilising the optimum sets of parameters indicated that the performance of the friction models in terms of the average prediction error of all investigated responses was nearly identical for K10/AISI 1045 tool-work material combination, although the adopted pressure dependent shear friction model in Deform 2D resulted in a slightly smaller percentage of the average error. This is due to the fact that the distribution of the error between the simulated responses varies by implementation of different friction models. Hence, for instance, while the pressure dependent shear friction model implemented in Deform 2D resulted in the least deviation from the experimental measurements of contact length and feed force for K10/AISI 1045 tool-work material combination at both cutting conditions, larger deviations were attained for the cutting force and chip thickness compared to the other adopted friction models. Therefore, the calculated average error becomes nearly identical for all friction models. As can be seen in Figure 4-9 to Figure 4-12, the distribution of the error between the simulated responses also varies for a certain friction model (e.g. sliding friction model) adopted in different FE codes. This perhaps stems from the differences in FE formulations in terms of the element type definition, thermo-mechanical coupling and the assumptions associated with the adaptive remeshing and ALE formulations in various FE codes. However, certain patterns can still be noted in the distribution of the error between the simulated responses. For instance, all FE models underestimated the feed force and the tool-chip contact length for the K10/AISI 1045 tool-work material combination, while the cutting force and the chip thickness were overestimated in most cases. On the other hand, for H13A/AISI 1080 tool-work material combination, the FE models only overestimated the chip thickness at both cutting conditions, independent of the FE code and the friction model used for simulation chip formation process. However, the calculated average errors in this case are typically smaller than those of K10/AISI 1045 tool/work material combinations shown in Figure 4-9 and Figure 4-10. This perhaps reflects the importance of the implementation of a well-defined constitutive model to describe the material deformation within the common range of strain, strain rate and temperature encountered in metal cutting process. As noted in section 3.2, the JC material parameters for the AISI 1080 carbon steel were obtained using inverse modelling of the orthogonal cutting process, which can perhaps better represent the material deformation during the chip formation process. The importance of a well-defined constitutive model to achieve reliable FE simulation results has also been stressed by other authors [19]. Özel [6] and Iqbal et al. [55] investigated the viability of various friction models to describe the frictional condition at the tool-chip interface. Özel [6] reported that the implementation of the variable shear friction model can significantly improve the feed force predictions, however, up to 50% error in cutting force estimations was still noted at various ranges of the cutting speeds. Iqbal et al. [55] showed that a realistic definition of the sticking-sliding contact lengths determined by SEM-EDX analyses of the contact region [38] on the rake face of the tools can enhance the reliability of FE simulation results. Yet, the authors reported as high as 30% error in cutting force predictions, despite a more realistic description of the sliding-sticking contact regions in the FE models. It was therefore concluded that the simulation errors cannot be further reduced, unless an appropriate constitutive model with well-defined parameters is adopted for FE simulation of chip formation process. A similar conclusion can be made by evaluation of the results in the current study, see for instance the calculated error percentage presented in Figure 4-9 to Figure 4-12 for the optimum sets of friction coefficients. Nevertheless, one may still critically discuss the viability of the friction models and the ranges of friction parameters adopted in the current study to represent the frictional condition at the tool-chip interface regardless of the influence of the constitutive model and FE formulations implemented for simulation of chip formation process. As mentioned in section 2, the velocity dependent Coulomb friction model (VD) in this study was derived based on the experimental data of a tailored tribometer test presented by Puls et al. [42]. The apparent Coulomb friction coefficient measured by the authors varied between 0.6 and 0.2 with increasing sliding velocity from 25 m/min to 200 m/min. It should be noted that this range of Coulomb friction coefficient has been widely accepted for FE modelling of the cutting process [30, 56, 57]. A similar range of friction coefficient was therefore adopted in the current study to evaluate the performance of the Coulomb friction (SL) model. However, as depicted in Figure 4-13, the calculation of the mean (apparent) friction coefficient based on the orthogonal cutting force analysis presented by Merchant [23] (see Eq. 4-4) suggests a significantly larger values for K10/AISI 1045 tool-work material combination. Furthermore, as evident from Figure 4-13, the mean friction coefficient varied with both feed rate and the cutting speed. Similar analyses by Merchant [23], Zorev [26], Usui et al. [24] and Bailey [58] showed that, in general, the mean friction coefficient in metal cutting varied with feed rate, cutting speed, the tool rake angle and the presence of lubrication. As shown by Usui et al. [24] and more recently by Atkins [25], the variation in the mean friction coefficient is, in fact, due to the variation in the relative proportion of sticking-sliding friction zones with the cutting parameters and the tool geometry. Obviously, such frictional behaviour cannot be fully reproduced by the tribometer tests and hence the measured values of the mean friction coefficient by those instruments may not represent the frictional condition within the entire

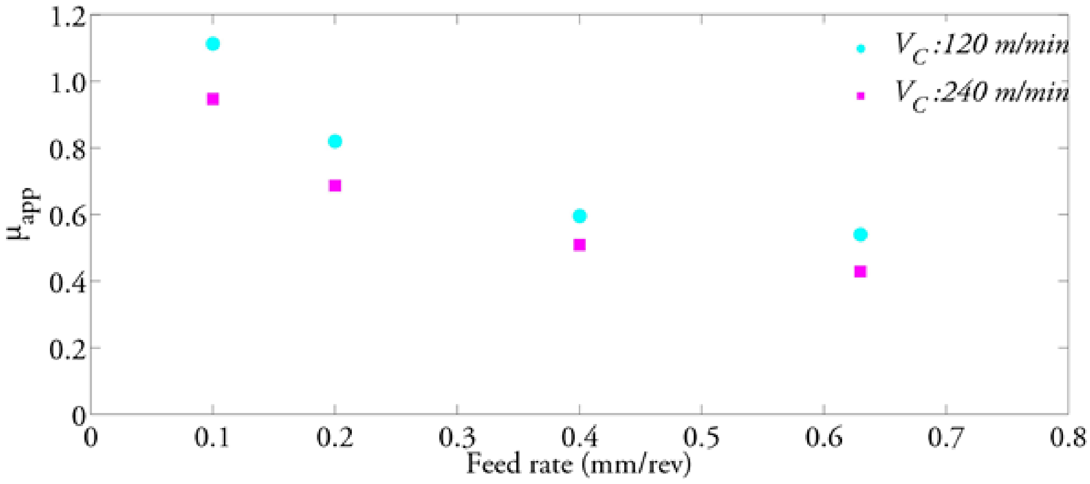

Figure 4-13. The variation in mean friction coefficient with feed rate and cutting speed calculated using Merchant [23] analysis of orthogonal cutting/feed force data provided by Jaspers [45] for K10/AISI1045 tool-work material combination.

range of cutting data and for all different tool geometries. The additional limitation of the tribometer test data is that the influence of sliding velocity and interface temperature on the measured mean friction coefficients cannot be easily separated, and therefore it is difficult to evaluate.

Figure 4-14 shows the variation of the velocity dependent friction coefficient (Eq. 4-5) as well as the estimated sliding velocity and the interface temperature along the contact length for H13A/AISI 1080 at cutting conditions B and C (see Table 4-3). As evident, the FE simulation results suggested that the sliding velocity increases along the contact length from zero near the cutting edge to nearly one third of the cutting speed (i.e. VS,Max≈1/3VC) as the chip leaves the rake face of the tool, while the interface temperature passes through its maximum in the middle of the contact region. In tribometer tests, however, the interface temperature and sliding velocity are directly proportional, i.e. with an increase in the sliding velocity the interface temperature increases. Hence, the mean friction coefficient obtained by tribometer instruments and the mathematical expression in the form of Equation 5 may not fully express of the tribological condition on the tool-chip interface.

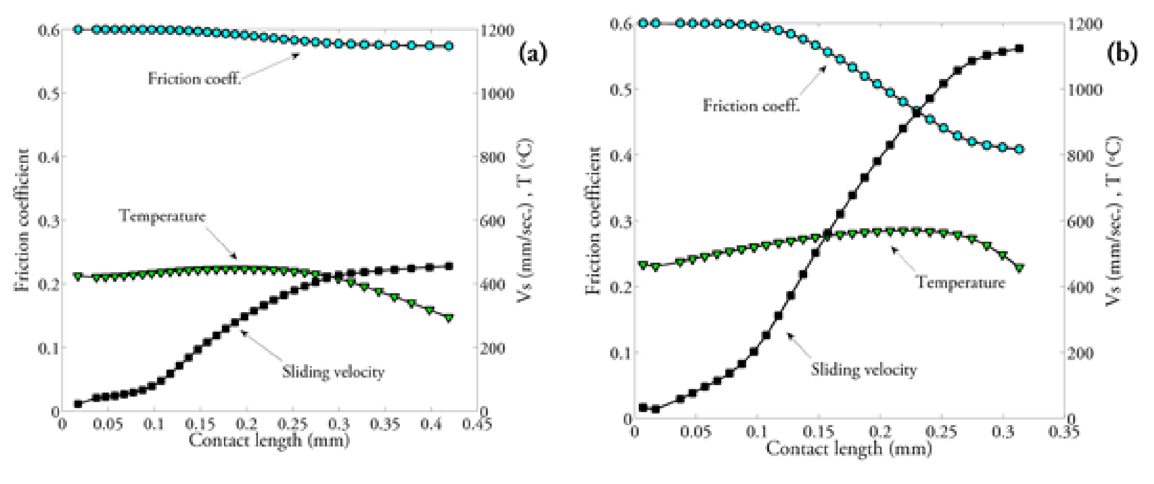

Figure 4-14. The variation of velocity dependent (VD) friction coefficient together with sliding velocity along the contact length: AISI 1080, cutting conditions B (a) and C (b). The process was simulated using Deform FE code.

In light of these considerations, the sliding-sticking and pressure dependent shear friction models are perhaps the most physically relevant expressions to describe the frictional condition at the tool-chip interface. Figure 4-15 shows the variation in pressure dependent shear friction coefficient as well as the predicted normal and shear stresses along the contact length. As evident, the shear friction coefficient reduces with decreasing the normal pressure according the Eq. 4-3. On the other hand, the shear strength of the work material varies with the strain, strain rate and temperature along the contact length according to the implemented constitutive model. Hence, in addition to the normal pressure, this model includes the influence of temperature and material deformation on the friction stress along the contact length in an indirect manner. As mentioned earlier, however, further improvement in prediction results is solely possible if a more viable constitutive model is adopted to describe the severe material deformation during the chip formation process.

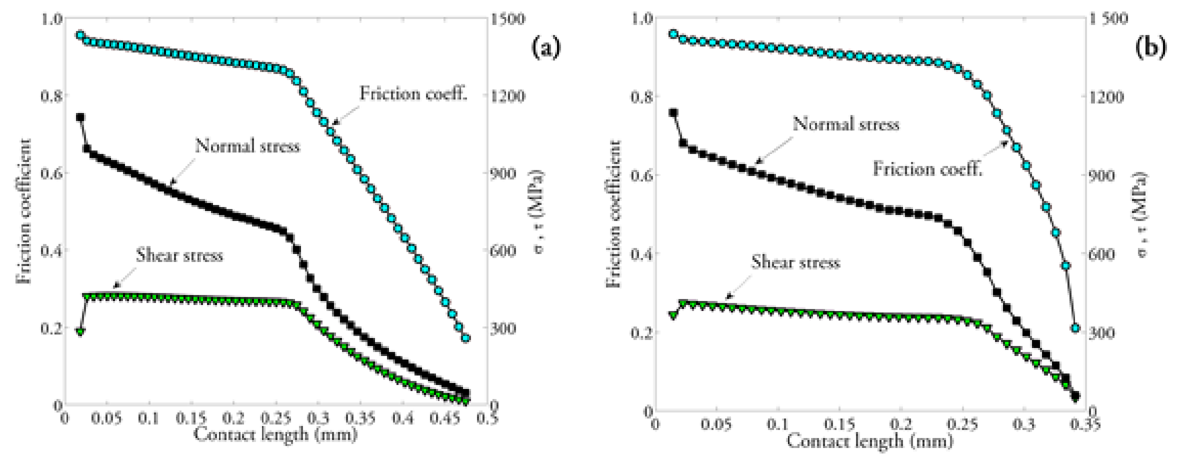

Figure 4-15. The variation of velocity dependent (VD) friction coefficient together with sliding velocity along the contact length: AISI 1080, cutting conditions B (a) and C (b). The process was simulated using Deform FE code.

4.6 Conclusions

In the current study, a systematic approach was presented to evaluate the performance of various friction models in FE simulation of the orthogonal cutting process using three different FE commercial codes; Deform 2D, Abaqus/Explicit and AdvantEdge. In this approach, the optimum sets of friction parameters that led to the least deviation from the experimental measurements of orthogonal cutting process were initially determined for each model and the viability of each one was assessed under its optimum condition. Two different working conditions have been considered (K10/AISI 1045 and H13A/AISI 1080) and the following conclusions can be summarized:

- The friction coefficients had a large influence on the FE simulation results. However, the results of the current study indicated that, for both tool-work material combinations and independently of the FE commercial code, nearly an identical range of minimum average error was attained for all adopted friction models.
- The similar range of average error is believed to be due to inability of the JC constitutive model to properly describe the severe deformation condition within the primary and secondary shear zones.
- The analysis of the experimental orthogonal cutting forces indicated the mean Coulomb friction coefficients as high as 1.2 at low ranges of the feed rate.
- The sliding-sticking and pressure dependent shear friction models provide the most physically relevant expressions for the simulation of frictional condition at the tool-chip interface.

4.7 Acknowledgement

The authors acknowledge VINNOVA (Swedish Agency for Innovation Systems) within the framework of the FFI programme and the Area of Advance Production at Chalmers University of Technology for financial support. Special thanks are also extended to Adjunct Professor Ibrahim Sadik from Sandvik Coromant for his support.

4.8 References

[1] Y. B. Guo, "An integral method to determine the mechanical behavior of materials in metal cutting," Journal of Materials Processing Technology, vol. 142, pp. 72-81, 2003.

[2] K.-D. Bouzakis, N. Michailidis, G. Skordaris, E. Bouzakis, D. Biermann, and R. M'Saoubi, "Cutting with coated tools: Coating technologies, characterization methods and performance optimization," CIRP Annals - Manufacturing Technology, vol. 61, pp. 703-723, 2012.

[3] A. Attanasio, E. Ceretti, A. Fiorentino, C. Cappellini, and C. Giardini, "Investigation and FEM-based simulation of tool wear in turning operations with uncoated carbide tools," Wear, vol. 269, pp. 344-350, 2010.

[4] A. Malakizadi, S. Cedergren, K. B. Surreddi, and L. Nyborg, "A methodology to evaluate the machinability of Alloy 718 by means of FE simulation," presented at the Advanced Manufacturing Engineering and Technologies NEWTECH, Stockholm, 2013.

[5] M. Binder, F. Klocke, and D. Lung, "Tool wear simulation of complex shaped coated cutting tools," Wear, vol. 330–331, pp. 600-607, 2015.

[6] T. Özel, "The influence of friction models on finite element simulations of machining," International Journal of Machine Tools and Manufacture, vol. 46, pp. 518-530, 2006.

[7] V. Kalhori, "Modelling and simulation of mechanical cutting " PhD, Mechanical Engineering, Lulea University of Technology 2001.

[8] J. Rech, P. J. Arrazola, C. Claudin, C. Courbon, F. Pusavec, and J. Kopac, "Characterisation of friction and heat partition coefficients at the tool-work material interface in cutting," CIRP Annals - Manufacturing Technology, vol. 62, pp. 79-82, 2013.

[9] A. Svoboda, D. Wedberg, and L. E. Lindgren, "Simulation of metal cutting using a physically based plasticity model," Modelling and Simulation in Materials Science and Engineering, vol. 18, pp. 1-19, 2010.

[10] H. Chandrasekaran, R. M'Saoubi, and H. Chazal, "Modelling of material flow stress in chip formation process from orthogonal milling and split Hopkinson bar tests," Machining Science and Technology, vol. 9, pp. 131-145, 2005.

[11] A. Malakizadi, S. Cedergren, I. Sadik, and L. Nyborg, "Inverse identification of flow stress in metal cutting process using Response Surface Methodology," Simulation Modelling Practice and Theory, vol. 60, pp. 40-53, 2016.

[12] D. Ulutan and T. Özel, "Determination of Constitutive Material Model Parameters in FE-Based Machining Simulations of Ti-6Al-4V and IN-100 Alloys: An Inverse Methodology," Proceedings of NAMRI/SME, vol. 41, 2013.

[13] M. Daoud, W. Jomaa, J. F. Chatelain, and A. Bouzid, "A machining-based methodology to identify material constitutive law for finite element simulation," The International Journal of Advanced Manufacturing Technology, vol. 77, pp. 2019-2033, 2015.

[14] A. Del Prete, L. Filice, and D. Umbrello, "Numerical Simulation of Machining Nickel-Based Alloys," Procedia CIRP, vol. 8, pp. 540-545, 2013.

[15] A. Malakizadi, I. Sadik, and L. Nyborg, "Wear Mechanism of CBN Inserts During Machining of Bimetal Aluminum-grey Cast Iron Engine Block," Procedia CIRP, vol. 8, pp. 188-193, 2013.

[16] D. Xu, P. Feng, W. Li, and Y. Ma, "An improved material constitutive model for simulation of high-speed cutting of 6061-T6 aluminum alloy with high accuracy," The International Journal of Advanced Manufacturing Technology, vol. 79, pp. 1043-1053, 2015.

[17] Y. Yang and W. Zhu, "Study on cutting temperature during milling of titanium alloy based on FEM and experiment," The International Journal of Advanced Manufacturing Technology, vol. 73, pp. 1511-1521, 2014.

[18] H. Chandrasekaran and D. V. Kapoor, "Photoelastic analysis of tool-chip interface stresses," Journal of Engineering for Industry, vol. 87, pp. 495-502, 1965.

[19] T. H. C. Childs, "Friction modelling in metal cutting," Wear, vol. 260, pp. 310-318, 2006.

[20] F. Zemzemi, J. Rech, W. Ben Salem, A. Dogui, and P. Kapsa, "Identification of a friction model at tool/chip/workpiece interfaces in dry machining of AISI4142 treated steels," Journal of Materials Processing Technology, vol. 209, pp. 3978-3990, 2009.

[21] J. Rech, C. Claudin, and E. D’Eramo, "Identification of a friction model—Application to the context of dry cutting of an AISI 1045 annealed steel with a TiN-coated carbide tool," Tribology International, vol. 42, pp. 738-744, 2009.

[22] D. Smolenicki, J. Boos, F. Kuster, H. Roelofs, and C. F. Wyen, "In-process measurement of friction coefficient in orthogonal cutting," CIRP Annals - Manufacturing Technology, vol. 63, pp. 97-100, 2014.

[23] M. E. Merchant, "Mechanics of the metal cutting process. I. orthogonal cutting and a type 2 chip," Journal of Applied Physics, vol. 16, pp. 267-275, 1945.

[24] E. Usui, K. Kikuchi, and K. Hoshi, "The theory of plasticity applied to machining with cut-away tools," Journal of Engineering for Industry, vol. 86, pp. 95-104, 1964.

[25] T. Atkins, "Prediction of sticking and sliding lengths on the rake faces of tools using cutting forces," International Journal of Mechanical Sciences, vol. 91, pp. 33-45, 2015.

[26] N. N. Zorev, Metal cutting mechanics. Oxford, England: Pergamon Press, 1966.

[27] P. Hedenqvist and M. Olsson, "Sliding wear testing of coated cutting tool materials," Tribology International, vol. 24, pp. 143-150, 1991.

[28] H. Puls, F. Klocke, and D. Lung, "Experimental investigation on friction under metal cutting conditions," Wear, vol. 310, pp. 63-71, 2014.

[29] K. Hosseinkhani and E. Ng, "A combined empirical and numerical approach for tool wear prediction in machining," Procedia CIRP, vol. 31, pp. 304-309, 2015.

[30] K. Hosseinkhani and E. Ng, "Analysis of the cutting mechanics under the influence of worn tool geometry," Procedia CIRP, vol. 8, pp. 117-122, 2013.

[31] H. Bil, S. E. Kılıç, and A. E. Tekkaya, "A comparison of orthogonal cutting data from experiments with three different finite element models," International Journal of Machine Tools and Manufacture, vol. 44, pp. 933-944, 2004.

[32] P. J. Arrazola, A. Villar, D. Ugarte, and S. Marya, "Serrated chip prediction in finite element modeling of the chip formation process," Machining Science and Technology, vol. 11, pp. 367-390, 2007.

[33] M. Vaz, Jr., D. R. J. Owen, V. Kalhori, M. Lundblad, and L. E. Lindgren, "Modelling and Simulation of Machining Processes," Archives of Computational Methods in Engineering, vol. 14, pp. 173-204, 2007.

[34] B. Shi and H. Attia, "Modeling the Thermal and Tribological Processes at the Tool-Chip Interface in Machining," Machining Science and Technology, vol. 13, pp. 210-226, 2009.

[35] H. Puls, F. Klocke, and D. Veselovac, "FEM-based prediction of heat partition in dry metal cutting of AISI 1045," The International Journal of Advanced Manufacturing Technology, pp. 1-9, 2015.

[36] P. J. Arrazola and T. r. Özel, "Investigations on the effects of friction modeling in finite element simulation of machining," International Journal of Mechanical Sciences, vol. 52, pp. 31-42, 2010.

[37] E. M. Trent and P. K. Wright, Metal cutting. Boston: Butterworth-Heinemann, 2000.

[38] S. A. Iqbal, P. T. Mativenga, and M. A. Sheikh, "Characterization of machining of AISI 1045 steel over a wide range of cutting speeds. Part 1: Investigation of contact phenomena," Proceedings of the Institution of Mechanical Engineers, Part B: Journal of Engineering Manufacture, vol. 221, pp. 909-916, 2007.

[39] I. Finnie and S. M. C., "The friction process in metal cutting," Transactions of ASME 78, vol. 78, pp. 1649-1657, 1956.

[40] T. Shirakashi and U. E., "Friction characteristics on tool face in metal machining " Journal of Japan Society for precision Engineering, vol. 39, pp. 966-972, 1973.

[41] T. Childs, K. Maekawa, T. Obikawa, and Y. Yamane, Metal Machining: Theory and Applications. Newyork, America: John Wiley & Sons Inc., 2000.

[42] H. Puls, F. Klocke, and D. Lung, "A new experimental methodology to analyse the friction behaviour at the tool-chip interface in metal cutting," Production Engineering, vol. 6, pp. 349-354, 2012.

[43] A. Bordin, S. Imbrogno, G. Rotella, S. Bruschi, A. Ghiotti, and D. Umbrello, "Finite Element Simulation of Semi-finishing Turning of Electron Beam Melted Ti6Al4V Under Dry and Cryogenic Cooling," Procedia CIRP, vol. 31, pp. 551-556, 2015.

[44] H. Demuth and M. Beale, Neural network toolbox for use with MATLAB: MathWorks, 1993.

[45] S. P. F. C. Jaspers, "Metal Cutting Mechanics and Material Behavior," PhD Technische Universiteit Eindhoven, 1999.

[46] T. D. Marusich and M. Ortiz, "Modelling and simulation of high-speed machining," International Journal for Numerical Methods in Engineering, vol. 38, pp. 3675-3694, 1995.

[47] J. Wang and M. S. Gadala, "Formulation and survey of ALE method in nonlinear solid mechanics," Finite Elements in Analysis and Design, vol. 24, pp. 253-269, 1997.

[48] S. M. T. Halim, "Finite element modeling of the orthogonal metal cutting process: modeling the effects of coefficient of friction and tool holding structure on cutting forces and chip thickness," PhD, McMaster University, 2008.

[49] Z. Guo, N. Saunders, J. P. Schillé, and A. P. Miodownik, "Material properties for process simulation," Materials Science and Engineering: A, vol. 499, pp. 7-13, 2009.

[50] F. Klocke, Manufacturing Processing I: Cutting, RWTH ed.: Springerlink, 2011.

[51] T. Thepsonthi and T. Özel, "3-D finite element process simulation of micro-end milling Ti-6Al-4V titanium alloy: Experimental validations on chip flow and tool wear," Journal of Materials Processing Technology, vol. 221, pp. 128-145, 2015.

[52] G. Rotella, O. W. Dillon Jr, D. Umbrello, L. Settineri, and I. S. Jawahir, "Finite element modeling of microstructural changes in turning of AA7075-T651 Alloy," Journal of Manufacturing Processes, vol. 15, pp. 87-95, 2013.

[53] F. Jafarian, M. Imaz Ciaran, D. Umbrello, P. J. Arrazola, L. Filice, and H. Amirabadi, "Finite element simulation of machining Inconel 718 alloy including microstructure changes," International Journal of Mechanical Sciences, vol. 88, pp. 110-121, 2014.

[54] G. S. Sekhon and J. L. Chenot, "Numerical simulation of continuous chip formation during non-steady orthogonal cutting " Engineering computations, vol. 10, pp. 31-48, 1993.

[55] S. A. Iqbal, P. T. Mativenga, and M. A. Sheikh, "Characterization of the Machining of AISI 1045 steel over a wide range of cutting speeds-Part 2: Evaluation of flow stress models and interface friction distribution schemes," Proceedings of the Institution of Mechanical Engineers Part B Journal of Engineering Manufacture vol. 221, pp. 917-926, 2007.

[56] F. Klocke, H. W. Raedt, and S. Hoppe, "2D-FEM simulation of the orthogonal high speed cutting process," Machining Science and Technology, vol. 5, pp. 323-340, 2001.

[57] E. G. Ng, D. K. Aspinwall, D. Brazil, and J. Monaghan, "Modelling of temperature and forces when orthogonally machining hardened steel," International Journal of Machine Tools and Manufacture, vol. 39, pp. 885-903, 1999.

[58] J. A. Bailey, "Friction in metal machining—Mechanical aspects," Wear, vol. 31, pp. 243-275, 1975.

5 PAPER 2: FINITE ELEMENT SIMULATION OF CUTTING PROCESS UNDER THE WORN TOOL EDGE GEOMETRIES

This chapter is a copy of the paper published in the Journal of Advanced Manufacturing Technology. It presents first phase of tool life prediction methodology and focuses on evaluating the accuracy of finite element simulation of cutting process under the worn tool geometry. For simulations, the experimentally obtained worn tool edge geometries are employed in the cutting simulations and the required thermal and mechanical process variables are determined. The simulated results were validated based on conventional direct a unique indirect method. The main conclusion of this paper was the validation of the finite element models of cutting process in simulating the process variables, which are going to be used as input in the empirical wear rate models.

Authors: Keyvan Hosseinkhani, E. Ng

The International Journal of Advanced Manufacturing Technology volume 116, pages 3991–4006 (2021)

Abstract.

Finite element (FE) technique has been used extensively to have a deeper understanding on the mechanics of metal cutting and for process optimization. The accuracy of the model is dependent on both the highly non-linear material plasticity model and the simulated friction condition between contacting surfaces. Hence majority of the predicted results were validated from direct or indirect experimental results. Measurement of cutting forces magnitude and temperature field are direct technique to validate the model. Indirect methods are chip morphology and residual stresses measurement from the newly generated surface. In this paper, a unique indirect method is proposed to validate the accuracy of the FE model. This method predicts the tool wear rate by using the average contact pressure and interface temperature acquired from finite element simulation, as the inputs for the Usui's tool wear rate equation. Orthogonal cutting experiments were performed in specific ranges of cutting speed and feed rate. The workpiece material used was AISI 1045 at 86 HRB and tool material was uncoated carbide. Tool cutting edge geometry was analyzed in different steps of the cutting process and worn edge geometries were obtained. The worn edge geometries were then used to build the FE cutting models. Based on the simulation results when the flank wear length increases, the temperature field prediction showed that the region of maximum temperature shifted from the rake face to the flank face region. The contact pressure increased substantially with cutting speed rather than feed rate. The predicted wear rate agreed well with experimental results. Using tool wear rate to predict the accuracy of the FE cutting model is limited to the orientation of the rake and flank face surfaces.

Keywords: Finite Element Simulation, Cutting and Feed Forces, Temperature, Contact Pressure, Tool Wear

5.1 Introduction

In machining, workpiece material undergoes large plastic deformation which is coupled with high strain rate and temperature. This complex nature of deformation makes the development of predictive, rather than descriptive, analytical models very challenging. At the same time experimentally developed empirical models, which are highly limited to specific boundary conditions, are time consuming and expensive to calibrate.

In recent years with the rapid advancement in computational capabilities, finite element (FE) models have been increasingly used for simulating the chip formation process in machining. FE simulations are numerical models which incorporate the constitutive material model as well as the friction model to simulate the complex workpiece deformation and tool-workpiece contact. Once a FE cutting model is validated, it can provide a unique insight into the process mechanics and reduce the number of design iterations required for process optimization and tool design. Also, in contrast to analytical models, FE models keep the history of the cutting process required for the analysis of sequential cuts.

To investigate the accuracy of the FE models, the simulated results are validated from direct or indirect experimental results. Comparing the simulated results with experimentally obtained measurements of forces and temperature field are direct technique to validate the models. Indirect techniques include the comparison of the predicted chip morphology and residual stresses with the experimental analysis of the chips and from the newly generated surfaces.

Movahhedy, et al. [1] simulated the chip formation process based on a unique approach known as Arbitrary Lagrangian-Eulerian (ALE). The FE models were validated by comparing the simulated forces, normal stresses, frictional stresses and temperature with experiments.

Ng, et al [2] simulated the continuous and segmental chip formation in high-speed machining in two- and three-dimensional environment based on a unique Lagrangian approach.

Ng validated the models by comparing the predicted forces and deformed chip thickness with experiment. The models were then used to investigate the temperature and plastic strain distribution in the cutting zone. The models were also used to simulate the effects of flank wear geometry on chip formation to provide insight on forces, temperature, and residual stresses in the cutting zone [3]. The simulation results showed that increase in the flank wear increased the temperature and tensile residual stresses in the newly machined surface.

Considering the importance of tool cutting edge geometry on the mechanics of machining, Yen, et al. [4] simulated the effect of tool cutting edge preparation on the chip formation process. Tool cutting edges were in the form of round and chamfered geometries. Yen validated the models by comparing the predicted cutting forces and chip geometries with the experiments when cutting with round cutting edges. The models were then used to investigate the temperature and plastic strain distributions. The validated models were also used to analyze the forces and temperature distribution for cutting with the chamfered tool edge. Nasr, et al [5] modelled the effects of tool-edge radius on the residual stresses in the newly generated surface using an ALE approach. To validate the results of the FE model, Nasr compared the predicted machining induced residual stresses in several depth from the machined surface with the experimental measurements.

Özel [6] simulated the effect of different friction models on the outputs of the chip formation process. To investigate the validity of the friction models, the predicted cutting and feed forces, shear angle, temperature and stress distribution on the rake face were compared with experimental data.

Considering the importance of tool wear on the mechanics of cutting, Li, et al. [7] simulated the effects of including the crater wear geometry on chip formation process. The FE models were validated by comparing the cutting and feed forces on a tool with no crater wear. The validated concept was then used to simulate and analyze the stresses, temperature, and forces when different crater wear geometries were included on the cutting tool. The simulation results showed that regardless of crater geometry, formation of crate wear resulted in both cutting and feed forces to decrease.

Hosseinkhani and Ng [8] simulated the effect of flank wear geometry on the chip formation process. To validate the models, the simulated results of cutting and feed forces and chip thickness were compared with experiments. The simulations were then used to provide insight into the effect of flank wear geometry on the temperature distribution and mechanical stresses in the cutting zone.

Sanchez, et al. [9] employed flank and crater wear geometries, on a round edge tool, to build finite element models in order to investigate the effects of wear on the residual stresses. The results of the FE simulations were validated by comparing the machining induced residual stresses with experiments. Based on the experimentally validated results, Sanchez concluded that formation of any type of wear results in higher induced tensile residual stresses in the workpiece material.

Boyd, et. al. [10] investigated the effect of temperature-dependent friction models on the FE simulation of the cutting process based on unworn and worn tool geometry. For validation, the simulated cutting and feed forces were compared with experiment. Boyd concluded that the cutting and feed forces were overestimated when the cutting process was simulated using an unworn tool. When the worn tool geometry was included in the simulation the cutting and feed forces were in closer agreement with experiment.

Wan, et. al. [11] investigated the feasibility FE modeling in estimating the near-surface residual stresses of Inconel 718 during ball-end milling process. To validate the models, Wang compared the estimated residual stresses with experimental measurements and concluded that the simulation results are efficient but still need improvement.

Duboust, et. al. [12] simulated the effect of cutting edge radius, cutting speed, fibre orientation and feed rate on the cutting forces when machining carbon fibre reinforced plastics. To validate the FE models, the simulated results of cutting forces were compared with experiment. While the increasing trend in the cutting force with the increase in the cutting edge radius was simulated successfully, the magnitude of cutting forces were under-estimated the experiment. It was also observed that cutting edge radius and feed rate have more significant influence on the cutting forces than fibre orientation and cutting speed. The simulations were then used to investigate the mechanical stresses and equivalent strain on the surface of the composites during machining.

Uçak, et. al. [13] simulated the drilling of Inconel 718 superalloy using an uncoated solid carbide drill. For validation, the simulated results of feed forces, torque and temperature were compared with experimental measurements which they all showed good agreement. Uçak concluded that the models can then be used confidently for process optimization and tool design.

The objective of this paper is to simulate the effects of tool wear geometries and process parameters when orthogonal cutting of AISI 1045 with uncoated carbide tool. Simulated results were validated from direct and indirect methods. In the direct method, both cutting and feed forces acquired from experiments were compared with predicted results. Following from here, a unique indirect method is used to validate the accuracy of the FE model. This method predicts the tool wear rate using Usui’s empirical tool wear rate equation. Usui’s equation is a function of contact pressure and temperature along the flank face of the tool, which is acquired from the finite element simulated results. Finally, the comparison of the predicted tool wear rate against the experimental wear rate is used to justify the validation of the FE models. If the unique indirect method proofs to be successful, it will reduce the time, cost and repeatability to validate the simulated results when compared to direct methods or other indirect methods.

5.2 Finite Element Simulation

The orthogonal cutting process was simulated based on the principles of Arbitrary Eulerian Lagrangian (ALE) technique and the assumptions that deformation was plane strain and chip formation was continuous type. The simulation was a dynamic temperature-displacement type, which allowed for including the temperature dependent properties and heat transfer. Explicit solver in ABAQUS was used, as the cutting process has transient and included high level of material and geometric nonlinearities. The elements used in the FE models were plane strain CPE4RT. These elements were quadrilateral and thermal-mechanical with reduced integration and automatic hourglass control properties. The hourglass control property has been used for handling high deformation induced by the cutting process.

5.2.1 Material properties

The physical and mechanical properties of the tool and work materials are detailed in Table 5-1. Tool material was considered fully elastic while elastic and plastic properties of workpiece material were included. The microstructural properties of tool and workpiece were neglected, and both were assumed to be homogenous and isotropic. The Johnson-Cook (J-C) constitutive model, Eq. 5-1, which is a particular type of Mises plasticity empirical model, was used to include the effect of strain, strain-rate, and temperature on the plastic deformation of the workpiece material [14].

$$\sigma=\left(A+B\varepsilon_{pl}^{n}\right)\left[1+C\,ln\left(\dot{\varepsilon}_{pl}/\dot{\varepsilon}_{0}\right)\right]\left\{1-\left[\left(T-T_{ref}\right)/\left(T_{melt}-T_{ref}\right)\right]^{m}\right\} \qquad \text{Eq. 5-1}$$

In the Johnson-Cook model σ, ε_{pl}, $\dot{\varepsilon}_{pl}$, $\dot{\varepsilon}_{0}$, and T, represent the Von Mises flow stress, the equivalent plastic strain and strain rate, the initial strain rate, and the operating temperature respectively. Table 5-2 lists the constants “*A*”, “*B*”, “*C*”, “*n*”, and “*m*” which were used in the

Material	Modulus of Elasticity (GPa)	Poisson's Ratio	Density (kg/m^3)	Thermal Conductivity (W/m°C)	Specific Heat Capacity (J/kg°C)	Thermal Expansion (°C^{-1}x10^6)
AISI 1045	205	0.33	7850	46 (20°C) 40 (250°C) 34 (500°C) 27 (750°C) 26 (1000°C)	470 (20°C) 535 (200°C) 635 (400°C) 800 (600°C)	10.1 (20°C) 12.0 (200°C) 13.0 (400°C) 15.3 (600°C)
Uncoated Carbide TNMG332QM-H13A	560	0.22	14500	34 (20°C) 38 (250°C) 42 (500°C) 45 (750°C) 47 (1000°C)	220	5.2(20°C) 5.3(200°C) 5.4(400°C) 5.6(600°C)

Table 5-1. Physical and mechanical properties of work and tool materials [16, 17].

A (MPa)	B (MPa)	n	C	$\dot{\varepsilon}_0$	T_{ref} (°C)	m
553.1	600.8	0.234	0.0134	1.0	25	1.0

Table 5-2. Johnson-Cook constants for AISI 1045 [11].

Johnson-Cook model for AISI 1045, as determined by [15]. T_{ref} is the reference temperature at which material constants have been obtained.

The *A* constant in the Johnson-Cook model represents the yield strength of material being plastically deformed [14]. The *A* value determined by Jaspers & Dautzenberg [15] was very close to the *A* value estimated based on the hardness measurement of the AISI 1045 samples and relating that to the yield strength according to [18]. Hardness was measured at different sections of the workpiece material and was found to be 87±1 HRB scale.

5.2.2 Geometry and boundary conditions

Figure 5-1 illustrates the geometries of tool and workpiece with respect to the orthogonal cutting configuration as well as the boundary conditions of an ALE cutting model. The workpiece elements in the region in front of the cutting edge have been constrained from moving in x and y directions [5]. As the result, the severe deformation of material in front of

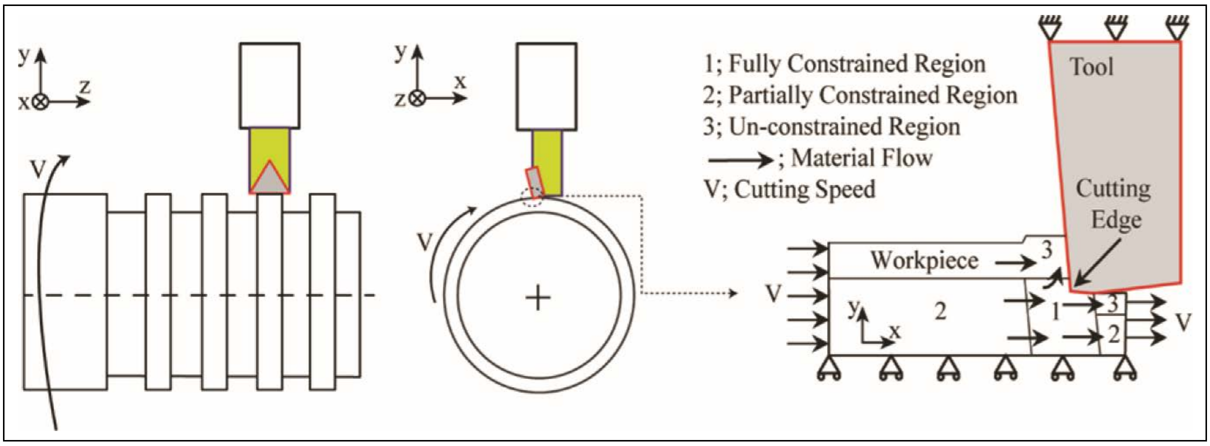

Figure 5-1. Geometry and boundary conditions in ALE model.

the tool tip does not lead to the severe element distortion. In the present study where the flank wear geometry was included in the simulation, the fully constrained region was extended to cover the workpiece elements below the tool flank – workpiece interface, as described in [8]. The workpiece elements in the region which form the chip and those which form the machined surface were kept un-constrained [5]. Therefore, the final chip geometry and the tool-chip contact length would be formed based on the natural deformation of the material. The elements in the rest of workpiece were only constrained from moving in y direction in order to increase the stability of simulation. In the current study, four different cutting edge geometries with specific flank wear lengths were employed. The orientation of the flank wear length will be discussed in the experimental work section.

5.2.3 Contact and friction

The interaction between the contacting surfaces has been modeled based on the Coulomb friction law in which the sticking and sliding conditions are functions of normal and shear stresses, as shown in Figure 5-2. Principles of coulomb friction The inequalities which represent the sticking and sliding regions are shown in Eq. 5-2 and Eq. 5-3 respectively:

$$\tau < \mu\sigma$$ Eq. 5-2

$$\tau \geq \mu\sigma \qquad \text{Eq. 5-3}$$

In Eq. 5-2 and Eq. 5-3, σ and τ are the normal and shear stresses acting the tool-workpiece interface and μ is the coefficient of friction (COF).

The COF data used in the current model was based on the experimental results acquired by Puls et.al. [19]. Puls et.al. employed a reverse orthogonal cutting set-up to determine the COF as a function of sliding velocity. In the experimental set-up, the workpiece was rotated in the opposite direction of the actual cutting process. The clearance angle of the tool acted as a highly negative rake angle, which caused severe plastic deformation of the workpiece material passing underneath. No chip is formed and the tool's cutting edge radius did not influence the measured normal and tangential forces. Therefore, the COF was determined as the ratio of tangential and normal forces measured on the inclined deformation plane. The results showed that COF decreased with higher cutting speed. The cutting speed range investigated were between 20 m/min to 200 m/min. Below 100 m/min, the COF ranged between 0.31 to 0.61. However above 100 m/min, the COF seemed to plateau between 0.20 to 0.31. In the current investigation, the magnitude of COF used is detailed in Table 5-3, which decreased by 0.01 with 50 m/min increased in cutting speed.

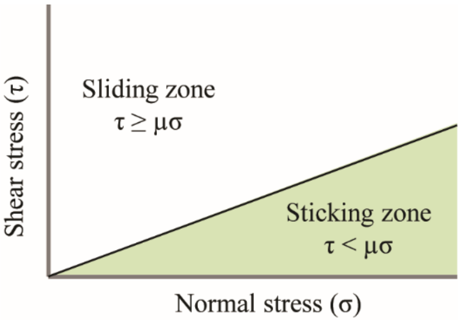

Figure 5-2. Principles of coulomb friction.

V (m/min)	200	250	300
μ	0.23	0.22	0.21

Table 5-3. Velocity dependent COF used in finite element simulations

5.2.4 Heat generation

Plastic deformation of workpiece and the sliding friction at the contacting interfaces are the main heat sources during metal cutting. The heat generated per unit volume due to plastic deformation of workpiece material has been detailed in Eq. 5-4:

$Q_{Pl}=\eta_m \sigma \dot{\varepsilon}$	Eq. 5-4

In Eq. 5-4, η_m is the inelastic heat fraction, σ is the plastic flow stress, and $\dot{\varepsilon}$ is the strain rate, [3]. Based on the Ng, et al. [2], the fraction of mechanical dissipation due to the plastic deformation of the work material which is converted into the heat is defined through the inelastic heat fraction and has been considered to be 0.9. This means that 90% of the mechanical energy due to plastic deformation has been converted into the heat.

The generated heat flux density due to the friction at interfaces is detailed in Eq. 5-5:

$q_f=\eta_f \tau_f (\Delta S/\Delta t)$	Eq. 5-5

In Eq. 5-5, τ_f is the frictional stress, ΔS is the incremental slip and Δt is the time increment [3]. The parameter η_f defines as the fraction of dissipated energy converted into heat which has been considered as 1.0 in the present study. The percentage of heat due to the friction which channelled into the chip or work, β_H, is shown in Eq. 5-6 and was related to the thermal emissivity of the workpiece material, E_w, and tool material, E_t. Eq. 5-7 shows the formula to determine the thermal emissivity of the workpiece and tool material.

$\beta_H= E_w/(E_w+ E_t)$	Eq. 5-6

$E_{w,t}= (k_{w,t} * \rho_{w,t} * c_{p_{w,t}})^{\frac{1}{2}}$	Eq. 5-7

In Eq. 5-7, k is the thermal conductivity, ρ is the density, and c_p is the specific heat capacity. The subscripts w and t refer to the work and tool respectively. Based on the properties listed in Table 5-1, β_H was calculated as 53%.

The heat losses through convection or radiation were neglected and the gap conductance between the interacting surfaces has been considered as 1E+8 W/m^2°C. An extreme value of gap conductance has been widely used in finite element simulation of cutting process [20, 21]. Such an extreme value decreased the required simulation time for reaching to a steady state condition [22].

In the FE simulation, the initial temperature was set to 20ºC which was similar to the starting value for the temperature dependent thermal physical properties of the tool and workpiece materials detailed in Table 5-1. The temperature dependent properties vary during the simulation as the result of heat generation and temperature increase.

5.3 Experimental Work

Orthogonal machining setup is shown in Figure 5-3. Orthogonal cutting was achieved through perpendicular movement of the cutting edge into the fins machined on the outer surface of a fully annealed AISI 1045 cylinder with hardness between 160 to 170 BHN. The insert was an uncoated tungsten carbide, with TNMG332QM-H13A designation. Depth of cut and rake angle were held constant at 3 mm and -6 deg respectively. Cutting tests were performed for nine combinations of cutting speed and feed rate, as shown in Figure 5-4. For each tool life test, flank wear and cutting time were recorded after machining each fin. The flank wear rate was then determined as the ratio of flank wear progression to the respective cutting time. Tests were stopped when the average flank wear reached 0.3 mm. Test for each cutting condition was repeated twice. In the setup, a piezo electric dynamometer (KISTLER 5210) was used for recording the forces in x, y and z directions.

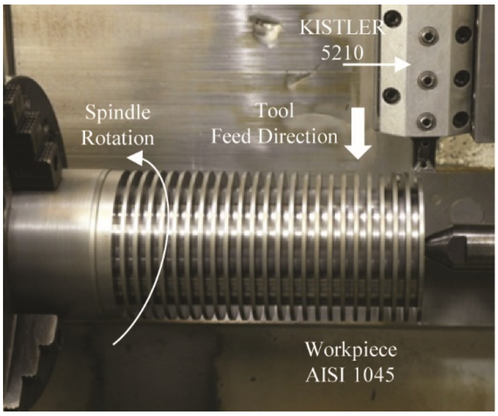

Figure 5-3. Orthogonal experimental setup.

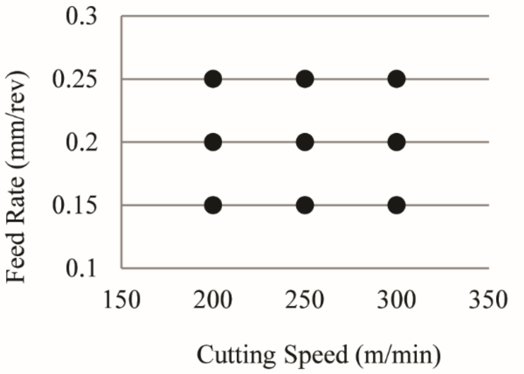

Figure 5-4. Nine combinations of cutting speed and feed rate.

Prior the cut and after machining each fin, the cutting edges were sectioned using Wire EDM, polished, etched, and analyzed under the optical microscope. Figure 5-5 (a) shows the micrograph of original cutting edge geometry in which edge radius was measured as 35-40 µm. The chip breaker was observed on the rake face at 230 µm from the intersection of the clearance and rake faces. Figure 5-5 (b) to (e) show the micro-graphs of cutting edges geometries at four stages when cutting at V=250 m/min and f=0.20 mm/rev. It was observed that the geometries of the worn edges, more specifically the angle between the flank face and horizontal axis were approximately 8 deg at different flank wear sizes.

Same trend in cutting edge geometries were observed when machining with different cutting speeds and feed rates which were specified in Figure 5-4. Figure 5-6 shows the micro-graphs of cutting edge geometries used at the lowest and highest process parameters respectively. It was concluded that when cutting speed and feed rate were varied only the wear rate was changed. Therefore, it was valid to assume that the orientation of flank face relative to the rake face did not change with different process parameters. Lane et al. [23] also observed similar phenomenon when machining AISI 1215 with diamond tools.

Based on the similarities observed on the worn edge geometries and for simplicity in comparing the process variables when cutting with different speeds and feed, it was valid to use the orientation of the flank face relative to the horizontal axis to be 8 deg for FE simulations of all the cutting conditions showed in Figure 5-4. Figure 5-7 shows the four different cutting edge geometries with specific flank wear lengths which were chosen. During the experiment, cutting time and forces were measured when the flank wear reached to 100, 200 and 300 µm.

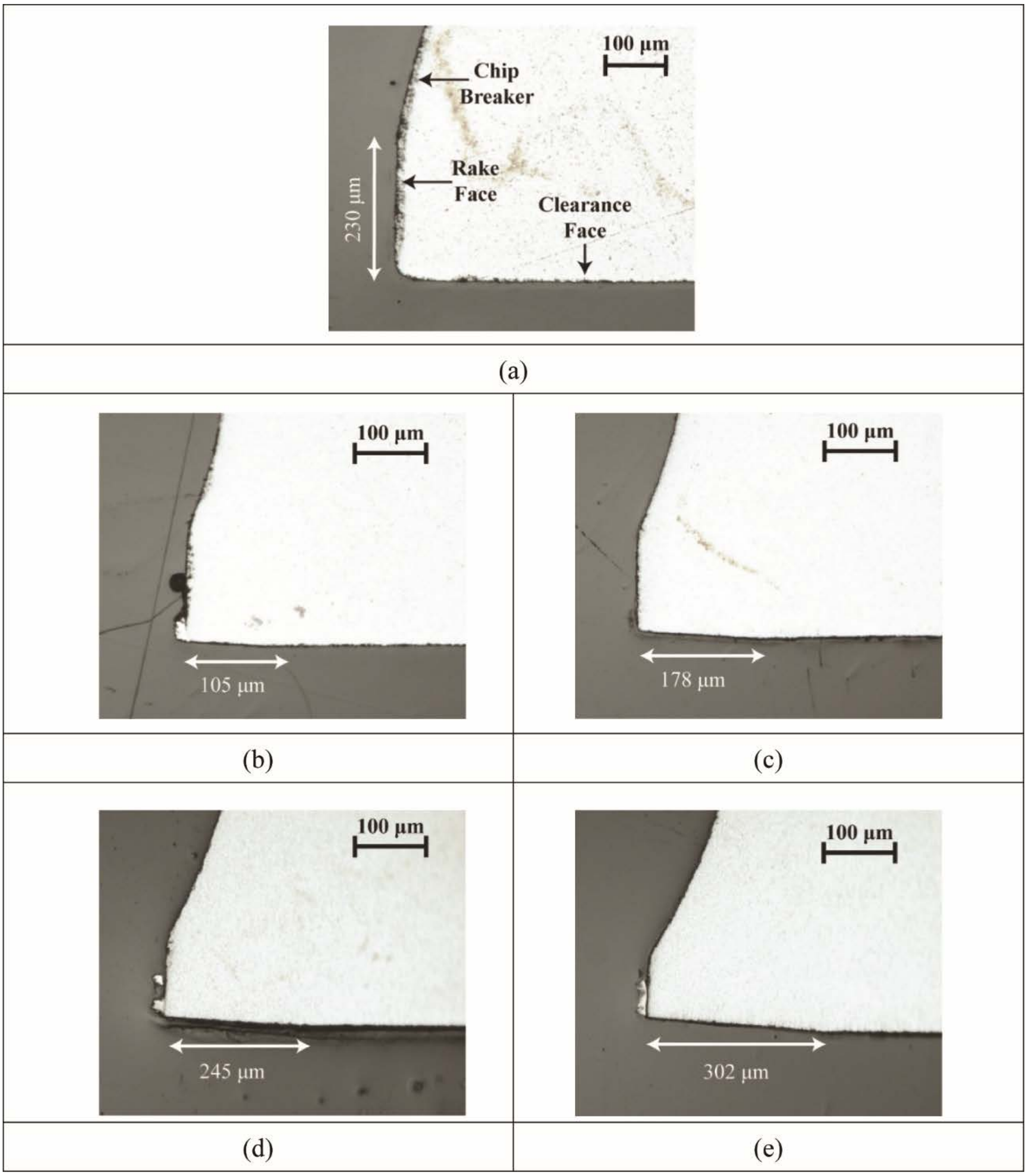

Figure 5-5. Micro-graphs of cutting edge geometries when V=250 m/min and f=0.20 mm/rev a) VB=105 µm, b) VB=178 µm, c) VB=245 µm and d) VB=302 µm.

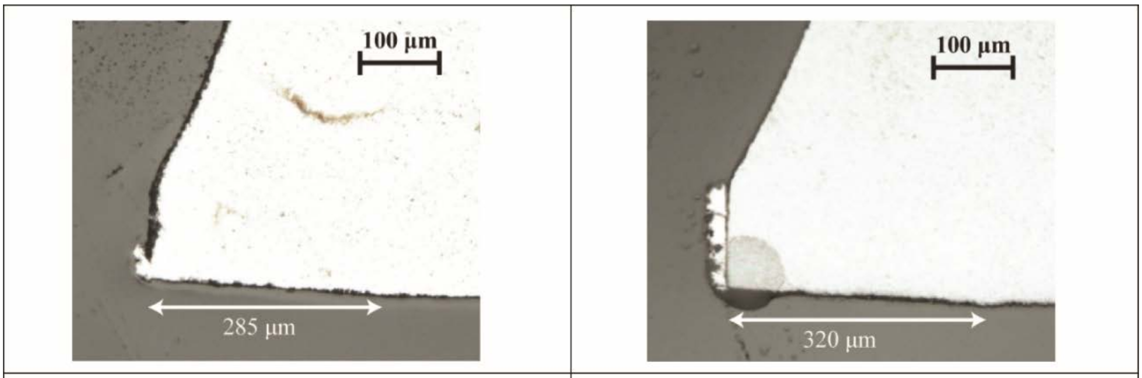

(a) V=200 m/min – f=0.15 mm/rev

(b) V=300 m/min – f=0.25 mm/rev

Figure 5-6. Geometry of worn edges at different cutting conditions.

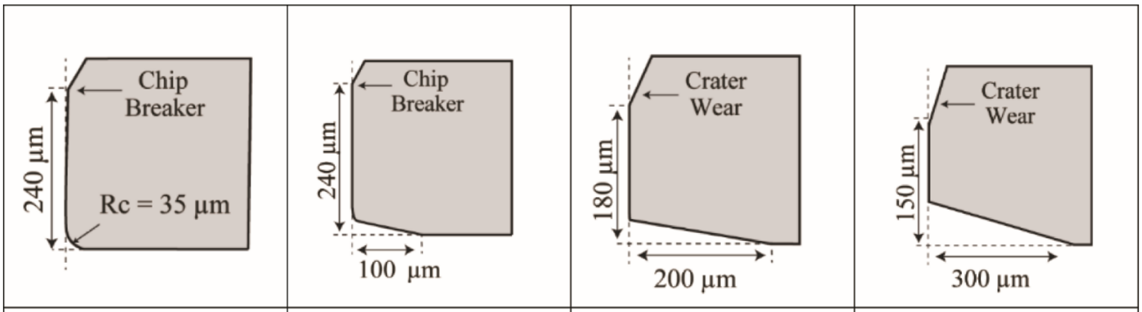

(a)

(b)

(c)

(d)

Figure 5-7. Tool edge geometries; a) VB=0, b) VB=100 µm, c) VB=200 µm, d) VB=300 µm.

5.4 Prediction of Tool Wear Rate

The tool wear rate was predicted based on a unique FE and empirical approach. The average interface temperature and contact pressure along the flank face-workpiece material interface results were determined with the FE model. These FE results were then used as data input into Usui’s wear rate model as shown in Eq. 5-8:

$$dW/dt = B_1 \sigma_n v_s exp(B_2 / T) \qquad \text{Eq. 5-8}$$

where, dW/dt is total wear rate (mm/s), σ_n is the contact pressure on the tool flank face (Pa), v_s is the sliding velocity of workpiece material passing over the tool flank (m/s), and T is average temperature along the contracting interface (deg C). B_1 and B_2 are constants which are dependent on the combination of the workpiece and tool materials and machining parameters. B_1 and B_2 are determined by model calibration.

Cutting speed (m/min)	Feed rate (mm/rev)
200	0.20
200	0.25
250	0.15
250	0.20
300	0.15
300	0.20

Table 5-4. Process parameters used to evaluate the accuracy of the FE model.

In the present study, only two process parameters were used for model calibration. These were i) 200 m/min cutting speed - 0.15 mm/rev feed and ii) 300 m/min cutting speed - 0.25 mm/rev feed. From the calibration, B_1 and B_2 magnitude were determined to be 1.95x10^{-8} m^2/MN and 3266 C respectively. Table 5-4 shows the six unique combination of cutting speeds and feed rates used to evaluate the accuracy of the FE models. The process parameters detailed in Table 5-4 were different from those used during model calibration. An extensive detail on the unique FE and empirical approach to predict tool wear rate can be found in [24].

5.5 Results and Discussion

5.5.1 Temperature

Figure 5-8 shows the effects of cutting speeds and feed rates on the average simulated flank face temperature at different flank wear length. The average flank face temperature was calculated when the nodal temperature on the tool flank face reached steady state condition.

In was observed that for each cutting condition the average flank face temperature increased with larger flank wear length. Similar trend was also observed in the FE simulation published by Malakizadi et. al, [22] and the experimental results presented by Thakare and Nordgren [25].

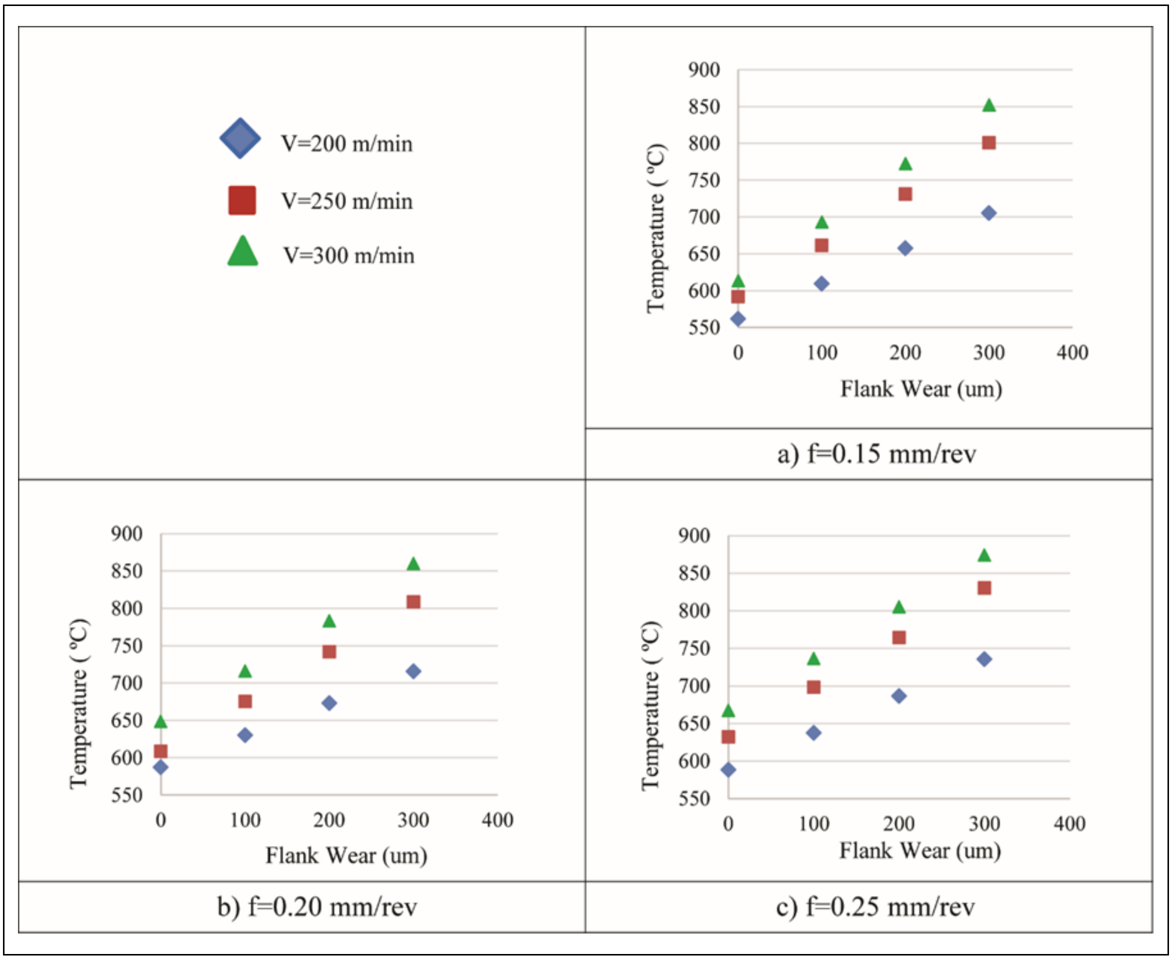

a) f=0.15 mm/rev

b) f=0.20 mm/rev

c) f=0.25 mm/rev

Figure 5-8. Simulated flank face temperature.

In metal cutting there are two main sources for heat generation; heat generated due to plastic deformation, and heat generation due to sliding friction, as detailed in Eq. 4 and Eq. 5. When the tool had zero flank wear, majority of heat was generated due to the plastic deformation and friction along the contacting surface in the primary deformation and secondary deformation zone regions. In this situation the size of tertiary deformation zone was limited to small area below the tool cutting edge, as shown in Figure 5-9 (a). Formation of flank wear resulted in the extension of the tertiary deformation zone, as illustrated in Figure 5-9 (b). As the contact area between tool flank face and work material in the tertiary deformation zone increased, the volume of plastically deformed material below the flank face also increased. This would result in higher heat generated by plastic deformation. At the same time, larger

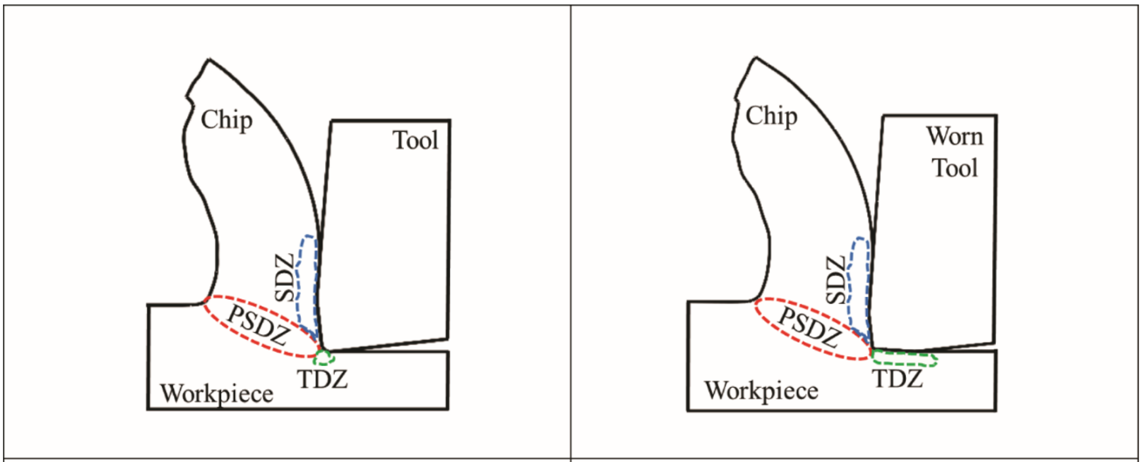

a) Chip formation zone – no wear

b) Chip formation zone- wear

Figure 5-9. Chip formation when cutting with a) tool with no wear and b) tool with flank wear.

flank wear increased the contact between work material and tool flank face which resulted in the increase of heat generated due to friction. Therefore, the increase in the flank wear length directly affected the heat generation due to plastic deformation and friction which increased the average flank face temperatures.

It was also observed that in each cutting condition, studied in this research, with the formation of flank wear the location of hottest zone on flank face gradually moved to a distance away from the tool tip. When flank wear length was 200 µm and 300 µm, maximum temperature was observed along the flank face away from the cutting edge. When flank wear was less than 100 µm, maximum temperature was found along the rake face away from the cutting edge. Figure 5-10 shows the isotherms distribution when flank wear length increases. Similar trend was also observed by Trigger [26] and Usui et. al, [27] from experiments, Ng et. al, [3] from FE simulation and Huang and Liang [28] from analytical modeling.

Based on results in Figure 5-8, it was also observed that the average flank face temperature increased with faster cutting speed and larger feed rate. However, the temperature increased is more substantial with cutting speed. This was because at higher cutting speed, the strain rate also increases. This will result in higher mechanical energy required to deform the material.

This mechanical energy is then finally converted to heat energy. Takeyama and Murata [25] experimental results also showed similar trend. Simulated results also showed that at higher cutting speed, the shearing stress along the tool flank face interface was higher, as detailed in Figure 5-11. In general, with higher shearing stress magnitude, the mechanical energy that was converted into heat energy also increases. Based on mechanical energy input into the system during orthogonal cutting, the increase in strain rate at faster cutting speed has a more substantial effect when compared to feed rate. Therefore, the average temperature increased along the flank face was smaller with change in feed rate when compared to cutting speed.

5.5.2 Forces

Figure 5-12, Figure 5-13 and Figure 5-14 show the effect of feed and flank wear length on cutting and feed forces at 200 m/min, 250 m/min and 300 m/min cutting speeds respectively. The predicted and experimental forces wear also compared in these figures.

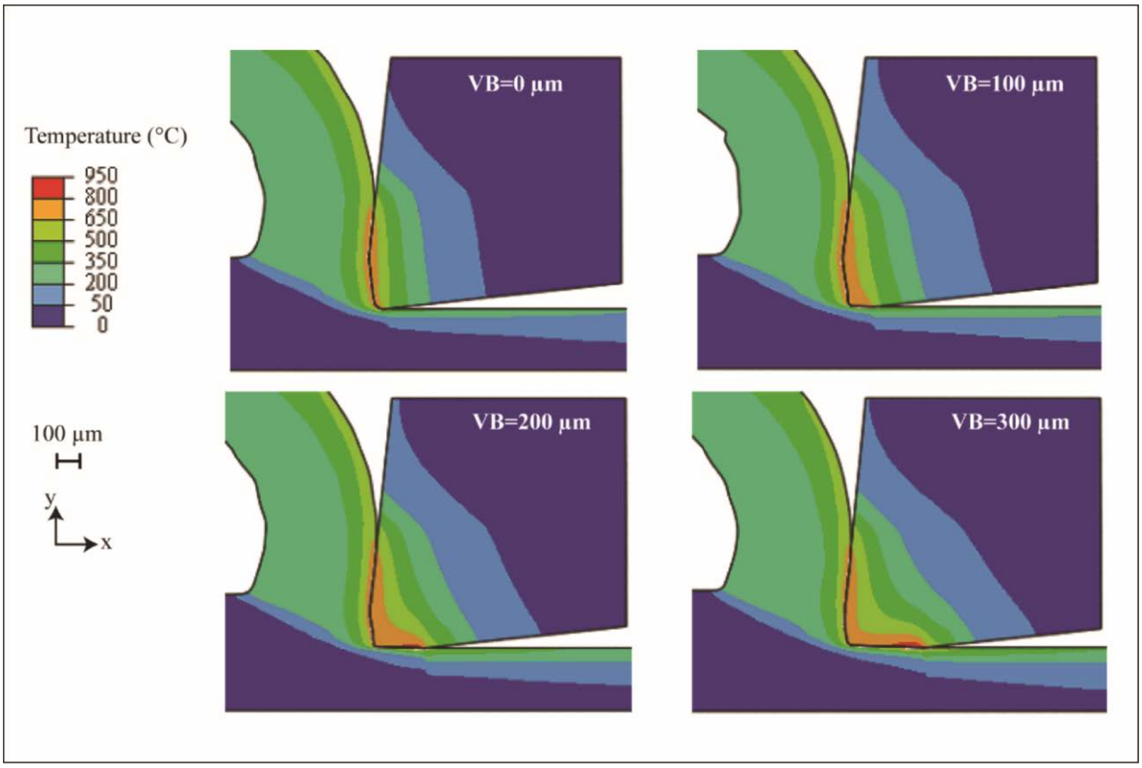

Figure 5-10. Location of the hottest zone on the tool flank face as flank wear is increased, V=250 m/min, f=0.20 mm/rev

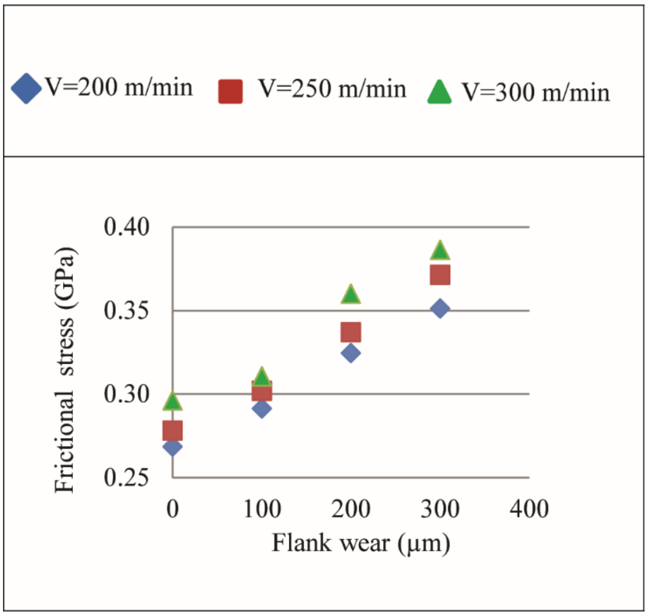

Figure 5-11. Average frictional (shear) stresses on the flank face, f=0.2 mm/rev

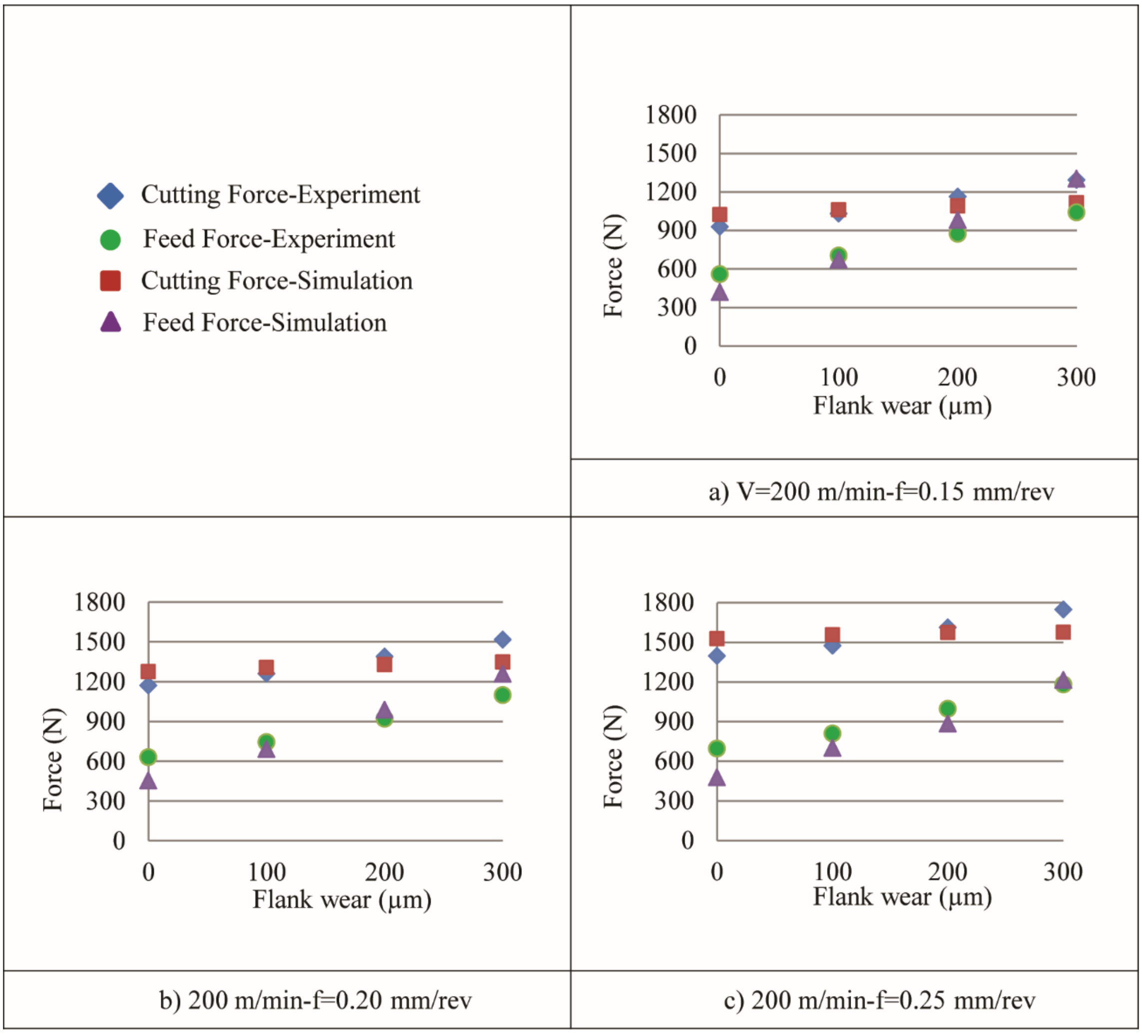

a) V=200 m/min-f=0.15 mm/rev

b) 200 m/min-f=0.20 mm/rev

c) 200 m/min-f=0.25 mm/rev

Figure 5-12. Effect of feed and flank wear on experimental and predicted forces at 200 m/min cutting speed

In each cutting condition the simulated cutting and feed forces increased with larger flank wear length. This was in agreement with the experimental observation. When the flank wear length increased, the contact area and friction between the tool flank face and newly generated workpiece material surface increases, which consequently increase the cutting and feed forces.

Both experiments and simulated results showed that feed forces had higher sensitivity to the change in flank wear length when compared to the cutting forces. According to Figure 5-15, when the material at the newly generated surface contacted the flank face, the normal force component relative to flank face, R_N, is the larger component. This R_N will be measured as the feed force direction relative to the force dynamometer. The trend on the effect on flank wear length on feed force was also observed experimentally by Thakare and Nordgren [25] and

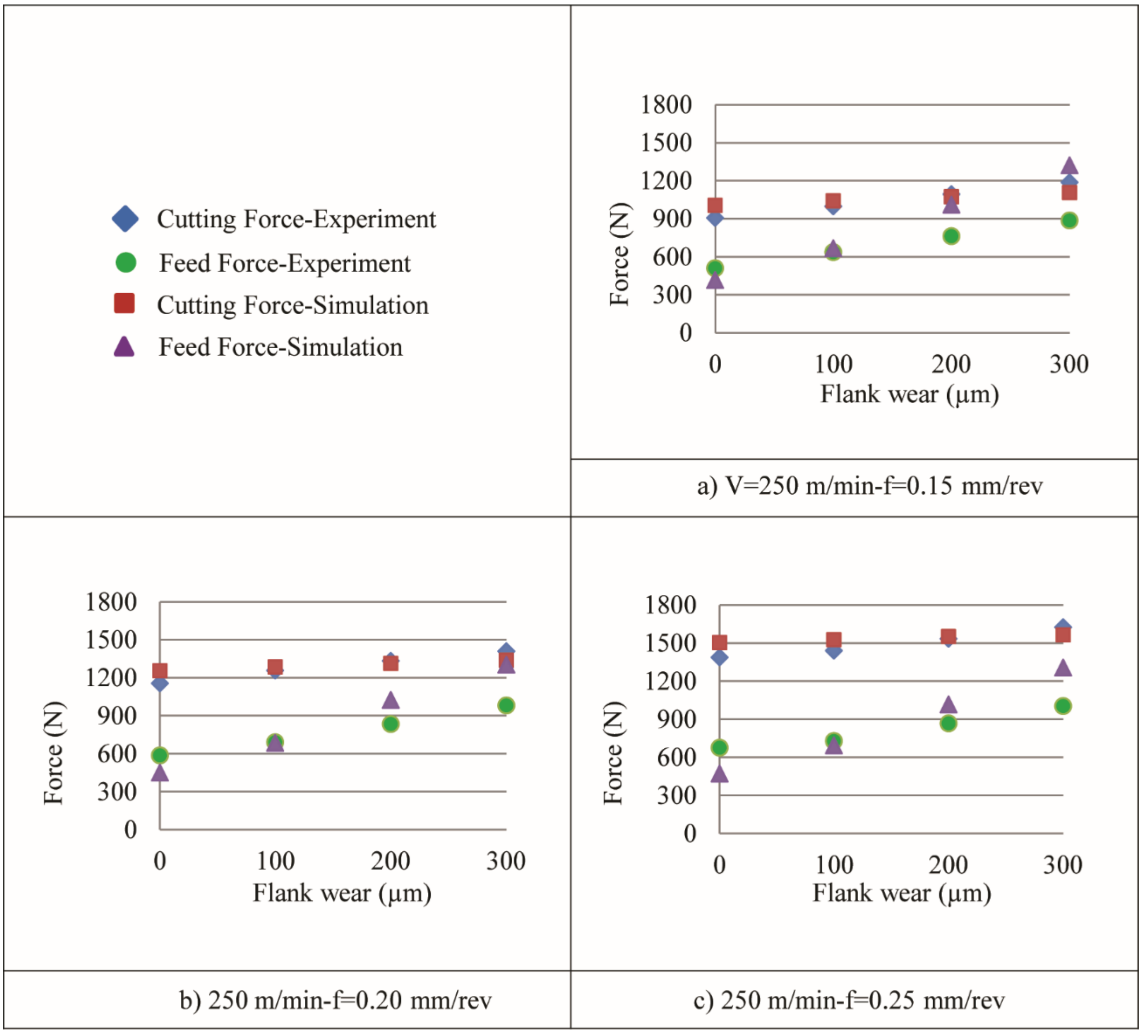

a) V=250 m/min-f=0.15 mm/rev

b) 250 m/min-f=0.20 mm/rev

c) 250 m/min-f=0.25 mm/rev

Figure 5-13. Effect of feed and flank wear on experimental and predicted forces at 250 m/min cutting speed

Kountanya et.al. [30]. This phenomenon resulted in higher increasing rate of feed force compared to the cutting force as the size of tertiary deformation zone increased.

In terms of cutting forces, in all conditions in Figure 5-12 to Figure 5-14, the increasing rate of cutting forces with flank wear length was simulated in close agreement with the experiment. In all the cutting conditions and for all flank wear lengths, the cutting forces were predicted in ±10% of average experimental forces.

In terms of feed forces, at zero flank wear length the simulated results under-predicted the experiments by 20% to 30%. Malakizadi et al. in [22] and [31] related the under-predictions in feed forces to the under-estimation in tool-chip contact length on the tool rake face. This observation was reported to be independent from the FE software packages and from the

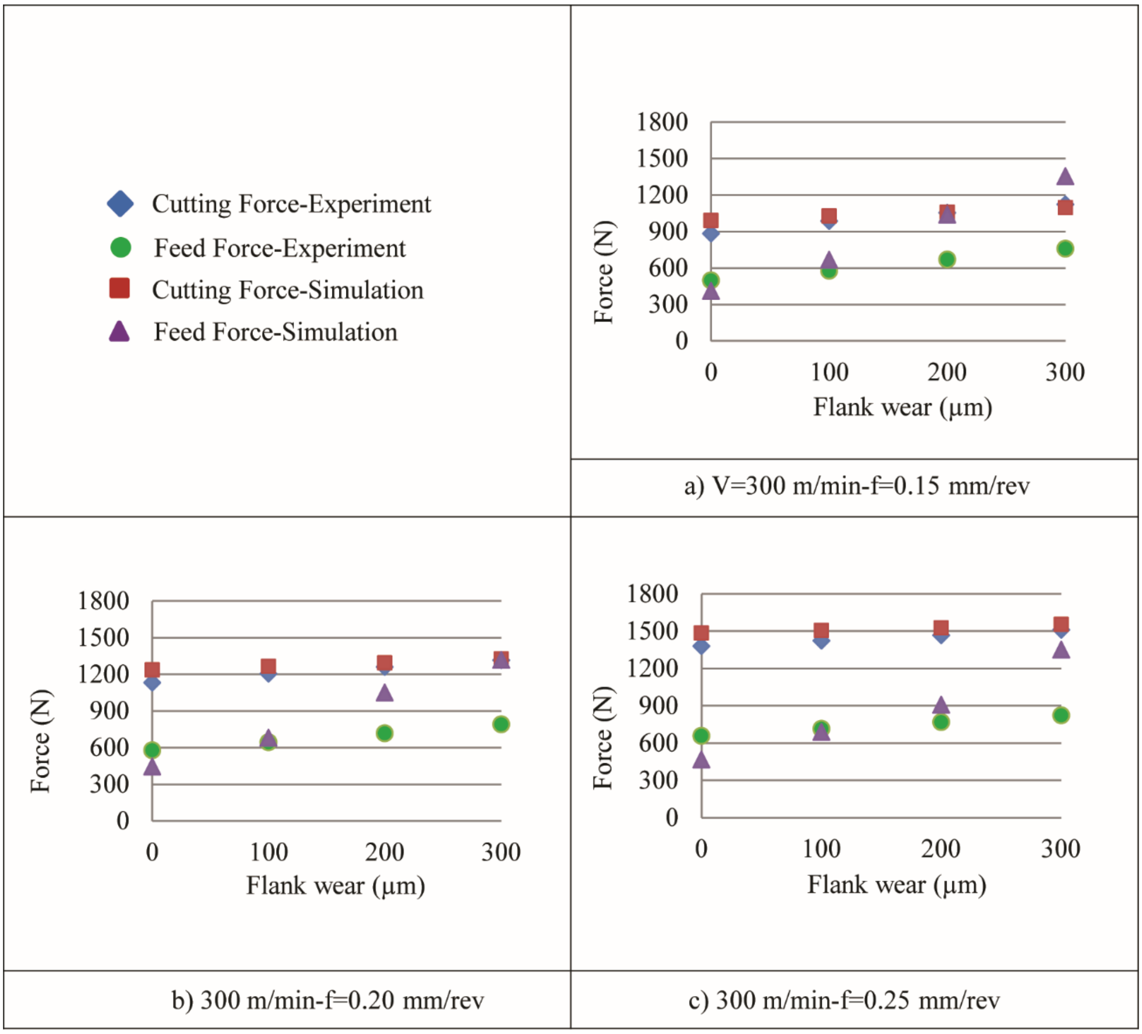

a) V=300 m/min-f=0.15 mm/rev

b) 300 m/min-f=0.20 mm/rev

c) 300 m/min-f=0.25 mm/rev

Figure 5-14. Effect of feed and flank wear on experimental and predicted forces at 300 m/min cutting speed.

friction models used. When flank wear was incorporated into the model, the simulated feed forces were in better agreement with experimental results at 200 m/min cutting speed. At higher cutting speeds, the simulated feed forces seemed to over predict from those acquired experimentally. This over prediction was of feed forces at larger flank lengths was also observed by Malakizadi et al. [22].

Experimental results from Figure 5-12 to Figure 5-14 showed that both the cutting and feed forces decreases when the cutting speed was increased, and feed rate held constant. The lower cutting forces with higher cutting speed was likely due to the increased in temperature generated during cutting, as observed in Figure 5-8. Experimental results published by Puls et. al. [19] showed that coefficient of friction was lower at higher temperature generated due to higher cutting speed. This decreasing trend in cutting forces at higher speed was also observed experimentally by Thakare and Nordgren [25]. The simulated feed forces also showed that at higher cutting speeds, feed force was lowered when the flank wear length was between 0 and 100 μm. However, at larger flank wear lengths of 200 μm and 300 μm simulated feed forces did not follow the decreasing trend and increased with speed. This is likely due to the over-simplification of the tool cutting edge geometry with the larger flank wear length.

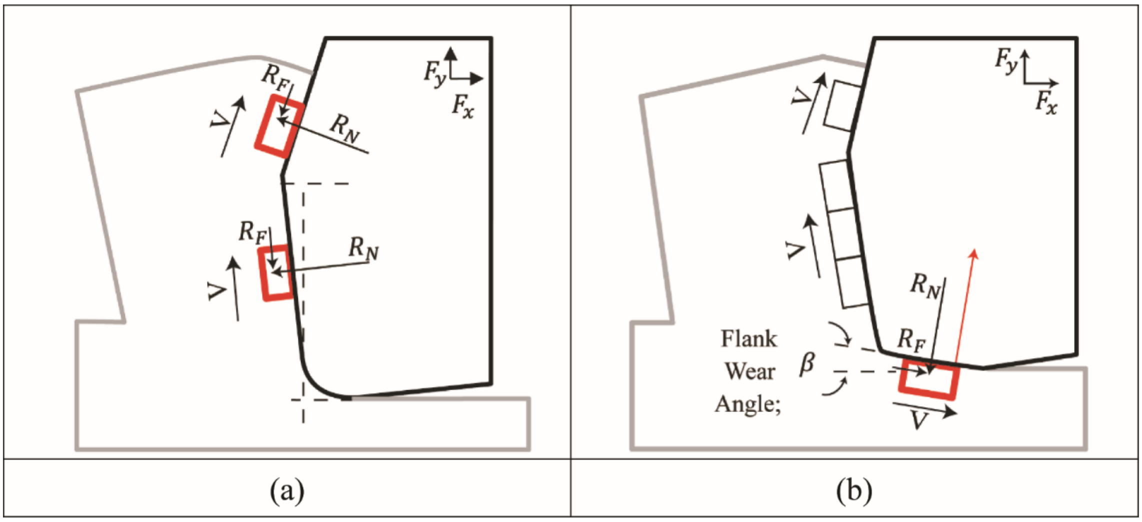

(a) (b)

Figure 5-15. Configuration of work material elements moving over the faces of a (a) new cutting edge and (b) worn cutting edge.

Figure 5-16 shows the effect of flank wear length and cutting speed on the average contact pressure along the flank face of the tool. The contact pressure at this region increased with larger flank wear and faster cutting speed. The contact pressure did not show substantial difference with the range of feed rate investigated.

5.5.3 Wear rate prediction

Figure 5-17 shows the comparison between the experimental and predicted flank wear rate in the flank wear interval of 100 to 200 µm and 200 to 300 µm. A more detailed explanation on the wear rate calculations has been provided in Hosseinkhani & Ng [24]. The process parameters used in Figure 5-17 can be found in Table 5-4. In general, the predicted wear rate had a similar trend to those acquired experimentally. The wear rate was higher with larger flank wear length as both predicted temperature and contact pressure increases. When the flank wear interval was between 100 to 200 µm, the difference between the predicted and experimental wear rate was between ±10%. A larger deviation of approximately 25% on the wear rate was observed between predicted and experimental results when the flank wear interval was between

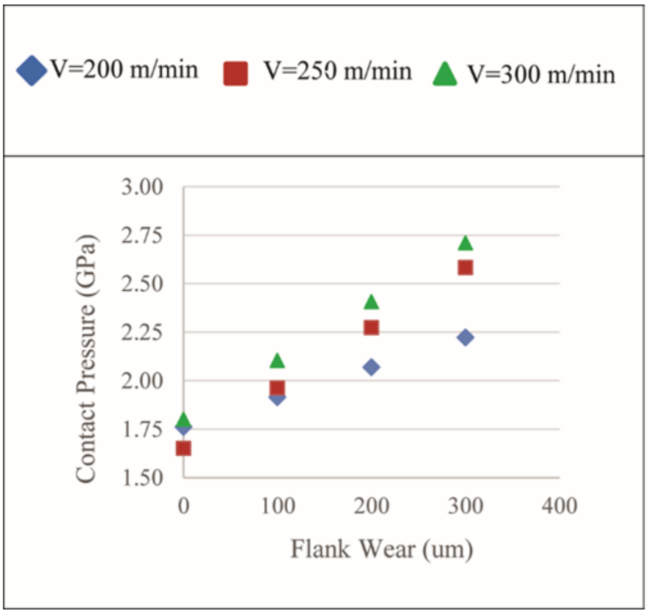

Figure 5-16. Average contact pressure on the flank face.

200 to 300 µm. Similar trend was also observed on the feed force when the flank wear length was between 200 to 300 µm, as shown in Figure 5-12 to Figure 5-14. The wear rate results showed that the model presented here is capable of predicting the stresses and temperature along the flank face trend accurately.

1

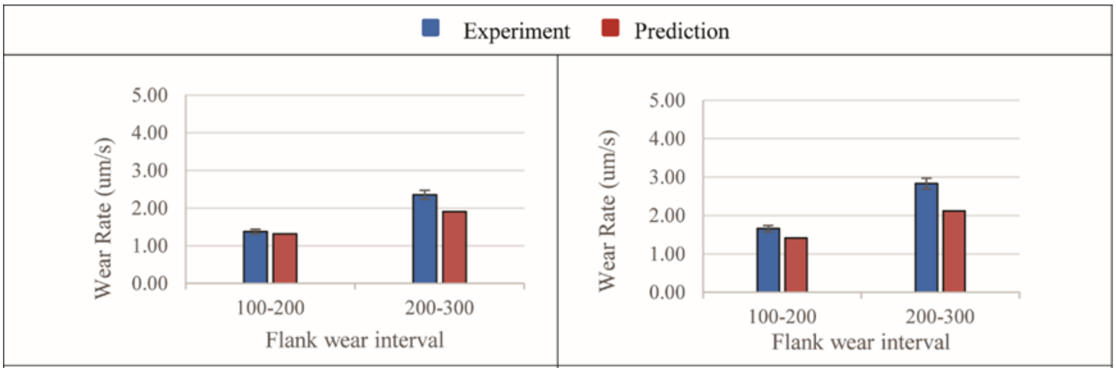

(a) V=200 m/min – f=0.20 mm/rev (b) V=200 m/min – f=0.25 mm/rev

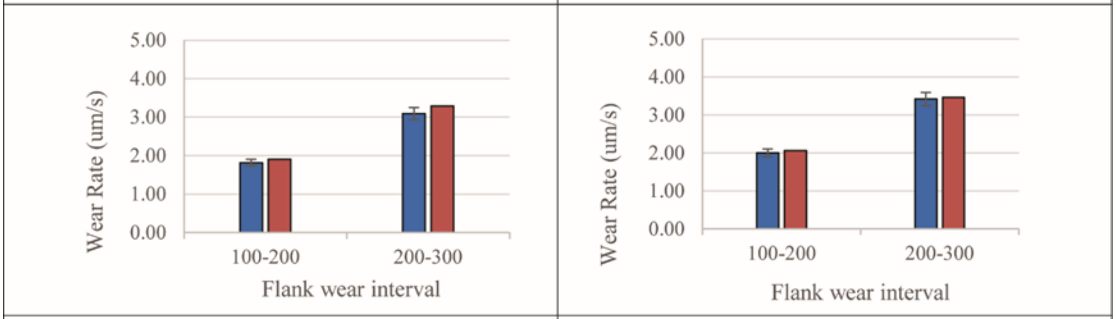

(c) V=250 m/min – f=0.15 mm/rev (d) V=250 m/min – f=0.20 mm/rev

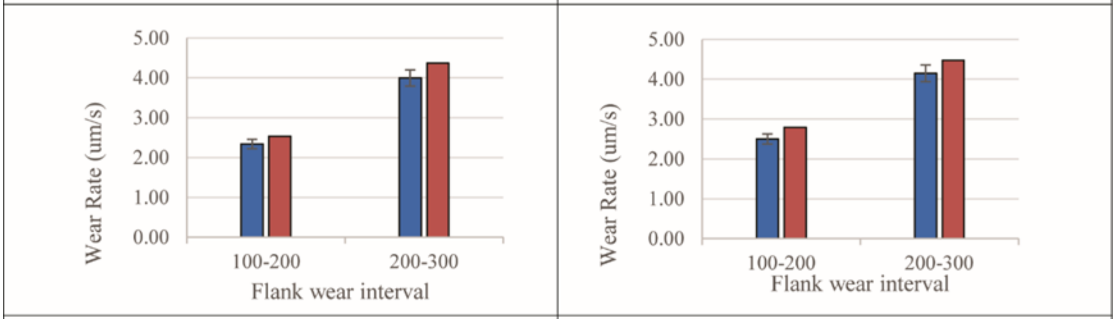

(e) V=300 m/min – f=0.15 mm/rev (f) V=300 m/min – f=0.20 mm/rev

Figure 5-17. Experimental and estimated wear rate in 100-200 µm and 200-300 µm flank wear intervals.

5.6 Conclusions

In this paper, the effect of flank wear length on cutting and feed forces, temperature and stresses were simulated using FE method with various combination of cutting speed and feed rate. The tool wear rate predicted with finite element results and Usui's model were also presented. Extensive experimental results were compared with simulated data. The following conclusions were made based on the orthogonal cutting of AISI 1045 with uncoated carbide tool and bounded by the associated process parameters used.

The average flank face temperature increased with the increase of flank wear length. The predicted temperature distribution showed that the position of maximum temperature shifted from the rake face to the flank face with larger flank wear length. The increase of frictional stress along the flank face interface was the cause of this shift. Simulations results showed that the increase in flank wear length increased the average shear stress and contact pressure on tool flank face.

Forces in the cutting and feed directions were increased with the increase in flank wear length. Modelling similar flank wear geometry with those observed during cutting tests was critical in predicting the cutting and feed forces accurately. Experimental results showed that the angle between the flank face and horizontal axis was constant with an increase in flank wear length. If this angle were to vary, the difference between the predicted and experimental forces will increase.

Both simulated and experimental wear rate showed that the change in wear rate was more substantial with cutting speed when compared to feed rate, and the wear rate also increased with larger flank wear length.

When the tool is worn, it is difficult to measure the stress, strain and temperature distribution with good repeatability. This research shows that using the tool wear rate results is one possibility to validate the model with limited wear model calibration.

5.7 Acknowledgment

The authors would like to thank the Mechanical Engineering Department at McMaster University and McMaster Manufacturing Research Institute (MMRI) for providing the laboratory infrastructure.

5.8 Declaration

Funding

This work was funded by Natural Sciences and Engineering Research Council of Canada (NSERC) through the Canadian Network for Research and Innovation in Machining Technology (CANRIMT) and Discovery Grant programs.

Authors Contribution

Conceptualization, methodology, experiment, finite element simulation and data analysis by Keyvan Hosseinkhani. Resources and funding acquisition by Eu-gene Ng. Writing—original manuscript draft preparation by Keyvan Hosseinkhani. Writing—review and editing by Eu-gene Ng. Project administration by Keyvan Hosseinkhani and Eu-gene Ng.

Conflicts of Interest/Competing Interests

The authors declare no conflict of interest.

Availability of Data and Material

All the data and material in this paper are original and available upon request

Code Availability

Not applicable

Ethics approval

Not applicable

Consent to participate

Not applicable

Consent for publication

We would like the manuscript entitled "Finite element simulation of cutting process under the Worn Tool Edge Geometries" by Keyvan Hosseinkhani and Eu-gene Ng to be considered for publication in the International Journal of Advanced Manufacturing Technology.

5.9 References

[1] Movahhedy MR, Gadala MS, Altintas Y (2000) Simulation of Chip Formation in Orthogonal Metal Cutting Process: An ALE Finite Element Approach. International Journal of Machining Science and Technology 4 (1): 15-42.

[2] Ng E, El-Wardany TI, Dumitrscu M, Elbestawi MA (2002) Physics-Based Simulation of High Speed Machining. International Journal of Machining Science and Technology 6 (3): 301-329.

[3] Ng E, El-Wardany TI, Elbestawi MA (2003) Influence of Flank Wear Lenght on Residual Stress and Workpiece Quality in Machined Surfaces. International Journal of Mechanical Production Systems, Issue April: 10-21.

[4] Yen Y.-C., Jain A, Altan T (2004) A Finite Element Analysis of Orthogonal Machining Using Different Tool Edge Geometries. Journal of Material Processing Technology 146 (1): 72-81.

[5] Nasr MN, Ng E-G, Elbestawi M (2007) Modelling the Effects of Tool-Edge Radius on Residual Stresses when Orthogonal Cutting AISI 316L. International Journal of Machine Tools and Manufacture 47 (2): 401-411.

[6] Özel T (2006) The Influence of Friction Models on Finite Element Simulations of Machining. International Journal of Machine Tools and Manufacture 46 (5): 518-530.

[7] Li K, Gao X.-L, Sutherland J (2002) Finite Element Simulation of the Orthogonal Metal Cutting Process for Qualitative Understanding of the Effects of Crater Wear on the Chip Formation Process. Journal of Materials Processing Technology 127 (3): 309-324.

[8] Hosseinkhani K, Ng E (2013) Analysis of the Cutting Mechanics Under the Influence of Worn Tool Geometry. Proceeding of the 14th international conference on modeling the machining operation (14th CIRP CMMO),Torino 8: 117-122.

[9] Sánchez A, Canteli J, Cantero J, Miguélez M (2011) Numerical Analysis of the Tool Wear Effect in the Machining Induced Residual Stresses. Journal of Simulation Modellling Practice and Theory 19 (2): 872-886.

[10] Boyd JM., Hosseinkhani K, Veldhuis SC, Ng E (2016) Improved Prediction of Cutting Forces Via Finite Element Simulations Using Novel Heavy-Load, High-Temperature

Tribometer Friction Data. International Journal of Advanced Manufacturing Technology, 86 (5): 2037–2045.

[11] Wan L, Wang D, Gao Y (2015) Investigations on the Effects of Different Tool Edge Geometries in the Finite Element Simulation of Machining. Journal of Mechanical Engineering, 61 (3): 157-166.

[12] Duboust N, Pinna C, Ghadbeigi H, Collis A, Ayvar-Soberanis S, Kerrigan K, Scaife R (2019) FE Modelling of CFRP Machining- Prediction of the Effects of Cutting Edge Rounding. 17th CIRP Conference on Modelling of Machining Operations (17th CIRP CMMO), 82: 59-64.

[13] Uçak N, Çiçek A, Oezkaya E, Aslantas K (2019) Finite Element Simulations of Cutting Force, Torque, and Temperature in Drilling of Inconel 718. 17th CIRP Conference on Modelling of Machining Operations (17th CIRP CMMO), 82:47-52.

[14] Johnson G.J, Cook WH (1983) A Constitutive Model and Data for Metals Subjected to Large Strains, High Strain Rates and High Temperatures. Proceedings of the 7th International Symposium on Ballistics: 541-547.

[15] Jaspers S, Dautzenberg JH (2002) Material Behaviour in Conditions Similar to Metal Cutting: Flow Stress in the Primary Shear Zone. Journal of Materials Processing Technology 122 (2-3): 322-330.

[16] Halim SMT (2008) Finite Element Modeling of the Orthogonal Metal Cutting Process: Modeling the Effects of Coefficient Of Friction and Tool Holding Structure on Cutting Forces and Chip Thickness. Dissertation, McMaster Univesity.

[17] Kalhori V (2001) Modelling and Simulation of Mechanical Cutting. Dissertation , Lulea University of Technology.

[18] Pavlina EJ, Van Tyne CJ (2008) Correlation of Yield Strength and Tensile Strength with Hardness for Steels. Journal of Materials Engineering and Performance 17 (6): 888–893

[19] Puls H, Klocke F, Lung D (2012) A New Experimental Methodology to Analyse the Friction Behaviour at the Tool-Chip Interface in Metal Cutting. Production Engineering - Research and Development 6: 349–354.

[20] Thepsonthi T, Özel T (2015) 3-D Finite Element Process Simulation of Micro-End Milling Ti-6Al-4V Titanium Alloy: Experimental Validations on Chip Flow and Tool Wear. Journal of Materials Processing Technology 221: 128-145.

[21] Bordin A, Imbrogno S, Rotella G, Bruschi S, Ghiotti A, Umbrello D (2015) Finite Element Simulation of Semi-finishing Turning of Electron Beam Melted Ti6Al4V Under Dry and Cryogenic Cooling. Procedia CIRP 31: 551-556.

[22] Malakizadi A, Gruber H, Sadik I, Nybor L (2016) An FEM-Based Approach for Tool Wear Estimation in Machining. International Journal of Wear 368–369: 10-24.

[23] Lane BM, Dow TA, Scattergood R (2013) Thermo-Chemical Wear Model and Worn Shapes for Single-Crystal Diamond Tools Cutting Steel. International Journal of Wear, 300 (1-2): 216-224.

[24] Hosseinkhani K, Ng E (2020) A Unique Methodology for Tool Life Prediction in Machining. Journal of Manufacturing and Materials Processing 4 (1): 1-16.

[25] Thakare A, Nordgren A (2015) Experimental Study and Modeling of Steady State Temperature Distributions in Coated Cemented Carbide Tools in Turning. Procedia CIRP 31: 234-239.

[26] Trigger K.J (1963) Temperatures in Machining and their Importance. Proceeding of International Research in Production Engineering ASME: 95-101.

[27] Usui E, Shirakashi T, Kitagawa T (1984) Analytical Prediction of Cutting Tool Wear. International Journal of Wear 100 (1-3): 129-151.

[28] Huang Y, Liang SY (2003) Modelling of the Cutting Temperature Distribution under the Tool Flank Wear Effect. Journal of Mechanical Engineering Science 217 (11): 1195-1208.

[29] Takeyama H, Murata R (1963) Basic Investigation of Tool Wear. Trasaction of ASME Journal of Engineering for Industry: 33-38.

[30] Kountanya RK, Endres WJ (2004) Flank Wear of Edge-Radiused Cutting Tools Under Ideal Straight-Edged Orthogonal Conditions. Journal of Manufacturing Science and Engineering 126 (3): 496-505.

[31] Malakizadi A, Hosseinkhani K, Mariano E, Ng E, Del Prete A, Nyborg L (2017) Influence of friction models on FE simulation results of orthogonal cutting process," The International Journal of Advanced Manufacturing Technology 88 (9–12): 3217–3232.

6 PAPER 3: A HYBRID EXPERIMENTAL AND NUMERICAL APPROACH TO EVALUATE AND CALIBRATE THE EMPIRICAL TOOL WEAR RATE MODELS FOR ORTHOGONAL MACHINING

This chapter is the copy of the paper published in the International Journal of Advanced Manufacturing Technology. It presents the second phase of the tool life prediction methodology and focuses on the calibration of the empirical tool wear rate models. The objective was to define the calibration framework for the Takeyama & Murata, Usui, Attanasio, and Akazawa wear rate models, which have been widely used in the tool wear prediction studies. The framework was based on the required data to be collected for efficient calibration of wear rate models which ultimately assisted in the selection of appropriate wear rate model. The main outcome of this paper was the selection of Usui's model as the most robust wear rate model to be used for wear rate prediction.

Authors: Keyvan Hosseinkhani, E. Ng

The International Journal of Advanced Manufacturing Technology volume 96, pages 2709–2724 (2018)

Abstract.

An important part of the tool wear prediction process is the calibration of empirical models which relate the process variables to the tool wear rate. In this paper, finite element simulations together with limited number of experiments were used to calibrate the empirical wear rate models. The cutting tool investigated was uncoated tungsten carbide which was used in orthogonal machining of AISI 1045. Four different wear rate models were evaluated during calibration from two aspects; the least amount of quantitative assumptions involved and independency from the proportions of dominant wear mechanisms. Following on from here, investigation was also carried out to determine the minimum number of experiments for calibrating the empirical models such that the predicted wear rates agree well with experimental results in specific range of cutting parameters. Results showed that Usui's wear rate model was the most robust as there was no restriction in selecting process parameter magnitude during calibration. It was also possible to calibrate Usui's model based on two cutting tests only. However, the number of experiments used during calibration should be increased when workpiece material is sensitive to either strain hardening or strain rate.

Keywords: Tool Wear Prediction, Wear Rate Models, Calibration and Finite Element Simulation

6.1 Introduction

In machining, tool wear is recognized as an inevitable phenomenon which changes the initial cutting edge geometry and affects the mechanics of cutting by increasing forces and temperature as well as the "unwanted" tensile residual stresses retained in the machined component. Therefore, for many decades, tool wear prediction has been the point of interest for improving process planning and productivity of the operation.

In recent years, with the improvements in computational capabilities, employing the finite element (FE) simulation of cutting process in combination with an empirical wear rate model for tool wear prediction has increased. Based on this approach, Yen et al. [1], Xie et al. [2] and Filice et al. [3] simulated the progression of both flank and crater wear during orthogonal cutting and Attanasio et al. [4] [5] modelled the formation of flank and crater wear in a 3-dimensional configuration.

In this approach, the efficiency of the FE in simulating the process variables and the selection and calibration of wear rate models are the key factors for achieving an accurate prediction. The focus of the current paper is on the calibration of the empirical models which relate the tool wear rate to the wear mechanisms in the cutting zone, as listed in Table 6-1. These models were proposed by Takeyama and Murata [6], Usui et al. [7], Akazawa et al. [8] and Attanasio et al. [4].

Takeyama and Murata model has been detailed in Eq. 6-1 a and b. In this model the total amount of wear rate is determined from separate expressions for mechanical abrasion and thermal diffusion. According to Takeyama and Murata, when interface temperatures is below the activation temperature of diffusion, T_{act}, wear due to abrasion is dominant, as shown in Eq. 1a. When interface temperature is higher than T_{act}, wear rate is mainly due to diffusion and the abrasive part of the model can be neglected, as shown in Eq. 6-1 b. In this model, abrasive wear rate has been directly related to the cutting speed and feed rate while diffusive wear rate was related to the tool–workpiece interface temperature.

In Usui’s model, as shown in Eq. 6-2, the total amount of wear rate is determined from a single expression [7]. In this model, the wear rate is related to the contact pressure on the tool face, the sliding velocity of the workpiece material passing over the tool face and the temperature of the tool – workpiece interface.

Wear Rate Equation	$T \le T_{act}$	$T > T_{act}$
Takeyama and Murata [6]	$dW/dt = dW_a/dt = A_1 fV$ Eq. 6-1a	$dW/dt = dW_d/dt = A_2 \exp(-E/RT)$ Eq. 6-1 b
Usui [7]	$dW/dt = dW_a/dt + dW_d/dt = B_1 \sigma_n v_s \exp(-B_2/T)$ Eq. 6-2	
Akazawa [8]	$dW/dt = dW_a/dt + dW_d/dt = C_1 v_s (H_w/H_t) + C_2 v_s \exp(-C_3/T)$ Eq. 6-3	
Attanasio [4]	$dW/dt = dW_a/dt =$ $D_1 \sigma_n v_s \exp(-D_2/T)$ Eq. 6-4a	$dW/dt = dW_a/dt + dW_d/dt =$ $D_1 \sigma_n v_s \exp(-D_2/T) + D_3 \exp(-E/RT)$ Eq. 6-4b
dW/dt; *total wear rate (µm/s)* dW_a/dt; *abrasive wear rate (µm/s)* dW_d/dt; *diffusive wear rate (µm/s)* *V; cutting speed (m/s)* *f; feed rate (m/rev)* v_s; *sliding velocity of the work material (m/s)* σ_n; *normal pressure on the tool face (Pa)* *T; temperature on the tool face (C)*		T_{act}; *activation temperature of diffusion (C)* *E; activation energy of the diffusion (KJ/molC)* *R; universal gas constant (KJ/mol)* H_w, H_t; *hardness of workpiece and tool* A_1, A_2, B_1, B_2, C_1, C_2, C_3, D_1, D_2, D_3,; *equation constants which depend on the combination of work and tool materials and cutting conditions*

Table 6-1. Empirical expressions for tool wear rate estimation.

In Akazawa model, as detailed in Eq. 6-3, the total wear rate is determined from separate expressions for abrasion and diffusion [8]. The first part of model specifies wear rate due to abrasion and the second part specifies wear rate due to diffusion. In Akazawa's model the wear rate due to abrasion was related to the sliding velocity of the work material passing over the tool face and the relative hardness of work, H_w, and tool, H_t. This is based on the fact that at higher temperature, hardness of tool was reduced as well as the abrasiveness of hard inclusions in the work material. Therefore, the relative hardness between these two plays the key role in the amount of abrasive wear. In Eq. 6-3 both H_w and H_t are functions of temperature. The diffusive wear rate in Akazawa model was related to sliding velocity of workpiece material passing over the interface and the tool – workpiece interface temperature.

Attanasio et al. [4] proposed a coupled abrasive and diffusive model for calculating the total wear rate by combining Takeyama & Murata and Usui models. This model assumes that when the interface temperature is lower than the activation temperature of the diffusion, T_{act}, the dominant wear mechanism is abrasion and wear rate is calculated based on Usui, as shown in Eq. 6-4 a. When the interface temperature is higher than Tact, a combination of Usui and Takeyama& Murata models are used for determining the total wear rate due to abrasion and diffusion, as detailed in Eq. 6-4 b.

In general the wear rate models should be calibrated based on the unique combination of tool and workpiece materials and for specific cutting conditions. Calibration refers to the process of determining the model’s constants which would result in the minimum difference between the model output and the experimental results. It has been realized that in previous wear estimation attempts, the calibration frameworks have not been clearly set in terms of the procedure for data collection and the optimum number of the experiments/simulations performed for data collection.

Lotfi et al. [9] and Filice et al. [3] used eleven and nine cutting conditions to calibrate the models respectively. While the predicted tool wear were in good agreement with experiment, the large number of cutting experiments seemed to be excessive and time intensive. On the other hand, Malakizadi et al. [10] and Attanasio et al. [4] employed one cutting condition to calibrate the wear rate model. Unfortunately, the wear rate predictions were different from experiment especially when there was a large difference between the cutting parameters and those used during calibration. Other published research did not elaborate on the cutting conditions and number of experiments performed during calibration, [11] [12] [13]. Xie et al. [2] and Yen et al. [1] did not calibrate the wear rate models for specific cutting conditions and tool/workpiece material combinations but rather used the calibration constants from literature, [14] [15].

The objective of the current paper is to define the calibration framework for the Takeyama & Murata, Usui, Attanasio, and Akazawa wear rate models, which have been widely used in the tool wear prediction studies [1] [2] [3] [4] [8]. The framework specifies the required data to be collected for efficient calibration of wear rate models. This ultimately will assist in the selection of appropriate wear rate model. The framework also suggests the optimum number of experiments and simulations to be performed for data collection which will prevent the excessive and redundant experiments and simulations. The research methodology is based on a hybrid experimental/simulation approach with emphasis on the flank wear rate and is outlined in the following section.

6.2 Methodology

The procedure for analyzing the calibration of wear rate models is described below:

1. Step one: Cutting experiments are performed to determine the worn cutting edge geometries and wear rate. The range of cutting parameters in which the wear rate models are desired to be effective is listed in Table 6-2. In this investigation, nine cutting conditions from this range have been considered and are shown in Figure. 6-1.
2. Step two: FE models are built based on the experimentally obtained worn tool edge geometries. Simulated flank face temperature and contact pressure data are collected.
3. Step three: Experimental and simulated data are analyzed. Based on the sensitivity of data to the variation in cutting speed and feed rate, several cutting conditions are selected for the calibration.
4. Step four: Wear rate models are calibrated based on the experimental/simulated data. The least squared error technique is used to determine the constants.

Cutting Speed (m/min)	200 to 300
Feed Rate (mm/rev)	0.15 to 0.25
Depth of Cut (mm)	3
Rake Angle (˚)	-6

Table 6-2. Cutting parameters.

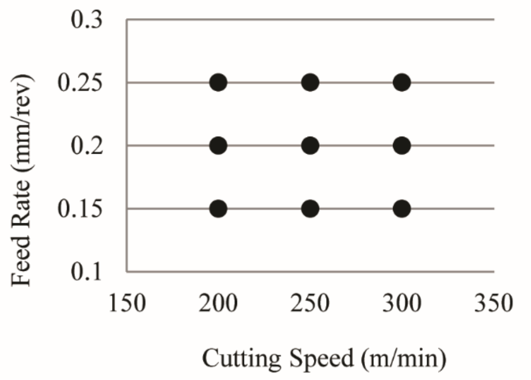

Figure. 6-1. Nine cutting conditions in the range of cutting parameters.

5. Step five: Tool wear models are compared from two aspects; 1) calibrating with least amount of assumptions or quantitative unknowns and 2) calibrating the wear rate model which is independent from the proportions of dominant wear mechanisms.
6. Step six: Calibrated constants based on different data sets are compared and the optimum number of simulation/experiment for data collection is determined.

6.3 Experiment

In step one, experiments were performed based on the setup shown in Figure 6-2. In Figure 6-2, orthogonal cutting was achieved by feeding the cutting tool into the fins on surface of the cylindrical workpiece. Cutting tool was uncoated tungsten carbide, with TNMG332QM-H13A designation, and workpiece material was fully annealed AISI 1045 to 165-190 BHN. Depth of cut and rake angle were held constant at 3 mm and -6˚ respectively. Tool life tests were performed for all the nine cutting conditions in Figure. 6-1. During each tool life test flank wear length and cutting time wear measured after cutting of each fin. Also the worn edge geometries were analyzed and flank wear rates were determined. Each test was repeated twice and was continued until the average flank wear reached 0.3 mm.

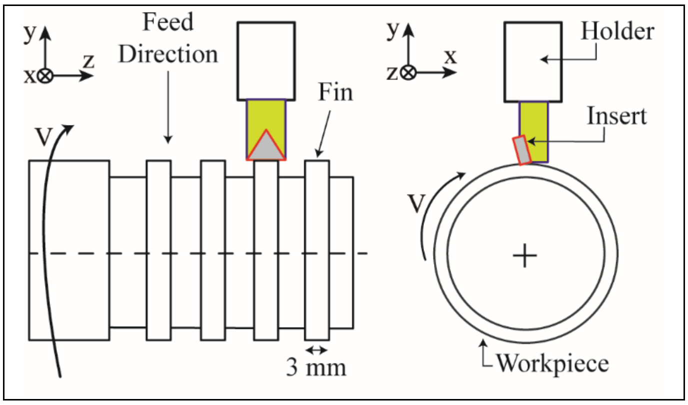

Figure 6-2. Orthogonal cutting setup.

To analyze the worn edge geometries, after machining each fin the process was stopped and worn edges were sectioned using wire electrical discharge machining (EDM). The sectioned inserts were then polished, etched, and analyzed under the optical microscope. Figure 6-3 (a) shows the micrograph of sharp cutting edge geometry and Figure 6-3 (b) to (d) show the micro-

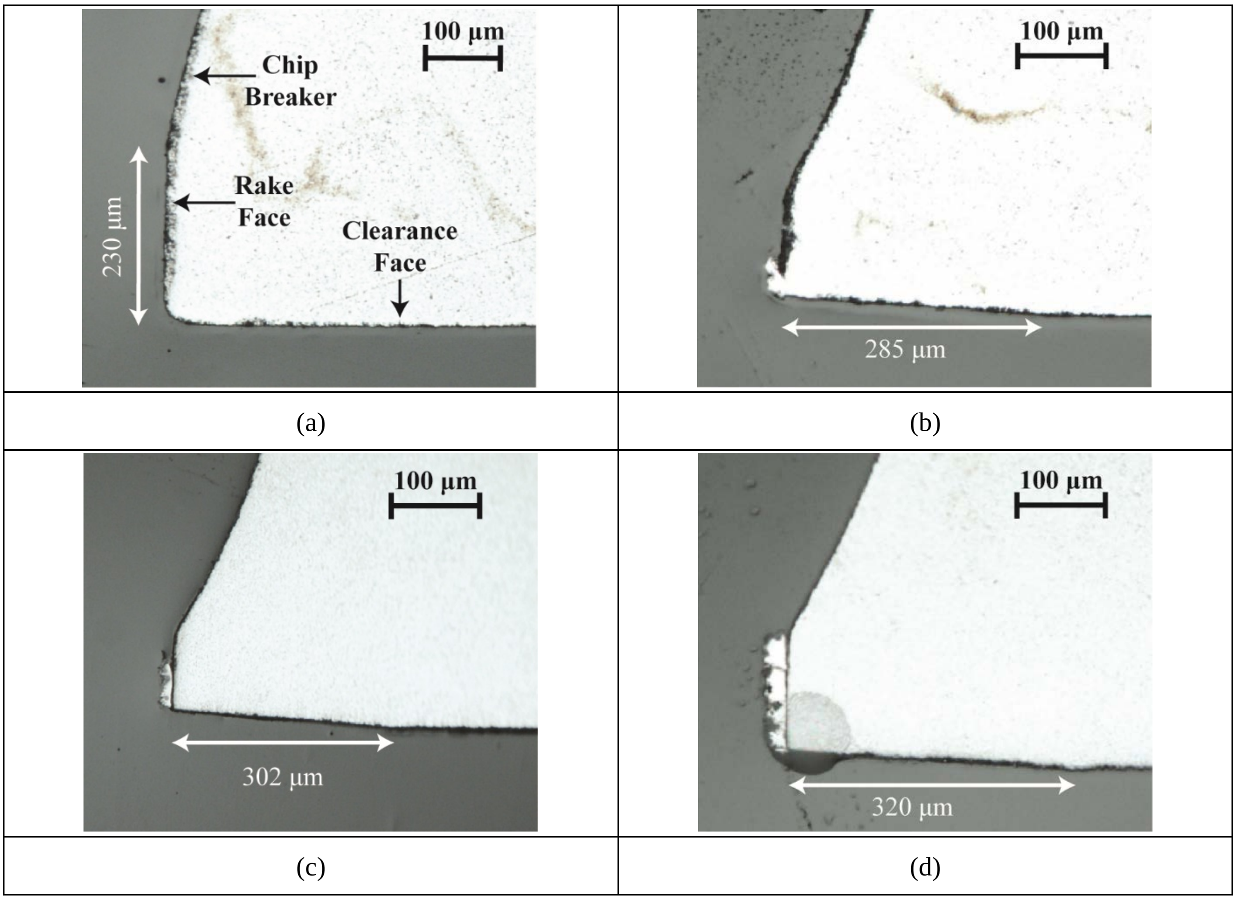

(a) (b)

(c) (d)

Figure 6-3. Cutting edge geometries a) VB=0, b) VB=285 µm when V=200 m/min, f=0.15 mm/rev c) VB=302 µm when V=250 m/min, f=0.20 and d) VB=320 µm when V=300 m/min, f=0.25 mm/rev.

graphs of cutting edge geometries used to cut at the lowest, mid-range, and highest process parameters respectively, shown in Table 6-2. It was observed that the geometries of the worn edges, more specifically the angle between the flank and rake faces, was approximately 8° at different flank wear sizes. This observation was independent from the cutting speeds and feed rates as shown in Figure 6-4. It was concluded that when cutting speed and feed rate were varied only the wear rate was changed. Therefore, it was valid to assume that the orientation of flank face relative to the rake face did not change with different process parameters investigated. Lane et al. [16] also observed similar phenomenon when machining AISI 1215 with diamond tools. Experimental observations showed that the worn edge geometries were different when cutting in low speed, 2 to 8 mm/s, medium speed, 71 to 284 mm/s, and high speed range, 1 to 4 m/s. However, in each range the angle between the flank and rake faces were similar [16].

Figure 6-5 shows the six cutting edge geometries with specific flank wear length that will be used in the FE models. During the cutting tests, time was measured when flank wear reached to approximately 100, 150, 200, 250 and 300 µm. The cutting processes were then divided into five flank wear length intervals of 0-100 µm, 100-150 µm, 150-200 µm, 200-250 µm and 250-300 µm and wear rates in these intervals were determined. Based on this approach, analysis was performed on the data obtained from the same flank wear length intervals at different cutting parameters.

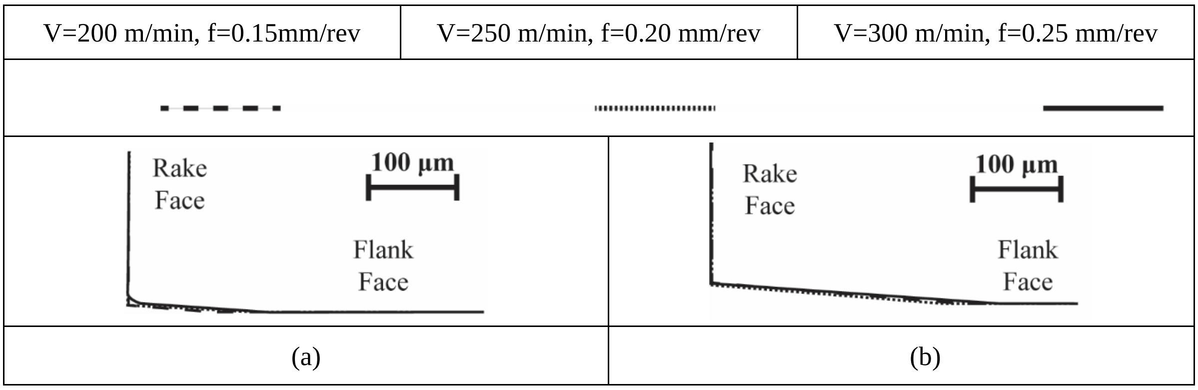

Figure 6-4. Geometry of worn edges at different cutting conditions when a) flank wear was approximately 100 µm and b) 300 µm.

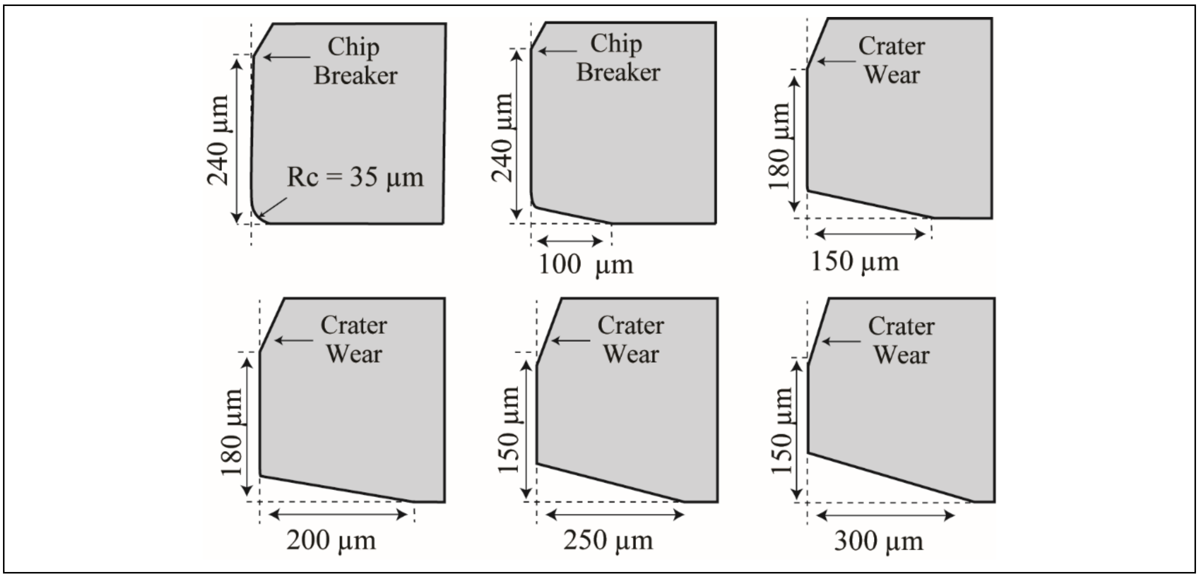

Figure 6-5. Tool edge geometries with 0, 100, 150, 200, 250 and 300 µm flank wear lengths.

A general tool life trend consists of three periods which are: a) the initial or running-in period, b) the secondary or steady-state period and c) the tertiary period [17]. Yen et al. [1] and Filice et al. [3], have reported that Takeyama & Murata and Usui models, which consider the gradual formation of wear, were unable to capture the wear rate during the initial cutting period. High wear rates are usually observed during the initial period due to micro-chipping or fracture. In present study, the data from the initial cutting period, 0-100 µm, has not been included during calibration.

Figure 6-6 shows the experimental wear rates at four flank wear intervals of 100-150 µm, 150-200 µm, 200-250 µm, and 250-300 µm when cutting based on the nine cutting conditions shown in Figure. 6-1. The flank wear interval range was arbitrary determined. The average wear rate in each flank wear interval was calculated from experiments, which were repeated twice. It was concluded that wear rate increased by increasing both cutting speed and feed rate with higher level of sensitivity to cutting speed.

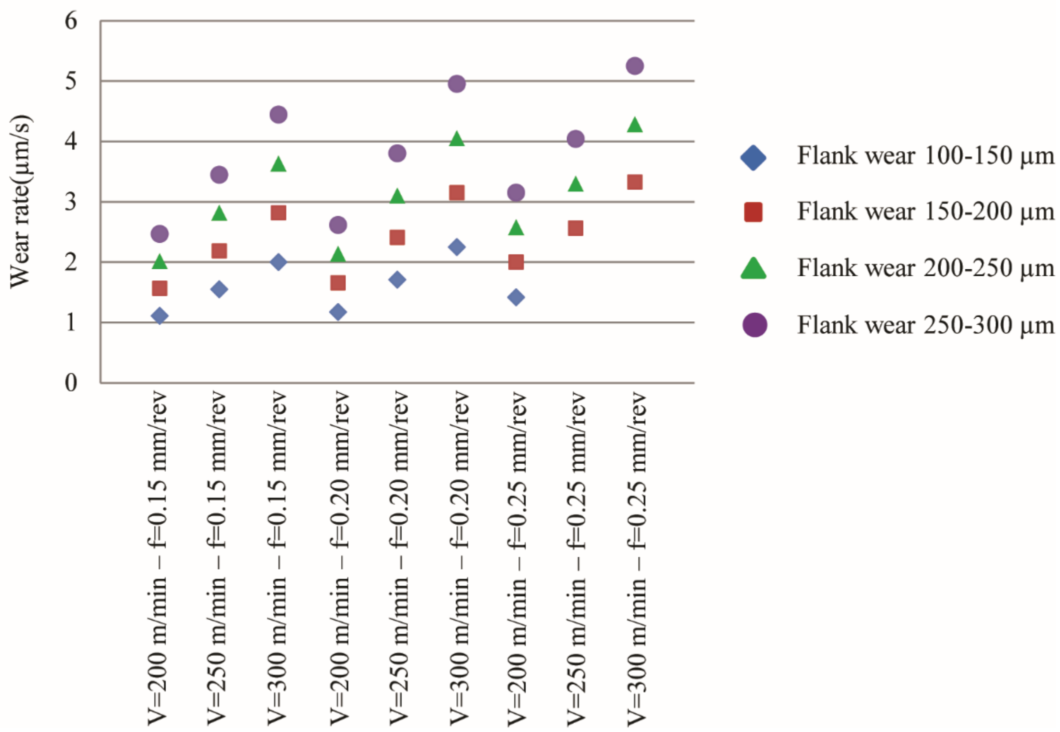

Figure 6-6. Experimental wear rate for VB=0-300µm for nine cutting conditions.

6.4 Finite Element Simulation

In step two, FE simulation was used to estimate the temperature and contact pressure on the flank face. FE models were built according to the Arbitrary Lagrangian-Eulerian (ALE) technique in Abaqus / Explicit. Figure 6-7 shows the schematic of an ALE cutting model. Based on the principles of ALE the workpiece mesh elements in the region in front of the cutting edge have been constrained from moving in x and y directions [21]. As the result, the severe deformation of material in front of the tool tip does not lead to the severe element distortion. The workpiece mesh elements in the region which form the chip and those which form the machined surface were kept un-constrained. Therefore, the final chip geometry and the tool-chip contact length would be formed based on the natural deformation of the material. The mesh elements in the rest of workpiece were only constrained from moving in y direction in order to increase the stability of simulation. The elements used in the FE models were plane strain CPE4RT. These elements were quadrilateral and thermal-mechanical with reduced

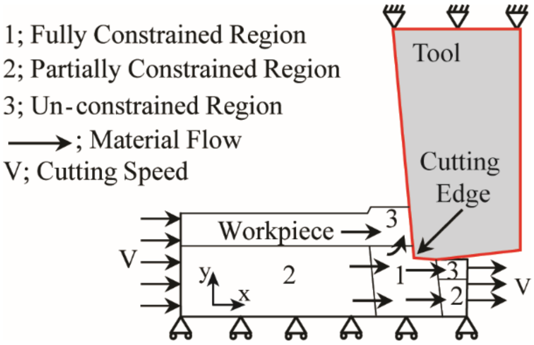

Figure 6-7. Geometry and boundary conditions of ALE cutting models.

integration and automatic hourglass control properties. The hourglass control property has been used for handling high deformation induced by the cutting process. The experimentally obtained cutting edge geometries of Figure 6-5 have been used in the FE simulations.

The Johnson-Cook (J-C) plasticity model, Eq. 6-5, was used to include the effects of strain, strain-rate, and temperature on the plastic flow stresses of the workpiece material, [18]. In the Johnson-Cook model "σ", "ε_{pl}", "$\dot{\varepsilon}_{pl}$", "$\dot{\varepsilon}_0$", and "T", represent the Von Mises flow stress, the equivalent plastic strain and strain rate, the initial strain rate, and the operating temperature respectively. Table 6-3 lists the constants "A", "B", "C", "n", and "m" which were used in the Johnson-Cook model for AISI 1045, as determined by [19]. "T_{ref}" is the reference temperature at which material constants have been determined.

$$\sigma = (A + B\varepsilon_{pl}^{n})[1 + C\ln(\dot{\varepsilon}_{pl}/\dot{\varepsilon}_0)]\{1 - [(T - T_{ref})/T_{melt} - T_{ref})]^{m}\} \quad \text{Eq. 6-5}$$

The interaction between the contacting surfaces has been modeled based on the Coulomb friction law in which the sticking and sliding conditions are the functions of normal and shear stresses. Eq. 6-6 and Eq. 6-7 show the inequalities which represent the sticking and sliding

A (MPa)	*B (MPa)*	*n*	*C*	$\dot{\varepsilon}_0$	T_{ref} (°C)	*m*
553.1	600.8	0.234	0.0134	1.0	25	1.0

Table 6-3. Johnson-Cook constants for AISI 1045 [19].

regions respectively.

$\tau < \mu\sigma$ ….. sticking region	Eq. 6-6

$\tau \geq \mu\sigma$ ….. sliding region	Eq. 6-7

In Eq. 6-6 and Eq. 6-7, σ and τ are the normal and shear stresses acting the interfaces and μ is the coefficient of friction (COF). Velocity dependent COF was used in the present work, which was based on the experimental observations by Puls et al. [20]. More details on the ALE technique in modeling the cutting process with non-worn and worn tool edge geometries can be found in Movahhedy et al. [21] and Hosseinkhani & Ng [22].

FE simulations were performed until the mechanical/thermal loadings at the interfaces reached the steady-state condition. In each simulation, the average interface temperature and contact pressure on the tool flank face were extracted and their mean values at the 100-150 µm, 150-200 µm, 200-250 µm, and 250-300 µm flank wear length intervals were calculated. Figure 6-8 shows temperature contours at 0.001s when flank wear reached 100 and 200 µm with cutting speed of 250 m/min feed rate of 0.2 mm/rev. The procedure for calculating the average temperature and pressure in each interval has been shown in Table 6-4. The temperature and contact pressure for any flank wear interval was calculated by taking the average magnitudes acquired at the start and end of the wear interval. Figure 6-9 and Figure 6-10 show the simulated

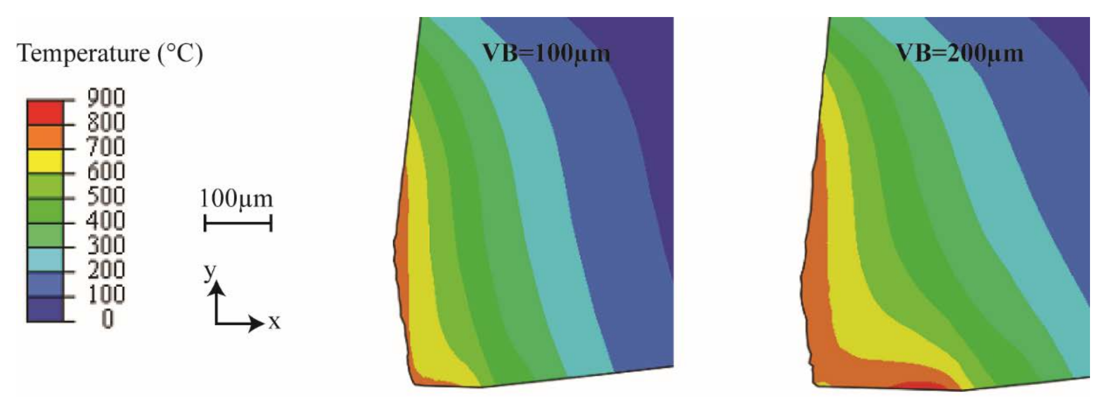

Figure 6-8. Temperature contours of the cutting tool with 100 and 200 µm flank wear lengths, V=250 m/min – f=0.2 mm/rev

Flank wear intervals	Average process variables
100-150 µm	$T_{100-150}=\frac{T_{100}+T_{150}}{2}, \sigma_{100-150}=\frac{\sigma_{100}+\sigma_{150}}{2}$
150-200 µm	$T_{150-200}=\frac{T_{150}+T_{200}}{2}, \sigma_{150-200}=\frac{\sigma_{150}+\sigma_{200}}{2}$
200-250 µm	$T_{200-250}=\frac{T_{200}+T_{250}}{2}, \sigma_{200-250}=\frac{\sigma_{200}+\sigma_{250}}{2}$
250-300 µm	$T_{250-300}=\frac{T_{250}+T_{300}}{2}, \sigma_{250-300}=\frac{\sigma_{250}+\sigma_{300}}{2}$

Table 6-4. Procedure to calculate the average process variables.

interface temperature and contact pressure in each interval for the nine cutting conditions respectively. The interface temperature and contact pressure were observed to increase linearly with an increase in the flank wear length. The magnitude of sliding velocity was assumed as unity. This is due to the fact that the effect of cutting speed has been already included in the simulated temperature and contact pressure.

It has been realized that the flank face temperature increased by the increase in both cutting speed and feed rate with more sensitivity to the cutting speed. Similar trend was observed in the experimental study by Takeyama & Murata [6]. Simulation results showed that the contact pressure on the flank face was only sensitive to the variation in cutting speed. Figure 6-11 shows the effect of cutting speed and feed rate on the simulated contact pressure on the tool flank face when flank wear length was 100 µm.

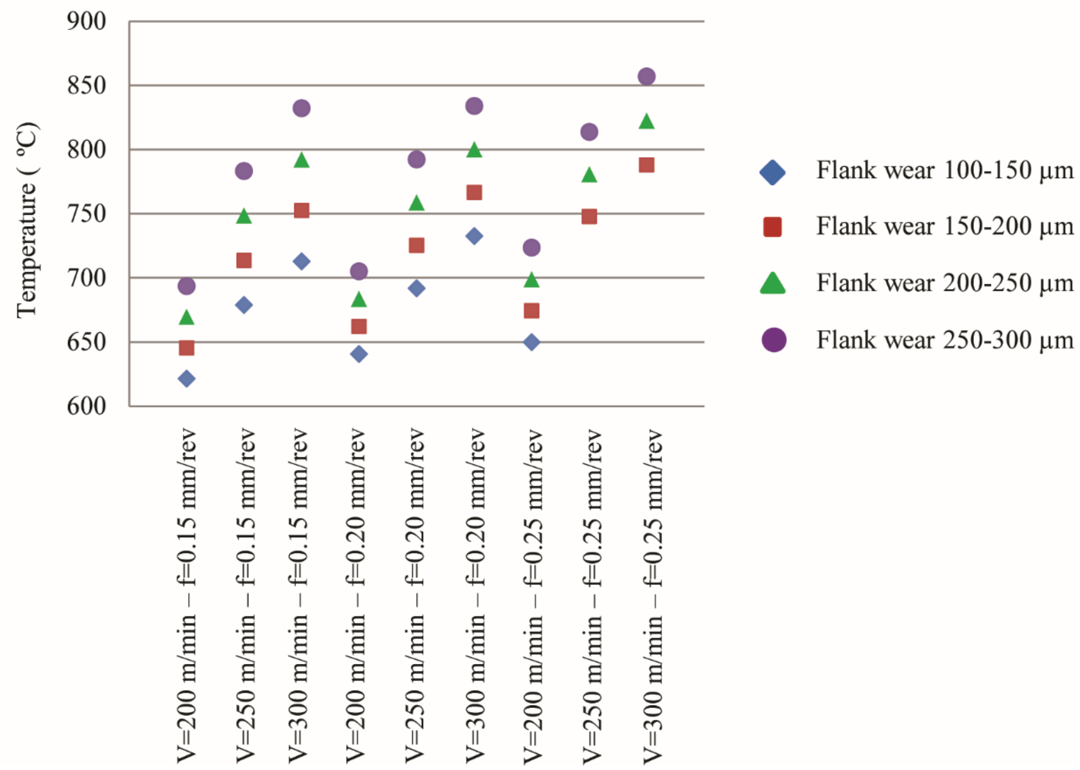

Figure 6-9. Simulated interface temperature for nine cutting conditions.

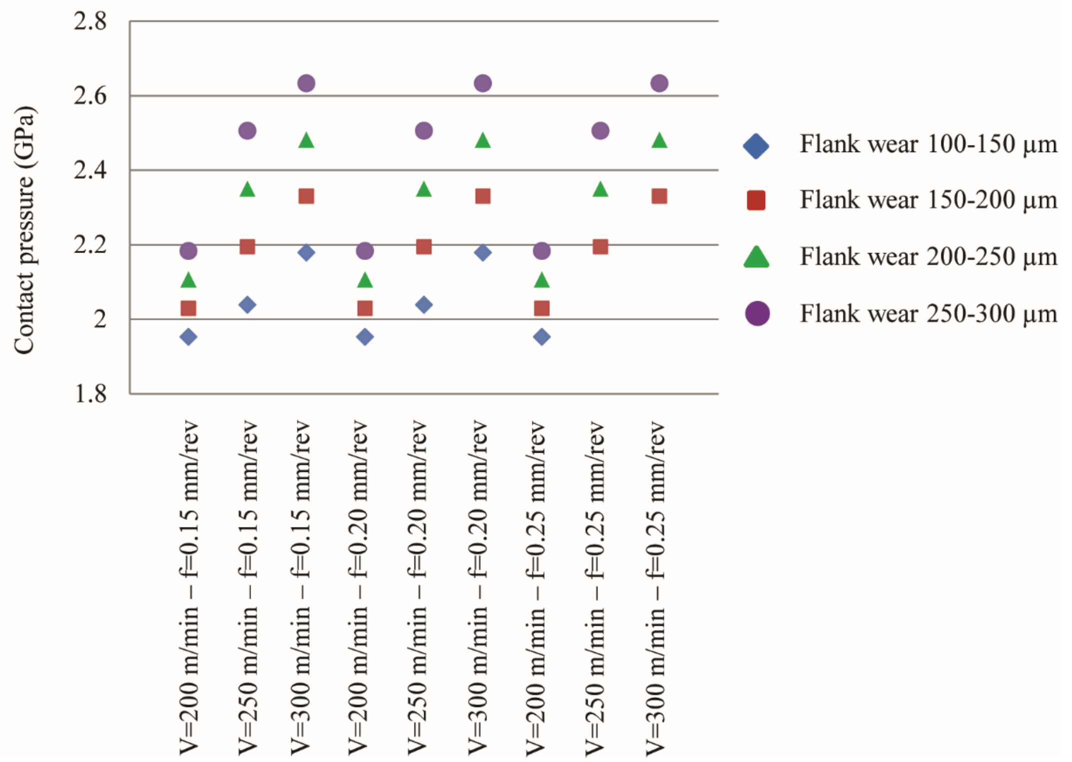

Figure 6-10. Simulated contact pressure for nine cutting conditions.

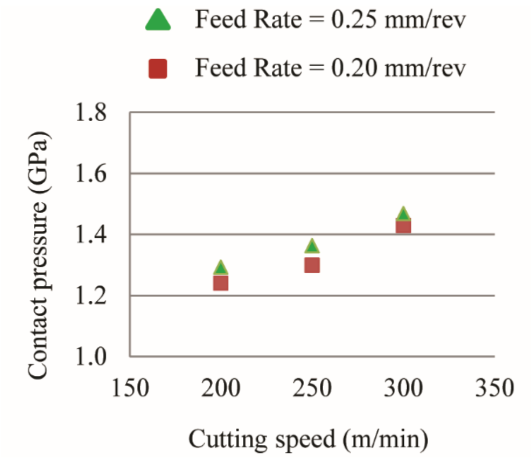

Figure 6-11. Average contact pressure on the flank face with respect to the variation in cutting speed and feed rate when flank wear was 100 µm.

6.5 Calibration Procedure

In step three and four, each of the wear rate models has been calibrated based on the hybrid procedure, as shown in the Figure 6-12. The experimental and simulated wear rates are compared and the equation constants are determined based on the principles of least squared errors. Four data sets from three different cutting conditions were chosen for calibrating the wear rate models which have been listed in Table 6-5. The four selected data sets provide different ranges of data for calibration. When data set “L” is used, all the wear rate models are calibrated based on the lowest magnitude of process variables. Similarly, when data set “M” and “H” are chosen, the models are calibrated based on the mid-range and highest magnitude of process variables respectively. Data set “LH” indicated that calibration is carried out with both the lowest and highest cutting parameters. The temperature, contact pressure and wear rate corresponding to data sets have been shown in Figure 6-13. Table 6-6 to Table 6-9 show the constants of the four wear rate models obtained by calibrating each of them based on four data sets.

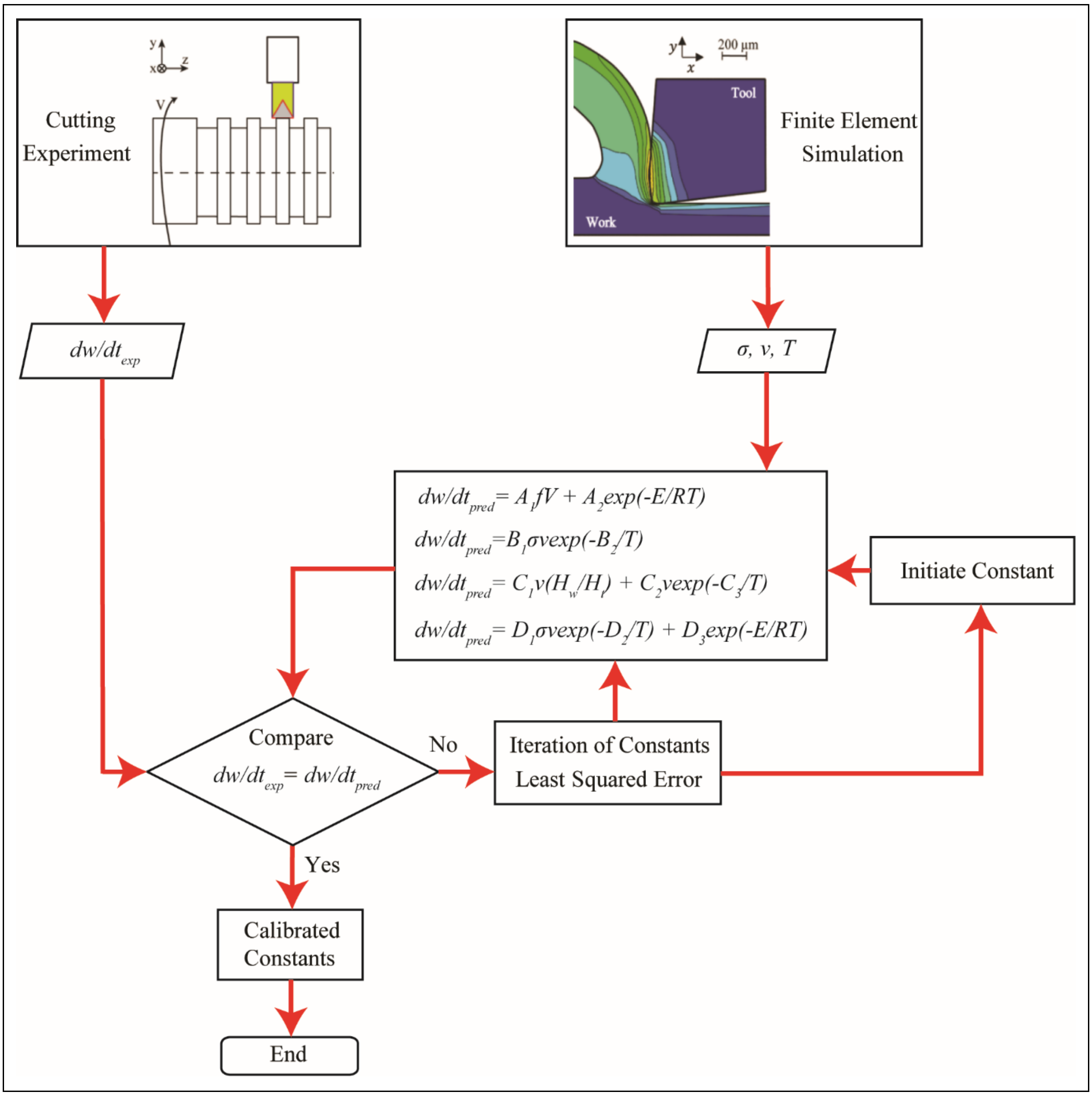

Figure 6-12. Hybrid experimental and numerical calibration procedure.

Condition	Data Set	Cutting Speed (m/min)	Feed Rate (mm/rev)
Lowest	L	200	0.15
Mid-range	M	250	0.20
Highest	H	300	0.25
Lowest / Highest	LH	200	0.15
		300	0.25

Table 6-5. Cutting conditions.

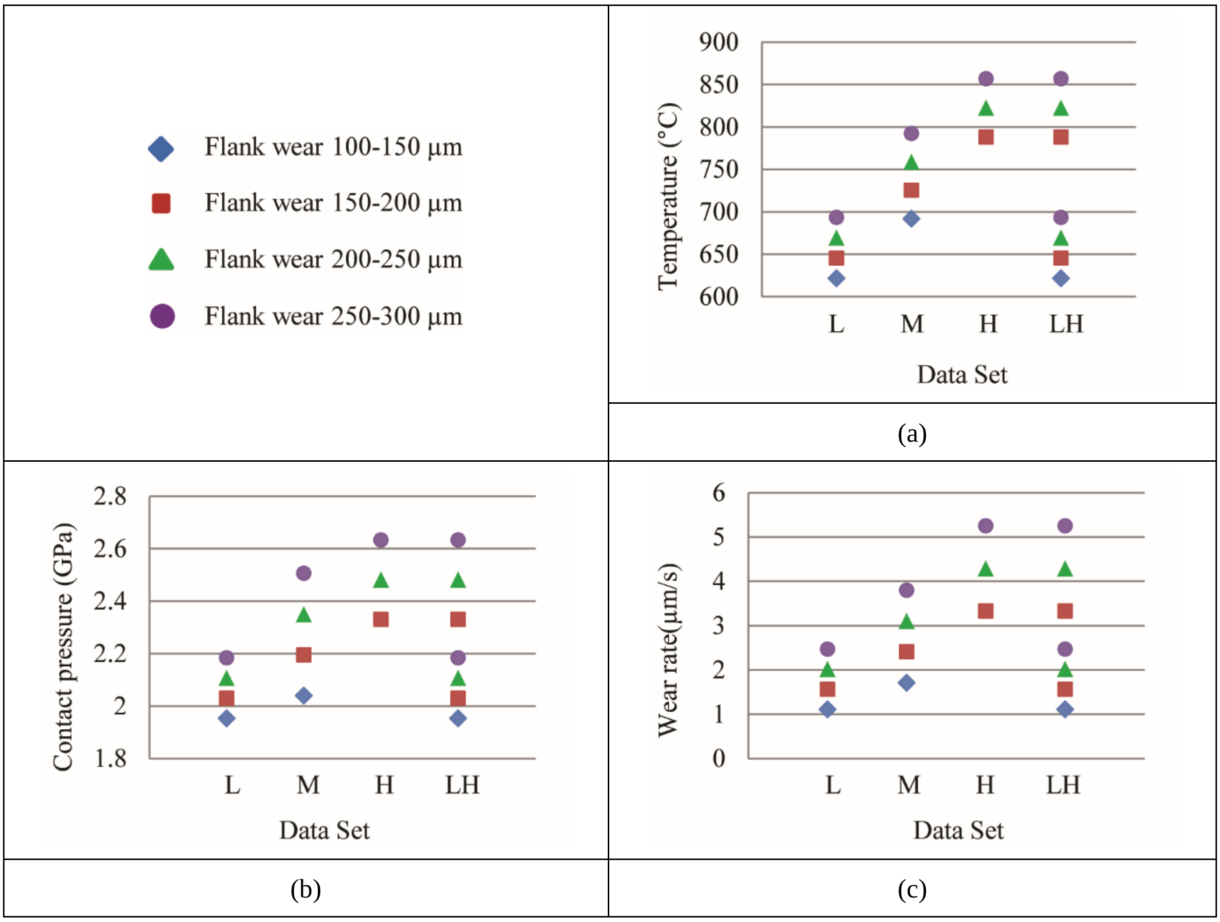

(a)

(b)

(c)

Figure 6-13. Process variables and wear rates for the four data sets to be used in calibration a) simulated temperature on flank face, b) simulated contact pressure on flank face and c) experimental flank wear rate.

Boundary Condition	Cutting Speed (m/min)	Feed Rate (mm/rev)	A_1(s/Mm)	$A_2=a_1T+a_2$	
				a_1(m/MsC)	a_2(m/Ms)
Lowest (L)	200	0.15	3500	N/A	N/A
Middle (M)	250	0.20	2000	0.0362	-24.55
Highest (H)	300	0.25	N/A	0.0325	-22.44
Lowest/Highest (LH)	200	0.15	3500	0.0326	-22.51
	300	0.25			

Table 6-6. Calibrated Takeyama & Murata model constants based on four boundary conditions.

Boundary Condition	Cutting Speed (m/min)	Feed Rate (mm/rev)	B_1(m^2/MN)	B_2(C)
Lowest (L)	200	0.15	1.24E-6	4814
Middle (M)	250	0.20	4.80E-7	4495
Highest (H)	300	0.25	3.94E-7	4483
Lowest/Highest (LH)	200	0.15	8.11E-8	3134
	300	0.25		

Table 6-7. Calibrated Usui model constants based on four boundary conditions.

Boundary Condition	Cutting Speed (m/min)	Feed Rate (mm/rev)	C_1(-)	C_2(-)	C_3(C)
Lowest (L)	200	0.15	10	6.47E+7	12200
Middle (M)	250	0.20	10	1.98E+4	6909
Highest (H)	300	0.25	10	4.62E+3	5885
Lowest/Highest (LH)	200	0.15	2	1.58E+3	6905
	300	0.25			

Table 6-8. Calibrated Akazawa model constants based on four boundary conditions.

Boundary Condition	Cutting Speed (m/min)	Feed Rate (mm/rev)	D_1(m^2/MN)	D_2(C)	$D_3=d_1T+d_2$	
					d_1(m/MsC)	d_2(m/Ms)
Lowest (L)	200	0.15	1.24E-6	4814	N/A	N/A
Middle (M)	250	0.20	2.93E-8	2547	0.0114	-7.94
Highest (H)	300	0.25	4.24E-9	1199	0.0150	-10.47
Lowest/Highest (LH)	200	0.15	7.78E-9	1583	0.0135	-9.301
	300	0.25				

Table 6-9. Calibrated Attanasio model constants based on four boundary conditions.

6.6 Results and Discussions

In step five, the calibration of four wear rate models are discussed in sections 7.6.1 and 7.6.2. In section 7.6.1, the calibration of four wear rate models is discussed in terms of their level of sensitivity to the dominant wear mechanism. In section.7.6.2, the calibration of four wear rate models is evaluated in terms of the least amount of assumptions or quantitative unknowns.

6.6.1 Effect of the activation temperature of diffusion on calibration

Total wear rate based on the Takeyama & Murata [6] and Attanasio et al., [4] models have been related to the activation temperature of diffusion, as shown in Table 6-1. Figure 6-13 (a) shows the average flank face temperature for the chosen four data sets. Attanasio et al, found that for similar combination of tool and work materials used in the current research, the activation temperature of diffusion was 700ºC [4]. This temperature criterion on the wear rate models affected the selection of data sets during calibration.

There was no temperature criterion imposed on the Usui and Akazawa models, as shown in Eq. 6-2 and Eq. 6-3 respectively. Therefore, these models could be calibrated based on any of the four collected data sets shown in Figure 6-13, which covered the calibration of their abrasive and diffusive sections. On the other hand, temperature criteria imposed on the Takeyama & Murata and Attanasio models limited the choice of data sets for covering the calibration of their abrasive and diffusive sections. When data set “L” was chosen, only the abrasive parts of Takeyama & Murata and Attanasio models could be calibrated as its temperature range, between 621 to 693°C, was below the activation temperature of diffusion. On the other hand, when the data set “H” was chosen, only the diffusive section of Takeyama & Murata model and the combined abrasive/diffusive section of Attanasio model could be calibrated, as its temperature range as between 753 to 857°C which was above the activation temperature of diffusion.

6.6.2 Effect of wear mechanism proportions on calibration

Takeyama & Murata together with Attanasio wear rate models required the information regarding the proportion of dominant wear mechanisms during calibration. During metal cutting when the worn edge geometries were analyzed, the total wear rate was mainly due to abrasion and diffusion wear mechanisms and it was impossible to separate the amount of removed tool material due to different wear mechanisms.

Takeyama & Murata total wear rate model was such that the abrasive wear rate was dominant as long as the temperature was below the activation temperature of diffusion, as detailed in Eq. 6-1 a. Above the activation temperature, the total wear rate was calculated based on an expression for diffusion, as shown in Eq. 6-1 b. This meant that the total wear rate below and above the activation temperature of diffusion was calculated based on two separate equations. Therefore, it was critical to know the activation temperature of diffusion when calibrating the Takeyama & Murata model.

The total wear rate according to Usui was based on one expression which included the effects of abrasion and diffusion coupled together as shown in Eq. 6-2. Therefore, there was no need to know the activation temperature of diffusion nor to consider the proportion of wear rate due to each mechanism during calibration.

Akazawa equation estimated the total wear rate based on a combined abrasive/diffusive expression, as detailed in Eq. 6-3. The abrasive wear proportion was based on the relative hardness between the tool and work materials which decreased at higher temperature. The diffusive wear was an exponential function of temperature and followed an increasing trend at higher temperature. Figure 6-14 (a) and (b) show the relative hardness and the abrasive and diffusive wear rate proportions with temperature respectively. The proportion of abrasion was estimated as the direct function of relative hardness and the reminder from total wear was diffusive wear. Therefore, there was no need to assume the proportion of abrasion and diffusion. The challenge was to collect data regarding the hardness of the specific tool and

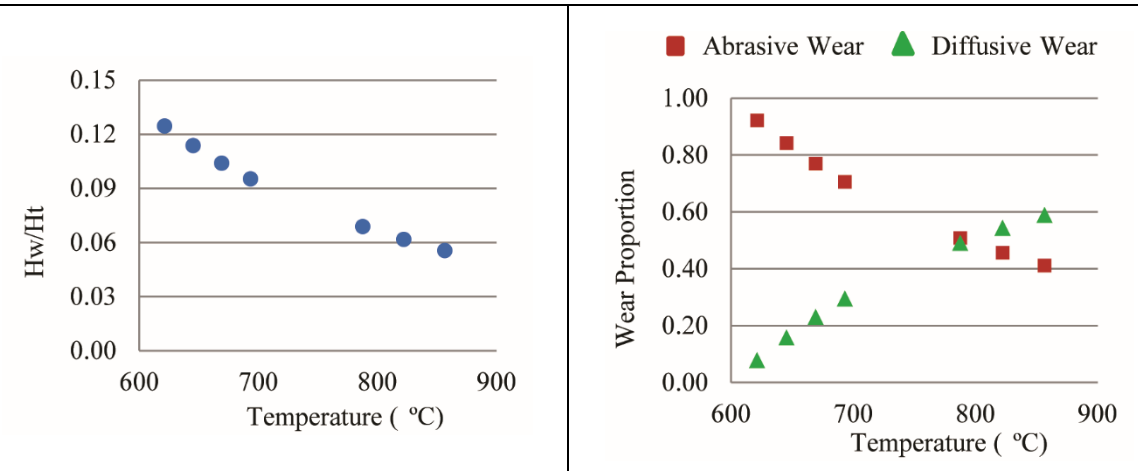

(a) (b)

Figure 6-14. Effect of temperature on a) relative hardness of work and tool materials [8] and b) proportion of abrasive and diffusive wear rates with respect to total wear rate.

work materials from room temperature to the elevated temperature of approximately 900°C. The relations between hardness and temperature shown in Figure 6-14 were based on the expressions provided by [8].

Attanasio model also required the activation temperature of diffusion, as it was required in calibrating Takeyama & Murata model. The total wear rate according to Attanasio was calculated from one expression for abrasion when the temperature was below the activation temperature of diffusion, as detailed in Eq. 6-4 (a). Above the activation temperature a combined abrasive/diffusive expression was used, where both abrasion and diffusion were exponential functions of temperature, as detailed in Eq. 6-4 (b). When calibrating Attanasio's model, assumptions had to be made on both abrasive and diffusive wear rate proportions with temperature since the proportions of wear mechanisms were impossible to determine experimentally. In the current evaluation of Attanasio's model, when the flank-workpiece interface temperature was below the activation temperature of diffusion, 100% of the tool wear rate was induced by abrasion. Above the activation temperature, it was assumed that the proportion of abrasion gradually decreased while the proportion of diffusion gradually increased. Figure 6-15 shows two arbitrary conditions which could be used during calibration. In the first condition, at the highest temperature of 857°C, the final proportion of both

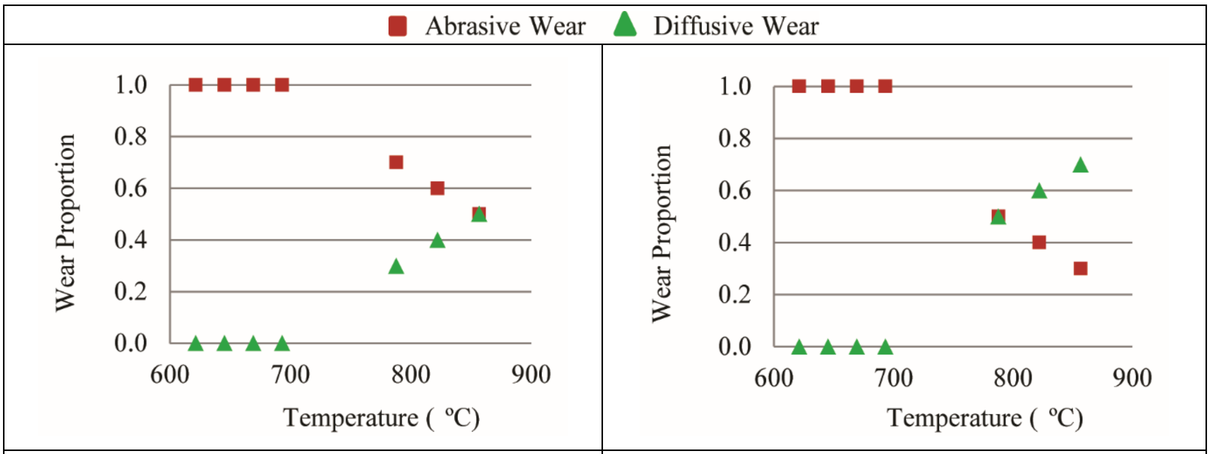

(a) (b)

Figure 6-15. Effect of temperature on the proportions of abrasive and diffusive wear rates when a) at the highest temperature both abrasion and diffusion were 50% of total wear and b) at the highest temperature abrasion was 30% and diffusion was 70%

mechanisms were assumed to be 50% of the total wear, as shown in Figure 6-15 (a). In the second condition, the final proportion of abrasion and diffusion were assumed to be 30% and 70% of total wear at 857°C, as shown in Figure 6-15 (b).

The wear rate model proposed by Usui was easiest to calibrate. There was no activation temperature of diffusion criterion imposed on the model which resulted in unbounded restriction in selecting cutting parameters for calibration. Also there was no need to gather information regarding the activation temperature of diffusion and the relative hardness of the work and tool materials. Furthermore, the calibration of Usui was less uncertain as the total wear rate was calculated according to a single expression. Therefore, the wear rate data obtained from experiment could be directly applied to the calibration and no extra assumptions regarding the proportions of wear due to different dominant wear mechanisms were required.

6.6.3 Optimum experiment/simulation for model calibration

In step six, the Usui model, which was calibrated based on four data sets, were compared and the optimum number of experiment/simulation for data collection was determined.

Figure 6-16 (a) to (f) show the predicted wear rates obtained by calibrating Usui model with the lowest “L”, mid-range “M”, highest “H” and combination of the lowest and highest “LH” process parameters. The constants of the calibrated models are listed in Table 6-10. Experimental wear rates were also included in Figure 6-16 and four data points in each graph

Boundary Condition	Cutting Speed (m/min)	Feed Rate (mm/rev)	$B_1(m^2/MN)$	$B_2(C)$
Lowest (L)	200	0.15	1.24E-6	4814
Middle (M)	250	0.20	4.80E-7	4495
Highest (H)	300	0.25	3.94E-7	4483
Lowest/Highest (LH)	200	0.15	8.11E-8	3134
	300	0.25		

Table 6-10. Calibrated model constants based on four boundary conditions

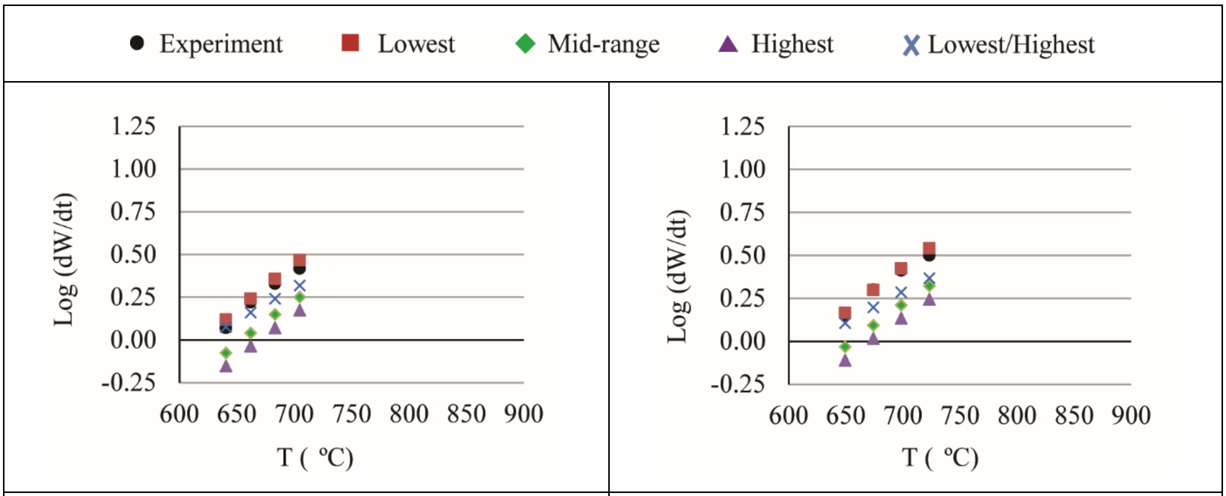

a) V=200 m/min – f=0.20 mm/rev

b) V=200 m/min – f=0.25 mm/rev

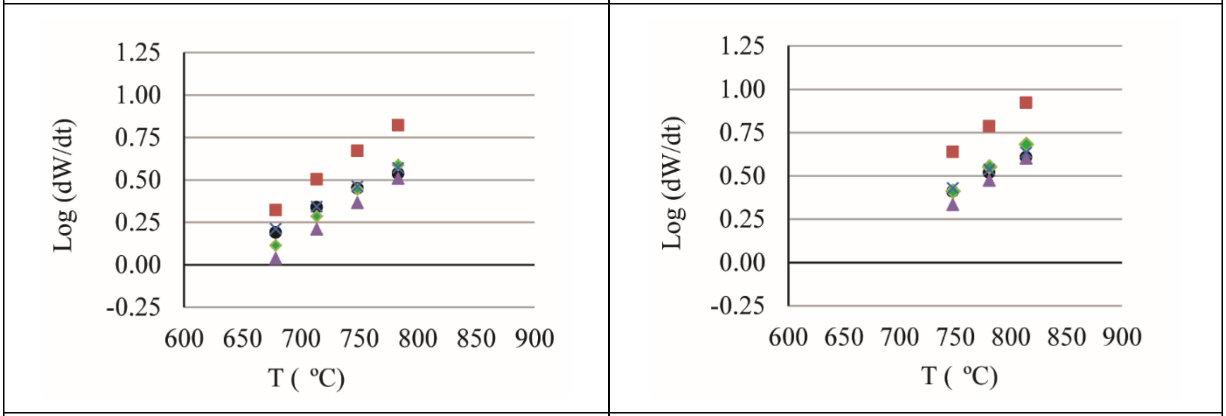

c) V=250 m/min – f=0.15 mm/rev

d) V=250 m/min – f=0.25 mm/rev

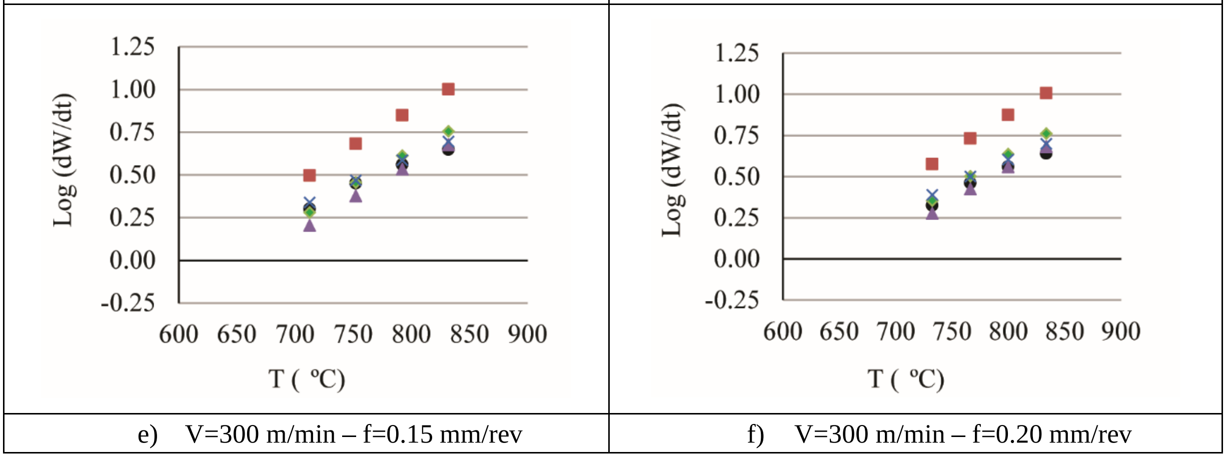

e) V=300 m/min – f=0.15 mm/rev

f) V=300 m/min – f=0.20 mm/rev

Figure 6-16. Comparison between predicted wear rates and experiment when Usui wear rate model was calibrated based on four sets of cutting parameters.

represent the wear rates in 100-150 µm, 150-200 µm, 200-250 µm, and 250-300 µm flank wear intervals.

Figure 6-17 and Figure 6-18 show the relation between the tool flank – workpiece interface temperature and contact pressure with the predicted and experimental wear rates respectively.

In Figure 6-17 (a) and Figure 6-18 (a), the calibrated constants were based on the lowest “L” magnitude of cutting speed and feed rate. In Figure 6-17 (a) both experimental and predicted results showed that wear rate has an exponential trend with respect to temperature. At lower temperature range, the predicted results agreed well with experimental results in terms of trend and magnitude. However, at higher temperature the predicted results diverged from experiments. In Figure 6-18 (a), the predicted wear rates were within the experimental wear rate range at low and high values of contact pressure. With reference to Figure 6-16 (a) and (b), the cutting speed was held at 200 m/min which was the same as the “L” cutting speed magnitude during calibration. The feed rate was 0.20 mm/rev and 0.25 mm/rev respectively which were higher than the feed rate of the “L” calibration parameter of 0.15 mm/rev. In general, increasing feed rate resulted in slight increase in the flank-workpiece interface temperature. Predicted flank-workpiece interface temperature showed that increasing feed rate from 0.15 mm/rev to 0.25 mm/rev only resulted in an increase of less than 40°C at all cutting speeds simulated. Therefore, the predicted and experimental wear rates were in close agreement in Figure 6-16 (a) and (b) when using the “L” process parameters for calibration. This observation is only valid if the workpiece material is insensitive to strain hardening.

At higher cutting speeds, the predicted wear rates using the calibrated constants from the “L” process parameter did not agree well with experimental results, as shown in Figure 6-16 (c) to (f). This was likely due to a substantial increase in flank-workpiece interface temperature at higher cutting speeds. Predicted flank-workpiece interface temperature was increased by at least 100°C when cutting speed was increased from 200 m/min to 300 m/min. This induced substantial difference between the predicted and experimental wear rates at higher temperatures as shown in Figure 6-17 (a). Attanasio made similar observation, where Eq. 4 was calibrated at the lowest speed and feed which resulted in large differences between predictions and experiments at the highest speed and feed [4].

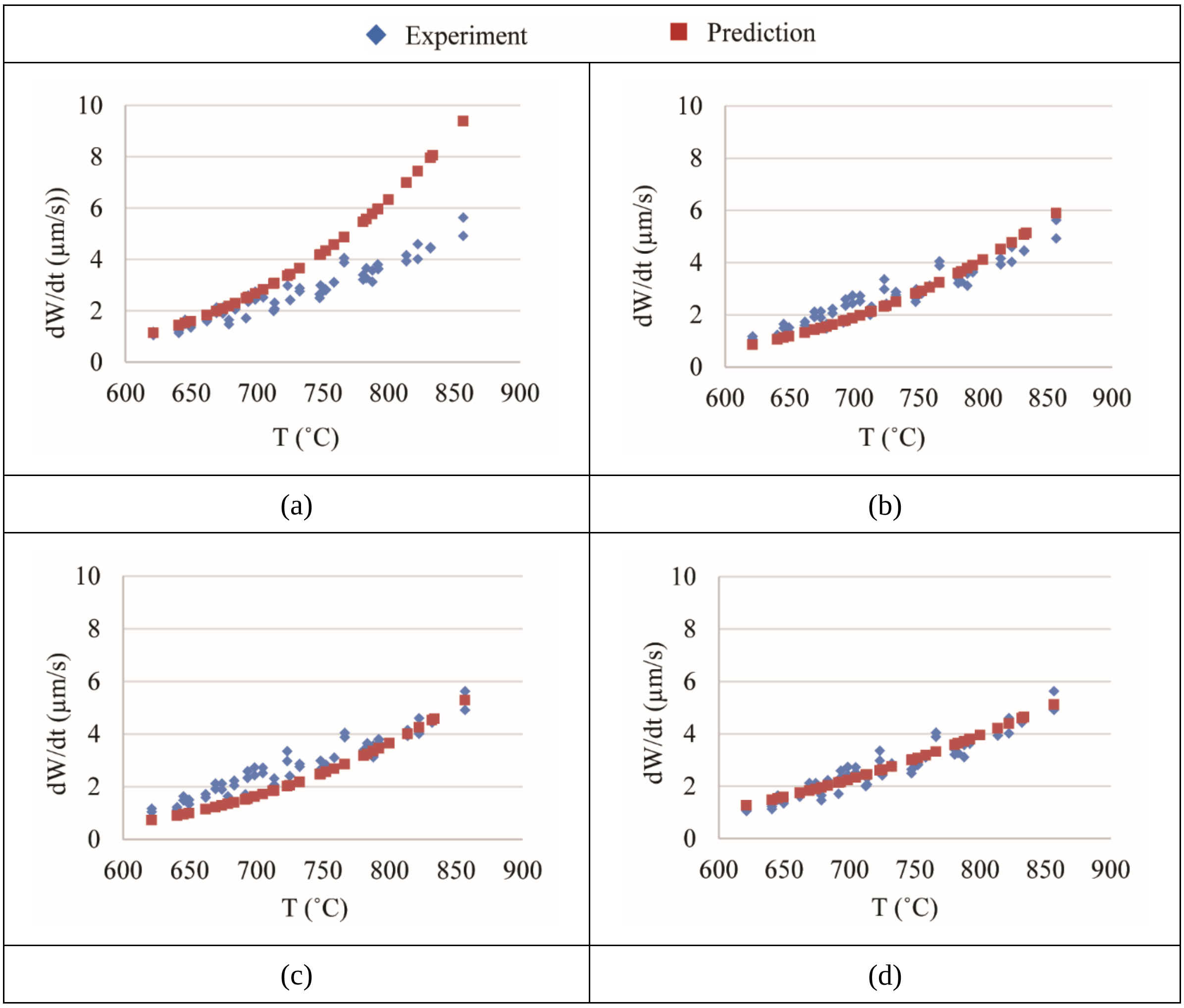

(a) (b) (c) (d)

Figure 6-17. Relation between experimental and predicted wear rates calculated as the exponential function of interface temperature. Calibration based on a) lowest, b) middle, c) highest and d) combined lowest/highest process parameters.

When the calibrated constants were based on the “M” process parameters with cutting speed of 250 m/min and feed rate of 0.2 mm/rev, the predicted wear rates agreed well with experimental results when cutting speed was held at 250 m/min and feed rates were between 0.15 mm/rev and 0.25 mm/rev, as shown in Figure 6-16 (c) and (d) respectively. However, when the cutting speed was 200 m/min with 0.20 mm/rev and 0.25 mm/rev feed rates, the predicted wear rates were lower than the experimental results as shown in Figure 6-16 (a) and (b) respectively. This was likely due to the under-prediction of wear rate at lower temperature, as shown in Figure 6-17 (b). In general, lower cutting speed tends to generate lower temperature along the primary shear zone and any contacting interfaces. Therefore, based on the lower cutting speeds in Figure 6-16 (a) and (b), lower contacting interface temperature was generated resulting in under-estimation in predicted wear rate. Similar trend was observed when cutting speed was increased to 300m/min, as shown in Figure 6-16 (e) and (f), except the predicted wear rates were higher than the experimental data. This was due to the over-prediction of wear rate at higher contacting temperature.

When the calibration constants were determined based on the highest process parameters, "H", with cutting speed of 300 m/min and feed rate of 0.25 mm/rev, the predicted wear rates were in close agreement with experimental data when cutting speed was held constant at 300 m/min and feed rate was between 0.15 mm/rev to 0.20 mm/rev, as shown in Figure 6-16

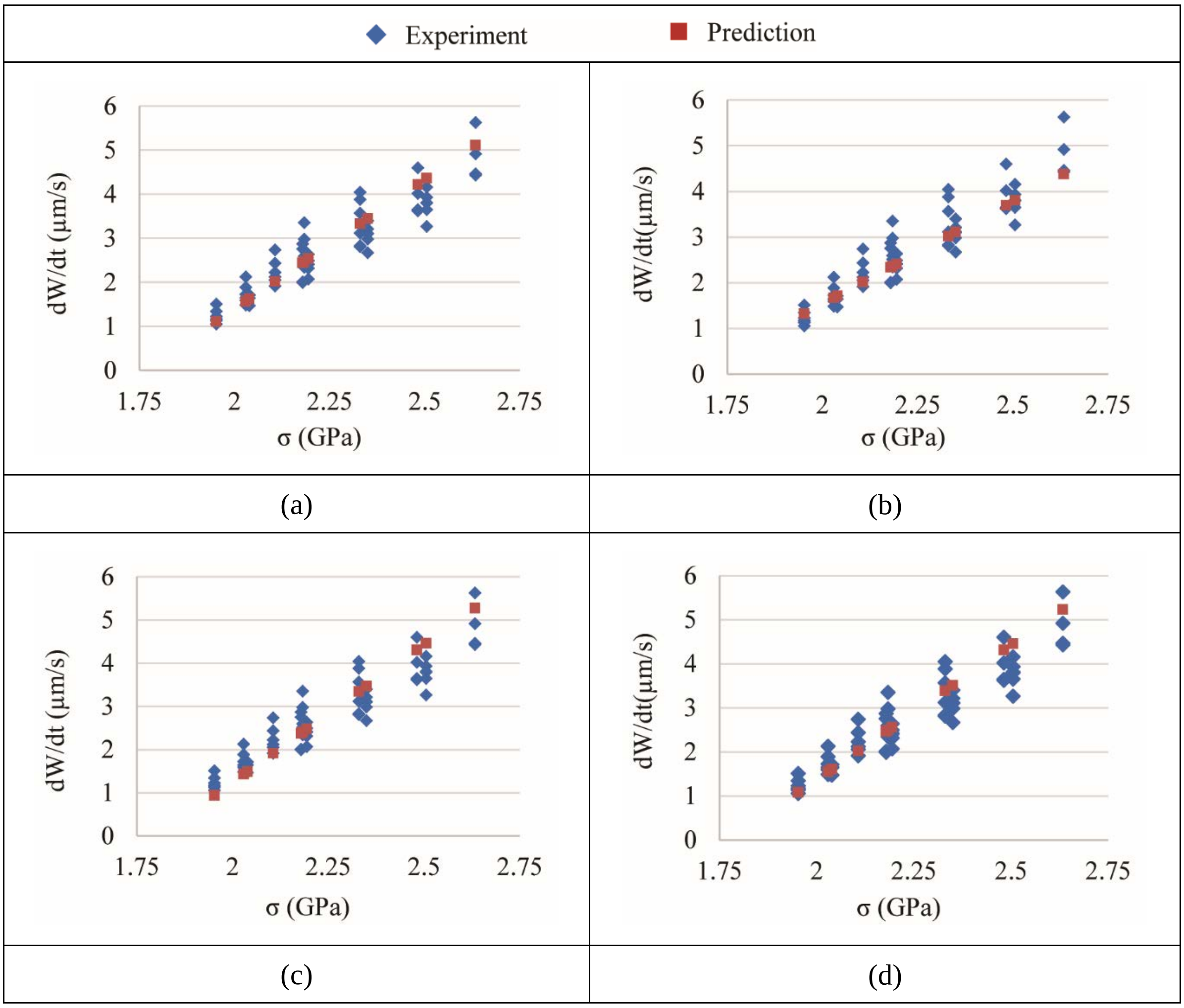

(a)

(b)

(c)

(d)

Figure 6-18. Relation between experimental and predicted wear rates calculated as the linear function of contact pressure. Calibration based on a) lowest, b) middle, c) highest and d) combined lowest/highest process parameters.

(e) and (f) respectively. With reference to Figure 6-16, the predicted wear rates based on the medium and highest process parameters were very close. This was due to the fact that the magnitudes of calibrated constants based on these two sets of process parameters were similar, as shown in Table 6-10. The effect of contact pressure and temperature on predicted wear rates based on calibrating with the lowest “L”, medium “M” and highest “H” process parameters, is detailed in Figure 6-19. It has been realized that regardless of temperature magnitude, the “M” and “H” process parameters predicted similar wear rates with respect to contact pressure.

When the calibrated constants were based on two sets of process parameters, the overall predicted wear rates agreed better with experiment when compared to calibrations based on other conditions, as shown in Figure 6-16 (a) to (f). One set of cutting parameters used for calibration had the lowest speed and feed, “L”, and the other set had the highest speed and feed, “H”.

With reference to Figure 6-17 (d), when calibration was performed based on the lowest and highest process parameters, the wear rate was controlled by the lowest and highest limits of the simulated temperature. Therefore, better convergence in the exponential relation between temperature and wear rate was achieved through the whole temperature range of 621°C to

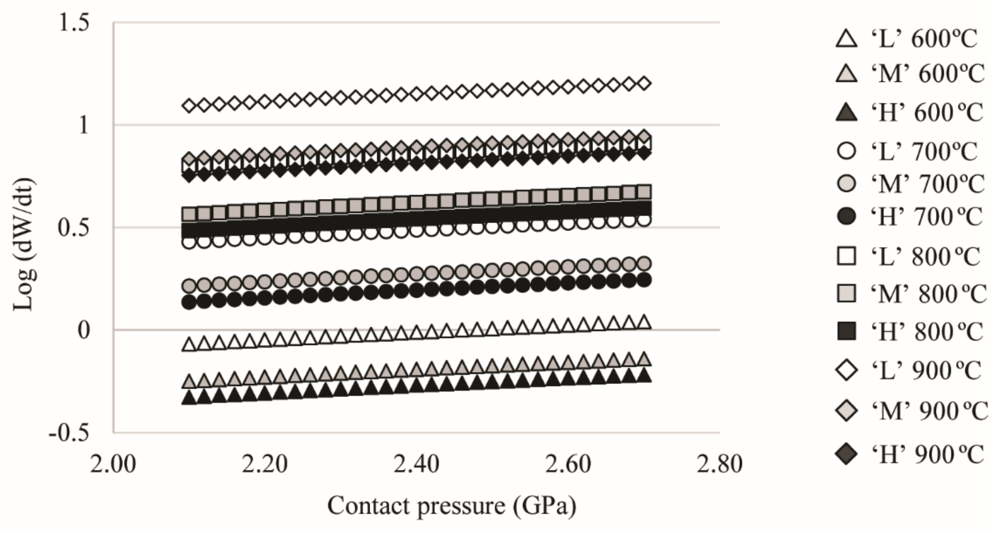

Figure 6-19. Effect of contact pressure, temperature and calibrated constants on wear rate predictions.

857°C when compared to when the lowest, mid-range or highest process parameters were used. Due to the linear relation between contact pressure and wear rate with this range of cutting parameters, imposing the lowest and highest limits did not improve the relation between pressure and wear rate, as shown in Figure 6-18 (a) to (d).

6.7 Conclusions

In this paper, a combined finite element simulation and experimental approach was used to calibrate different wear rate models. The following conclusions were made based on orthogonal cutting of AISI 1045 with uncoated tungsten carbide tool and process parameters detailed in Table 6-2:

- Both Usui and Akazawa wear models can be calibrated without knowing the dominant wear mechanism of either abrasion or diffusion. However, Akazawa model requires the detail description on how temperature affects hardness for both workpiece and tool material.
- Prior knowledge of the flank face temperature is critical when calibrating both Takeyama & Murata and Attanasio models. When the magnitude of the flank face temperature was lower than activation temperature of diffusion, only the abrasive component of the equation could be calibrated. This condition affects the selection of process parameters magnitude during the experimental phase for model calibration. Moreover, limited information could be found on activation temperature of diffusion relative to different workpiece and tool material combinations.
- Usui wear rate model was the most robust when compared to the other models investigated. This was because there is unbounded restriction in selecting process parameters during model calibration. Also the information regarding the dominant wear

mechanism as a function of temperature is not required. Furthermore, latter information is very difficult to determine quantitatively with experiments.

- When calibrating Usui's wear model, the predicted wear rate was controlled by the lower and upper limit of the simulated flank face temperature. Therefore, it is critical to perform experiments that are capable of capturing the lower and upper limit of the operating temperature during model calibration.
- With the current combination of the workpiece and tool material used, calibrating Usui's wear model based on combination of lowest and highest process parameters showed to be most efficient. The number of experiments to be carried out should increase if the workpiece material is sensitive to strain rate and strain hardening.

6.8 Acknowledgement

The author is thankful for the financial support provided by NSERC CANRIMT and Discovery Grant.

6.9 References

[1] Yen YC, Söhner J, Lilly B, Altan T (2004) Estimation of tool wear in orthogonal cutting using the finite element analysis. Journal of Material Processing Technology 146: 82-91

[2] Xie LJ, Schmidt J, Schmidt C, Biesinger F (2005) 2D FEM estimate of tool wear in turning operation. International Journal of Wear 258:1479-1490

[3] Filice L, Micari F, Settineri L, Umbrello D (2007) Wear modelling in mild steel orthogonal cutting when using uncoated carbide tools. International Journal of Wear 262:545-554

[4] Attanasio A,Ceretti E, Fiorentino A, Cappellini C, Giardini C (2010) Investigation and FEM-based simulation of tool wear in turning operations with uncoated carbide tools. International Journal of Wear 269:344-350

[5] Attanasio A, Ceretti E, Giardini C (2011) 3D FEM simulation of flank wear in turning. 14th International ESAFORM Conference on Material Forming, Belfast 561-566.

[6] Takeyama H, Murata R (1963) Basic investigation of tool wear. Trasaction of ASME, Journal of Engineering for Industry 33-38

[7] Usui E, Shirakashi T, Kitagawa T (1984) Analytical prediction of cutting tool wear. International Journal of Wear 100:129-151

[8] Akazawa K, Ozaki K, Shamoto E (2009) Development of a System to Predict Tool Wear Considering Cutting Conditions and Workpiece Components. Journal of the Japan Society for Precision Engineering 75:396-401

[9] Lotfi M, Jahanbakhsh M, Akhavan Farid A (2016) Wear estimation of ceramic and coated carbide tools in turning of Inconel 625: 3D FE analysis. Tribology International 99:107–116

[10] Malakizadi A, Cedergren S, Surreddi KB, Nyborg L (2013) A methodology to evaluate the machinability of Alloy 718 by means of FE simulation. Proceedings of Advanced Manufacturing Engineering and Technologies NEWTECH. Stockholm 95-106

[11] Haddag B, Nouari M (2013) Tool wear and heat transfer analyses in dry machining based on multi-steps numerical modelling and experimental validation. International Journal of Wear 302:1158–1170

[12] Binder M, Klocke F, Doebbeler B (2017) An advanced numerical approach on tool wear simulation for tool and process design in metal cutting. Simulation Modelling Practice and Theory 70:65–82

[13] Zanger F, Schulze V (2013) Investigation on mechanisms of tool wear in machining of ti-6al-4v using fem simulation. Proceeding of the 14th international conference on modeling the machining operation (CMMO), Torino 8:158-163

[14] Kitagawa T, Maekawa K, Shirakashi T, Usui E (1988) Analytical prediction of flank wear of carbide tools in turning plain carbon steels, part 1: Characteristic equation of flank wear. Bulletin of the Japan Society of Precision Engineering, 22:263-269

[15] Kitagawa T, Maekawa M, Shirakashi T, Usui E (1989) Analytical prediction of flank wear of carbide tools in turning plain carbon steels, part 2: prediction of flank wear. Bulletin of the Japan Society of Precision Engineering, 23:126-133

[16] Lane BM, Dow TA, Scattergood R (2013) Thermo-chemical wear model and worn shapes for single-crystal diamond tools cutting steel. International Journal of Wear, 300: 216-224

[17] Shaw MC (2005) Metal Cutting Principles. Oxford University Press Inc

[18] Johnson GJ, Cook WH (1983) A constitutive model and data for metals subjected to large strains, high strain rates and high temperatures. Proceedings of the 7th International Symposium on Ballistics, 541-547

[19] Jaspers S, Dautzenberg JH (2002) Material behaviour in conditions similar to metal cutting: flow stress in the primary shear zone. Journal of Materials Processing Technology, 122:322-330

[20] Puls H, Klocke F, Lung D (2012) A new experimental methodology to analyse the friction behaviour at the tool-chip interface in metal cutting. Journal of Production Engineering, 6:349–354

[21] Movahhedy M, Gadala MS, Altintas Y (2000) Simulation of the orthogonal metal cutting process using an arbitrary Lagrangian–Eulerian finite-element method. Journal of Materials Processing Technology 103:267–275.

[22] Hosseinkhani K, Ng E (2013) Analysis of the cutting mechanics under the influence of worn tool geometry. Proceeding of the 14th international conference on modeling the machining operation (CMMO), Torino 3:117-122

7 PAPER 4: A UNIQUE METHODOLOGY FOR TOOL LIFE PREDICTION IN MACHINING

This chapter is the copy of the paper published in the Journal of Manufacturing and Materials Processing. It presents the third phase of the tool life prediction methodology where the outcomes from the first and second phases were used in a unique approach for estimating tool life. The uniqueness of this methodology referred to its capability to substantially reduce the computational time compared to similar approaches. Tool life experiments were carried out to identify the operating limits of such approach and validate the predicted tool life.

Authors: Keyvan Hosseinkhani, E. Ng

Journal of Manufacturing and Materials Processing. 2020, 4(1), 16

Abstract

In this paper, a unique approach for estimating tool life using a hybrid finite element method coupled with empirical wear rate equation is presented. In the proposed approach, the computational time was significantly reduced when compared to nodal movement technique. However, to adopt such an approach, the angle between tool's rake and flank faces must be constant through the process and at least two cutting experiments need to be performed for empirical model calibration. It is also important to predict the sliding velocity along the tool/flank face interface accurately when using Usui's model to predict the tool wear rate. Model validations showed that when the sliding velocity was assumed to be equivalent to the cutting speed, poor agreement between the predicted and measured wear rate and tool life was observed, especially at low cutting speed. Furthermore, a new empirical model to predict tool wear rate in the initial or break-in period as a function of Von Mises stress field was developed. Experimental validation shows that the newly developed model substantially improved the initial tool wear rate in terms of trend and magnitude.

Keywords: tool wear prediction; worn edge geometries; finite element simulation; wear rate equations

7.1 Introduction

In machining, the tool is gradually worn and loses its effective geometry. The wear is usually due to the severe thermal and mechanical loading conditions along the contacting interfaces. As wear reaches to a critical size, the tool is reached to the end of its efficient life and must be replaced. Otherwise, it affects the dimensional accuracy and surface integrity of the machined component.

Traditionally there have been two main approaches used to predict tool life: In the first approach, empirical equations were developed based on the relations between tool life and process parameters such as cutting speed, feed rate, and depth of cut. One of the most famous examples is the Taylor's tool life equation [1], as shown in Table 7-1. Although the Taylor equation is easy to use, its calibrations require extensive amount of tool life tests and data fitting [2]. Also the operating boundaries of the Taylor equation is very narrow and recalibration is usually required when the cutting tool geometry changes. In the second approach, tool wear rate has been described based on the wear mechanisms in the cutting zone. In this approach, rate of tool wear has been related to the thermomechanical process variables as shown in Table 7-2. These relationships were proposed by Shaw and Dirke [3] and Trigger and Chao [4]. Following them, other researchers have developed more or less similar relations. Among them the equation proposed by Usui [5], as shown in Table 7-2, is one of the most commonly used.

Usui's equation was developed based on the principles of Shaw's equation [3] for adhesive wear and introduction of the thermal softening factor. The total wear rate was related to the interface temperature, contact pressure, and sliding velocity of the chip or work material passing over the tool rake or flank faces respectively. Kitagawa et al. [6,7] showed that flank and crater wear on carbide tools can be predicted by Usui equation when cutting carbon steels with 0.15–0.46% C.

Taylor's Model [1]	$TV^{1/n}f^{1/m}b^{1/l}=C$ ……………… Eq. 7-1
T = tool life (s) V = cutting speed (m/s) f = chip thickness (m) b = depth of cut (m)	n, m, l, C = equation constants which depend on the combination of work and tool materials and cutting conditions

Table 7-1. Tool life expressions developed based on the first approach.

Usui's model [2]	$dW/dt = B_1 \sigma_n v_S e^{-B_2/T}$……… Eq. 7-2
dW/dt: total wear rate (μm/s) v_S ; sliding velocity of the work material (m/s) σ_n ; normal pressure on the tool face (Pa) T; temperature on the tool face (°C)	B_1, B_2; equation constants which depend on the combination of work and tool materials and cutting conditions

Table 7-2. Tool wear rate equation developed based on the second approach.

With the improvements in computational capabilities over the past decade, finite element method (FEM) has been used as a modelling technique for simulating the cutting process and estimating the temperature and stress distributions along the contacting interfaces that were difficult to measure or formulate based on either experimental or analytical techniques [8,9].

Combining the advantages of FEM and wear rate equations, researchers have attempted to develop physics-based methodologies for two dimensional [10–13] and three-dimensional tool wear predictions [14,15]. In all these wear prediction attempts, the cutting process with defined tool edge geometry was simulated with FEM until the mechanical and thermal loadings on the cutting tool reached steady state. Depending on the wear rate equation the required variables on interfacial nodes such as temperature, contact pressure, and sliding velocity were determined from the simulation. Following on from here, the wear rate at each node and the interfacial nodal displacements were calculated at a specified time increment. Finally, the tool geometry was updated, and the length of flank wear, *VB*, or depth of crater, *KT*, was determined. If the tool wear criterion has not been reached, the updated tool geometry was inserted back in the cutting simulation and same cycle was continued until the wear criterion was achieved. The flow chart of this methodology is shown in Figure 7-1. Regardless of the wear prediction accuracy, two key factors have been identified: The first referred to the nodal wear rate and displacement calculation. Calculating the displacement rate of each node along the tool–workpiece interface highly relies on the state of contact simulation, which is very complex in metal cutting. The complexity generally resulted in uncertainties in the simulated process variables such as sliding velocity which could lead to errors in nodal displacement calculation and consequently irregularity on updated worn geometry [16]. To overcome this issue, Malakizadi et. al [17] and Hosseinkhani and Ng [18] developed methodologies to determine the rate of tool material loss on the flank face from average values of interface temperature and contact pressure instead of calculating the individual nodal displacement rates.

The other factor refers to the iterative nature of tool wear prediction procedure which makes the overall computational time long and expensive. When using the approach detailed in Figure 7-1, a simulated cutting time increment should be defined based on which nodal displacements are calculated and cutting edge geometry is updated. Generally, the magnitude of simulated cutting time increment with respect to the total cutting time specifies the number of iterations required until the wear criterion is reached. Based on the selected time increment, Filice et al. [12], Attanasio et al. [14], and Malakizadi et al. [17] went through 10, 16, and 8 iterations, respectively. The iterative approach of Figure 7-1 is referred to as the series since the start of each iteration depends on the completeness of the previous iteration.

In the present paper, a new methodology for tool life prediction has been proposed and its feasibility has been investigated. This unique approach adopts the parallel processing rather than the series, which will substantially reduce the computational time. However, to adopt this approach, the angle between the tool rake and flank faces cannot vary with the increase in the flank wear length. Tool life experimental tests were carried out to identify the operating limits

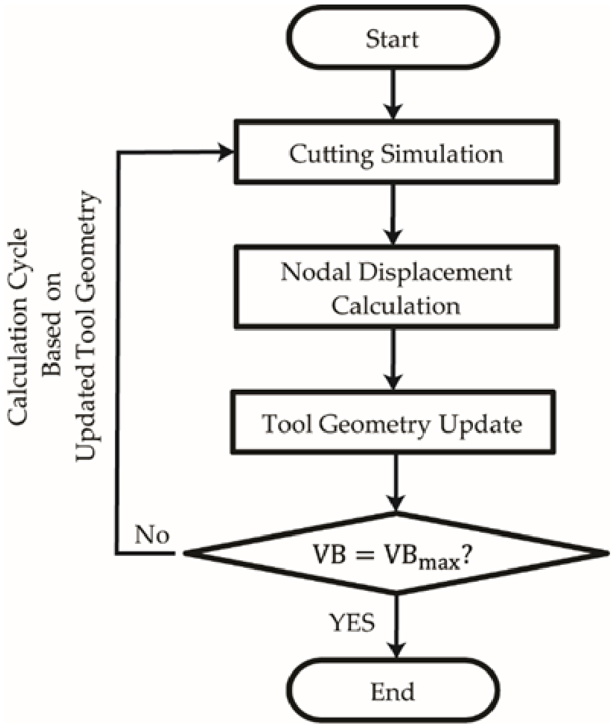

Figure 7-1. Conventional tool wear prediction approach using finite element method and empirical wear rate equation.

of such approach and validate the predicted tool life. A medium carbon steel was used in this research and orthogonal cutting was performed with an uncoated carbide tool. The motivation behind proposing this methodology was to improve the hybrid finite element/empirical based tool life prediction in terms of the wear rate calculation approach and overall computational time, which were introduced as challenges in the previous paragraphs.

7.2 Experimental Work

Cutting experiments were performed based on the orthogonal cutting configuration as shown in Figure 7-2. The ranges of cutting parameters used in this research have been listed in Table 7-3. Cutting tool was uncoated tungsten carbide, with TNMG332QM-H13A designation, and work material was fully annealed AISI 1045 with hardness of 165–190 BHN. Depth of cut and rake angle were held constant at 3 mm and −6° respectively.

Figure 7-3 shows nine combinations of cutting speed and feed rate. For each combination of parameters, tool life test was performed twice and worn tool geometries were analyzed during the tests. Each test was repeated twice. Flank wear of 0.3 mm was considered as the tool life criterion for ending each tool life test which was in accordance to ISO Standard 3685 for the tool life criterion.

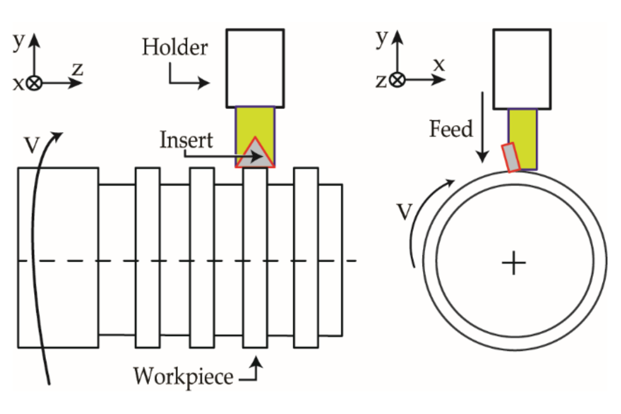

Figure 7-2. Schematic of orthogonal cutting process.

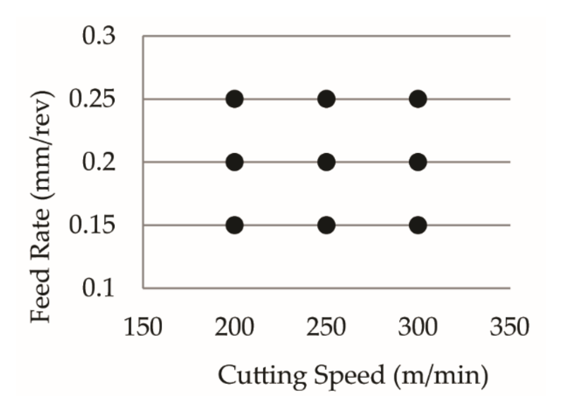

Figure 7-3. Cutting conditions in the range of cutting parameters.

Cutting Speed (m/min)	200 to 300
Feed Rate (mm/rev)	0.15 to 0.25
Depth of Cut (mm)	3
Rake Angle (°)	−6

Table 7-3. Cutting parameters

During the tool wear pattern cutting tests, after each fin was removed, the process was stopped, and tool edges were sectioned using wire electric discharge machining. The sectioned tools were then cold mounted, polished, etched, and analyzed under the optical microscope. It was observed that regardless of cutting speed and feed rate, the angle between flank and rake faces were approximately 98° at different flank wear sizes. The schematics of non-worn and worn edge geometries are shown in Figure 7-4. It was concluded that when cutting speed and feed rate were varied only the rate of tool wear was varied. Figure 7-5 a–c shows the micro-graphs of tool edge geometries after machining the first fin, and Figure 7-5 d–f shows the tool edge micro-graphs after machining the last fin with the lowest, mid-range, and highest process parameters, respectively. Lane [19] also observed similar phenomenon when machining AISI 1215 with diamond tools.

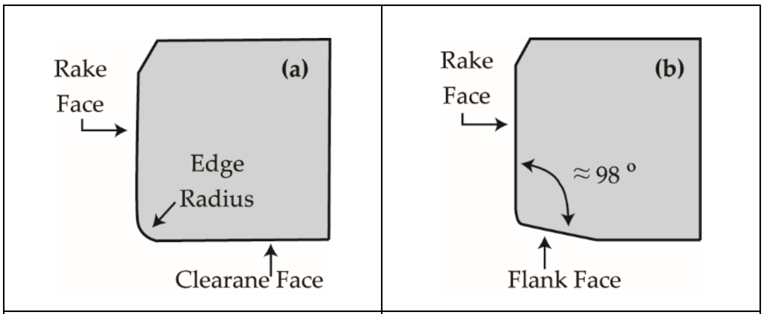

(a) Non-worn edge geometry

(b) Worn edge geometry

Figure 7-4. Schematics of edge geometries: (a) non-worn and (b) worn edge geometries.

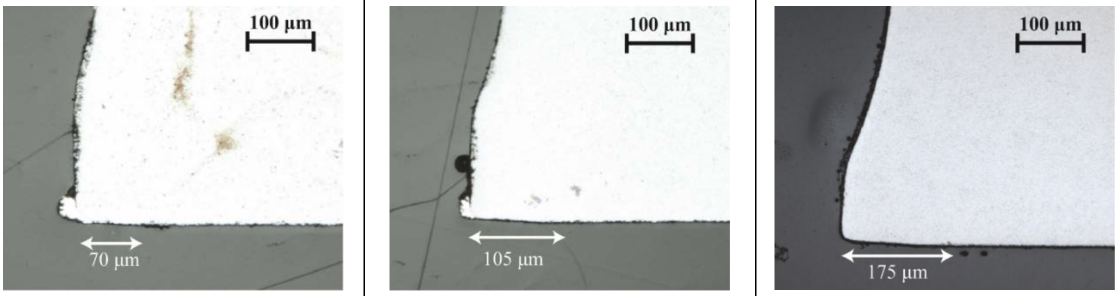

(**a**) V = 200 m/min, f = 0.15 mm/rev (**b**) V = 250 m/min, f = 0.20 mm/rev (**c**) V = 300 m/min, f = 0.25 mm/rev

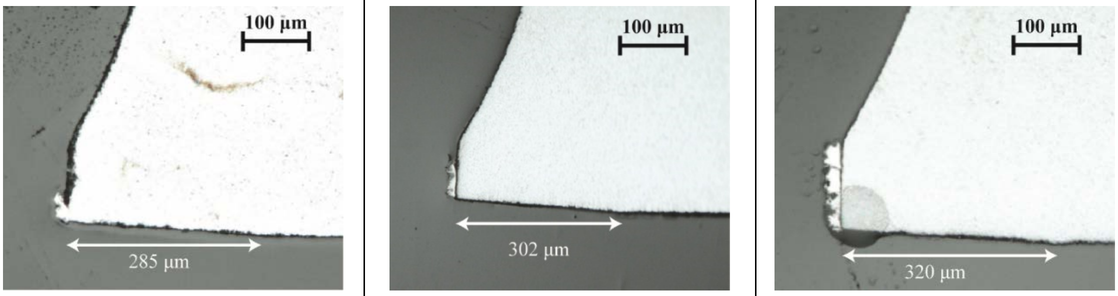

(**d**) V = 200 m/min, f = 0.15 mm/rev (**e**) V = 250 m/min, f = 0.20 mm/rev (**f**) V = 300 m/min, f = 0.25 mm/rev

Figure 7-5. Geometry of worn edges after machining first (a–c) and last (d–f) fin with the lowest, mid-range, and highest process parameters.

7.3 Tool Life Prediction Approach

Figure 7-6 details the overall procedure of the current approach which has been divided into three stages. In stage one, finite element simulation is used to model the effect of flank wear length on the temperature and contact pressure at the tool flank face and workpiece interface. Six simulations are carried out in parallel for each unique set of process parameters. Each simulation will have a particular flank wear length dimension. In the current research, flank wear lengths simulated were 0, 100, 150, 200, 250, and 300 µm. In stage two, the tool life period is divided into five intervals: 0–100 µm, 100–150 µm, 150–200 µm, 200–250 µm, and 250–300 µm. The tool wear rate for each interval is calculated based on Usui’s wear rate equation together with the interface temperature and contact pressure results predicted by finite element simulation. Finally, in stage three, the tool life is calculated.

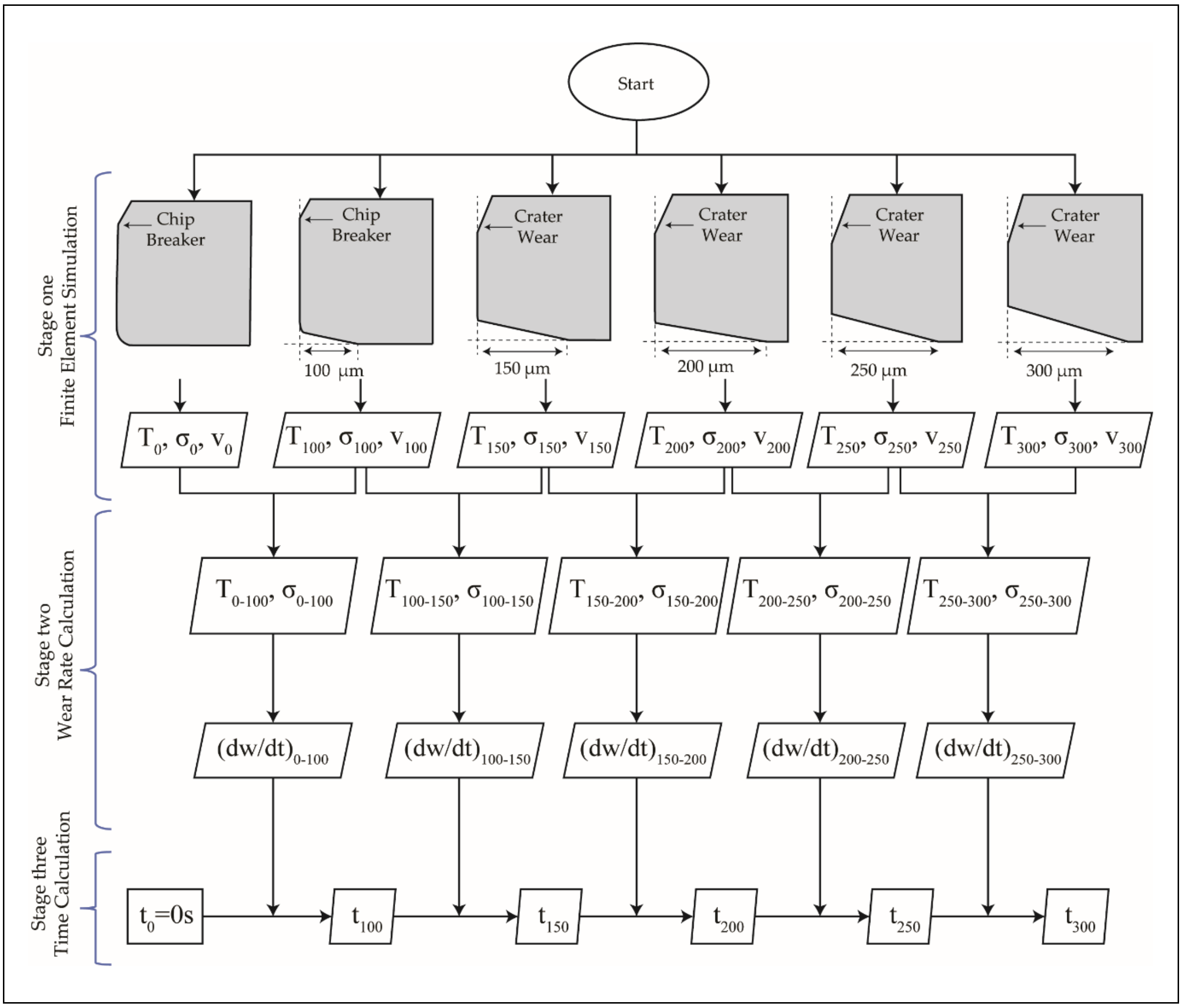

Figure 7-6. Overall procedure of the proposed methodology.

7.3.1 Finite element simulation

In stage one, FE models were built based on the principles of Arbitrary Lagrangian–Eulerian (ALE) technique. Figure 7-7a shows the schematic of an ALE cutting model with the associated boundary conditions. Details of the ALE technique in modeling the cutting process with non-worn and worn tool edge geometries can be found in [20]. Explicit solver in Abaqus was used with adaptive meshing. The plane strain CPE4RT elements were used for meshing the workpiece and tool which were quadrilateral with thermal-mechanical properties. The Johnson–Cook (J–C) constitutive model was used to include the effect of strain, strain rate, and temperature on the plastic deformation of the workpiece material. The interaction between the contacting surfaces has been modeled based on the Coulomb friction law in which the sticking and sliding conditions are the functions of normal and shear stresses. Figure 7-7b shows the resulting chip formation simulation and the location where the temperature and contact pressure were extracted for the analysis.

For any combination of cutting speed and feed rate, simulations based on the defined edge geometries were performed in parallel until mechanical-thermal fields reached steady states at the tool–workpiece interface. Parallel simulations completely eliminate the need for defining the time increment and the gradual tool geometry update, which reduced the overall computation time significantly when compared to the series approach. Based on the defined simulated cutting time increment, Filice et al. [12] and Attanasio et al. [14] had to go through the iterations 10 and 16 times, respectively. An iteration is defined here as restarting the cutting simulation with updated cutting edge geometry. Based on the approach proposed in the current research, only six simulations were performed in parallel without any iteration. Therefore, the overall tool life prediction process based on the current parallel simulation approach only requires a few hours when compared to series approach which requires at least 48 h per iteration.

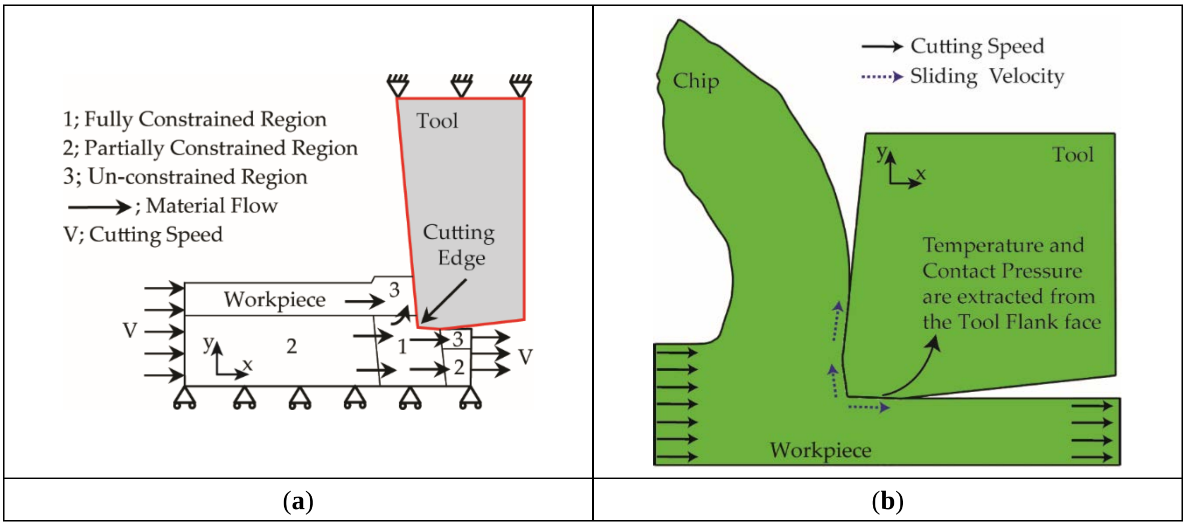

(**a**) (**b**)

Figure 7-7. Geometry and boundary conditions of orthogonal Arbitrary Lagrangian–Eulerian (ALE) cutting models. (b) Chip formation in orthogonal ALE simulation: temperature, contact pressure, and sliding velocity at flank wear–workpiece interface.

Usui's wear rate model is a function of interface temperature, contact pressure and sliding velocity. The temperature and pressure on the flank face were stable when simulation reached steady state. However, instability was observed in the simulated sliding velocity. This is likely due to the numerical errors associated with the continuous re-mapping of the workpiece elements throughout the simulation. Therefore, cutting speed was used in the wear rate calculations instead of sliding velocity. Malakizadi [16] also made similar observation regarding the instability and used cutting speed instead of sliding velocity.

From each simulation, the temperature and contact pressure on the tool flank face were extracted. Figure 7-7b indicated where the temperature and contact pressure were extracted from the models. Details on the simulated results have been reported in [21]. From the simulated results, flank face temperature and contact pressure increased as the flank wear increased. Flank face temperature was also a direct function of cutting speed and feed rate with more sensitivity to cutting speed. Contact pressure on the other hand, was only sensitive to the cutting speed and did not show substantial sensitivity to the variation in feed rate.

7.3.2 Wear rate calculation

In stage two, the average values of the interface temperature and contact pressure along the tool flank face were calculated with respect to the flank wear intervals of 0–100 µm, 100–150 µm, 150–200 µm, 200–250 µm, and 250–300 µm. The procedure for calculating average interface temperature and contact pressure in each interval has been shown in Table 7-4.

The calculated wear rate in each interval, dW/dt, represented the ratio of the distance between flank faces at the beginning, and end of that interval, Δw, to the time corresponding to that interval, Δt, as shown in Figure 7-8.

7.3.3 Cutting time calculation

In stage three, the cutting times corresponding to the flank wear length intervals are determined. The calculated wear rate in each interval is shown in Eq. 7-3:

$$dW/dt = (W_{i+1}-W_i)/(t_{i+1}-t_i) \qquad \text{Eq. 7-3}$$

where W_{i+1} and W_i are known from defined cutting edge geometries and t_i is known from the calculation of the previous interval. Eq. 7-4 was used to estimate t_{i+1}.

$$t_{i+1} = [(W_{i+1}-W_i)/(dW/dt)]+t_i \qquad \text{Eq. 7-4}$$

This procedure was continued until the cutting time corresponding to 0.3 mm flank wear was reached, which was accordance to the ISO Standard 3685 for the tool life criterion.

Flank Wear Intervals	**Average Temperature and Pressure**
0–100	$T_{0\text{-}100} = \frac{T_0+T_{100}}{2}$, $\sigma_{0\text{-}100} = \frac{\sigma_0+\sigma_{100}}{2}$
100–150	$T_{100\text{-}150} = \frac{T_{100}+T_{150}}{2}$, $\sigma_{100\text{-}150} = \frac{\sigma_{100}+\sigma_{150}}{2}$
150–200	$T_{150\text{-}200} = \frac{T_{150}+T_{200}}{2}$, $\sigma_{150\text{-}200} = \frac{\sigma_{150}+\sigma_{200}}{2}$
200–250	$T_{200\text{-}250} = \frac{T_{200}+T_{250}}{2}$, $\sigma_{200\text{-}250} = \frac{\sigma_{200}+\sigma_{250}}{2}$
250–300	$T_{250\text{-}300} = \frac{T_{250}+T_{300}}{2}$, $\sigma_{250\text{-}300} = \frac{\sigma_{250}+\sigma_{300}}{2}$

Table 7-4. Procedure to calculate the average process variables.

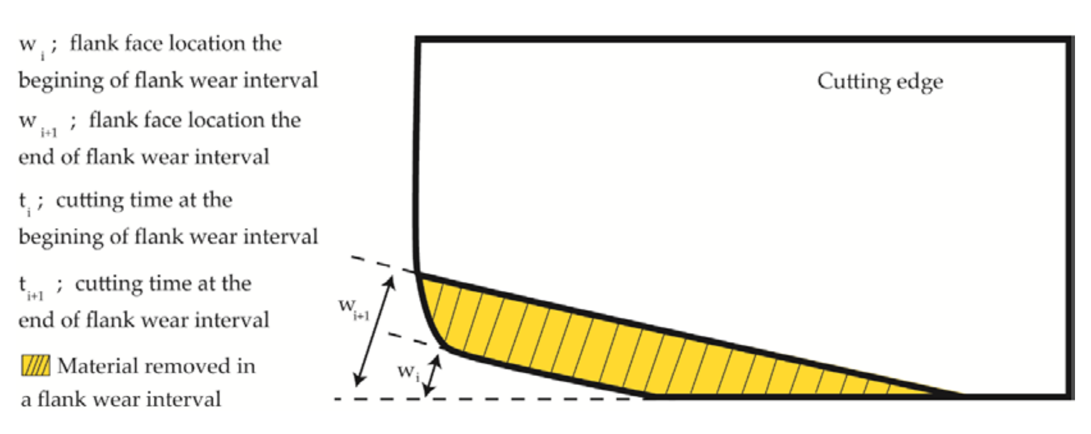

Figure 7-8. Schematic of wear rate calculation in a flank wear interval.

7.3.4 Wear rate model calibration

A general tool life trend consists of three periods which are (a) the initial or running-in period, (b) the secondary or steady-state period, and (c) the tertiary period [22]. Based on the collected experimental data in the current research, the high wear rate in the beginning of the cut differentiated the initial period from the secondary and tertiary periods. However, no extreme transition in the wear rate between secondary and tertiary periods was observed in all the nine cutting conditions carried out in this research. Therefore, the wear rate equation was calibrated in two periods. First, it was calibrated for the initial cutting period, 0–100 µm flank wear interval, and then it was calibrated for the combined second and third periods, which consisted of 100–150 µm, 150–200 µm, 200–250 µm, and 250–300 µm flank wear intervals. The calibration in each period was performed according to a hybrid experimental/simulation approach and based on the data from two cutting conditions; V = 200 m/min – f = 0.15 mm/rev and V = 300 m/min and f = 0.25 mm/rev [21]. The constants for the calibrated equation are detailed in Table 7-5. It was observed from experiments that the flank face surface orientation with respect to the rake face remained unchanged throughout the cut and tool material was continuously removed from the same direction. Therefore, in the present research, the calculation of nodal displacement rate was replaced by calculating the flank face displacement rate. Calculating the displacement rate of each node along the interface highly relies on the state of contact simulation, which is very challenging and unstable in metal cutting. In case of calculating the displacement rate of flank face, average values of temperature and contact

Period	**B_1 (m^2/MN)**	**B_2 (°C)**
Initial Period	1.89×10^{-6}	7141
Secondary/Tertiary Periods	1.95×10^{-8}	3266

Table 7-5. Calibrated constants of the wear rate model.

pressure which represented all the nodal values on the interface were used. Therefore, the possibility of including the uncertainties involved in estimating the nodal displacement was eliminated.

7.4 Results and Discussions

7.4.1 Tool life

Figure 7-9 shows the effect of cutting speed and feed rate on the experimental and predicted tool life. In Figure 7-9, both experimental and predicted tool life decreased at higher cutting speed and feed rate. Binder et al. [23] and Palmai [24] made similar observations when machining AISI 1045 with carbide tools. However, in terms of tool life magnitude, the difference between predicted tool life and experiment was larger at lower cutting speeds. As shown in Figure 7-9 (a) and (b), at cutting speed of 200 m/min together with 0.2 mm/rev and 0.25 mm/rev feed rate, the predicted tool life were 80% and 85% longer, respectively, when compared to experiment. The difference between prediction and experiment was 30% when cutting speed was held at 250 m/min and was 10% when cutting speed was at 300 m/min regardless of feed rate, as shown in Figure 7-9 (c) to (e).

7.4.2 Wear rate predictions in the initial cutting period

The predicted wear rates in the initial cutting periods for five cutting conditions are shown in Figure 7-10. The flank wear interval during the initial cutting period was between 0 and 100 µm. The predicted wear rates increased with higher cutting speed and feed rate which were similar to those observed in experiment. However, the magnitudes of predictions were not in good agreement with experiment. In the five cutting conditions analyzed, the predicted wear rates were 40% to 55% lower when compared to experiment.

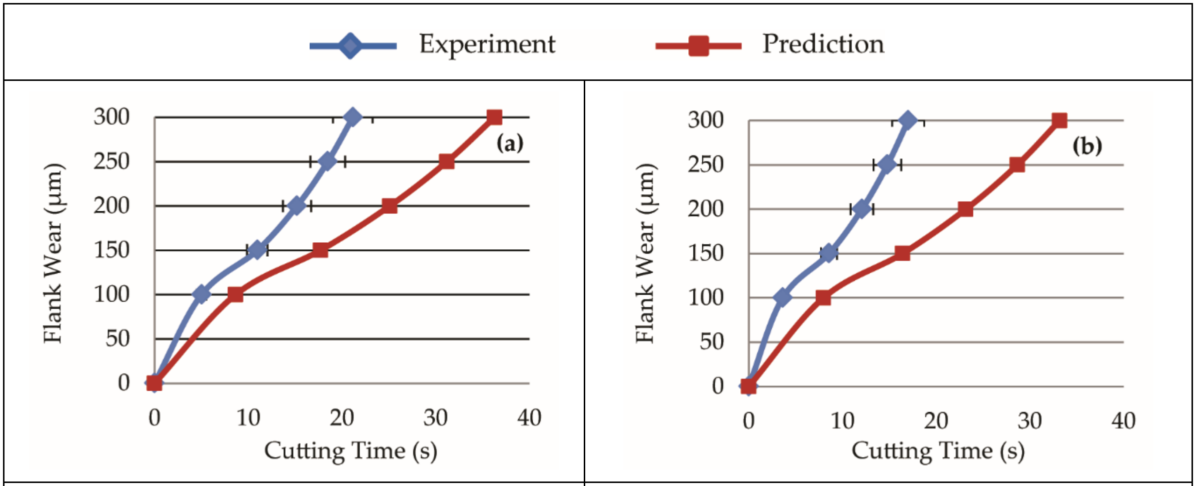

V = 200 m/min, f = 0.20 mm/rev

V = 200 m/min, f = 0.25 mm/rev

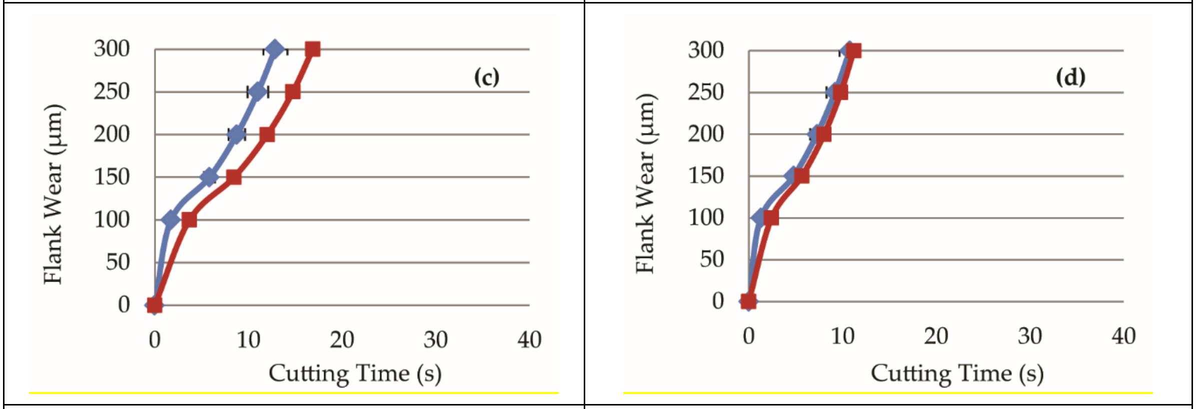

V = 250 m/min, f = 0.20 mm/rev

V = 300 m/min, f = 0.15 mm/rev

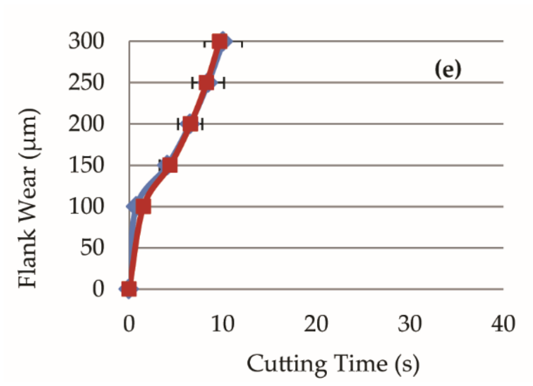

V = 300 m/min, f = 0.20 mm/rev

Figure 7-9. Predicted tool life in comparison with experimental results.

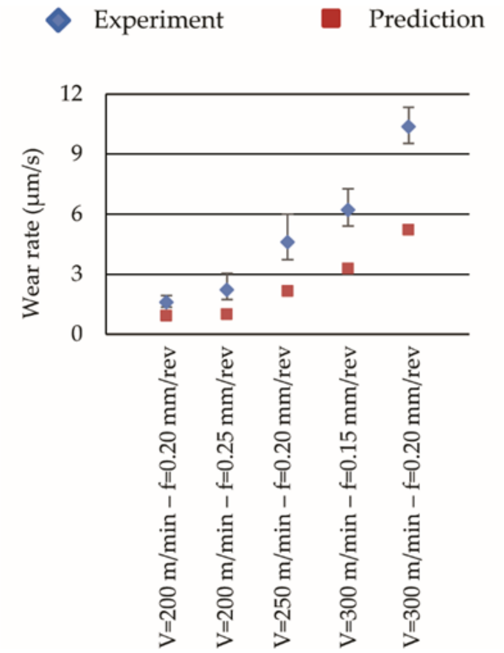

Figure 7-10. Wear rates predictions corresponding to the initial cutting period.

The difference in the wear rate prediction in the initial period did not influence the predicted tool life in conditions with 250 m/min and 300 m/min speeds as much as it did in conditions with 200 m/min speed. This was likely due to the fact that the cutting times corresponding to the initial period were shorter in conditions with 250 m/min and 300 m/min speeds, which reduced the difference of wear rate predictions on the overall tool life.

The difference of the predictions in initial period, as shown in Figure 7-10, did not necessarily relate to the methodology proposed in the current research but rather due to the limitations of Usui’s model. Yen [10] referred to Usui model as an expression developed based on the principles of adhesive wear which might be better representing the flank wear rate at higher temperature and unable to capture the high initial wear rates due to micro-chipping or fracture.

7.4.3 Recommendation for improvement in wear rate estimation during initial period

The importance of successful estimation of wear rate in initial period cannot be neglected due to its influence on the overall tool life estimation, as shown in Figure 7-9 a and b.

Based on the hypothesis that mechanical stresses are the main cause of tool wear in the initial period, a methodology was developed to predict the initial wear rate. First, the flank wear length and orientation with respect to time during initial cutting period, up to 100 µm, was measured. Orthogonal cutting process with no flank wear was then simulated and stress contour plot was obtained. Figure 7-11 shows the contour of Von Mises stresses in the tool for the lowest, mid-range and highest magnitudes of cutting parameters listed in Table 7-3.

Following on from here, the measured flank wear length and orientation were superimposed onto the stress contour plot and average stress along the flank wear length was calculated. Dotted rectangles in Figure 7-11 show the flank area in the simulated tool where the stresses have been obtained Finally, the experimentally obtained wear rate in the initial period was related to the calculated average stress. Figure 7-12 shows the experimentally obtained wear rates, *dW/dt*, plotted against the simulated Von Mises stresses. Referring to the coefficient of determination, R^2, it was concluded that the exponential function fitted the relation better than the linear function. The equation representing the relation is detailed in Eq. 7-5:

$dW/dt = Ce^{(D\sigma)}$	Eq. 7-5

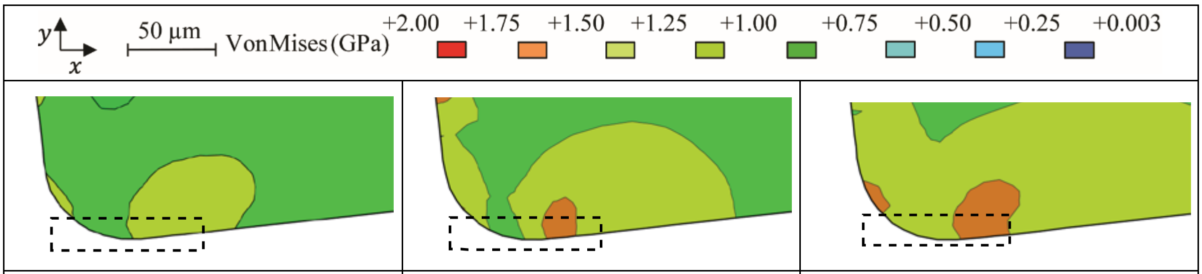

(a) V = 200 m/min, f = 0.15 mm/rev

(b) V = 250 m/min, f = 0.20 mm/rev

(c) V = 300 m/min, f = 0.25 mm/rev

Figure 7-11. Contour of Von Mises stresses developed in the tool cutting edge when machining at different cutting conditions.

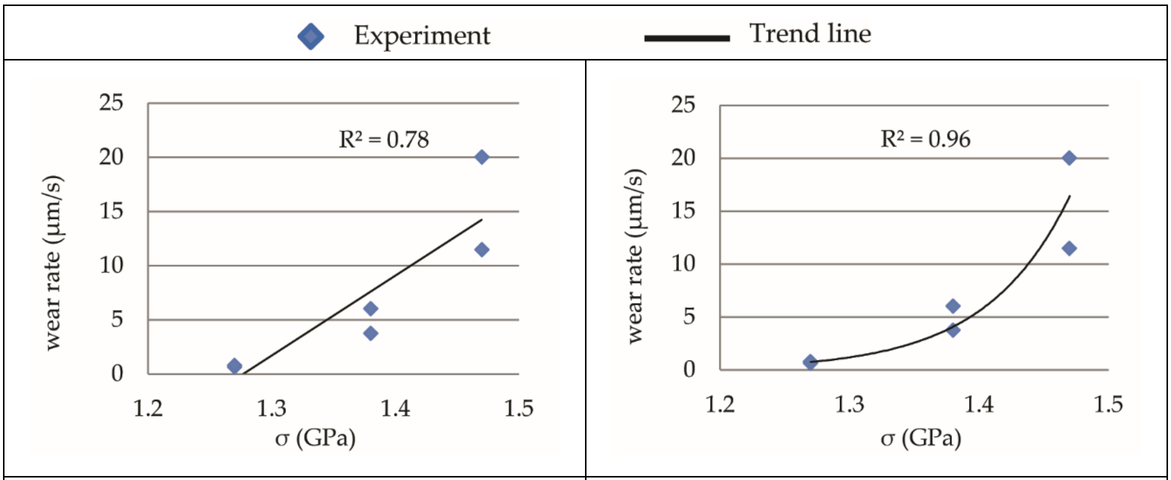

(**a**) Linear fit (**b**) Exponential fit

Figure 7-12. Relation between the experimental wear rate in the initial cutting period and the simulated Von Mises stresses.

in which *C* and *D* are the constants to be determined through calibration. Employing the experimental and simulated data in Figure 7-12, the calibrated constants *C* and *D* were 1.26 × 10−9 µm/s and 1.59 × 10−8 m^2/N, respectively.

Figure 7-13 compares the predicted wear rates when using Usui and newly proposed equation, with experimental results. In the five conditions analyzed, 0.75 to 5 µm/s differences between predictions and experiments were improved to 0.45 to 2 µm/s. The most significant improvement in the predicted wear rate was at 300 m/min cutting speed and 0.2 mm/rev feed rate. At this condition, Usui precited wear rate was 5.22 µm/s. However, with the proposed

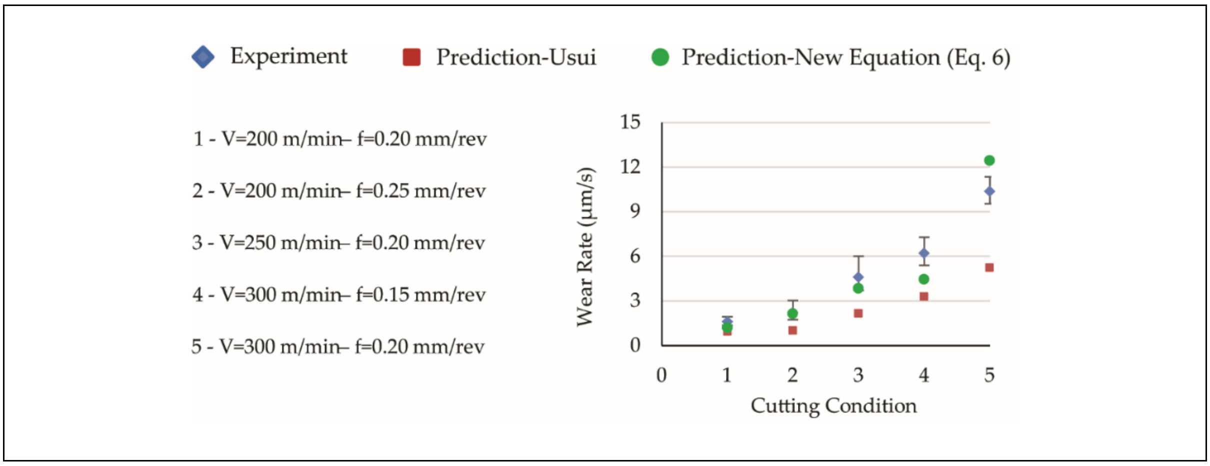

Figure 7-13. Predictions of wear rate in the initial period of cutting based on original Usui and new equations.

equation, the predicted wear rate was 12.42 µm/s which agrees better with the experimental data of 10.36 µm/s.

7.4.4 Wear rate predictions in the secondary and tertiary cutting periods

Figure 7-14 shows the effect of simulated temperature on tool wear rates acquired experimentally and predicted with Usui model for different cutting parameters during the secondary and tertiary tool life periods. The simulated temperatures along the flank face/ workpiece interface were compared to experimental results performed by Filice et al. [25]. The difference between predicted temperature and those acquired experimentally were less than 70 °C for two different sets of process parameter. With reference to Equation (2), wear rate is an exponential function of temperature. Zanger [13] showed that in the Usui model, the sensitivity of wear rate to temperature was much higher than to contact pressure and velocity. Therefore, in Figure 7-14, the estimated wear rates have been plotted with respect to the corresponding temperature. The four data points in each graph of Figure 7-14 represented the wear rates in 100–150 µm, 150–200 µm, 200–250 µm, and 250–300 µm flank wear intervals. At 250 m/min and 300 m/min cutting speed, the wear rates were predicted in better agreement with experiments compared to the predictions in conditions with 200 m/min. In Figure 7-14 (a) and (b), for conditions with 200 m/min speed, the predicted wear rate was approximately 40% to 50% lower when compared to experiment. On the other hand, in Figure 14 (c)–(e), for conditions with higher speeds of 250 m/min and 300 m/min, wear rates at any flank wear interval were predicted within in ±20% when compared to experiment.

In the current FE simulations, the average temperature and pressure on the flank face were stable while instability was observed in the sliding velocity of work material passing over the tool face. As the result, the sliding velocity equivalent to cutting speed magnitude was used in the wear rate model instead of simulated sliding velocity. Malakizadi [16] observed similar instability in the sliding velocity and used cutting speed instead of sliding velocity.

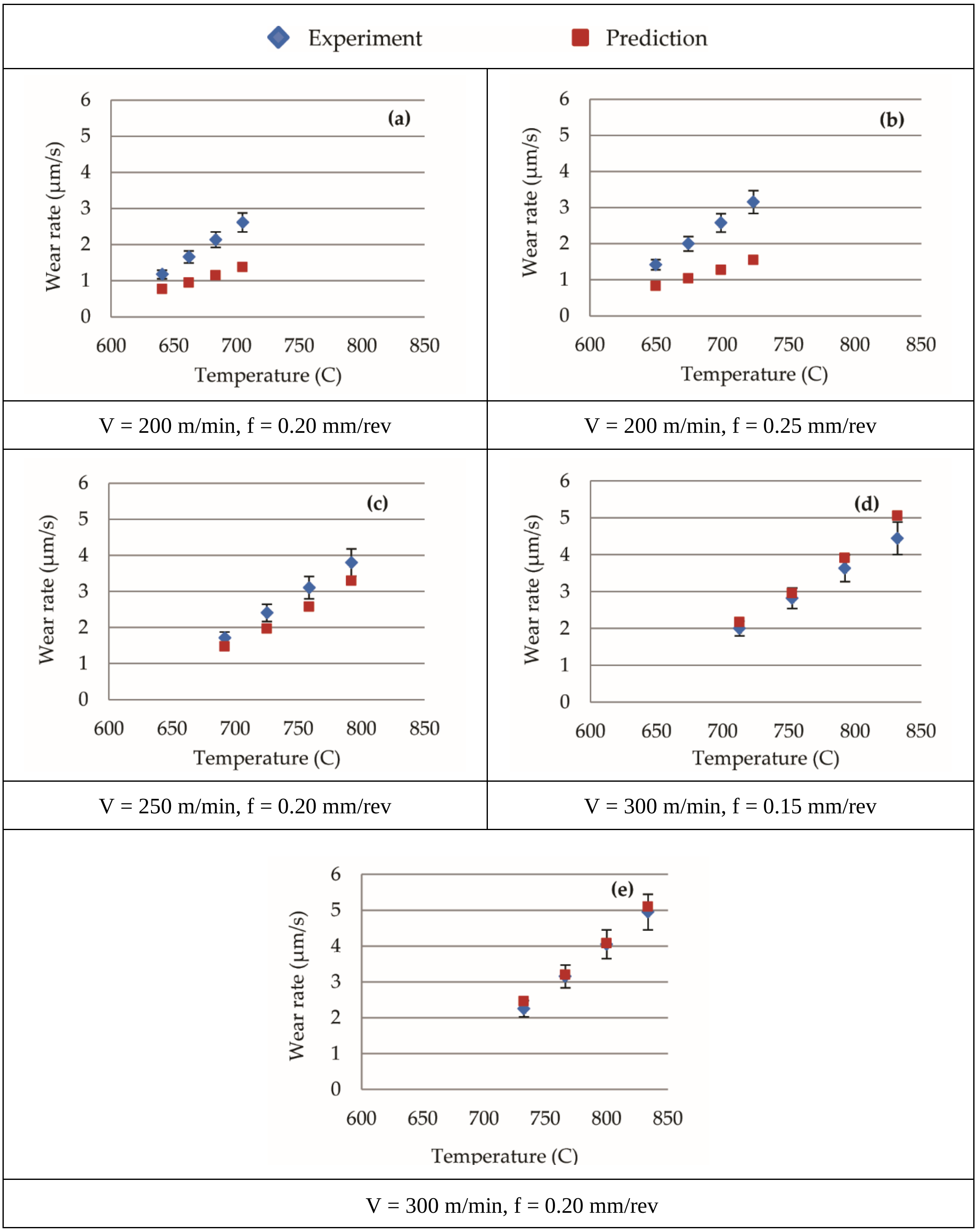

V = 200 m/min, f = 0.20 mm/rev

V = 200 m/min, f = 0.25 mm/rev

V = 250 m/min, f = 0.20 mm/rev

V = 300 m/min, f = 0.15 mm/rev

V = 300 m/min, f = 0.20 mm/rev

Figure 7-14. Effect of temperature on tool wear rates acquired experimentally and predicted with Usui model for different cutting parameters.

In the next section a methodology is detailed to calculate the workpiece sliding velocity from strain field distribution and stable time increment.

7.4.5 Strain and velocity distributions beneath the newly generated surface

Figure 7-15 shows the predicted plastic strain distribution beneath the newly generated surface when the flank wear was at 200 µm. The plastic strain was parallel to the cutting velocity vector and the newly generated surface was still in contact with the flank face/workpiece interface. For all the cutting speed investigated, the plastic strain was at its maximum at the flank face/workpiece interface and decay to approximately zero at a depth of 15 µm. The high plastic strain induced on the surface was likely due to strain hardening effect when the material was fractured to form the chip or newly generated surface and also due to friction along the flank face/workpiece interface. Han et.al. [25] also found similar trend during experimental orthogonal cutting test of annealed AISI 1045 with carbide tool. Experimentally acquired micrographs showed the surface with intense bending of the cementite plates within the pearlite phase and in some cases the formation of white layer. The white layers are generally formed due to rapid heating and cooling, severe plastic deformation and reaction of the surface with the environment. The bending of the cementite plates was observed up to a depth of less than 10 µm, which was similar to the depth predicted in Figure 7-15.

The cutting speed had no substantial effect in surface plastic strain. Han et al. [26] also made similar observation when increasing cutting speed on the thickness of formed white layer. Han et al. found that when cutting speed was increased from 100 to 200 m/min with a flank wear length of 100 µm, the formation of white layer measured depths were 1 µm to 2 µm, respectively, which is not a substantial difference. This shows that increased cutting speed has insignificant effect on the plastic strain induced on the newly generated surface.

Figure 7-16 details the simulated velocity distribution beneath the newly generated surface. This velocity is parallel to the cutting speed and was acquired in the region when the newly generated surface was still in contact with the flank face of the tool. The velocity distribution was calculated using the relative strain history distribution, $\varepsilon_{t(i)}$-$\varepsilon_{t(i-1)}$, divided by the stable simulated time increment, t_s, and multiplied with the corresponding distance travelled, $d_{(i-1)}$, as shown in Eq. 7-6. This approach will eliminate any instability as observed here as well by Malakizadi [16].

$v_s = \left[(\varepsilon_{t(i)}-\varepsilon_{t(i-1)})/t_s\right] \times d_{(i-1)}$	Eq. 7-6

As expected, the velocity was lower near the newly generated surface. This was due to plastic deformation that occurs in the region as shown in Figure 7-15. Further away from the newly generated surface, the velocity increased to its prescribed cutting speed. At 7.5 µm depth beneath the flank face/workpiece interface, the velocity range bar overlapped one another regardless of the cutting speed simulated. At 10 µm depth, the range bar did not overlap. This was likely due to the contact interfaces were simulated with stick-slip condition, which is

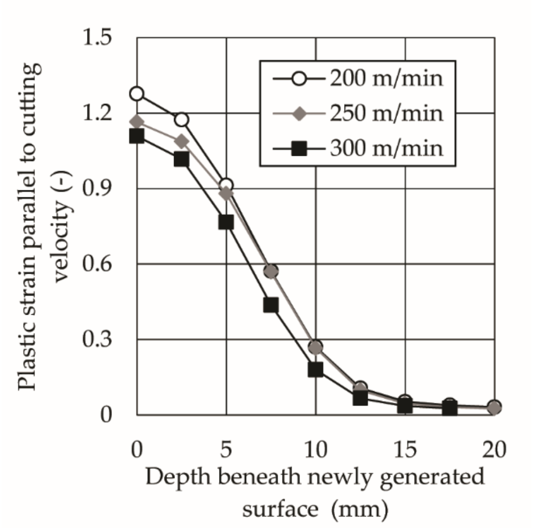

Figure 7-15. Effect of cutting speed on predicted plastic strain distribution beneath newly generated surface.

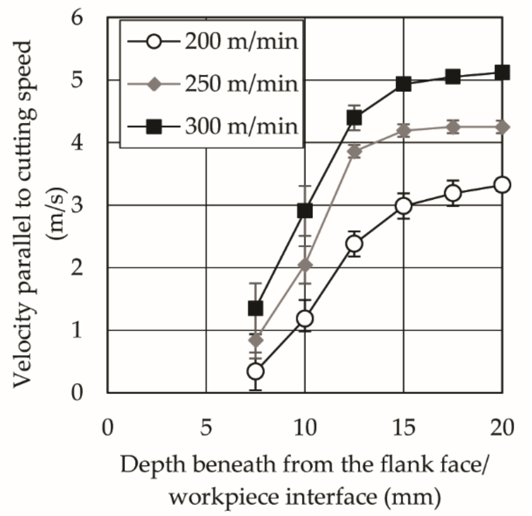

Figure 7-16. Velocity distribution beneath the newly generated surface.

dependent on the normal pressure acting along the contacting surfaces. When the node undergoes a transition between sticking to slipping, the node will have high relative kinetic energy. In the sticking region, the difference between the sliding velocity and cutting velocity is high. In the slipping region, this difference was substantially reduced, and therefore the node will experience high kinetic energy resulting in oscillation of the predicted velocity. This was not observed when the depth of the newly generated surface was increased as no plastic deformation was observed.

Therefore, it was concluded that the sliding velocity of 0.86 m/s, which was calculated by taking the average of the maximum and minimum velocity for all the cutting conditions simulated, could be used in the wear rate predictions. Table 7-6 shows the new calibrated constants based on using the constant sliding velocity of 0.86 m/s and Figure 7-17 shows the corresponding new predicted wear rates. The current approach of acquiring sliding velocity together with Usui model improved the wear rate predictions in all the conditions, especially in those with cutting speed of 200 m/min. The difference between predicted and experimental results at 200 m/min cutting speed was reduced to within 20% from 40% to 50%. The wear rate predictions at condition with 250 m/min and 300 m/min cutting speed was also reduced to 10% from 20%.

Figure 7-18 (a) and (b) show the tool life results from experiment, predictions when using cutting speed as sliding velocity, and predictions when using the 0.86 m/s calculated average sliding velocity. Tool life prediction agreed better with experiment when the calculated average sliding velocity was used. In this case, at cutting speed of 200 m/min together with feed rates

Region	**B_1 (m^2/MN)**	**B_2 (°C)**
Initial Period	9.14×10^{-5}	7005
Secondary/Tertiary Periods	9.42×10^{-8}	3135

Table 7-6. Model constants for the calibrated equation based on two boundary conditions.

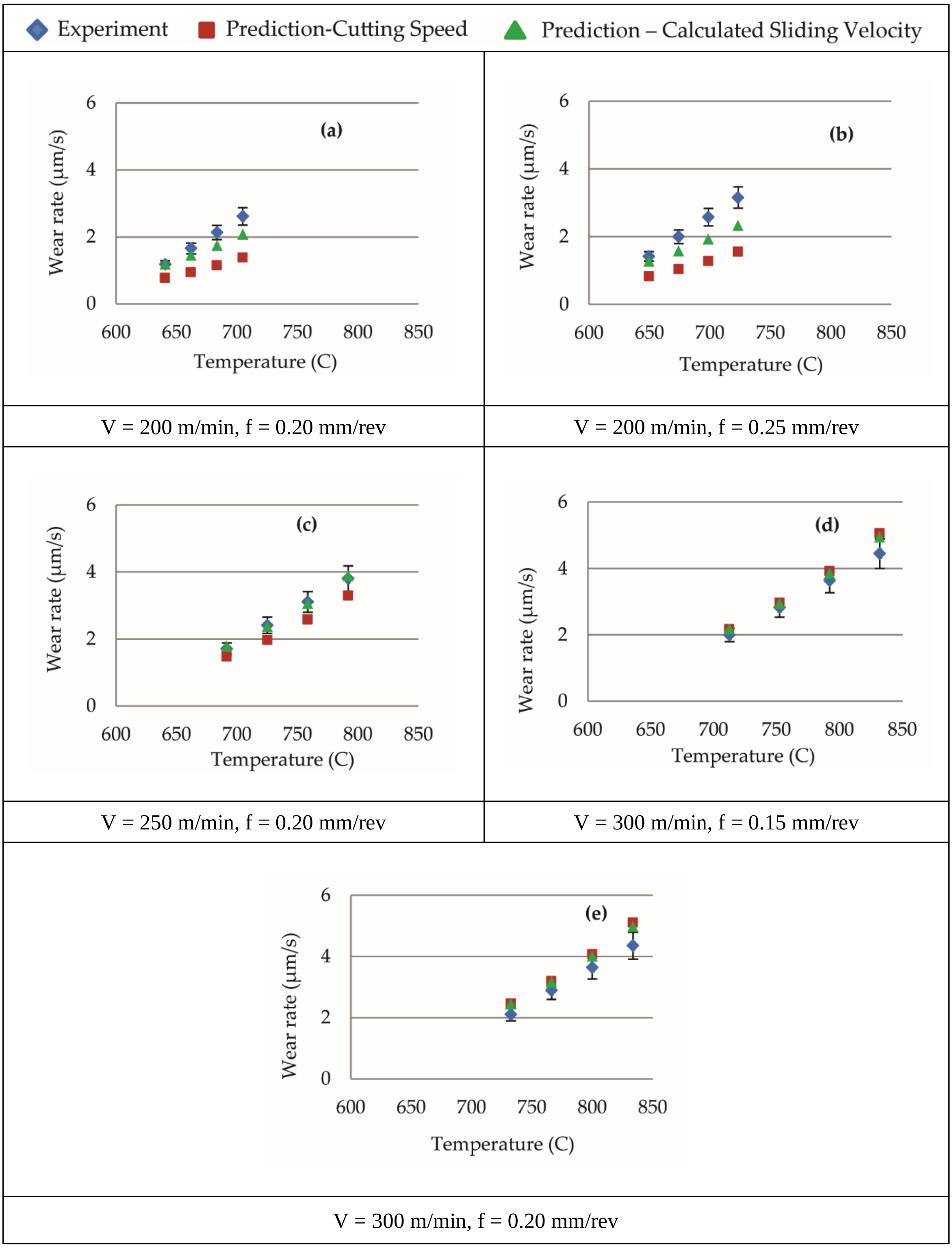

V = 200 m/min, f = 0.20 mm/rev

V = 200 m/min, f = 0.25 mm/rev

V = 250 m/min, f = 0.20 mm/rev

V = 300 m/min, f = 0.15 mm/rev

V = 300 m/min, f = 0.20 mm/rev

Figure 7-17. Predicted wear rate according to the modified Usui model in comparison with experiment.

of 0.20 mm/rev and 0.25 mm/rev, the difference between predicted tool life with experiment at 0.3 mm flank wear were approximately 14% and 20% respectively. However, when the cutting speed was assumed to be equal to the sliding velocity, the difference for both feed rates

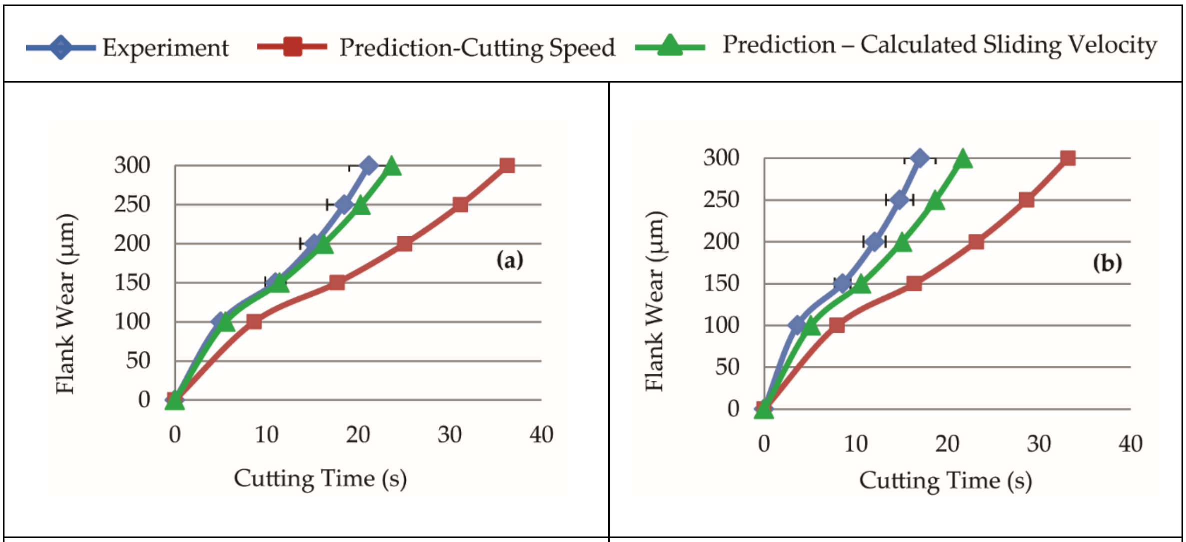

V = 200 m/min, f = 0.20 mm/rev

V = 200 m/min, f = 0.25 mm/rev

Figure 7-18. Predicted tool life according to original Usui and modified Usui in comparison with experiment.

were between 73% and 110%. Similar trends were observed at the higher cutting speeds with corresponding feed rates.

7.4.6 Computational time improvement

Based on the current methodology proposed here, FE simulations with worn edge geometries were carried out in parallel, which were independent from each other. Simulations were completed when temperature and stresses reached study state. This approach substantially reduced the overall computation time when compared to the methodologies published by other researchers [12,14,17], where simulations were performed in series, as shown in Figure 7-1. Eq. 7-7 shows the overall computational time when the series approach was used,

$$Computational\ time\ in\ series = (t_P \times t_R)/(t_s \times i_s) \qquad \text{Eq. 7-7}$$

where t_P is the time required to generate 0.3 mm flank wear, t_R is the real computational time for a specific number of increments, t_S is the stable time increment, and i_S is the specific number of increments. The computational time shown in Eq. 7-7 is highly dependent on the time required to generate 0.3 mm flank wear.

The computational time in parallel that was developed in this research can be calculated using Eq. 7-8,

$$\textit{Computational time in parallel} = (t_{SS} \times t_R \times n_i)/(t_s \times i_s) \qquad \text{Eq. 7-8}$$

where t_{SS} is the time taken for the cutting forces and cutting temperature to reach steady state and n_i is the number of wear intervals. The definition on the rest of the terms found in Equation (9) were similar to those listed in Eq. 7-7.

The computation time in Eq. 7-8 is substantially lower when compared Eq. 7-7, as the time taken for the cutting forces and temperature to reach steady state is dependent on the length of cut simulated divided by the cutting speed, whereas the time required to generate 0.3 mm flank wear using Eq. 7-7 is dependent on the real tool wear rate. Table 7-7 details the computational time calculation using Eq. 7-7 and Eq. 7-8. When using series approach, the actual computational time increased with the time required to generate 0.3 mm flank wear, whereas with the parallel approach, which was developed in this research, the computational time was independent to tool wear rate. For example, when the time required to generate 0.3 mm flank wear was fixed at 30s, the computation time for series approach was 10 times longer when compared to the method detailed in this paper.

	Computational Time in Series Approach, Equation (8)			**Computational Time in Parallel Approach, Equation (9)**		
t_P (s)	30	300	3000	30	300	3000
t_{SS} (s)				0.5	0.5	0.5
t_S (s)	5×10^{-8}	5×10^{-8}	5×10^{-8}	5×10^{-8}	5×10^{-8}	5×10^{-8}
i_S	250,000	250,000	250,000	250,000	250,000	250,000
t_R (s)	120	120	120	120	120	120
n_i	-	-	-	6	6	6
Actual computational time	0.28×10^{6}s 4800 min	2.88×10^{6}s 48,000 min	28.8×10^{6}s 480,000 min	28.8×10^{3}s 480 min	28.8×10^{3}s 480 min	28.8×10^{3}s 480 min

Table 7-7. Effect of time required to generate 0.3 mm flank wear and computational time with series and parallel simulation.

7.5 Conclusions

In this paper, a hybrid finite element method coupled with empirical wear rate equation to predict tool life was presented and validated experimentally. The following conclusions were made based on the orthogonal cutting of AISI 1045 with uncoated carbide with the associated process parameters.

Experimental results showed that Usui’s equation had limitation predicting the tool wear rate during the initial tool wear period, which is dominated by mechanical stresses. A new empirical equation was proposed here which predict the initial tool wear rate as a function of Von Mises stress together with calibrated constants. Experimental validation showed evidence that the newly developed empirical equation substantially improved the predicted tool wear rate. The limitations of this approach were that a 100 µm initial flank wear length was assumed and empirical model calibration was required.

Due to the inherent instable of the sliding velocity from the stick-slip condition at the contacting surface, the relative strain history and stable simulated time increment was used to calculate the sliding velocity distribution beneath the newly generated surface. The average sliding velocity used at the tool/flank face interface for the cutting conditions investigated was 0.86 m/s. When using this sliding velocity magnitude, the tool wear rate and tool life predicted during the secondary and tertiary cutting periods agreed better with experimental results regardless of cutting speed or tool wear life.

In the current research approach, the FE computational time was significantly reduced. This reduction was due to the fact that the FE simulation with different flank wear lengths could be computed in parallel and for each flank wear length interval, the simulated cutting time is dependent on the duration when the mechanical and thermal field becomes steady state. When using the nodal movement technique together with series approach, the FE computational time is coupled to the tool wear rate, which can have long computational time.

However, there are also two limitations is the current approach, which are (i) the angle between the rake face and flank face must not vary with tool life and (ii) at least two sets of experiments are required for model calibration.

Author Contributions: "Conceptualization methodology: Keyvan Hosseinkhani; software, Keyvan Hosseinkhani.; validation, Keyvan Hosseinkhani..; formal analysis, Keyvan Hosseinkhani.; investigation, Keyvan Hosseinkhani.; resources, Eu-gene Ng.; data curation, Keyvan Hosseinkhani and Eu-gene Ng.; writing—original draft preparation, Keyvan Hosseinkhani.; writing—review and editing, Eu-gene Ng.; visualization, Keyvan Hosseinkhani.; supervision, Eu-gene Ng.; project administration, Keyvan Hosseinkhani and Eu-gene Ng.; funding acquisition, Eu-gene Ng. All authors have read and agreed to the published version of the manuscript.",

Funding: This research was funded by NSERC CANRIMT and NSERC Discovery Grant. Acknowledgment. The authors would like to thank the Mechanical Engineering Department at McMaster University and McMaster Manufacturing Research Institute (MMRI) for providing the laboratory infrastructure**.**

Conflicts of Interest: The authors declare no conflict of interest.

7.6 References

[1] Taylor, F.W. On the art of cutting metals. Transactions of the American Society of Mechanical Engineers 1907, 28, 31-58.

[2] Li, B. A review of tool wear estimation using theoretical analysis and numerical simulation technologies. International Journal of Refractory Metals and Hard Materials 2012, 35, 143–151.

[3] Shaw, M. C.; Dirke, S. O. On the wear of cutting tools. Microtecnic (english ed) 1956, 10, 187–193.

[4] Trigger, K. J.; Chao, B. T. The mechanism of crater wear of cemented carbide tools. Transaction of ASME 1956, 78, 1119, 1956.

[5] Usui, E.; Shirakashi, T.; Kitagawa, T. Analytical prediction of cutting tool wear. International Journal of Wear 1984, 100, 129-151.

[6] Kitagawa, T.; Maekawa, K.; Shirakashi, T.; Usui, E. Analytical prediction of flank wear of carbide tools in turning plain carbon steels, part 1: Characteristic equation of flank wear. Bull. Japan Soc. of Prec. Engg 1988, 22 (4), 263-269.

[7] Maekawa, K.; Kitagawa, T.; Shirakashi, T.; Usui, E. Analytical prediction of flank wear of carbide tools in turning plain carbon steels, part 2: prediction of flank wear. Bull. Japan Soc. of Prec. Engg 1989, 23 (2), 126-133.

[8] Denkena, B.; Köhler, J.; Mengesha, M. S. Influence of the cutting edge rounding on the chip formation process: Part 1. Investigation of material flow, process forces, and cutting temperature. Production Engineering 2012, 6 (4), 329–338.

[9] Sanchez, A. M.; Canteli, J. A.; Cantero, J. L.; Miguelez, M. H. Numerical analysis of tool wear effect in machining induced residual stresses. Simulation Modelling Practice and Theory 2011, 19, 872-886.

[10] Yen, Y. C.; Söhner, J.; Lilly, B.; Altan, T. Estimation of tool wear in orthogonal cutting using the finite element analysis. Journal of Material Processing Technology 2004, 146 (1), 82-91.

[11] Xie, L.-J.; Schmidt, J.; Schmidt, C.; Biesinger, F. 2D FEM estimate of tool wear in turning operation. International Journal of Wear 2005, 258 (10), 1479-1490.

[12] Filice, L.; Micari, F.; Settineri, L.; Umbrello, D. Wear modelling in mild steel orthogonal cutting when using uncoated carbide tools. International Journal of Wear 2007, 262 (5-6), 545-554.

[13] Zanger, F.; Schulze, V. Investigation on Mechanisms of Tool Wear in Machining of Ti-6Al-4V using FEM Simulation. Procedia CIRP, Torino 2013, 8, 158-163.

[14] Attanasio, A.; Ceretti, E.; Fiorentino, A.; Cappellini, C.; Giardini, C. Investigation and FEM-based simulation of tool wear in turning operations with uncoated carbide tools. International Journal of Wear 2010, 269 (5-6), 344-350.

[15] Attanasio, A.; Ceretti, E.; Giardini, C. 3D FEM Simulation of Flank Wear in Turning, 14th International ESAFORM Conference on Material Forming, Belfast 2011, 561-566.

[16] Malakizadi, A.; Gruber; H.; Sadik, I.; Nyborg, L. An FEM-based approach for tool wear estimation in machining. International Journal of Wear 2016, 368–369, 10–24.

[17] Malakizadi, A.; Cedergren, S.; Surreddi, K. B.; Nyborg, L. A methodology to evaluate the machinability of Alloy 718 by means of FE simulation. Proceedings of Advanced Manufacturing Engineering and Technologies NEWTECH. Stockholm 2013, 95-106.

[18] Hosseinkhani, K; Ng, E. A Combined Empirical and Numerical Approach for Tool Wear Prediction in Machining," Procedia CIRP, Karlsruhe 2015, 31. 304-309.

[19] Lane, B. M.; Dow, T. A.; Scattergood, R. Thermo-chemical wear model and worn shapes for single-crystal diamond tools cutting steel. International Journal of Wear 2013, 300 (1-2), 216-224.

[20] Hosseinkhani, K; Ng, E. Analysis of the cutting mechanics under the influence of worn tool geometry. Procedia CIRP, Torino 2013, 8, 117-122.

[21] Hosseinkhani, K; Ng, E. A hybrid experimental and simulation approach to evaluate the calibration of tool wear rate models in machining. International Journal of Advanced Manufacturing Technology 2018, 96 (5-8), 2709-2724.

[22] Shaw, M. C. Metal Cutting Principles, 2 ed., Oxford University Press Inc, 2005.

[23] Binder, M.; Klocke, F.; Doebbeler, B. An advanced numerical approach on tool wear simulation for tool and process design in metal cutting. Simulation Modelling Practice and Theory 2017, 70, 65–82.

[24] Palmai, Z. Proposal for a new theoretical model of the cutting tool's flank wear. International Journal of Wear 2013, 303 (1-2), 437-445.

[25] Filice L., Umbrello D., Beccasri S., Micari F., On the FE Codes Capability for Tool Temperature Calculation in Machining Processes, Journal of Materials Processing Technology 2006, 174, 286-292

[26] Han, S.; Melkote, S. N.; Haluska, M. S.; Watkinsc, T. R. White Layer Formation Due to Phase Transformation in Orthogonal Machining of AISI 1045 Annealed Steel. Materials Science and Engineering 2008, 488 (1-2), 195-204.

8 CONCLUSION AND FUTURE WORK

This chapter summarizes the key discovery in this research. Following this the ideas that can potentially improve the current achievements and enhance their applications are presented in the future work section.

8.1 Conclusion

The objective of the present research was to develop a tool wear prediction methodology by combining the finite element simulation of the orthogonal cutting process and the available empirical wear rate characteristic models. The research was divided into three phases.

The objective of phase one was set to evaluate the results of mechanical and thermal process variables from FE simulation of the cutting process based on sharp (new) and worn tool edge geometries. In this phase, one of the key performance measures was to ensure that FE cutting simulations were numerically valid.

Phase two was aimed to define the calibration framework for the empirical wear rate models which have been widely used in the tool wear prediction studies. The framework specifies the required data to be collected for efficient calibration of wear rate models. This ultimately will assist in the selection of appropriate wear rate model. The framework also suggests the optimum number of experiments and simulations to be performed for data collection which will prevent the excessive and redundant experiments and simulations. The research methodology is based on a hybrid experimental/simulation approach with emphasis on the flank wear rate.

The objective of phase three was to develop a methodology for tool life prediction using a hybrid finite element simulation coupled with calibrated empirical wear rate models. The methodology should minimize the challenges involved in the nodal displacement calculations and should reduce the computational time when compared to nodal movement technique.

The experimental data of the wear formation, cutting edge geometry, wear rate, tool life and machining forces was collected based on performing the cutting tests in a defined range of cutting speed and feed rate. The experimental data of the friction and temperature magnitude and distribution were collected from literature. Ultimately the collected data was used in all three phases of this research to evaluate the simulated and predicted results. The following sections were the main conclusions of each phase and the respective discovery.

8.1.1 Phase one

In phase one the accuracy of simulated process variables in terms of their trend and magnitude, with respect to the experimentally available data, was investigated. The effect of flank wear length on machining forces, temperature and stresses were simulated using FE method with various combination of cutting speed and feed rate. The predicted tool wear rate with finite element results and Usui's model were also presented. Extensive experimental results were compared with simulated data. The following concluding remarks were achieved in the phase one:

The average flank face temperature increased with the increase of flank wear length. This direct relation of flank face temperature and flank wear length agreed with the experimental data from literature. The predicted temperature distribution showed that the position of maximum temperature shifted from the rake face to the flank face with larger flank wear length. This results also agreed with the experimental data from literature. The increase of frictional stress along the flank face interface was the cause of this shift. Simulations results showed that the increase in flank wear length increased the average shear stress and contact pressure on tool flank face.

Machining forces in the cutting and feed directions were increased with the increase in flank wear length. This direct relation of forces and flank wear length agreed with the experimental data. Modelling similar flank wear geometry with those observed during cutting tests was critical in predicting the cutting and feed forces accurately. Experimental results showed that the angle between the rake face and flank face was constant with an increase in flank wear length. If this angle were to vary, the difference between the predicted and experimental forces will increase.

Both simulated and experimental wear rate showed that the change in wear rate was more substantial with cutting speed when compared to feed rate, and the wear rate also increased with larger flank wear length.

Based on the result from this phase of research, it was also concluded that the predicted tool wear rate results is one possibility to validate the model with limited wear model calibration.

8.1.2 Phase two

In phase two, a combined finite element simulation and experimental approach was used to define the calibration framework for the Takeyama & Murata, Usui, Attanasio, and Akazawa wear rate models. The framework specifies the required data to be collected for efficient calibration of wear rate models. The framework also suggests the optimum number of experiments and simulations to be performed for data collection which will prevent the excessive and redundant experiments and simulations. The framework definition ultimately assisted in the selection of appropriate wear rate model to be used in phase three for tool life prediction. The following concluding remarks were achieved in phase two:

Both Usui and Akazawa wear rate models can be calibrated without knowing the dominant wear mechanism of either abrasion or diffusion. However, Akazawa model requires the detail description on how temperature affects hardness for workpiece and tool materials.

Prior knowledge of the flank face temperature is critical when calibrating both Takeyama & Murata and Attanasio models. When the magnitude of the flank face temperature was lower than activation temperature of diffusion, only the abrasive component of the equation could be calibrated. This condition affects the selection of process parameters magnitude during the experimental phase for model calibration. Moreover, limited information could be found on activation temperature of diffusion relative to different workpiece and tool material combinations.

Usui wear rate model was the most robust when compared to the other models investigated. This was because there is unbounded restriction in selecting process parameters during model calibration. Also the information regarding the dominant wear mechanism as a function of temperature is not required. Furthermore, latter information is very difficult to determine quantitatively with experiments.

When calibrating Usui's wear model, the predicted wear rate was controlled by the lower and upper limit of the simulated flank face temperature. Therefore, it is critical to perform experiments that are capable of capturing the lower and upper limit of the operating temperature during model calibration.

With the current combination of the workpiece and tool material used, calibrating Usui's wear model based on combination of lowest and highest process parameters showed to be most efficient. The number of experiments to be carried out should increase if the workpiece material is sensitive to strain rate and strain hardening.

8.1.3 Phase three

In phase three, a new methodology for tool life prediction was proposed and its feasibility was investigated. This unique approach adopted the parallel processing rather than the series, which substantially reduced the computational time. The motivation behind proposing this methodology was to improve the hybrid finite element/empirical based tool life prediction in terms of the wear rate calculation approach and overall computational time, which were introduced as challenges in the previous works done by other researchers. The achievements from phases 1 and 2 were used as the inputs in calibration of wear rate model and calculating the wear rate at the contact interfaces. The following concluding remarks were achieved in phase three:

The FE computational time was significantly reduced. This reduction was due to the fact that the FE simulation with different flank wear lengths could be computed in parallel and for each flank wear length interval; the simulated cutting time is dependent on the duration when the mechanical and thermal field becomes steady state. When using the nodal movement technique together with series approach, the FE computational time is coupled to the tool wear rate, which can have long computational time. There are two limitations in the proposed approach, which are (i) the angle between the rake face and flank face must not vary with tool life and (ii) at least two sets of experiments are required for model calibration.

Due to the inherent instable of the sliding velocity from the stick-slip condition at the contacting surface, the relative strain history and stable simulated time increment was used to calculate the sliding velocity distribution beneath the newly generated surface. The average sliding velocity used at the tool/flank face interface for the cutting conditions investigated was 0.86 m/s. When using this sliding velocity magnitude, the tool wear rate and tool life predicted during the secondary and tertiary cutting periods agreed better with experimental results regardless of cutting speed or tool wear life.

Experimental results showed that Usui’s equation had limitation predicting the tool wear rate during the initial tool wear period, which is dominated by mechanical stresses. A new empirical equation was proposed here which predicts the initial tool wear rate as a function of Von Mises stress together with calibrated constants. Experimental validation showed evidence that the newly developed empirical equation substantially improved the predicted tool wear rate. The limitations of this approach were that a 100 μm initial flank wear length was assumed, and empirical model calibration was required.

8.2 Future Work

The intent of this research was to prove the concept of using the combined empirical and finite element method to predict tool wear rate/life and identify its operating limits. The current research was based on the orthogonal cutting process and continuous chip formation. In general, most chip formation processes observed in practice are mostly the non-continuous or segmental type and in oblique or non-orthogonal cutting configuration. Finite element simulation of the cutting process for non-continuous chip type and oblique cutting configuration is substantially more complex and requires more advanced crack propagation to be added on subroutine. Therefore, future work should focus on applying the methodology developed in this research with oblique cutting configuration, which include the cutting nose radius and non-continuous type. This proposed future work should be built on the hypothesis of performing simple and fast orthogonal cutting tests for tool wear empirical model calibration and applying to more complex machining configuration. More time should be focused on developing the subroutine for advanced crack propagation to simulate non continuous chip type.

9 REFERENCES

[Akazawa, 2009] Akazawa K., Ozaki K. & Shamoto E., 2009. Development of a System to Predict Tool Wear Considering Cutting Conditions and Workpiece Components. Journal of the Japan Society for Precision Engineering, 75(3), pp. 396-401.

[Albrecht, 1960] Albrecht P., 1960. New Developments in the Theory of the Metal-Cutting Process: Part I. The Ploughing Process in Metal Cutting. Journal of Engineering for Industry, 82(4), pp. 348-357.

[Altintas, 2009] Altintas Y., 2000. Manufacturing Automation. New York: Cambridge University Press.

[Archard, 1953] Archard J. F., 1953. Contact and Rubbing of Flat Surfaces. Journal of Applied Physics, 24(8), p. 981.

[Arrazola, 2008] Arrazola P. J., Ugarte D. & Domínguez X., 2008. A New Approach for the Friction Identification During Machining Through the Use of Finite Element Modeling. International Journal of Machine Tools and Manufacture, 48(2), pp. 173-183.

[Arsecularatne, 1996] Arsecularatne J., Fowle R., Mathew P. & Oxley P., 1996. Prediction of Tool Life in Oblique Machining with Nose Radius Tools. International Journal of Wear, 198(1-2), pp. 220-228.

[Arsecularatne, 2006] Arsecularatne J., Zhang L. & Montross C., 2006. Wear and Tool Life of Tungsten Carbide, PCBN and PCD Cutting Tools. International Journal of Machine Tools and Manufacture, 46(5), pp. 482-491.

[Astakhov, 2004] Astakhov V., 2004. The Assessment of Cutting Tool Wear. International Journal of Machine Tools and Manufacture, 44(6), pp. 637-647.

[Astakhov, 2006] Astakhov V., 2006. Tribology of Metal Cutting. 1 ed. Elsevier Science.

[Astakhov, 2008] Astakhov V. & Davim J., 2008. Tools (Geometry and Material) and Tool Wear. Springer: London.

[Attanasio, 2008a] Attanasio A., Ceretti E., Giardini C., Filice L. & Umbrello D., 2008. Criterion to Evaluate Diffusive Wear in 3D Simulations when Turning AISI 1045 Steel, International Journal of Material Forming, 1, pp. 495-498.

[Attanasio, 2008b] Attanasio A., Ceretti E., Rizzuti S., Umbrello D., & Micari F., 2008. 3D Finite Element Analysis of Tool Wear in Machining. CIRP Annals, 57(1), pp. 61-64.

[Attanasio, 2009] Attanasio A. & Umbrello D., 2009. Abrasive and Diffusive Tool Wear FEM Simulation. International Journal of Material Forming, 2, pp. 543-546.

[Attanasio, 2010] Attanasio A., Ceretti E., Fiorentino A., Cappellini C., & Giardini C., 2010. Investigation and FEM-Based Simulation of Tool Wear in Turning Operations with Uncoated Carbide Tools. International Journal of Wear, 269, pp. 344-350.

[Attanasio, 2011] Attanasio A., Ceretti E. & Giardini C., 2011. 3D FEM Simulation of Flank Wear in Turning. The 14th International ESAFORM Conference on Material Forming, 1353, pp. 561-566.

[Berhrens, 1999] Berhrens A. & Westhoff B., 1999. Finite Element Modeling of High Speed Machining Process. 2nd International Conference on High Speed Machining, pp. 185-190.

[Bil, 2004] Bil H., Kılıç S. & Tekkaya A., 2004. A Comparison of Orthogonal Cutting Data From Experiments with Three Different Finite Element Models. International Journal of Machine Tools and Manufacture, 44(9), pp. 933-944.

[Binder, 2015] Binder M., Klocke F. & Lung D., 2015. Tool Wear Simulation of Complex Shaped Coated Cutting Tools. Wear, 330-331, pp. 600-607.

[Binder, 2017] Binder M., Klocke F. & Doebbeler B., 2017. An Advanced Numerical Approach on Tool Wear Simulation for Tool and Process Design in Metal Cutting. Simulation Modelling Practice and Theory, 70, pp. 65–82.

[Boothroyd, 1985] Boothroyd G., 1985. Fundamentals of Metal Machining and Machine Tools. 9th ed. Washington , D.C.: Scripta Book Company.

[Bordin, 2015] Bordin A., Imbrogno S., Rotella G., Bruschi S., Ghiotti A. & Umbrello D., 2015. Finite Element Simulation of Semi-finishing Turning of Electron Beam Melted Ti6Al4V Under Dry and Cryogenic Cooling. Procedia CIRP, 31, pp. 551-556.

[Ceretti, 1999] Ceretti E., Lucchi M. & Altan T., 1999. FEM Simulation of Orthogonal Cutting: Serrated Chip Formation. Journal of Materials Processing Technology, 95(1-3), pp. 17-26.

[Chen 2004] Chen L., El-Wardany T. & Harris W., 2004. Modelling the Effects of Flank Wear Land and Chip Formation on Residual Stresses. CIRP Annals, 53(1), pp. 95-98.

[Choudhury, 2000] Choudhury S. & Kishore K., 2000. Tool Wear Measurement in Turning using Force Ratio. International Journal of Machine Tools and Manufacture, 40(6), pp. 899-909.

[Coelho, 2007] Coelho R. T., Ng E.-G. & Elbestawi, M., 2007. Tool Wear when Turning Hardened AISI 4340 with Coated PCBN Tools Using Finishing Cutting Conditions. International Journal of Machine Tools and Manufacture, 47(2), pp. 263-272.

[Coromant, 1994] Coromant A. S., 1994. Modern Metal Cutting: A Practical Handbook. Sandviken, Sweden: Sandvik Coromant.

[Denkena, 2011] Denkena B., Lucas A. & Bassett E., 2011. Effects of the Cutting Edge Microgeometry on Tool Wear and its Thermo-Mechanical Load. CIRP Annals, 60(1), pp. 73-76.

[Denkena, 2012] Denkena B., Kohler J. & Mengesha M. S., 2012. Influence of the Cutting Edge Rounding on the Chip Formation Process: Part 1. Investigation of Material Flow, Process Forces, and Cutting Temperature. Production Engineering Research and Development, 6, pp. 329-338.

[Fang, 2007] Fang N. & Fang G., 2007. Theoretical and Experimental Investigations of Finish Machining with a Rounded Edge Tool. Journal of Materials Processing Technology, 191(1-3), pp. 331-334.

[Filice, 2006] Filice L., Umbrello D., Beccari S. & Micari F., 2006. On the FE Codes Capability for Tool Temperature Calculation in Machining Processes. Journal of Materials Processing Technology, 174(1-3), pp. 286-292.

[Filice, 2007a] Filice L., Micari F., Rizzuti S. & Umbrello D., 2007. A Critical Analysis on the Friction Modelling in Orthogonal Machining. International Journal of Machine Tools and Manufacture, 47(3-4), pp. 709-714.

[Filice, 2007b] Filice L., Micari F., Settineri L. & Umbrello D., 2007. Wear Modelling in Mild Steel Orthogonal Cutting when using Uncoated Carbide Tools. International Journal of Wear, 262, pp. 545-554.

[Glaeser, 1971] Glaeser W., 1971. Friction and Wear. IEEE Transactions on Parts, Hybrids, and Packaging, 7(2), pp. 99-105.

[Grzesik,2002] Grzesik W., Zalisz Z. & Nieslony P., 2002. Friction and Wear Testing of Multilayer Coatings on Carbide Substrates for Dry Machining Applications. Surface and Coatings Technology, 155(1), pp. 37-45.

[Haddag, 2013] Haddag B. & Nouari M., 2013. Tool Wear and Heat Transfer Analyses in Dry Machining Based on Multi-Steps Numerical Modelling and Experimental Validation. Wear, 302(1-2), pp. 1158-1170.

[Haglund, 2008] Haglund A. J., Kishawy H. A. & Rogers R. J., 2008. An Exploration of Friction Models for The Chip–Tool Interface using an Arbitrary Lagrangian–Eulerian Finite Element Model. Wear, 265(3-4), pp. 452-460.

[Halim, 2008] Halim S. M. T., 2008. Finite Element Modeling of the Orthogonal Metal Cutting Process: Modeling the Effects of Coefficient of Friction and Tool Holding Structure on Cutting Forces and Chip Thickness, Master Thesis, McMaster Univesity.

[Hoffman, 1984] Hoffman E. G., 1984. Fundamentals of Tool Design. Dearborn: Society of Manufacturing Engineers.

[Hoier, 2019] Hoier P., Malakizadi A., Klement U. & Krajnik P., 2019. Characterization of Abrasion- and Dissolution-Induced Tool Wear in Machining. Wear, 426-427, pp. 1548-1562.

[Hosseinkhani, 2015] Hosseinkhani K. & Ng E., 2015. A Combined Empirical and Numerical Approach for Tool Wear Prediction in Machining. Procedia CIRP, 31, pp. 304-309.

[Huang, 1996] Huang J. M. & Black J. T., 1996. An Evaluation of Chip Separation Criteria for the FEM Simulation of Machining. Journal of Manufacturing Science Engineering, 118(4), pp. 545-554.

[Huang, 2003] Huang Y. & Liang S. Y., 2003. Modelling of the Cutting Temperature Distribution under the Tool Flank Wear Effect. Journal of Mechanical Engineering Science, 217, pp. 1195-1208.

[Iqbal, 2007] Iqbal S., Mativenga P. & Sheikh M., 2007. Characterization of Machining of AISI 1045 Steel Over a Wide Range of Cutting Speeds. Part 1: Investigation of Contact Phenomena. Journal of Engineering Manufacture, 221, pp. 917-926.

[Jaspers, 2002] Jaspers S. & Dautzenberg J., 2002. Material Behaviour in Metal Cutting: Strains, Strain Rates and Temperatures in Chip Formation. Journal of Materials Processing Technology, 121(1), pp. 123-135.

[Johnson, 1983] Johnson G. J. & Cook W. H., 1983. A Constitutive Model and Data for Metals Subjected to Large Strains, High Strain Rates and High Temperatures, Proceedings of the 7th International Symposium on Ballistics, pp. 541-547.

[Joyot, 1998] Joyot P., Rakotomalala R., Pantalé O., Touratier M. & Hakem N., 1998. A Numerical Simulation of Steady State Metal Cutting. Proceedings of the Institution of Machanical Engineers, Part C: Journal of Mechanical Engineering Science, 212(5), pp. 331-341.

[Kalhori, 2001] Kalhori V., 2001. Modelling and Simulation of Mechanical Cutting, PhD Thesis, Lulea: Lulea University of Technology.

[Kitagawa, 1988] Kitagawa T., Maekawa K., Shirakashi T. & Usui E., 1988. Analytical Prediction of Flank Wear of Carbide Tools in Turning Plain Carbon Steels, Part 1: Characteristic Equation of Flank Wear. Bulletin of the Japan Society of Precision Engineering, 22(4), pp. 263-269.

[Kitagawa, 1989] Kitagawa T., Maekawa M., Shirakashi T. & Usui E., 1989. Analytical Prediction of Flank Wear of Carbide Tools in Turning Plain Carbon Steels, Part 2: Prediction of Flank Wear. Bulletin of the Japan Society of Precision Engineering, 23 (2), pp. 126-133.

[Klocke, 2001] Klocke F., Raedt H.-W. & Hoppe S., 2001. 2D-FEM Simulation of the Orthogonal High Speed Cutting Process. Machining Science and Technology, 5(3), pp. 323-340.

[Klocke, 2002] Klocke F., Beck T., Hoppe S., Krieg T., Müller N., Nöthe T., Raedt H-W & Sweeney K., 2002. Examples of FEM Application in Manufacturing Technology. Journal of Materials Processing Technology, 120(1-3), pp. 450-457.

[Komvopoulos, 1991] Komvopoulos K. & Erpenbeck S. A., 1991. Finite Element Modeling of Orthogonal Metal Cutting. Journal of Manufacturing Science and Engineering, 113(3), pp. 253-267.

[Koshy, 2011] Koshy P., 2011. Lecture Notes - Manufacturing Processes I, Hamilton: McMaster University.

[Kountanya, 2004] Kountanya R. K. & Endres W. J., 2004. Flank Wear of Edge-Radiused Cutting Tools Under Ideal Straight-Edged Orthogonal Conditions. Manufacturing Science and Engineering, 126(3), pp. 496-505.

[Lane, 2013] Lane B. M., Dow T. A. & Scattergood R., 2013. Thermo-Chemical Wear Model and Worn Shapes for Single-Crystal Diamond Tools Cutting Steel. International Journal of Wear, 300, pp. 216-224.

[Li, 2002] Li K., Gao X.-L. & Sutherland J. W., 2002. Finite Element Simulation of Orthogonal Metal Cutting Process for Qualitative Understanding of the Effects of Crater Wear on Chip Formation Process. Journal of Materials Processing Technology, 127, pp. 309-324.

[Li, 2012] Li, B., 2012. A Review of Tool Wear Estimation using Theoretical Analysis and Numerical Simulation Technologies. International Journal of Refractory Metals and Hard Materials, 35, pp. 143-151.

[Long, 2010] Long Y. & Huang Y., 2010. Combined Effect of Flank and Crater Wear on Cutting Force Modelling in Orthogonal Machining-Part I: Model Development. Machining Science and Technology, 14, pp. 1-23.

[Lorentzon, 2008] Lorentzon J. & Järvstråt N., 2008. Modelling Tool Wear in Cemented-Carbide Machining Alloy 718. International Journal of Machine Tools and Manufacture, 48(10), pp. 1072-1080.

[Lotfi, 2016] Lotfi M., Jahanbakhsh M. & Akhavan Farid A., 2016. Wear Estimation of Ceramic and Coated Carbide Tools in Turning of Inconel 625: 3D FE Analysis. Tribology International, 99, pp. 107-116.

[Luo, 2005] Luo X., Cheng K., Holt R. & Liu X., 2005. Modeling Flank Wear of Carbide Tool Insert In Metal Cutting. International Journal of Wear, 259, pp. 1235-1240.

[Malakizadi, 2013] Malakizadi A., Cedergren S., Surreddi K. B. & Nyborg L., 2013. A Methodology to Evaluate the Machinability of Alloy 718 by Means of FE Simulation. International Conference on Advanced Manufacturing Engineering and Technologies. Stockholm: NEWTECH, pp. 95-106

[Malakizadi, 2015] Malakizadi A., 2015. Optimisation of Machining Operations by means of Finite Element Method and Tailored Experiments. PhD Thesis, Chalmers University of Technology.

[Malakizadi, 2016] Malakizadi A., Gruber H., Sadik I. & Nyborg L., 2016. An FEM-Based Approach for Tool Wear Estimation in Machining. Wear, 368-369, p. 10-24.

[Malakizadi, 2020] Malakizadi, A., Shi, B., Hoiera, P., Attia, H., Krajnik, P., 2020. Physics-Based Approach for Predicting Dissolution–Diffusion Tool Wear in Machining. CIRP Annals-Manufacturing Technology, 69, pp. 81-84.

[Mamalis, 2001] Mamalis A., Horváth M., Branis A. & Manolakos D., 2001. Finite Element Simulation of Chip Formation in Orthogonal Metal Cutting. Journal of Materials Processing Technology, 110(1), pp. 19-27.

[Marksberry, 2008] Marksberry P. & Jawahir I., 2008. A Comprehensive Tool-Wear/Tool-Life Performance Model in the Evaluation of NDM (Near Dry Machining) for Sustainable Manufacturing. International Journal of Machine Tools and Manufacture, 48(7-8), pp. 878-886.

[Marusich, 2001] Marusich T. D., Thiele J. D. & Brand C. J., 2001. Simulation and Analysis of Chip Breakage in Turning Processes. 5th CIRP Intenational Workshop on Modelling of Machining, pp. 139-148

[Mathew, 1989] Mathew P., 1989. Use of Predicted Cutting Temperatures in Determining Tool Performance. International Journal of Machine Tools and Manufacture, 29, pp. 481-497.

[Merchant, 1945] Merchant M. E., 1945. Mechanics of the Metal Cutting Process. II. Plasticity Conditions in Orthogonal Cutting. Journal of Applied Physics, 16, pp. 318-324.

[Mills, 1983] Mills B. & Redford A., 1983. Machinability of Engineering Materials. London: Springer, Dordrecht.

[Movahhedy, 2000] Movahhedy M., Gadala M. S. & Altintas Y., 2000. Simulation of the Orthogonal Metal Cutting Process using An Arbitrary Lagrangian–Eulerian Finite-Element Method. Journal of Materials Processing Technology, 103(2), p. 267-275.

[Nasr, 2007] Nasr M. N., Ng E.-G. & Elbestawi, M., 2007. Modelling the Effects of Tool-Edge Radius on Residual Stresses when Orthogonal Cutting AISI 316L. International Journal of Machine Tools and Manufacture, 47(2), pp. 401-411.

[Ng, 2002a] Ng E.-G. & Aspinwall D. K., 2002. Modelling of Hard Part Machining. Journal of Materials Processing Technology, 127(2), pp. 222-229.

[Ng, 2002b] Ng E., El-Wardany T. L., Dumitrscu M. & Elbestawi M. A., 2002. Physics-Based Simulation of High Speed Machining. Machining Science and Technology, 6(3), pp. 301-329.

[Ng, 2003] Ng E., El-Wardany T. I. & Elbestawi M., 2003. Influence of Flank Wear Lenght on Residual Stress and Workpiece Quality in Machined Surfaces. International Journal of Mechanical Production Systems, Issue April, pp. 10-21.

[Niebel, 1989] Niebel B. W., Draper A. B. & Wysk R. A., 1989. Modern Manufacturing Process Engineering. New York: McGraw-Hill.

[Olsson, 1989] Olsson M., Söderberg S., Jacobson S. & Hogmark S., 1989. Simulation of Cutting Tool Wear by a Modified Pin-On-Disc Test. International Journal of Machine Tools and Manufacture, 29(3), pp. 377-390.

[Oxley, 1977] Oxley P. L. B. & Hastings W. F., 1977. Predicting the Strain Rate in the Zone of Intense Shear in which the Chip is Formed in Machining from The Dynamic Flow Stress Properties of the Work Material and the Cutting Conditions. Proceedings of the Roal Society of London, 356(1686), pp. 395-410.

[Oxley, 1989] Oxley P., 1989. Mechanics of Machining: An Analytical Approach to Assessing Machinability. Chichester, West Sussex, England: Ellis Horwood Limited.

[Özel, 2000] Özel T. & Altan T., 2000. Determination of Workpiece Flow Stress and Friction at the Chip–Tool Contact for High-Speed Cutting. International Journal of Machine Tools and Manufacture, 40(1), pp. 133-152.

[Özel, 2006] Özel T., 2006. The Influence of Friction Models on Finite Element Simulations of Machining. International Journal of Machine Tools and Manufacture, 46(5), pp. 518-530.

[Özel, 2010] Özel T., Sima M., Srivastava A. & Kaftanoglu B., 2010. Investigations on the Effects of Multi-Layered Coated Inserts in Machining Ti–6Al–4V Alloy with Experiments and Finite Element Simulations. CIRP Annals, 59(1), pp. 77-82.

[Palmai, 2013] Palmai Z., 2013. Proposal for a New Theoretical Model of the Cutting Tool's Flank Wear. Wear, 303(1-2), pp. 437-445.

[Poulachon, 2001] Poulachon G., Moisan A. & Jawahir I., 2001. Tool-Wear Mechanisms in Hard Turning with Polycrystalline Cubic Boron Nitride Tools. Wear, 250(1-12), pp. 576-586.

[Puls, 2012] Puls H., Klocke F. & Lung D., 2012. A New Experimental Methodology to Analyze the Friction Behaviour at the Tool-Chip Interface in Metal Cutting. Journal of Production. Engineering – Research and Development, 6, pp. 349-354.

[Quinto, 1988] Quinto D. T., 1988. Mechanical Property and Structure Relationships in Hard Coatings for Cutting Tools. Journal of Vacuum Science & Technology A, 6, pp. 2149–2157.

[Rabinowicz, 1980] Rabinowicz E., 1980. An Adhesive Wear Model Based on Variations in Strength Values. Wear, 63(1), pp. 175-181.

[Rabinowicz, 1966] Rabinowicz E. & Tanner R., 1966. Friction and Wear of Materials. Journal of Applied Mechanics, 33(2), p. 479.

[Raczy, 2004] Raczy A., Elmadagli M., Altenhof W. J. & Alpas A. T., 2004. An Eulerian Finite-Element Model for Determination of Deformation State of a Copper Subjected to Orthogonal Cutting. Metallurgical and Materials Transactions A, 35A, pp. 2393-2400.

[Rech, 2013] Rech J., Arrazola P.J., Claudin C., Courbon C., Pusavec F. & Kopac J., 2013. Characterisation of Friction and Heat Partition Coefficients at the Tool-Work Material Interface in Cutting. CIRP Annals - Manufacturing Technology, 62, pp. 79-82.

[Ren, 2000] Ren H. & Altintas, Y., 2000. Mechanics of Machining with Chamfered Tools. Manufacturing Science and Technology, 122(4), pp. 650-659

[Sadik, 2014] Sadik M.I. & Jalilian E., 2014. Characterization and Performance Evaluation of Mono-Grain and Bi-Modal PCD Grade in Machining of MMC. 6th CIRP International Conference on High Performance Cutting, 14, pp. 200-204

[Saini, 2012] Saini S., Ahuja I. S. & Sharma V. S., 2012. Residual Stresses, Surface Roughness, and Tool Wear in Hard Turning: A Comprehensive Review. Materials and Manufacturing Processes, 27(6), pp. 583-598.

[Salvatore, 2013] Salvatore F., Saad S. & Hamdi H., 2013. Modeling and Simulation of Tool Wear During the Cutting Process. 14th CIRP Conference on Modeling of Machining Operations (CIRP CMMO), 8, pp. 305-310.

[Sanchez, 2011] Sanchez A. M., Canteli J. A., Cantero J. L. & Miguelez M. H., 2011. Numerical Analysis of Tool Wear Effect in Machining Induced Residual Stresses. Simulation Modelling Practice and Theory, 19, pp. 872-886.

[Sartkulvanich, 2005] Sartkulvanich P., Altan T. & Göcmen A., 2005. Effects of Flow Stress and Friction Models in Finite Element Simulation of Orthogonal Cutting—A Sensitivity Analysis. Machining Science and Technology, 9(1), pp. 1-26.

[Schey, 1987] Schey J. A., 1987. Introduction to Manufacturing Processes. New York: McGraw-Hill.

[Schulze, 2011] Schulze V. & Zanger F., 2011. Development of a Simulation Model to Investigate Tool Wear in Ti-6Al-4V Alloy Machining. Advanced Materials Research, 223, pp. 535-544.

[Shaw, 1956] Shaw M. C. & Dirke S. O., 1956. On the Wear of Cutting Tools. Microtecnic, 10, pp.187.

[Shaw, 2005] Shaw M. C., 2005. Metal Cutting Principles. 2nd ed. New York: Oxford University Press.

[Shet, 2000] Shet C. & Deng X., 2000. Finite Element Analysis of the Orthogonal Metal Cutting Process. Journal of Materials Processing Technology, 105(1-2), pp. 95-109.

[Shi, 2002] Shi G., Deng X. & Shet C., 2002. A Finite Element Study of the Effect of Friction in Orthogonal Metal Cutting. Finite Element in Analysis and Design, 38(9), pp. 863-883.

[Shi, 2004] Shi J. & Liu C. R., 2004. The Influence of Material Models on Finite Element Simulation of Machining. Journal of Manufacturing Science and Engineering, 126(4), pp. 849-857.

[Simoneau, 2006] Simoneau A., Ng E. & Elbestawi M., 2006. Chip Formation during Microscale Cutting of a Medium Carbon Steel. International Journal of Machine Tools and Manufacture, 46(5), pp. 467-481.

[Simoneau, 2007] Simoneau A., Ng E. & Elbestawi M. A., 2007. Modeling the Effects of Microstructure in Metal Cutting. International Journal of Machine Tool and Manufacture, Volume 47, pp. 368-375.

[Takeyama, 1963] Takeyama H. & Murata R., 1963. Basic Investigation of Tool Wear. Trasaction of ASME, Journal of Engineering for Industry, pp. 33-38.

[Taylor, 1907] Taylor F. W., 1907. On the Art of Cutting Tools, Transactions of American Society of Mechancial Engineers, 28, pp., 31-350

[Thepsonthi, 2013] Thepsonthi T. & Özel T., 2013. Experimental and Finite Element Simulation Based Investigations on Micro-Milling Ti-6Al-4V Titanium Alloy: Effects of CBN Coating on Tool Wear. Journal of Materials Processing Technology, 213(4), pp. 532-542.

[Thepsonthi, 2015] Thepsonthi T. & Özel T., 2015. 3-D Finite Element Process Simulation of Micro-End Milling Ti-6Al-4V Titanium Alloy: Experimental Validations on Chip Flow and Tool Wear. Journal of Materials Processing Technology, 221, pp. 128-145.

[Toenshoff, 2013] Toenshoff H. K. & Denkena B., 2013. Basics of Cutting and Abrasive Processes. 1st ed. Germany: Springer.

[Trent, 2000] Trent E. M. & Wright P. K., 2000. Metal Cutting. 4th edition. Woburn, United States of America: Butterworth-Heinemann..

[Trigger, 1963] Trigger K. J., 1963. Temperatures in Machining and their Importance. Proceeding of the International Production Engineering Research Conference, pp. 95-101

[Trigger, 1956] Trigger K. J. & Chao B. T., 1956. The Mechanism of Crater Wear of Cemented Carbide Tools. Transaction of ASME, 78(5), pp. 1119-1126.

[Usui, 1978a] Usui E., Hirota A. & Masuko M., 1978. Analytical Prediction of Three Dimensional Cutting Process—Part 1: Basic Cutting Model and Energy Approach. ASME. Journal of Engineering for Industry, 100(2), pp. 222–228.

[Usui, 1978b] Usui E. & Hirota A., 1978. Analytical Prediction of Three Dimensional Cutting Process—Part 2: Chip Formation and Cutting Force with Conventional Single-Point Tool. ASME. Journal of Engineering for Industry, 100(2), pp. 229-235.

[Usui, 1982] Usui E. & Shirakashi T., 1982. Mechanics of Machining - from Descriptive to Predictive Theory. In on the Art of Cutting Metals-75 years later. ASME, 7, pp. 13-35.

[Usui, 1984] Usui E., Shirakashi T. & Kitagawa T., 1984. Analytical Prediction of Cutting Tool Wear. International Journal of Wear, 100(1-3), pp. 129-151.

[Wang, 1986] Wang H.-P. & Wysk R. A., 1986. An Expert System for Machining Data Section. Computers & Industrial Engineering, 10(2), pp. 99-107.

[Wang, 2019] Wang Y., Su H., Dai J. & Yang S., 2019. A Novel Finite Element Method for the Wear Analysis of Cemented Carbide Tool During High Speed Cutting Ti6Al4V Process. The International Journal of Advanced Manufacturing Technology, 103, pp. 2795-2807.

[Wanigarathne, 2005] Wanigarathne P., Kardekar A.D., Dillon O.W., Poulachon G. & Jawahir I.S., 2005. Progressive Tool-Wear in Machining with Coated Grooved Tools and its Correlation with Cutting Temperature. Wear, 259(7), pp. 1215-1224.

[Xiang, 2018] Xiang J. Pang S., Xie L., Gao F., Hu X., Yi J. & Hu F., 2018. Mechanism-Based FE Simulation of Tool Wear in Diamond Drilling of SiCp/Al Composites. Materials, 11(2), p. 252.

[Xie, 2004] Xie L., 2004. Estimation of Two-Dimensional Tool Wear Based on Finite Element Method, Karlsruhe, Germany: University of Karlsruhe.

[Xie, 2005] Xie L.-J., Schmidt J., Schmidt C. & Biesinger F., 2005. 2D FEM Estimate of Tool Wear in Turning Operation. International Journal of Wear, 258, pp. 1479-1490.

[Yang, 2002] Yang X. & Liu C., 2002. A New Stress-Based Model of Friction Behavior in Machining and its Significant Impact on Residual Stresses Computed by Finite Element Method. International Journal of Mechanical Sciences, 44(4), pp. 703-723.

[Yang, 2013] Yang S., Zhu G., Xu J. & Fu Y., 2013. Tool Wear Prediction of Machining Hydrogenated Titanium Alloy Ti6Al4V with Uncoated Carbide Tools. The International Journal of Advanced Manufacturing Technology, 68, pp. 673-682.

[Yen, 2004a] Yen Y.-C., Jain A. & Altan T., 2004. A Finite Element Analysis of Orthogonal Machining using Different Tool Edge Geometries. Journal of Material Processing Technology, 146(1), pp. 72-81.

[Yen, 2004b] Yen Y.-C., Jain A., Chigurupati P., Wu W.T. & Altan T., 2004. Computer Simulation of Orthogonal Cutting using a Tool with Multiple Coatings. Machining Science and Technology, 8(2), pp. 305-326.

[Yen, 2004c] Yen, Y.-C., Söhner, J., Lilly, B. & Altan, T., 2004. Estimation of Tool Wear in Orthogonal Cutting using the Finite Element Analysis. Journal of Materials Processing Technology, 146(1), pp. 82-91.

[Yussefian, 2010] Yussefian N., Koshy P., Buchholz S. & Klocke F., 2010. Electro-Erosion Edge Honing of Cutting Tools. CIRP Annals, 59(1), pp. 215-218.

[Zanger, 2013] Zanger F. & Schulze V., 2013. Investigation on Mechanisms of Tool Wear in Machining of Ti-6Al-4V using FEM Simulation. Procedia CIRP, 8, pp. 158-163

[Zemzemi, 2008] Zemzemi F. Bensalem W., Rech J., Dogui A., Kapsa P., 2008. New Tribometer Designed for the Characterisation of the Friction Properties at the Tool/Chip/Workpiece Interfaces in Machining. Tribotest, 14(1), pp. 11-25.

[Zerilli, 1987] Zerilli F. J. & Armstrong R. W., 1987. Dislocation-Mechanics-Based Constitutive Relations for Material Dynamics Calculations. Journal of Applied Physics, 61(5), pp. 1816-1825.

[Zhao, 2002] Zhao H., Barber G. C. & Zou Q., 2002. A Study of Flank Wear in Orthogonal Cutting with Internal Cooling. International Journal of Wear, 253, pp. 957-962.

[Ziada, 2013] Ziada Y., 2013. Improved Residual Stress Prediction In Metal Cutting, PhD Thesis, McMaster University.

[Zorev, 1963] Zorev N. N., 1963. Interrelation Between Shear Processes Occurring Along Tool Face and on Shear Plane in Metal Cutting. ASME, pp. 42-49.